Evading the Storm: BET Inhibitor Resistance and the Leukaemia Stem Cell

Chun Yew Fong

ORCID: 0000-0001-5773-103X

February 2017

Sir Peter MacCallum Department of Oncology, The University of Melbourne

Submitted in total fulfilment of the requirements for the degree of Doctor of Philosophy

Abstract

Bromodomain and Extra Terminal protein (BET) inhibitors are first-in-class, epigenetic targeted therapies that deliver a new therapeutic paradigm by directly targeting protein-protein interactions at chromatin. Early clinical trials have shown significant promise, particularly in acute myeloid leukaemia (AML), suggesting that these compounds are likely to form an important component of future anti-cancer regimes. However, therapeutic resistance is an inevitable consequence of most cancer therapies, therefore the evaluation of resistance mechanisms is of utmost importance in order to optimise the clinical utility of this novel class of drugs.

This work utilises primary murine hematopoietic stem and progenitor cells (HSPC) immortalised with MLL-AF9 to generate several clonal cell lines demonstrating robust resistance, *in vitro* and *in vivo* to the prototypical BET inhibitor, I-BET151. Resistant clones harbour cross-resistance to the chemically distinct BET inhibitor JQ1, as well as resistance to genetic knockdown of BET proteins. Moreover, resistance is stably maintained across subsequent cell generations in the absence of ongoing selective pressure. Immunophenotypic immaturity is identified in resistant clones and, through functional limiting dilution assays, resistance is definitively demonstrated to emerge from leukaemia stem cells (LSCs). This finding is further confirmed using an independently generated *in vivo* model of resistance and in patient derived xenograft (PDX) models of human leukaemia.

The underlying mechanism of resistance is identified through examination of the transcriptome and chromatin interface utilising high throughput sequencing techniques. Consistent with the adoption of alternative transcriptional pathways, expression of key target oncogenes such as *Myc* remain unaltered in resistant clones despite the global loss of chromatin-bound Brd4. Alternatively, increased Wnt/β-catenin signalling in human and mouse leukaemia cells is demonstrated to account, in part, for resistance to BET inhibitors and functions to maintain expression of malignant oncogenes. Negative regulation of this pathway restores sensitivity to I-BET151 *in vitro* and *in vivo* and highlights a potential rational combination therapy strategy to circumvent or prevent the development of BET inhibitor resistance.

The emergence of BET inhibitor resistance from a LSC population prompted further exploration of rational combination therapies with sound mechanistic basis. LSD1 inhibitors have demonstrated pre-clinical promise in the treatment of AML underpinned by the induction of differentiation of leukaemia cells and the loss of LSC capacity. Using the derived model BET inhibitor resistance, LSD1 inhibitors are demonstrated to function synergistically with BET inhibitors and restore sensitivity to BET inhibitor resistant clones. Induction of differentiation is demonstrated in immunophenotypic and transcriptome assays and suggest a further potential combination therapy approach to enhance the clinical utility of both drugs.

Collectively, these findings give insight into the basic biology of AML, demonstrate the role of epigenetically mediated intratumoural heterogeneity and transcriptional plasticity in the evasion of targeted therapies and provide a base from which further investigation of the LSC can occur to identify vulnerabilities which may be exploited for therapeutic gain.

Declaration

This is to certify that:

(i) the thesis comprises only my original work towards the PhD except where indicated in the Preface,

(ii) due acknowledgement has been made in the text to all other material used,

(iii) the thesis is fewer than 100 000 words in length, exclusive of tables, maps, bibliographies and appendices.

Preface

This thesis includes experiments performed with the assistance of others. I sincerely thank the following people for their contributions:

Dr Omer Gilan for his assistance in obtaining biological replicate data for β-catenin ChIP and Western blot expertise.

Dr Enid Lam and Dr Alan Rubin for their assistance in the analysis of genomic data sets.

Mr Nathan Pinnawala for his assistance in preparation of RNA-seq samples following LSD1 inhibitor therapy.

Professor Anthony Papenfuss for his assistance in the analysis of correlation between WNT/β-catenin pathway and target gene expression and outcomes following treatment of primary human samples with BET inhibitors.

Dr Richard Gregory of the GSK Medicines Research Centre for his assistance with the performance quantitative mass spectrometry and subsequent data analysis.

The remainder of the experimentation and written work is my own.

Acknowledgements

The completion of this project has been a journey of many miles, unexpected highs, eye opening lows and unbelievable opportunities.

I want to sincerely thank Mark for taking a chance on a completely unknown quantity, supporting my scientific development and having me along for an incredible ride. The success of your lab is a testament to your unrelenting mentorship, vision and dedication to our individual development.

To the members of the Dawson laboratory, past and present, we have laughed together, cried together and done amazing work together. Thank you for the kind words, unkind words, years of friendship and unquestioning support. Science is only a small part of what I've learnt from you all.

To Brian and Tony, thank you for hosting an Australian refugee in Cambridge. Brian, your valued guidance and mentorship has been much appreciated. Tony, your generosity knows no bounds.

To Ricky and the Johnstone laboratory, thank you for your support when a new face arrived in East Melbourne.

To the Peter Mac research family, your support has been immeasurable and I continue to be amazed by the genuine warmth and generosity of the research department.

To the Leukaemia Foundation of Australia, Haematology Society of Australia and New Zealand, Royal Australasian College of Physicians and the Victorian Comprehensive Cancer Centre who have provided scholarship funding and travel assistance I express my gratitude for supporting my scientific and research development.

To my loving wife Liz, nothing is impossible when we are together. When we begun this journey we could not have foreseen the path it has taken but I could not have faced it without you. All of my achievements are your achievements as they could never have happened without you.

Table of Contents

List of tables, figures and illustrations

Figures

Tables

Abbreviations

Nucleotide abbreviations

A	Adenine	K	Guanine or Thymine
C	Cytosine	M	Adenine or Cytosine
G	Guanine	B	Cytosine or Guanine or Thymine
T (or U)	Thymine (or Uracil)	D	Adenine or Guanine or Thymine
R	Adenine or Guanine	H	Adenine or Cytosine or Thymine
Y	Cytosine or Thymine	V	Adenine or Cytosine or Guanine
S	Guanine or Cytosine	N	Any base
W	Adenine or Thymine	-	Gap

Other abbreviations

2HG	2-hydroxyglutate
5fC	5-formylcytosine
5hmC	5-hydroxymethylcytosine
5mC	5-methylcytosine
α-KG	α-ketoglutarate
ABC	ATP-binding cassette
ALL	Acute Lymphoblastic Leukaemia
AML	Acute Myeloid Leukaemia
APC	Allophycocyanin
BCR	Breakpoint Cluster Region
BSA	Bovine Serum Albumin
bp	Base pair
cDNA	Complementary Deoxyribonucleic Acid
CFC	Colony forming cell
CFSE	Carboxyfluorescein diacetate succinimidyl ester
ChIP	Chromatin Immunoprecipitation
ChIP-seq	Chromatin Immunoprecipitation followed by massively parallel sequencing
CML	Chronic Myeloid Leukaemia
CMML	Chronic Myeloonocytic Leukaemia
Cy5	Cyanine 5
Cy5.5	Cyanine 5.5
Cy7	Cyanine 7
Da	Dalton
DAPI	4',6-diamidino-2-phenylindole
ddH_2O	Double distilled water
DMEM	Dulbecco's Modified Eagle Medium
DMSO	Dimethyl sulfoxide
DNA	Deoxyribonucleic Acid
DNMT	DNA methyltransferase
dNTP	Deoxyribonucleoside triphosphate

EDTA	Ethylenediaminetetraacetic acid
EPO	Erythropoietin
ESC	Embryonic Stem Cell
FACS	Fluorescence Activated Cell Sorting
FBS	Fetal Bovine Serum
FITC	Fluorescein isothiocyanate
FSC	Forward scatter
g	gram
GSEA	Gene Set Enrichment Analysis
GMP	Granulocyte Macrophage Progenitor
H3K27ac	Acetylation of lysine 27 on histone H3
HDAC	Histone deacetylase
HDACi	Histone deacetylase inhibitor
HEK	Human embryonic kidney
HEPES	4-(2-hydroxyethyl)-1-piperazineethanesulfonic acid
HPLC	High Performance Liquid Chromatography
HSC	Haematopoietic Stem Cell
HSPC	Haematopoietic Stem and Progenitor Cell
IGV	Integrative Genomics Viewer
IL-3	Interleukin 3
IL-6	Interleukin 6
IP	Intraperitoneal
IRES	Internal Ribosome Entry Site
kb	kilobase
kg	kilogram
KAT	Lysine Acetyltransferase
KDM	Lysine Demethylase
KMT	Lysine Methyltransferase
LDA	Limit Dilution Analysis
L-GMP	Leukaemic Granulocyte Macrophage Progenitor
Lin	Lineage
LMPP	Lymphoid-primed multipotent progenitors
LPC	Leukaemia Progenitor Cells

LSC	Leukaemia Stem Cell
M	molar
mAU	mili-Anson unit
MBP	Methyl CpG binding protein
MDR	Multidrug resistance
MDS	Myelodysplastic Syndrome
mL	millilitre
MLL	Mixed Lineage Leukaemia
MLLfp	Mixed Lineage Leukaemia Fusion Protein
mm	millimetre
mM	millimolar
MPN	Myeloproliferative Neoplasm
MTD	Maximal tolerated dose
ng	nanogram
nm	nanometre
nM	nanomolar
NSG	Nod SCID gamma
OS	Overall Survival
PAFc	Polymerase-associated factor complex
PBS	Phosphate Buffered Saline
PcG	Polycomb group
PCR	Polymerase Chain Reaction
PDX	Patient Derived Xenograft
PerCP	Peridinin Chlorophyll
PHD	Plant Homeo Domain
PI	Propidium iodide
PVDF	Polyvinylidene Fluoride
PRC	Polycomb Repressive Complex
PRMT	Protein arginine methyltransferases
PTEFb	Positive Transcription Elongation Factor b
qRT-PCR	Quantitative Real-Time Polymerase Chain Reaction
RBC	Red Blood Cell
RNA	Ribonucleic Acid

RNAi	Ribonucleic Acid Interference
RNA-seq	Ribonucleic Acid Sequencing
rpm	Revolutions per minute
RPMI	Roswell Park Memorial Institute
shRNA	Short Hairpin Ribonucleic Acid
SAM	S-adenosyl methionine
SCF	Stem Cell Factor
SDS	Sodium Dodecyl Sulfate
SDS-PAGE	Sodium Dodecyl Sulfate - Polyacrylamide Gel Electrophoresis
SEC	Super Elongation Complex
SNP	Single Nucleotide Polymorphism
SSC	Side scatter
TKI	Tyrosine Kinase Inhibitor
TSS	Transcription Start Site
U	units
μg	microgram
μL	microlitre
μM	micromolar
μm	micrometre
V	volt
v/v	volume/volume
WT-MLL	Wild Type Mixed Lineage Leukaemia
WB	Western Blot
WES	Whole exome sequencing
w/v	weight/volume
YFP	Yellow Fluorescent Protein

Chapter 1 - Introduction

1.1 The role of epigenetic mechanisms of disease in malignancy

Our expanding knowledge of the genome and epigenome in cancer cells has highlighted the central role that aberrant regulation of the chromatin interface plays in the pathogenesis of many malignancies. The unparalleled view of the epigenetic landscape provided by the advent and application of next generation genomic technologies has afforded us the opportunity to gain significant insights into key pathways and nodes of chromatin regulation in both normal and malignant contexts. In particular, recurrent somatic alterations in the haematological malignancies of key proteins involved in DNA methylation, post-translational histone modification and chromatin remodelling underline the importance of epigenetic regulation in the initiation, maintenance and progression of cancer.[1-4]

In each mammalian cell, approximately 2 m of DNA is packaged as chromatin in a nucleus which is less than 10 μm wide. Approximately 146 bp of DNA is wound around a protein core consisting of an octamer of histone proteins (two copies each of H2A, H2B, H3 and H4) to form the basic functional unit of chromatin, the nucleosome.[5,6] Tight regulation of the chromatin environment is essential to facilitate the normal progression of essential DNA templated processes such as transcription, replication and repair. The dynamic regulation of the chromatin environment involves a complex interplay of multiple regulatory proteins which do not function in isolation, but as components of multi-subunit protein complexes, the functional integrity of which are critical to exert their respective regulatory roles.[7]

It is not surprising that disruptions to the tightly co-ordinated chromatin environment can lead to the gain of autonomous abilities which are the hallmarks of cancer.[8] However, the plasticity of the epigenome affords an opportunity for therapeutic manipulation through small molecule approaches. A number of potentially viable compounds that modulate the activities of various proteins which control the epigenetic landscape are in active development.[7,9]

Ultimately, the development and rational use of therapies directed against epigenetic targets requires a thorough understanding of the underlying mechanisms of malignant transformation driven by aberrant epigenetic regulators. This understanding will enhance our ability to deliver effective novel compounds to clinical practice. An overview of the major protagonists in epigenetic regulation, their aberrant role in the haematological malignancies focussing on myeloid malignancies, prognostic significance and potential for therapeutic targeting is presented below.

1.1.1 DNA methylation

The regulation and maintenance of DNA methylation is essential for appropriate embryonic development, cellular differentiation and genome stability.[10] In eukaryotes, the family of enzymes known as DNA methyltransferases (DNMTs) catalyse the addition of a methyl group to the five-carbon position of cytosine bases in CpG dinucleotides, yielding 5-methylcytosine (5mC).

DNA methylation has traditionally been thought to mediate transcriptional silencing and the formation of repressive chromatin states in addition to maintaining gene expression patterns through mitotic cell division. These functions are achieved through mechanisms which include the direct obstruction of transcriptional activators from their cognate promoters and the recognition of 5mC and consequent recruitment of co-repressor complexes by methyl CpG binding proteins (MBP).

Although aberrant hypermethylation and silencing of tumour suppressor genes has been found in almost all forms of cancer, tumorigenesis can result from both hypomethylation and hypermethylation of promoter CpG islands adversely affecting the expression of protein coding genes and non-coding RNAs.[11,12] These changes are disease specific with distinctive methylation patterns able to distinguish between hematologic malignancies and even subtypes of these malignancies.[13,14]

The establishment and maintenance of DNA methylation is mediated by three main DNMT enzymes. DNMT1, a maintenance methyltrasferase, recognizes hemimethylated CpG sites and restores symmetry to newly synthesized nucleotides following DNA replication.[15] Whilst also capable of maintenance,[16] DNMT3A and DMNT3B function primarily in de novo methylation during embryogenesis.[17] Of key interest in the

myeloid malignancies is the identification of recurrent somatic mutations in DNMT3A in acute myeloid leukaemia (AML).

Aberrant regulation of DNA methylation in the myeloid malignancies

High throughput DNA sequencing techniques have identified recurrent DNMT3A mutations in approximately 20% of patients with AML.[18-20] DNMT3A mutations are enriched in cytogenetically normal, intermediate risk AML and commonly co-occur with mutations in Fms-Related Tyrosine Kinase 3 (FLT3), Nucleophosmin 1 (NPM1) and isocitrate dehydrogenase (IDH) 1/2.[21] DNMT3A mutations have also been identified in patients with myelodysplastic syndromes (MDS)[22] and myeloproliferative neoplasms (MPN),[23] and are associated with increased likelihood of progression to AML. Intriguingly, DNMT3A mutations are also frequently found in patients demonstrating clonal haematopoiesis well before the development of overt malignancy.[24] Indeed, in some studies, the same DNMT3A mutation as the antecedent hematologic disorder is identified in secondary AML, suggesting that these mutations may be an early event in malignant clonal evolution.[25]

Somatic mutations cause premature truncation of the protein or affect a single amino acid, R882, resulting in attenuation of enzymatic activity. Heterozygous mutations predominate with R882 DNMT3A mutations exerting a dominant negative effect through inhibition of DNMT3A oligomerisation.[26-28] The role of DNMT3A as an early event in malignant evolution is highlighted by the demonstration of DNMT3A loss in hematopoietic stem cells leading to a block in differentiation and an expansion of the stem cell pool without overt leukaemia in murine models.[29] These haematopoietic stem cells (HSC) have a competitive multi-lineage repopulation advantage over wild-type HSCs, and furthermore, are demonstrated to persist following chemotherapy thereby acting as a reservoir for therapeutic resistance.[30] However, the role of DNMT3A in malignant transformation is yet to be fully elucidated. Analysis of global methylation levels by liquid chromatography-tandem mass spectrometry (LC-MS) does not demonstrate a significant difference in DNMT3A mutant leukemic cells. Furthermore, although differential methylation of key promoter CpG islands is observed, there is a lack of correlation between methylation changes and differential gene expression.[18,20]

Although DNMT3A mutations are associated with poorer outcomes in AML, modulation of this association through tailoring of conventional chemotherapeutic

regimens with the addition of high-dose daunorubicin results in improvement of overall survival (OS).[3,31,32] The impact of DNMT3A mutations in AML on sensitivity to hypomethylating agents is unclear. Retrospective examination of small therapeutic cohorts suggesting that hypomethylating agents abrogate the negative impact of DNMT3A mutations[33,34] but further investigation in prospective clinical trials is warranted.[23,24]

Therapeutic targeting of DNA methylation

Emerging therapeutic strategies targeting epigenetic mechanisms of disease have shown significant promise with the establishment of DNMT inhibitors as a cornerstone of management in MDS.[35-37] DNMT inhibitors such as 5-azacitadine and 5-aza-2'-deoxycytidine are nucleoside analogues that covalently trap DNMT1 following incorporation into DNA resulting in genome-wide hypomethylation through passive dilution of 5mC.

The hypomethylating effects of these agents are at non-cytotoxic dose ranges limiting the severity of side effects. Interestingly, the effectiveness of these agents is not reliant in attaining a complete remission, with improved survival, transfusion independence and reduced hospitalization observed despite persistent disease.[38] Further development of the treatment paradigm has suggested that less toxic regimens (lower doses with more frequent dosing) and the use of maintenance DMNT inhibitors as adjunct therapy or in combination with other novel therapies such as lenalidomide may be effective in subsets of patients with high-risk MDS/AML.[39-41]

DNA demethylation pathways, α-ketoglutarate and the link between metabolism and disordered epigenetic regulation

Although DNA methylation was initially believed to be a relatively stable DNA modification, genome-wide high resolution mapping of 5mC during cellular differentiation and the recent identification of the Ten-Eleven-Translocation (TET) enzymes has revealed a more dynamic state of affairs.[42-44] The three TET enzymes (TET1-3) are α-ketoglutarate (α-KG) and Fe2+-dependent dioxygenase enzymes, which catalyse the successive oxidation of 5mC to 5-hydroxymethylcytosine (5hmC), 5-formylcytosine (5fC) and 5-carboxycytosine.[43-46]

Although the exact function of the 5mC derivatives is yet to be fully established, it is evident that they play an important role in transcriptional regulation. They have been shown to alter DNA confirmation, act as essential intermediates in both active and passive DNA demethylation, modulate the binding and recruitment of chromatin regulators including the polycomb repressive complexes (PRC), and are involved in the reversal of transcriptional silencing.[47,48] Additionally, mapping of 5hmC and 5fC in mouse embryonic stem cells has highlighted its role in the establishment and maintenance of pluripotency through context-dependent promoter hypomethylation of pluripotency factors or modulation of PRC recruitment.[49]

Mutations of TET2 in myeloid malignancies were first described in MDS and MPN through single nucleotide polymorphism (SNP) arrays identifying a minimally deleted region on chromosome 4q24.[50,51] Subsequently, TET2 has been shown to be mutated in myeloid malignancies including AML, MDS and MPN with a high proportion of patients with MDS and chronic myelomonocytic leukaemia (CMML) harbouring mutations.[52,53] In MDS, TET2 mutations have been demonstrated to act as a biomarker for response to hypomethylating agents.[2,54,55] In AML, TET2 mutations are enriched in patients presenting with a normal karyotype and is associated with poorer OS.[53] Likewise, in CMML TET2 mutations are associated with poorer OS but they are not predictive regarding clinical outcome in MPN.[52,56]

Recurrent somatic mutation of the cytosolic enzyme IDH1, or its mitochondrial homolog IDH2, have been identified in approximately 20% of AML genomes and less commonly in other hematologic malignancies.[1,57] These abnormalities, in a core cellular metabolic pathway, are associated with specific epigenetic signatures.[58] IDH1 and IDH2 normally catalyse the conversion of isocitrate to α-KG. However, the most common *IDH1* (R132) and *IDH2* (R140, R172) mutations result in acquisition of neomorphic enzymatic activity that generates high intracellular concentrations of the aberrant oncometabolite 2-hydroxyglutate (2-HG).[59,60] 2-HG, a structural analogue of α-KG, results in competitive inhibition of Fe2+ and α-KG dependent demethylases including the TET enzymes and JmjC-domain containing lysine demethylases (KDMs).[61] Inhibition results in aberrant DNA and histone methylation, altered gene expression and impaired lineage specific differentiation.[61,62] Consistent with a common role in AML pathogenesis, *IDH1/2* and *TET2* mutations are mutually exclusive but associated with overlapping specific hypermethylation signatures.[58] Mice expressing the *IDH2*

mutations demonstrate an expansion of hematopoietic stem and progenitor cells. Interestingly, these models were also used to show co-operation with clinically relevant mutations such as *FLT3-ITD* in the development of AML.[63,64]

The overall effect of *IDH1/2* mutations on clinical outcome in AML is still unclear, as the prognostic impact appears to be dependent on the mutant allele present in the context of other co-existing molecular abnormalities.[65-69] In particular, *IDH1/2* mutations are demonstrated to modulate the outcome of patients defined as molecular low-risk (*NPM1*-mutant/*FLT3-ITD* negative) where *IDH1-R132* and *IDH2-R172* mutant alleles are associated with impaired outcome and *IDH2-R140* mutations are associated with favourable outcomes. Recently, a number of novel small molecule inhibitors targeting the aberrant gain-of-function consequent to mutant IDH alleles have demonstrated promising specific *in vitro* potency through induction of differentiation and apoptosis in IDH mutant leukaemia cell lines.[70,71] This has led to the initiation of early phase clinical trials targeting specific IDH1/2 mutants with early reports presented in abstract form showing promising outcomes in relapsed/refractory AML as a single agent.[72]

1.1.2 Histone modifications

Post-translational modification of histone tails by chromatin modifying enzymes has significant impact on intra- and inter-nucleosomal interactions. A considerable number of histone residues can be modified and the diversity of modifications result in complex, orchestrated chromatin environments that are dynamically regulated in specific cellular contexts. Post-translational histone modifications not only have the ability to regulate the binding of effector molecules essential to DNA processes including transcription, repair and replication, but also the ability to regulate higher order chromatin structure and stability.[73] Unsurprisingly, derangement of these modifications and the enzymes involved in their addition, removal and recognition features strongly during malignant transformation.

Chromatin modifying enzymes are often found in multi-protein complexes, which serve to modulate substrate specificity, enzyme activity and recruitment to target loci. Further layers of complexity and control are introduced through crosstalk between different histone and DNA modifications. In this situation, one modification may influence the

deposition, removal or interpretation of another chromatin modification on a separate site. This may occur through the obstruction of binding to target substrates by the presence of an adjacent modification, competitive antagonism of modification pathways for the same substrate, dependence of a chromatin-modifying enzyme on the presence of another modification, or co-operation between modifications to recruit specific factors.[74]

Critical protein-protein interactions and essential co-factors for enzymatic activity have been identified as viable therapeutic targets and demonstrate significant promise in the treatment of malignancies arising from abnormalities in epigenetic regulation.[75] Although much progress has been made in demystifying the 'epigenetic landscape', the mechanisms by which histone modifications and chromatin modifying enzymes exert their influence remains to be fully elucidated. A summary of key histone modifications and the chromatin-modifying enzymes deranged in the haematological malignancies responsible for writing, reading and erasing them is presented below (Figure 1).

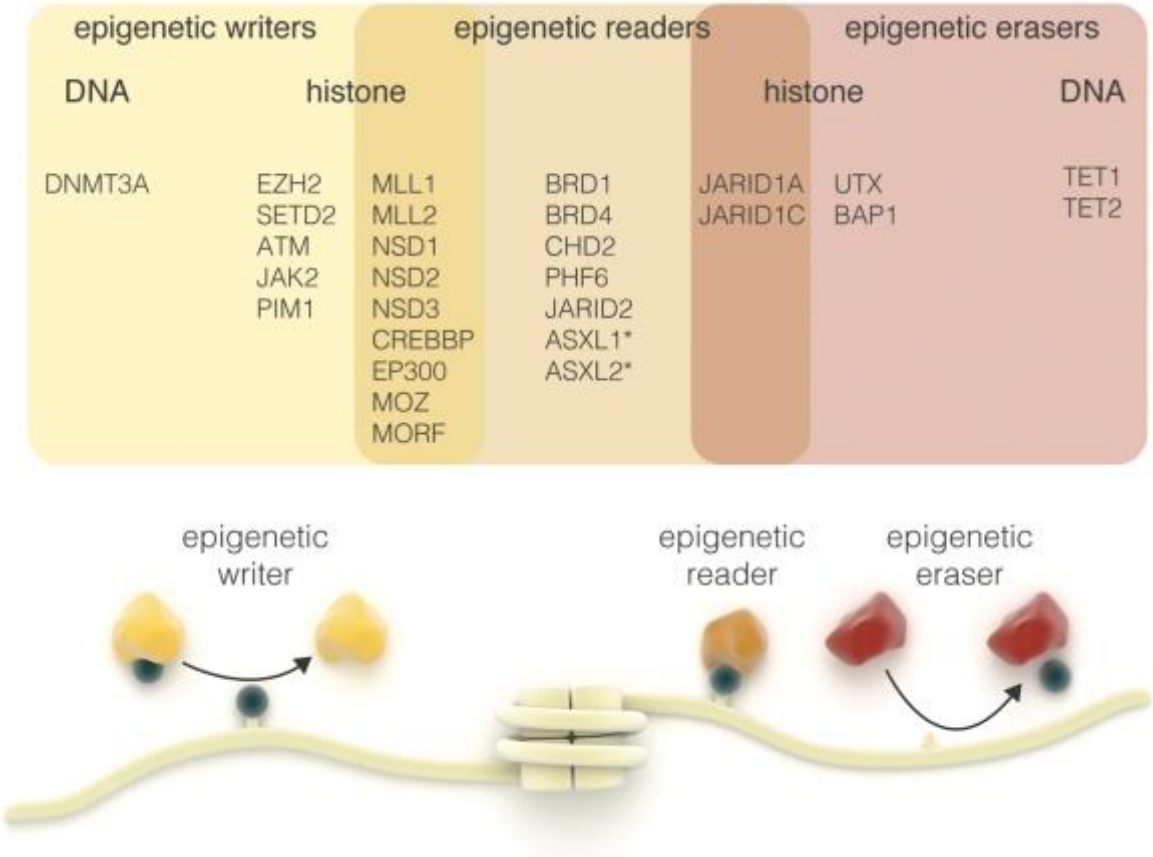

Figure 1 – Epigenetic writers, readers and erasers mutated or translocated in the haematological malignancies.

*Epigenetic writers catalyse the addition of chemical modifications to amino acids on histones and the cytosine base of DNA. Epigenetic erasers catalyse the removal of these modifications and epigenetic readers recognize these modifications and recruit larger macromolecular complexes to chromatin. A number of epigenetic writer and erasers also have domains that allow them to function as epigenetic readers (highlighted in the overlap shaded areas). *ASXL1 and ASXL2 have a PHD domain that may allow them to function as epigenetic readers; however, there is still no conclusive evidence for this.*

Acetylation

Histone acetylation, one of the best studied histone modifications, is dynamically controlled by two opposing families of enzymes: lysine acetyltransferases (KATs) and histone deacetylases (HDACs).[76]

The catalytic activity of KATs result in transfer of an acetyl group from the common co-factor acetyl CoA to the ε-amino group of lysine side chains in histones.[77] Consequent neutralisation of the positive charge weakens interactions between histones and negatively-charged DNA. This results in open chromatin conformations thereby facilitating access of chromatin associated proteins and is functionally consistent with the identification of KATs as transcriptional co-activators. KATs are subdivided on the basis of intracellular localization into predominantly nuclear (type A) or cytoplasmic (type B) subtypes. Enzymes found in the CBP/p300, MYST and GNAT families are type A KATs.

Recurrent mutations in CBP and p300 are noted in a range of hematologic malignancies, especially the lymphoid neoplasms.[78,79] Similarly, chromosomal translocations involving KATs (e.g. *MLL-CBP*[80,81] and *MOZ-TIF2*[82]) are found in myeloid malignancies. In particular, the KAT domain and bromodomain of CBP were demonstrated to be essential for leukemic transformation following an initial myeloproliferative phase in murine models of MLL-CBP leukaemia.[83] Similarly, the MOZ-TIF2 fusion protein is sufficient for leukemic transformation through its ability to bind nucleosomes and recruit CBP to aberrant sites, resulting in the activation of a self-renewal program and the acquisition of stem cell properties.[84,85]

The acetyltransferase activity of KATs is not limited to histone substrates and can regulate protein-protein interactions and the activity of target non-histone proteins. For example, acetylation of the leukemic fusion protein AML1- ETO by KAT3B (p300) has been demonstrated to be essential for conferring self-renewal ability and leukemogenicity. Pharmacological inhibition of KAT3B leads to improved survival in a murine AML1-ETO model.[86]

In general, therapeutic targeting of KATs has thus far been hampered by their low substrate specificity and broad involvement in multi-protein complexes that define their molecular activity. However, recent structure based *in silico* approaches have identified

a commercially available, specific, small molecule p300/CBP inhibitor, C646.[87] C646 resulted in selective *in vitro* inhibition of primary human AML bearing the AML1-ETO translocation through induction of cell cycle arrest and apoptosis and has further been demonstrated to be effective across a broader range of AML subtypes. This was associated with a dose-dependent reduction in global histone H3 acetylation, decreased expression of c-kit and bcl-2 and gene expression changes consistent with modulation of genes associated with genome integrity.[88,89]

HDACs reverse lysine acetylation restoring the positive charge and, consistent with their predominant role as transcriptional repressors, result in the stabilization of local chromatin architecture.[90] Eighteen human iso-enzymes of HDACs have been identified and are grouped into four classes on the basis of sequence homology. Similar to KATs, HDACs can target both histone and non-histone proteins with substrate specificity determined by the members of component protein complexes.[74]

Notably, recurrent mutations of HDAC's are not observed in cancer genomes yet HDAC inhibitors have broadly been trialled in a range of malignancies. This is primarily because they are aberrantly recruited by various oncoproteins to inappropriately initiate or maintain malignant gene expression programs. For instance, the leukemic fusion proteins PML-RARα and PZLF-RARα have been shown to recruit HDAC containing repressor complexes resulting in aberrant gene silencing.[91-94] In murine models of APML, the use of HDAC inhibitors (HDACi) is effective in potentiating or restoring the retinoid-induced differentiation of retinoic acid sensitive and resistant tumours resulting in improved survival.[95]

The efficacy of HDACi in the treatment of cutaneous T-cell lymphoma has been established. However, the broader application of this class of therapies in other hematologic malignancies is yet to be clinically proven.[90] HDACi pre-dominantly function by specifically blocking the entry of required co-factors to the active site.[96] A myriad of cellular responses, including modulation of pathways involved in cell cycle progression, differentiation, angiogenesis, immune function and apoptosis, result in malignant cell death. Although initially regarded as straightforward activators of transcription through direct histone hyperacetylation, a greater appreciation of the non-histone effects of HDACi on proteins such as p53 and key members of the proteasome/aggresome pathways, HSP90 and tubulin have emerged.[97] Indeed, recent mechanistic insight into the anti- leukemic activity of HDACi in t(8;21) AML

demonstrates the induction of terminal myeloid differentiation following HDACi mediated proteasomal degradation of the AML1/ETO9a fusion protein.[98]

Acetylation of lysine residues is primarily recognized by protein binding motifs named bromodomains. Over 40 bromodomain containing proteins in eight subfamilies with functionally diverse roles such as chromatin remodelling, post-translational histone modification and transcriptional co-activation have been identified. The activity of bromodomain containing proteins is not limited to histone targets with binding to non-histone targets such as the NF-κB subunit RelA and GATA1 described.[99,100] Whilst critical residues required for the recognition of acetylated lysines within the hydrophobic binding pocket of bromodomains are highly conserved, considerable variation of residues at the opening of the pocket allows for variability in the specificity of individual bromodomains. This also provides the opportunity to develop specific small molecule inhibitors targeting certain families of bromodomains.

For example, highly specific small molecule inhibitors targeting the protein-protein interactions of the Bromodomain and Extra Terminal (BET) proteins (BRD2, BRD3, BRD4 and BRDt) have emerged as promising therapeutic avenues in inflammation and cancer.[75,101,102] Further discussion of therapeutic targeting of the BET protein family is undertaken in section 1.3 found on page 45.

Methylation

Histone methylation occurs predominantly on lysine and arginine residues and is mediated by lysine methyltransferases (KMTs) and protein arginine methyltransferases (PRMTs).[103] Lysine residues can be mono-, di- or tri- methylated whereas arginine can be mono-, symmetrically or asymmetrically di-methylated. Histone methylation does not alter the charge on histone tails but influences the affinity of reader proteins to methylated residues. KMTs and PRMTs are highly substrate specific and transfer methyl groups from S-adenosyl methionine (SAM) to target amino acid residues.

The vast majority of KMTs contain a conserved SET catalytic domain, a sequence of approximately 130 amino acids initially characterized as a common motif in drosophila Suppressor of position-effect variegation [Su(var)], Enhancer of Zeste [E(z)] and Trithorax genes. The only exception is the catalytic domain of the H3K79 methyltransferase, KMT4/DOT1L (disruptor of telomeric silencing 1-like), which more closely resembles that of PRMTs. The degree of lysine modification is determined by

key residues within the SET domain.[104] In addition to the SET domain, KMTs have I-SET, pre-SET and post-SET domains which vary in sequence and are present in different combinations. These domains serve as a scaffold for substrate and co-factor interaction and determine substrate specificity.[105]

The functional impact of histone methylation is contextual and can lead to both transcriptional activation and repression. The best-characterized sites of histone lysine methylation include H3K4, H3K9, H3K27, H3K36, H3K79 and H4K20. These modifications are associated with both actively transcribed genes in euchromatin (H3K4, H3K36 and H3K79) and silenced genes in heterochromatin (H3K9, H3K27 and H4K20).[106] Adding to the complexity, the methylation state of individual histone residues also influences functional relevance. For example, monomethylation of H3K9 is associated with active transcription whereas trimethylation is associated with repression[106] and, whilst H3K4me2/3 is associated with transcriptional start sites (TSSs) of active genes,[107] H3K4me1 is associated with active enhancers.[108] Furthermore, although H3K79me has been predominantly associated with actively transcribed genes, the functional role of this modification in negative regulatory contexts has been described.[109]

Aberrant methyltransferase activity resulting in alterations to the location and amplitude of histone methylation can play a critical role in malignant transformation. Key examples in the haematological malignancies include abnormalities in the *MLL* and enhancer of zeste homolog 2 (*EZH2*) genes. Abnormalities in both result in the misappropriation of key components of gene regulatory machinery. See section 1.2 located on page 40 for a discussion of the role of MLL translocations in malignancy.

The role of the polycomb group proteins in haematological malignancy

Polycomb group (PcG) proteins are transcriptional repressors, which are crucial for the regulation of genes involved in cell fate decisions. Two distinct complexes, PRC1 and PRC2, work in concert to establish specific post-translational histone modifications resulting in the initiation and stable maintenance of transcriptional silencing. PRC2 consists of the core components EZH1/2, EED and SUZ12. EZH2, and the closely related EZH1, are H3K27 methyltransferases, which form the enzymatic core of PRC2. Subsequent recognition of H3K27 methylation by PRC1 occurs through component chromobox (Cbx) family members that target the complex to specific loci.[110] PRC1-

mediated H2AK119 ubiquitylation and chromatin compaction follows, resulting in transcriptional silencing.[111,112]

EZH2 is the most frequent PcG member implicated in the pathogenesis of malignancy. Enzymatic hyperactivity of EZH2 has been linked to aberrant repression of tumour suppressor genes in diverse cancers, including germinal centre B-cell lymphomas.[113,114] In particular, recurrent mono-allelic somatic mutations observed in lymphoma at Y641 of the SET domain confers enhanced catalytic activity and a preference for di- and tri-methylation of H3K27.[115] Selective small molecule inhibition of EZH2 is effective in inhibiting the proliferation of EZH2 mutant lymphoma cell lines and mouse xenografts.[116] A number of small molecule inhibitors of EZH2 have now commenced in early phase clinical trials with early results suggesting clinical activity.[117]

Intriguingly, loss of function mutations of *EZH2* predominate in myeloid malignancies.[118,119] Prognostically, these mutations portend a poorer OS in CMML, MDS and primary myelofibrosis.[2,120-122] The biological implications of inactivating *EZH2* mutations in haematopoiesis are unclear. Inactivating mutations of other core PRC2 components in myeloid malignancies are less common suggesting that EZH2 plays an important non-redundant role in haematopoiesis.[123,124] Nonetheless, the dichotomous role played by EZH2 as both an oncogene and tumour suppressor in the development of malignancies highlights the tissue specific role of H3K27 methylation.

Inactivating *ASXL1* mutations have also been linked to loss of PRC2 mediated H3K27 methylation.[125] Mutations have been identified in a wide range of myeloid malignancies, most commonly in patients with CMML, MDS or MPN, and are biomarkers of adverse outcome.[2,3,126] Although *ASX*, the orthologue of human *ASXL1* in *D. Melanogaster*, has been demonstrated to function as part of the polycomb-repressive deubiquitylase complex, no significant changes in H2AK119 ubiquitylation are observed in human ASXL1 mutant cells.[125,127] Instead, *ASXL1* mutations resulted in global decrease of H3K27 methylation and upregulation of transcriptionally poised genes normally bivalently marked with H3K27me3 and H3K4me3. This, coupled with identification of a direct interaction between ASXL1 and EZH2 through co-immunoprecipitation assays and the loss of EZH2 occupancy at *HOXA* genes highlight the specific role of ASXL1 in epigenetic regulation of gene expression by facilitating the recruitment/stabilization of PRC2 at target loci.[125]

Other PcG proteins that have also been demonstrated to play important roles in haematopoiesis are members of PRC1 and include the cbx family and BMI-1. Target selectivity of the PRC1 complex is dependent upon the sole constituent cbx family member. In HSCs, cbx family members cbx7 and cbx8 have been demonstrated to mediate the balance between self-renewal and differentiation through co-regulation of a set of common genes.[110] Cbx7 overexpression in murine models results in enhanced self-renewal and induction of leukaemia whereas cbx8 overexpression is associated with lineage commitment and HSC exhaustion. Similarly, BMI-1 is critical for both hematopoietic and leukemic stem cell self renewal.[128,129] It is an interchangeable subunit of PRC1 which is specifically expressed in immature hematopoietic cells and enhances the H2AK119 ubiquitin ligase activity of the core members, RING1A and RING1B.[130,131] Increased expression of *BMI-1* is associated with impaired survival in CML,[132] MDS[133] and AML[134] and may be a useful prognostic marker in myeloid malignancies.

Demethylation

Analogous to DNA methylation, the discovery of enzymes capable of reversing lysine methylation has highlighted the dynamic nature of histone modifications. Two classes of KDMs have been identified. Class one enzymes are amine oxidases consisting of only two members including the first identified KDM, lysine-specific demethylase 1 (LSD1) or KDM1A.[135] The second, more expansive class of KDMs, contain a Jumonji domain (JmjC) which functions as a Fe2+ and α-KG dependent dioxygenase.

Aberrant regulation of KDMs has been linked to malignant progression; however, compared to the extensively studied KMTs, very little is known about how histone demethylation results in abnormal gene expression patterns. *UTX/KDM6A* was the first mutated KDM to be linked to malignant transformation.[136] Deletions or loss-of-function point mutations occurring within the JmjC domain of *UTX* inactivate H3K27 demethylase activity and have been identified in a wide variety of cancers, including multiple myeloma and acute lymphoblastic leukaemia.[136,137] The development of specific UTX/JMJD3 inhibitors through rational, structure-guided and chemoproteomic approaches, has served to highlight the critical role of KDM6 family members as determinants of pro-inflammatory gene activation in macrophages.[138] However, the

potential application of these small molecule inhibitors as potential anti-cancer therapy is yet to be established.

Aberrant KDM activity has been demonstrated to play a key role in the facilitation of malignant gene expression in AML.[139,140] KDM1A/LSD1 (hereafter referred to as LSD1) has a dual role in normal cells as both a transcriptional activator and repressor through interactions with multiple protein complexes. The most well described role of LSD1 is in the removal of methyl groups from H3K4me2 and H3K4me1 resulting in repression of gene transcription which is further augmented through interactions with the repressor proteins or protein complexes such as HDAC1/2 and CoREST.[141] The role of LSD1 as a transcriptional activator has been demonstrated in the regulation of androgen receptor dependent transcription through the demethylation of H3K9me2 and H3K9me1.[142]

High expression of LSD1 is observed in patients with AML[143] and is thought to perturb the balance between transcriptional activation and repression in the regulation of transcription normally modulated by LSD1.[144] In MLLfp models, LSD1 is required for leukaemia stem cell function with pharmacological inhibition resulting in induction of differentiation and loss of colony forming ability in both murine and primary human MLL-FP cells.[139] In cell line models of other subtypes of AML, pharmacological inhibition of LSD1 in combination with ATRA results in reactivation of ATRA-dependent differentiation pathways.[140] These effects were associated with gene-specific, selective increases in H3K4me2 and were respectively associated with downregulation of genes bound by MLLfp and upregulation of genes associated with myeloid differentiation and highlight the potential role of LSD1 inhibition as a therapeutic strategy.

Methyl-binding proteins and readers of histone methylation

More distinct recognition motifs are able to recognize lysine methylation than any other modification and are broadly divided into two families, the Royal Family [Tudor domains, chromo domains and malignant brain tumour (MBT) domains] and plant homeo domain (PHD) fingers. Akin to abnormalities in methyl-lysine writers and erasers, aberrant function of methyl-lysine readers are causally linked to the pathogenesis of hematologic malignancy.

For example, leukemogenesis of a subset of NUP98 translocated AML is dependent on the retained function of H3K4me3 reader PHD finger located in the C-terminal portion of translocation partners JARID1A and PHF23. The aberrant function of these fusion proteins results in upregulation of many critical oncogenes such as *HOXA9* and *MEIS1* through the blockade of PcG-mediated H3K27me3 deposition.[145] Although functional compensation through the substitution of other PHD fingers is possible, these recognition motifs specifically require H3K4me3 binding ability. The specificity of this protein-protein interaction resulting in malignant transformation makes methyl-lysine readers an attractive therapeutic target.

Phosphorylation

Kinases and phosphatases control the addition and removal of phosphate groups on serine, threonine and tyrosine residues of component histone proteins. Transfer of a phosphate group from ATP to the hydroxyl group of target amino acids results in the addition of a significant negative charge. Histone phosphorylation results in gross changes in chromatin structure and has been implicated in the regulation of gene transcription, DNA repair and chromatin condensation.

Aberrant kinase activity is one of the most commonly observed processes in malignant transformation.[8] Whilst attention has focused upon the cytoplasmic role of these master regulators of intracellular signal transduction, it has recently been recognized that some kinases may also have critical nuclear functions including histone phosphorylation.[146]

Constitutive activation of JAK2, a non-receptor tyrosine kinase crucial for cytokine signalling in normal haematopoiesis, commonly occurs in MPN. JAK2 is demonstrated to specifically phosphorylate H3Y41 within the nucleus, resulting in the exclusion of transcriptional repressor HP1α from chromatin and the activation of hematopoietic oncogenes such as *LMO2*.[147] Jak2 nuclear activity is closely correlated with levels of H3Y41ph. Interestingly, genomic profiling of H3Y41ph demonstrates that only a small subset of genes are uniquely heavily blanketed with this histone modification.[148] Several genes marked with H3Y41ph are also bound by members of the STAT family suggesting that the functional interaction with JAK kinases and STAT family members may not be confined to the cytoplasm but may extend all the way to chromatin.

Aberrant JAK2 function also has indirect effects at chromatin. The most common mutation, JAK2 V617F, interacts with PRMT5 in the cytoplasm and nucleus of

hematopoietic cells. This interaction results in a novel gain of function whereby JAK2 phosphorylates PRMT5.[149] Abrogation of histone methyltransferase activity ensues with global decrease of H2/H4 R3 methylation and altered gene expression. Inhibition of PRMT5 activity results in promotion of progenitor cell proliferation and erythrocytosis.

The identification of multiple pathogenic consequences of aberrant signalling kinase activity at chromatin broadens the therapeutic scope of kinase inhibitors currently in clinical development. Several kinase inhibitors result in global reduction of histone modification laid down by target enzymes (e.g. JAK2 and Aurora kinase inhibitors) and thus can be considered as potential epigenetic therapies.

1.2 MLL leukaemias as a model of disordered epigenetic regulation

Wild-type MLL (WT-MLL) plays an integral role in normal embryogenesis and haematopoiesis.[150] It is a 430 kDa protein post-translationally cleaved by taspase-1 into N-terminal and C-terminal fragments that subsequently re-associate to form the MLL complex.[151] The C-terminal fragment contains a SET domain which methylates H3K4. WT-MLL also has 3 HMG-like AT hooks and a DNMT1-like CxxC domain which bind DNA; whilst four PHD fingers, a bromodomain, host cell factor binding motif and transactivation domain mediate interactions with several protein complexes (Figure 2). The recruitment and stabilization of WT-MLL to target genes is mediated by these interactions.

Translocations involving this essential epigenetic regulator account for the vast majority of infantile and approximately 10% of adult leukaemias.[152] Resultant leukaemias may be characterized as AML, acute lymphoblastic leukaemia (ALL) or bi-phenotypic leukaemias. MLL leukaemias follow an aggressive clinical course with poor response to conventional chemotherapy and frequent early relapse.

The aberrant gene expression signatures in MLL leukaemias result from the abnormal stabilisation of MLLfp at malignant target genes through the acquisition of new interactions with various protein complexes. The breakpoint cluster region (BCR) in virtually all *MLL* translocations is located between the CxxC domain and the PHD fingers resulting in fusion proteins which lack the SET domain.[153] More than 70 MLL translocation partners have been identified, many of which are members of multi-subunit protein complexes that alter the structure and function of chromatin.[154] The 5 most common MLL fusion partners (*AFF1/AF4*, *MLLT3/AF9*, *MLLT1/ENL*, *MLLT10/AF10* and *ELL*, accounting for approx. 80% of MLL rearrangements) are components of the super elongation complex (SEC) or DOT1L complex (Figure 2). These complexes, in association with the polymerase-associated factor complex (PAFc), play a central role in the regulation of transcriptional elongation.[155,156]

The functional integrity of the SEC and DOT1Lc are critical for MLLfp mediated malignant transformation and offers a rational target for epigenetic therapies with compounds directed against various components of these complexes.[7,9] In addition to

the therapeutic targeting of BET proteins (described in detail in section 1.3 found on page 45), attention has focused upon targeting KMT4 (DOT1L) and the menin-MLL interaction.[157,158]

The direct or indirect recruitment of KMT4 (DOT1L) is frequently linked with leukemogenic *MLL* translocations.[159-162] DOT1L, the only human H3K79 methyltransferase, plays a central role in normal haematopoiesis[163-165] and has been reported to be involved in a variety of cellular processes including telomeric silencing, cell cycle progression, DNA repair and replication and transcriptional control.[156] Much of the emphasis in studying the role of DOT1L in leukaemia has centred on understanding the transcriptional programs controlled by this methyltransferase. Misdirected H3K79 methylation has been shown to sustain the expression of key pro-leukemic genes such as the *HOXA* genes and *MEIS1*.[166,167] Moreover, the disruption of DOT1L function by genetic means or a selective small molecule inhibitor blocks cellular H3K79 methylation, abrogates malignant gene expression signatures and has *in vivo* efficacy in MLL xenograft models.[157,168] This pre-clinical data has led to the initiation of early phase clinical trials with DOT1L inhibitors.[169]

The rationale for targeting multiple components of putative MLLfp complexes for synergistic therapeutic effect has been bolstered by the establishment of the presence of pharmacological targets BRD4 and DOT1L in independent protein complexes.[170] BRD4 and its associated positive transcription elongation factor b complex (PTEFb) [composed of cyclin T1, cyclin T2 and cyclin-dependent kinase 9 (CDK9)] were demonstrated, by quantitative mass spectrometry of immunoprecipitated native protein complexes and size exclusion chromatography of nuclear fractions, to exist in distinct macromolecular complexes to DOT1L. Functional interdependence of BRD4 and DOT1L, particularly at genes regulated by superenhancers, was shown to occur through H3K79me mediated regulation of chromatin accessibility to transcription factor complexes including the H4 acetyltransferase, EP300. Subsequent recognition of H4K5ac by BRD4 and binding of associated protein complexes facilitated transcription of target genes. Pharmacological and genetic inhibition of both BRD4 and DOT1L resulted in synergistic efficacy against MLLfp leukaemia *in vitro* and *in vivo* thereby demonstrating the possibility of successful combination epigenetic targeted therapy approaches directed against independent, parallel transcriptional regulatory pathways.[170] These findings highlight that sound understanding of underlying molecular mechanisms

can improve the utility and mitigate concerns of potential antagonism of combination therapy approaches.

Other therapeutic avenues currently being explored in MLLfp leukaemia includes the disruption of the menin-MLL interaction.[158] Menin, which directly binds the N-terminal fragment of MLL retained in all MLLfp, is an essential oncogenic co-factor required for the leukemogenic activity of MLLfp.[171,172] Novel small molecules identified using high throughput screening and structure-based design has led to a refinement of selectivity in targeting critical residues in the large binding site. Interruption of the menin-MLL interaction results in selective induction of apoptosis and differentiation, a block in proliferation and reversal of malignant gene expression signatures in cell lines bearing MLLfp.[158,173] Finally, whilst a selective inhibitor to the catalytic activity of MLL1 has been developed,[174] the role of the SET domain of wild-type MLL1 in the initiation and maintenance of leukaemia is not fully resolved.[175]

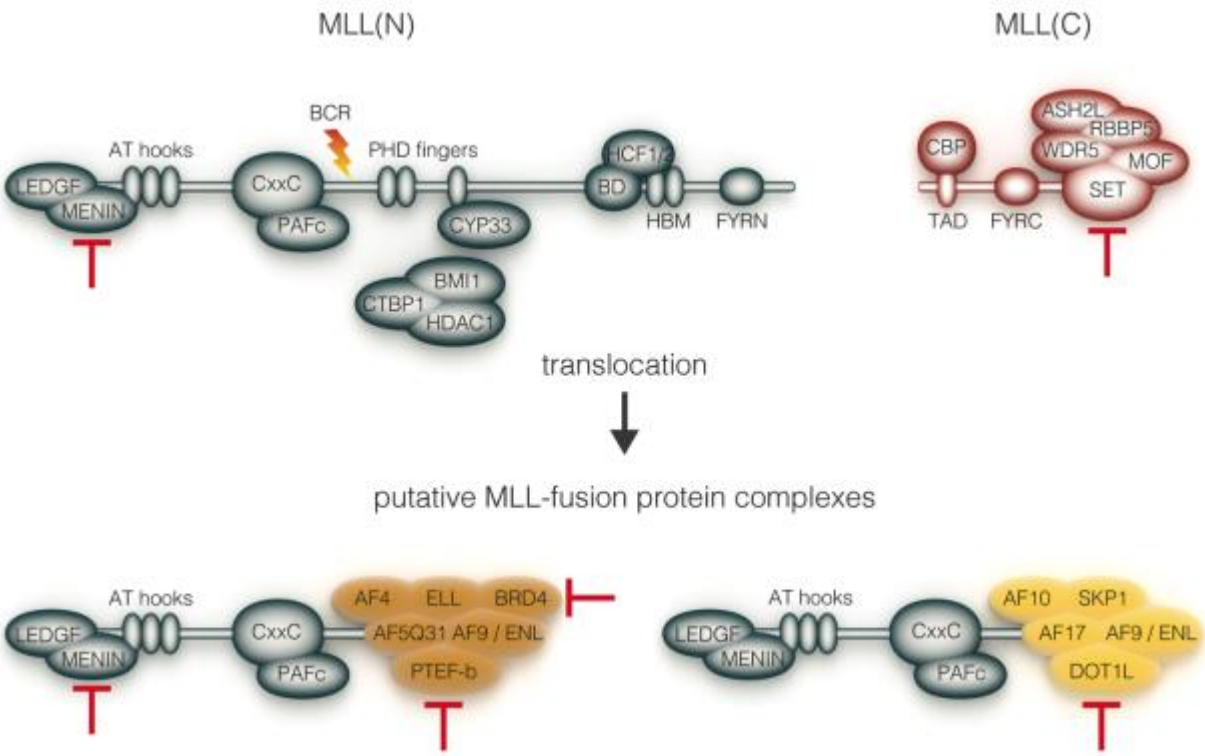

Figure 2 – MLLfp as targets for small molecule inhibition.

Schematic diagram of wild-type MLL illustrating the various specialized domains and the protein-protein interactions mediated by them. Also illustrated are the purported MLL-fusion protein complexes. Following translocation, a fragment of the N-terminal portion of MLL is fused in frame with translocation partners leading to the formation of novel MLL-fusion protein complexes including the SEC and DOT1L complex. Highlighted in red inhibitory arrows are key components, essential to the leukaemogenic capacity of wild-type MLL or MLL-fusion proteins, against which targeted small molecules have been developed. These include the Menin-MLL interaction, SET domain inhibitors, BET inhibitors targeting BRD4, PTEF-b/CDK9 inhibitors and DOT1L inhibitors. HBM: host cell factor binding motif; TAD: transactivation domain.

1.2.1 Murine models of MLLfp driven leukaemias

One of the best characterised models of epigenetic dysregulation in leukaemia utilises retroviral transduction of MLLfp into primary murine haematopoietic stem and progenitor cells (HSPC). In particular, retroviral insertion of MLL-AF9 or MLL-ENL, the two most common MLLfp associated with AML,[154] are able to initiate leukaemia which faithfully mimics the human disease in a flexible murine model system.[176-178] Indeed, use of these retroviral models have lead to key cellular and molecular insights into leukaemogenesis.

Akin to the human disease, immunophenotypic analysis of murine cells following MLLfp insertion is consistent with the development of AML with the bulk tumour expressing markers of granulocyte/macrophage differentiation (Gr-1/CD11b).[176,177] These immortalised leukaemic cells can be maintained in indefinite *in vitro* cell culture. Unlike human cell lines, murine models generated through retroviral insertion have a relatively clean genetic background with few passenger mutations or structural rearrangements. Furthermore, robust development of AML from this potent oncogene *in vivo* following transplantation into syngeneic or immunodeficient hosts with moderate latency of disease allows for studies of novel compounds targeting AML in animals.

Importantly, these models have been used to dissect the immunophenotype, gene expression programs and functional properties of leukaemia stem cells (LSCs) through *in vitro* colony forming assays and *in vivo* modelling and are the best characterised model of the LSC hierarchy.[153] Seminal observations include the demonstration that leukaemogenic fusion proteins result in the activation of a subset of genes required for stem cell function and can transform not only HSC but also committed progenitors into LSC.[177-179] Although debate ensues regarding the precise immunophenotypic characteristics of the LSC compartment in MLLfp driven leukaemia; studies consistently identify cells with leukaemia initiating capacity downstream of the normal stem cell compartment with c-kit positive, granulocyte macrophage progenitor-like (GMP-like) cells at the apex of the LSC hierarchy.[176-178]

1.3 Targeting epigenetic reader proteins for therapeutic gain

Although interest in targeting components of the epigenetic machinery for therapeutic gain have initially been aimed at altering the catalytic activity of chromatin modifying enzymes, advances in medicinal chemistry have now made it possible to exploit protein-protein interactions at the chromatin interface.[9,101,102] The success of this approach is highlighted by the development of the BET inhibitors where promising pre-clinical data has translated to early phase clinical trial activity within three years of their initial description in malignant contexts.

BET proteins are a family of epigenetic reader proteins containing tandem N-terminus bromodomains and an extra-terminal domain at their C-terminus. The tandem bromodomains exhibit high levels of sequence conservation.[180] Ubiquitous expression of BRD2, BRD3 and BRD4 is observed, whereas BRDT expression is restricted to germ cells. Whilst BET proteins do not independently demonstrate enzymatic activity at chromatin, following bromodomain mediated localization to acetylated histones, the extra-terminal domain acts as a scaffold for the recruitment of general transcription factors or chromatin modifying enzymes. Indeed, determination of the complete BET protein interactome, utilizing a tripartite proteomic approach, prominently identifies components of core transcriptional regulatory machinery. Notably, this includes components of the PAFc and SEC which are critical to the pathogenesis of MLLfp mediated leukaemias.[75] Additionally, BET proteins are identified as integral components of nuclear protein complexes which play a role in DNA replication, chromatin remodelling and DNA damage response.

Pharmacological BET inhibition shows remarkable efficacy *in vitro* and *in vivo* against MLLfp leukaemia through rapid induction of cell cycle arrest and apoptosis.[75,181] BET inhibitors from two chemically distinct groups are under current development. I-BET151 (GSK2820151) is a highly specific and potent isoxazoloquinoline based BET inhibitor whereas JQ1 and I-BET762 (GSK525762), are novel benzodiazepine based BET inhibitors which demonstrate similar efficacy in pre-clinical studies (Figure 3).[75,101,102,181] Broader extension of pharmacological BET inhibition to other genetically distinct AML subgroups results in the identification of a core transcriptional program

including critical oncogenic targets such as *BCL2* and *C-MYC*. This suggests a role for BET proteins as a common terminal effector of malignant transcription and is supported by the efficacy of BET inhibition in NPM1c mutant leukaemia.[182]

Originally identified in the BET interactome, wild-type NPM1 is demonstrated to exert a repressive effect on BRD4 binding to target loci resulting in decreased transcription. Loss of inhibition resulting from mislocalisation of NPM1c, consequent to gain of an aberrant NPM1 nuclear export signal, results in release of BRD4 repression and activation of aberrant transcription.[182] Downregulation of the core transcriptional program underlies sensitivity to BET inhibition in AML and may serve as biomarkers of response to BET inhibitors. Interestingly, many of the genes identified are associated with super-enhancers, large enhancer regions containing high levels of BRD4 and mediator that are exquisitely sensitive to BET inhibition.[183]

The efficacy of BET inhibition has been replicated in a broad range of hematologic malignancies including multiple myeloma,[184] non-Hodgkin lymphoma[185] and ALL.[186] These serve as proof of principle for epigenetic targeted therapies directed against protein-protein interactions, and have formed the basis for the initiation of early phase clinical trials.

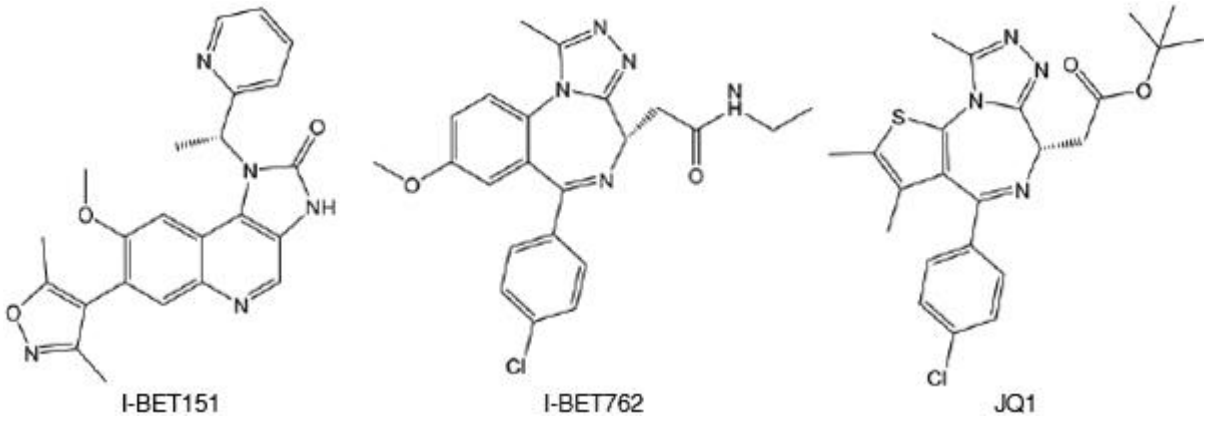

Figure 3 – Structural backbones of BET inhibitors in active development

Two chemically distinct families of BET inhibitors are under active development. The structure I-BET151 is based upon an isoxazoloquinoline backbone, whereas I-BET762 and JQ1 are based upon a benzodiazepine backbone.

1.3.1 BET inhibitor clinical trial outcomes

A number of BET inhibitor compounds are in active development in early phase clinical trials (Table 1.1).

Drug	Phase	Setting	Clinicaltrials.gov identifier
BMS-986158 (BMS)	I/II	Advanced solid tumours	NCT02419417
CPI-0610 (Constellation)	I	Progressive lymphoma	NCT01949883
	I	Acute Leukaemia, MDS, MDS/MPN and Myelofibrosis	NCT02158858
	I	Multiple Myeloma	NCT02157636
FT-1101 (Forma)	I	AML/MDS	NCT02543879
GSK525762 (GlaxoSmithKline)	I/II	Relapsed/refractory haematological malignancies	NCT01943851
	I/II	NUT midline carcinoma	NCT01587703
GSK2820151 (GlaxoSmithKline)	I	Advanced or Recurrent Solid Tumours	NCT02630251
INCB054329 (Incyte)	I/II	Advanced haematological and non-haematological malignancies	NCT02431260
INCB057643 (Incyte)	I/II	Advanced haematological and non-haematological malignancies	NCT02711137
MK-8628 (MSD)	I	Selected haematological malignancies	NCT02698189
	I	Advanced solid tumours	NCT02698176
OTX015 (OncoEthix)	I	Haematological malignancies	NCT01713582
	I	Advanced solid tumours	NCT02259114
TEN-010 (Tensha)	I	AML and MDS	NCT02308761
	I	Solid tumours	NCT01987362
ZEN003694 (Zenith)	I	Metastatic castration-resistant prostate cancer	NCT02705469

Table 1.1: Active BET inhibitor clinical trials

Preliminary results have been recently reported from studies utilising the BET inhibitor compound, OTX015, in acute leukaemia[187] and lymphoma or multiple myeloma[188]. In both phase I dose escalation studies, a recommended dose for oral single agent OTX015 therapy of 80 mg on a 14 days on, 7 days off schedule, has been established for phase II studies. In the non-leukaemia study, the most common grade 3-4 toxicities were haematological (thrombocytopenia, anaemia and neutropenia) with gastrointestinal events, elevated bilirubin and fatigue highlighted as dose limiting toxicities in both studies. Severe toxicities resolved rapidly after OTX015 cessation.

In the leukaemic cohort, patients with relapsed/refractory AML following at least two prior lines of therapy demonstrated clinical responses at a range of dose levels (40 mg to 160 mg daily, n = 41). These included complete remissions (CR, n = 2), complete remission with incomplete recovery of platelets (CRi, n = 1) and partial responses (PR, n = 2). Responses were short lived, with all five patients who demonstrated a response relapsing whilst on OTX015 treatment after two to five months. In these small cohorts, no predictive biomarkers for response were identified. In particular, no correlation was observed between genetic abnormalities and response (including patients with leukaemias harbouring MLL translocations). Unexpectedly, no change in expression was observed in bone marrow samples of seven oncogenes (*c-MYC*, *BCL2*, *CCND1*, *NF-κB*, *BRD2*, *BRD3*, and *BRD4*) however the authors have attributed this to collection and processing difficulties.

These findings are not dissimilar to other early phase clinical trials of single agent therapies in AML and serve to highlight the significant challenges in the management of these patients.[189] Although significant interest surrounds targeting epigenetic mechanisms of disease for therapeutic gain, a key controversy in the clinical use of epigenetic agents surrounds their effectiveness in the face of overwhelmingly rapidly progressive disease. Recognition of a requirement of time to effect disease control and delay to maximal response has prompted a re-evaluation of the role and timing of these agents. Therefore, further delineation of the determinants of response and resistance are essential to improving the clinical utility of these novel agents which have a strong scientific rationale and have demonstrated substantial pre-clinical efficacy. Key to this is identifying molecular mechanisms of resistance and the development of rational combination therapy approaches.

1.4 Drug resistance in cancer

The effectiveness of all cancer therapeutics is limited by the development of treatment resistance. Resistance, to both traditional cytotoxic agents and targeted therapies, may be intrinsic or acquired.[190] Intrinsic resistance arises from pre-existing tumour factors which render therapies ineffective from the outset, often acting as a guide to avoidance of futile therapies in varying tumour types. Of increased clinical relevance is the development of acquired resistance, where initially effective therapies lose their effectiveness. This distressing development leads to clinical progressive disease refractoriness or relapse. It is this situation which is the major cause of treatment failure and death in AML. Indeed, despite aggressive chemotherapeutic and immunological salvage therapies, disease relapse following initial remission portends extremely poor prognosis in AML with 5 year OS rates of 5 to 12% observed in multicentre Australian data.[191,192]

It is important to consider the complex interplay between factors mediating resistance at the level of an individual cancer cell and also the host environment. Mechanisms of acquired resistance in individual malignant cells include alterations in drug targets, drug influx/efflux and drug metabolism; blunted responses to DNA damage/repair pathways; activation of pro-survival or inhibition of pro-apoptotic pathways; and activation of downstream or alternative signalling pathways.[190,193] At the level of a whole organism, persistence of malignant cells in the face of therapy has been demonstrated to occur as a result of variations in systemic drug distribution thereby allowing tumours to avoid drug exposure through disease compartmentalisation. A prime example of this is the inability of some drugs to access privileged sites such as the central nervous system.[194] Additionally, host factors such as the absence of enzymatic machinery to convert pro-drug to active drug compounds, or the increased function of metabolic pathways which result in the inactivation of therapeutic compounds can impact the effectiveness of drug compounds.[195,196]

A key mediator of malignant cell adaptation to conventional chemotherapeutic agents is in the increased activity of ATP-binding cassette (ABC) transporter family members. This results in increased efflux of cytotoxic drugs, thus reducing intracellular drug concentrations below the effective chemotherapeutic level. ABC transporters are able to function upon multiple structurally and mechanistically unrelated chemotherapeutic

agents leading to the phenomenon of multidrug resistance (MDR). Indeed, the first described drug transporter, P-glycoprotein (ABCB1, MDR1) has been studied extensively and has been demonstrated to function upon a broad number of chemotherapeutic agents including taxanes, anthracyclines and vinca alkaloids.[197,198] Similarly, other members of this family, including MDR-associated protein 1 (MRP1; also known as ABCC1) and breast cancer resistance protein (BCRP; also known as ABCG2), have been demonstrated to play a role in cancer drug resistance. Collectively, they are capable of actively transporting a wide range of substrates in addition to chemotherapeutic agents including ions, sugars, amino acids, lipids and toxins.[199] Overexpression of ABC transporters is seen in many tumours resulting in intrinsic drug resistance and can be induced by chemotherapy.[190] Furthermore, ABC transporter activity has been demonstrated to protect cancer stem cells from chemotherapeutic agents.[200] Of note, molecular targeted therapies can also be substrates for ABC drug transporters.[201]

In contrast, drug inactivation or metabolism resulting in cancer cell resistance is highly drug class specific. For example, the rate limiting enzymatic step in the catabolism of the antimetabolite 5-fluorouracil (5-FU) is action of dihydropyrimidine dehydrogenase, overexpression of which confers resistance to 5-FU.[202] Similarly, increased expression or allosteric activation of cytidine deaminase has been demonstrated to play a role in the resistance of acute myeloid leukaemias to cytarabine arabinoside (ara-c).[203]

Despite initial promise, our clinical experiences with targeted therapies such as tyrosine kinase inhibitors in various solid and haematological malignancies have illustrated the problems resulting in acquired resistance to targeted therapies.[204-207] Whilst targeting oncogenic drivers with single agent therapies has proven to be highly efficacious it is seldom curative. Prominent examples include the identification of T315 BCR-ABL gatekeeper mutations following imatinib therapy in chronic myeloid leukaemia (CML) resulting in resistance through alteration of drug target[205]; amplification of MET resulting in 'oncogenic bypass' through activation of the alternative PI3K signalling pathway mediating resistance following EGFR inhibitor therapy in non small cell lung cancer[206]; and downstream activation of JAK-STAT signalling through heterodimerisation of JAK2 and JAK1 or TYK2 resulting in transphosphorylation and reactivation of JAK2 despite small molecule JAK2 kinase inhibition[204].

1.4.1 Overcoming resistance to cancer therapeutics

Various strategies have been developed to overcome or circumvent resistance to cancer therapeutics. These approaches have included designing second or third generation drugs to overcome alterations in drug targets; targeting parallel or downstream signalling pathways; and developing combination strategies targeting orthogonal oncogenic mechanisms.

The strategies utilised to overcome resistance to tyrosine kinase inhibitor (TKI) therapy in BCR-ABL driven malignancies highlights these approaches.[208] The third generation TKI, ponatinib, was developed utilising structure-based design to overcome the limitation of first and second generation TKIs requiring the formation of a hydrogen bond to T315 for high affinity binding. Ponatinib contains a carbon-carbon triple bond linkage which enforces correct positioning and productive hydrophobic contact with I315 to ensure kinase inhibition of the T315I BCR-ABL mutant.[209] This approach has been demonstrated to be effective in overcoming clinical resistance.[210] Additionally, rational combination therapy approaches, through parallel targeting of the auto-regulatory domain of ABL1 with a second small molecule, have been demonstrated to circumvent the development of resistance to TKIs in Philadelphia chromosome bearing malignancies.[211,212] This promising approach, where a small molecule compound functionally mimics the auto-regulatory role of the myristoylated N-terminus of ABL1 lost upon fusion with BCR, thereby restoring negative regulation of kinase activity, is now in early phase clinical trials (NCT02081378).

Appropriate temporal sequencing of drug combinations must be taken into account to circumvent the development of resistance and maximise the anti-tumour activity of combination approaches.[213] For example, taxane exposure induces an adaptive response in breast cancer cells through the activation of Src kinases. This induces a phenotypic change resulting in a chemotolerant state and the suppression of apoptosis. The development of Src kinase inhibitors provides promise in the form of rational combination therapies potentially overcoming taxane resistance. Indeed, the temporal sequencing of Src kinase inhibitors following taxane exposure results in sensitisation of taxane tolerant cells to chemotherapy. However, the same is not observed during concurrent exposure with persistent acquired resistance to taxanes observed. Therefore,

in this setting, only the appropriate temporal sequencing of anticancer drugs is able to overcome adaptive resistance.[214]

The importance of rational temporal sequencing of therapeutic combinations is further reinforced by the challenges faced when combining conventional chemotherapy with targeted FLT3 inhibition in AML.[215,216] Nucleoside analogues such as ara-c require leukaemic cells to enter S-phase to have maximal effect. Pre-treatment with a FLT3 inhibitor induces cell cycle arrest thereby antagonising the effect of ara-c.[217,218] However, marked synergy is observed when leukaemic cells are exposed first to ara-c and subsequently to FLT3 inhibitors. These pre-clinical observations have had a significant impact on the design of treatment regimens containing FLT3 inhibitors in AML. These examples highlight the caution required in designing rational novel therapeutic combinations, with consideration given not only to maximisation of therapeutic efficacy but also avoidance of antagonism between agents.

Notably, the examples discussed only encompass conventional chemotherapeutic agents and targeted therapies directed against the aberrant catalytic activity of malignant oncoproteins. Resistance to therapies directed against protein-protein interactions and epigenetic targeted therapies have not been thoroughly investigated.

1.4.2 The concept of a leukaemia stem cell

By their very nature, tumours are highly adaptable and are able to evolve in order to overcome therapeutic pressures.[219] The therapeutic resilience of cancer occurs as a consequence of tumour heterogeneity underpinned by intratumoural genetic diversity and epigenetic plasticity. This dynamic evolutionary process has been highlighted by the advent of massively parallel sequencing technologies and the development of novel techniques which allow exploration of single cell genomes and transcriptomes.[220-222] At the heart of this process is the cancer/leukaemia stem cell - often purported to be the nidus for the emergence of therapeutic resistance.[223,224]

Normal stem cells make cell fate decisions to either self-renew or differentiate during the process of asymmetric cell division, a capacity provided by epigenetic plasticity. These decisions are guided by environmental cues in response to steady state demands or extrinsic stressors.[225] In cancer cells, this balance shifts towards self-renewal. These self-renewing cells sustain tumour growth and may be viewed as units of evolutionary

selection driving cancer development. In the face of selective pressure, they either possess or acquire enabling characteristics which are the hallmarks of cancer, resulting in resistance to therapy.[8,219] Indeed, acquired resistance may be driven by stochastic mutational load or adaptive epigenetic changes which confer a fitness advantage to sub-populations of co-existent malignant cells. A better understanding of cancer stem cells and their ability to adapt will allow us to manage and potentially guide cancer evolution for therapeutic gain.

With this in mind, the haematopoietic developmental hierarchy serves as a blueprint for understanding the mechanisms of self-renewal in both normal and malignant contexts. Analogous to the hierarchical organisation of normal haematopoiesis, leukaemic clones have significant morphologic, phenotypic and functional heterogeneity and appear to organise themselves in loose hierarchies with a small sub-population of leukaemia stem cells (LSC) at their apices.[224,226] In this context, LSC are characterised by two major features: (i) they have unlimited self-renewal capacity and (ii) the ability to initiate, sustain, and regenerate the primary malignancy when transplanted into an appropriate host. Studies utilising limiting dilution transplant assays (LDA) have demonstrated that LSC are a rare population in AML and vary in frequency from between 1 in 1×10^3 to 1 in 1×10^6 leukaemic cells.[223,227] Eradication of the LSC compartment is essential for sustained cure and increasing efforts have been directed towards identifying and targeting the LSC.[223]

Our collective clinical experience demonstrates that resistance to cancer therapies is inevitable and understanding the cellular and molecular mechanisms of resistance is imperative to enhancing the clinical utility of novel therapeutics. This understanding, our ability to identify determinants of response and our ability to circumvent therapeutic futility, is strengthened by the application of new analytical techniques which allow for effective interrogation of the response of malignant cells to therapeutic pressures.

To this end, an exploration of the mechanisms of resistance to targeted epigenetic therapy with the BET inhibitors in a murine MLLfp driven leukaemia model is presented in this thesis.

Chapter 2 - Materials and Methods

2.1 Materials

All general laboratory chemicals were obtained from Sigma-Aldrich unless otherwise stated. Tissue culture plasticware was manufactured by Corning. Cell culture media and antibiotics were obtained from Life Technologies (Thermo Fisher Scientific) unless otherwise stated.

2.1.1 Buffers and Bacterial Growth Media

The composition of bacterial media and stock solutions are shown below in Table 2.1.

Name	**Composition per litre**
Annealing Buffer	10 mM Tris-HCl pH 7.5, 50 mM NaCl, 1 mM EDTA
Annexin V Binding Buffer	10 mM HEPES pH 7.4; 140 mM NaCl; 2.5 mM $CaCl_2$
FACS Buffer	150 mM NaCl, 2.5 mM KCl, 10 mM Na_2HPO_4, 2 mM K_2HPO_4, 5% [v/v] FBS, 5 mM EDTA
K Buffer	10 mM Tris-HCl pH 7.5, 50 mM KCl, 1.5 mM $MgCl_2$, 0.5% Tween-20
LB	5 g NaCl, 5 g yeast extract, 10 g bacto-tryptone
MACS buffer	150 mM NaCl, 2.5 mM KCl, 10 mM Na_2HPO_4, 2 mM K_2HPO_4, 0.5% BSA, 2 mM EDTA
PBS	150 mM NaCl, 2.5 mM KCl, 10 mM Na_2HPO_4, 2 mM K_2HPO_4
RBC Lysis Buffer	150 mM NH_4Cl, 10 mM $NaHCO_3$, 1 mM EDTA
Resazurin solution	150 mg resazurin, 25 mg methylene blue, 1 M potassium hexacyanoferrate (III) and 1 M potassium hexacyanoferrate (II) trihydrate
SOC	20 g bacto-tryptone, 5 g bacto-yeast, 0.58 g NaCl, 0.19 g KCl, 10 mM $MgCl_2$, 10 mM $MgSO_4$ and 0.4% [w/v] glucose

TBE	90 mM Tris-borate, 2 mM EDTA pH 6.5
TBS	150 mM NaCl, 20 mM Tris-Hcl pH 7.6

Table 2.1: Standard solutions

2.1.2 Cell Culture Media and Additives

Media and additives used are shown below in Table 2.2.

Item	**Manufacturer**	**Catalogue #**
DMEM	Thermo Fisher Scientific	11965
Fetal Bovine Serum	Sigma Aldrich	12003C
Gentamycin	Thermo Fisher Scientific	15750
L-alanyl-L-glutamine	Thermo Fisher Scientific	35050
Methylcellulose-Based Medium with Recombinant Cytokines and EPO for Mouse Cells (Methocult™)	Stemcell Technologies	M3434
Opti-MEM®	Thermo Fisher Scientific	31985
Penicillin/Streptomycin/Amphotericin-B	Thermo Fisher Scientific	15240
Recombinant Human IL-6	PeproTech	AF-200-06
Recombinant Murine IL-3	PeproTech	213-13
Recombinant Murine Stem Cell Factor	PeproTech	AF-250-03
RPMI-1640	Thermo Fisher Scientific	11875

Table 2.2: Media additives

2.1.3 Investigational compounds

Investigational compounds used are shown below in Table 2.3.

Compound	In Vitro Drug Vehicle	In Vivo Drug Vehicle
I-BET151	DMSO	IP - 0.9% saline containing 5% [v/v] DMSO and 10% [w/v] Kleptose HPB
Pyrvinium	DMSO	IP - 0.9% saline containing 15% [v/v] DMSO
IMG98	DMSO	-
JQ1	DMSO	-

Table 2.3: Investigational compounds

2.1.4 Antibodies

Antibodies used for chromatin immunoprecipitation (ChIP) and Western blot (WB) assays are shown in Table 2.4. Antibodies used in flow cytometric analyses are shown in Table 2.5. Antibodies used for magnetic bead selection are shown in Table 2.6.

Target	Manufacturer	Catalogue #	Application
BRD2	Bethyl Labs	A302-583A	ChIP, WB
BRD3	Bethyl Labs	A302-368A	ChIP, WB
BRD4	Bethyl Labs	A301-985A	ChIP
BRD4	abcam	ab128874	ChIP
c-MYC	Cell Signalling Technology	9402S	WB
H3K27ac	abcam	ab4729	ChIP
HSP60	Santa Cruz Biotechnology	sc-13966	WB
β-actin	Sigma-Aldrich	A1978	WB
β-catenin	BD Biosciences	610154	ChIP

Table 2.4: ChIP and WB antibodies

Target	Species	Fluorochrome	Manufacturer	Catalogue #
Annexin V		APC	BD Biosciences	550475
Biotin		V500 streptavidin	BD Biosciences	561419
CD11b	Mouse	BV605	BioLegend	101237
CD117	Mouse	APC/Cy7	BioLegend	105826
CD123	Human	PE/Cy5	eBioscience	15-1239-41
CD16/32	Mouse	PerCP/Cy5.5	BioLegend	101324
CD19	Human	Biotin	BD Biosciences	555411
CD3	Human	Biotin	BD Biosciences	555338
CD33	Human	PE/Cy7	BD Biosciences	333946
CD34	Human	APC	BD Biosciences	555824
CD34	Mouse	eFluor 660	eBioscience	50-0341-82
CD38	Human	BV711	BD Biosciences	563965
CD45	Human	FITC	eBioscience	11-9459-42
CD45.1	Mouse	APC/Cy7	BioLegend	110716
CD45RA	Human	PerCP/Cy5.5	eBioscience	45-0458-42
CD86	Mouse	PE	BioLegend	105008
CD90	Human	PE	BD Biosciences	561970
Gr-1	Mouse	Alexa Fluor 700	BioLegend	108422
Lineage antibody cocktail	Mouse	Biotin	Miltenyi Biotec	120-001-547
Ly-6A (sca-1)	Mouse	Pacific Blue	BioLegend	122520
Ter119	Mouse	eFluor 450	eBioscience	48-5921-82

Table 2.5: Flow cytometry antibodies

Target	Species	Manufacturer	Catalogue #
CD117	Mouse	Miltenyi Biotec	130-091-224

Table 2.6: Antibodies used for magnetic bead selection

2.1.5 Cell lines

The human embryonic kidney 293T cell line was used for production of viral particles and was available as a stock in the Dawson laboratory (Peter MacCallum Cancer Centre).

2.1.6 Bacterial strains

The E. coli strain TOP10F (Thermo Fisher Scientific) was used for transformation and plasmid DNA production.

TOP10F genotype: F- mcrA Δ(mrr-hsdRMS-mcrBC) φ80lacZΔM15 ΔlacX74 nupG recA1 araD139 Δ(ara-leu)7697 galE15 galK16 rpsL(StrR) endA1 λ-

2.1.7 Vectors

The plasmids used for the various applications detailed below are summarised in Table 2.7. The plasmid containing DKK1 was a kind gift from Dr Steve Lane (QIMR Berghofer Medical Research Institute, Brisbane, Australia). The pLMN-mCherry plasmids were a kind gift from Dr Johannes Zuber (The Research Institute of Molecular Pathology, Vienna, Austria). The TtRMPVIR plasmid was purchased from addgene (ID 27995). The remaining plasmids were present as stocks in the Dawson laboratory (Peter MacCallum Cancer Centre).

Backbone	**Insert**	**Application**
pGIPZ	shRNA	shRNA source for sub-cloning
pMSCV-IRES-YFP	MLL-AF9	Transfection into mammalian cells and protein expression
pMSCVneo	DKK1	Transfection into mammalian cells and protein expression
pMSCVneo	MLL-ENL	Transfection into mammalian cells and protein expression
pQCXIX	TtRMPVIR[228]	Transfection into mammalian cells and tetracycline inducible shRNA expression
pLMPC	mirE	Transfection into mammalian cells and constitutive shRNA expression
pCL-Eco	gag/pol/env	Transfection into mammalian cells for retroviral particle production

Table 2.7: Vectors

2.1.8 PCR primers

cDNA primers used for gene expression analysis by qRT-PCR for murine (Table 2.8) and human (Table 2.9) genes are listed below. Primers used for ChIP qRT-PCR analysis of murine samples are listed below in Table 2.11. Custom oligonucleotides were purchased from Sigma-Aldrich and resuspended as 200mM stock solutions.

Amplicon	Forward primer	Reverse primer
Apc	GGAGTGGCAGAAAGCAACAC	AAACACTGGCTGTTTCGTGA
B2m	GAGCCCAAGACCGTCTACTG	GCTATTTCTTTCTGCGTGCAT
Brd2	TGGGCTGCCTCAGAATGTAT	CCAGTGTCTGTGCCATTAGG
Brd3	GCCAGTGAGTGTATGCAGGA	GCCTGGGCCATTAGCACTAT
Brd4	TCTGCACGACTACTGTGACA	GGCATCTCTGTACTCTCGGG
Ccnd2	CAAGCCACCACCCCTACA	TTGCCGCCCGAATGG
Dkk1	CTGCATGAGGCACGCTATGT	AGGAAAATGGCTGTGGTCAG
Dvl1	ATCACACGCACCAGCTCTTC	GGACAATGGCACTCATGTCA
Fzd5	GGCTACAACCTGACGCACAT	CAGAATTGGTGCACCTCCAG
Gapdh	GGTGCTGAGTATGTCGTGGA	CGGAGATGATGACCCTTTTG
Gsk3 β	TTGGAGCCACTGATTACACG	CCAACTGATCCACACCACTG
Myc	TGAGCCCCTAGTGCTGCAT	AGCCCGACTCCGACCTCTT

Table 2.8: Mouse cDNA primers

Amplicon	Forward primer	Reverse primer
AXIN2	CGGACAGCAGTGTAGATGGA	CTTCACACTGCGATGCATTT
CCND1	GCTGTGCATCTACACCGACA	CCACTTGAGCTTGTTCACCA
CTNNB1	GACCACAAGCAGAGTGCTGA	CTTGCATTCCACCAGCTTCT
FZD5	TTCCTGTCAGCCTGCTACCT	CGTAGTGGATGTGGTTGTGC
MYC	CTGGTGCTCCATGAGGAGA	CCTGCCTCTTTTCCACAGAA
TCF4	ATGGCAAATAGAGGAAGCGG	TGGAGAATAGATCGAAGCAAG
ACTIN	TTCAACACCCCAGCCATGT	GCCAGTGGTACGGCCAGA
GAPDH	ACGGGAAGCTTGTCATCAAT	TGGACTCCACGACGTACTCA

Table 2.9: Human cDNA primers

Target	Forward primer	Reverse primer
BRD4 exon 3	TCCTAGCCATCCTGACCAGT	CACTGTGGACACTGGTGGTT
BRD4 exon 4	TCCCCCTTGTGAATACAACC	TGTCCTTGGGCTCCTTAGAA
BRD4 exon 5	AGATTGTAGCCCCCTGGAGT	CATGGGACTTCCTAGGAGCA

Table 2.10: Sanger sequencing primers

Amplicon	Forward primer	Reverse primer
MYC enhancer	TCTTTGATGGGCTCAATGGT	TTCCCTTCACCTGATGAACC
MYC TSS	GTCACCTTTACCCCGACTCA	TCCAGGCACATCTCAGTTTG
Negative control region	TGAAACCGTGACAGATGAGC	ACCCCTGAAATTGCTCCTTC

Table 2.11: ChIP PCR primers

2.1.9 DNA restriction enzymes

Restriction enzymes used are detailed below in Table 2.12.

Enzyme	Manufacturer	Catalogue Number
BglII	New England Biolabs	R0144
EcoRI	New England Biolabs	R0101
EcoRV	New England Biolabs	R0195
MluI	New England Biolabs	R0198
XhoI	New England Biolabs	R0146

Table 2.12: DNA restriction enzymes

2.1.10 Patient material

Peripheral blood or bone marrow containing >80% blasts was obtained from patients following informed consent and under full ethical approval at each involved institute.

2.2 Methods

2.2.1 Cell culture

All tissue culture manipulations were carried out in sterile conditions in a standard laminar flow hood. All cell cultures were maintained in a humidified incubator at 37°C in 5% CO_2. Suspension cell lines were maintained in 25cm^2 flasks and passaged every 48-72 hours to maintain a cell density between 1×10^4 to 2×10^6 cells/mL.

Primary murine haematopoietic progenitors and derived cell lines were cultured in RPMI-1640 supplemented with IL-3 (10 ng/mL), 20% [v/v] fetal bovine serum, penicillin (100 units/mL), streptomycin (100 μg/mL), amphotericin B (250 ng/mL) and gentamycin (50 μg/mL). Primary human leukaemia cells were cultured in RPMI-1640 supplemented with IL-3 (10 ng/mL), IL-6 (10 ng/mL), SCF (50 ng/mL) and 20% [v/v] fetal bovine serum. HEK 293T cells were cultured in DMEM supplemented with 10% [v/v] fetal bovine serum.

Cell cultures were cryopreserved in fetal bovine serum supplemented with 10% [v/v] DMSO. A controlled rate of cooling (−1°C/minute) was achieved by using Mr Frosty™ Freezing Containers (ThermoFisher Scientific).

2.2.2 Mycoplasma contamination testing

Cell lines were routinely tested for mycoplasma contamination by PCR. A 1 mL sample of media was obtained from cultures following at least 72 hours growth. These samples were then centrifuged at >13,000 g for 2 minutes to pellet contents and the supernatant aspirated. Pellets were lysed in 50 μL of K buffer containing 1 μg/mL proteinase K, incubated at 55°C for 60 minutes then 95°C for 10 minutes. 2 μL of the lysate was then used as template DNA for PCR. PCRs were carried out using a Mastercycler® nexus gradient (Eppendorf) thermal cycler. GoTaq® DNA polymerase (Promega) was used according to manufacturer's instructions. The primers (Table 2.13), reaction mix and protocol (Table 2.14) are detailed below. After PCR, 10 μL of the sample was run on a 2% [w/v] agarose gel. 2% [w/v] agarose gels were made by dissolving agarose in 100 mL TBE and adding 10 μL of SYBR® Safe DNA Gel Stain (ThermoFisher Scientific). The gel was poured into a mould, allowed to set and then mounted in an electrophoresis

tank and covered with TBE. Mycoplasma contamination was determined if a 520 bp band was present in conjunction with a 375 bp cytochrome b band (PCR reaction positive control).

Amplicon	Forward primer	Reverse primer
Mycoplasma	YGCCTGVGTAGTAYRYWCGC	GCGGTGTGTACAARMCCCGA
Cytochrome b	GCTGTGCATCTACACCGACA	CCACTTGAGCTTGTTCACCA

Table 2.13: PCR primers for mycoplasma testing

	Mycoplasma PCR
Reaction mix (made up to 25 μL in ddH_2O)	5x reaction buffer, 2.5 mM MgCl2, 1 mM dNTP mix, 1.25 μM mycoplasma forward primer, 0.3 μM mycoplasma reverse primer, 0.6 μM cytochrome b forward primer, 0.6 μM cytochrome b reverse primer, 2 μL sample lysate
Enzyme	1.25 units Promega GoTaq
Protocol	95°C, 3 minutes 95°C, 1 minute; 50°C, 1 minute; 72°C, 1 minute (35 cycles) 72°C, 10 minutes

Table 2.14: PCR reaction mix and protocol for mycoplasma testing

Any cell lines which were deemed positive were treated with 25 μg/mL Plasmocin™ (InvivoGen) for a two week period prior to retesting to confirm successful eradication of mycoplasma contamination.

2.2.3 DNA cloning techniques

DNA cloning techniques utilised in this work are described below in general with specific applications detailed in subsequent sections.

To anneal complimentary oligonucleotides, equal volumes of equimolar (200 nM) oligonucleotides were mixed in a 1.5 mL micro-centrifuge tube and placed on a heat block at 95°C for 5 minutes. After allowing the mixture to cool to room temperature on the bench for 60 minutes, annealed oligonucleotides were placed at 4°C until utilisation in downstream applications.

Restriction enzyme digestion of DNA templates were performed according to manufacturer's instructions and reaction conditions are detailed in Table 2.15. All reactions were carried out in 50 μL reaction volumes at 37°C for 60 minutes. Restriction enzymes were subsequently heat inactivated at 65°C for 20 minutes.

Enzyme(s)	**Condition**
EcoRI	10 units EcoRI enzyme, 1 μg DNA, 5 μL 10× NEBuffer EcoRI
XhoI & MluI	10 units XhoI enzyme, 10 units MluI enzyme, 1 μg DNA, 100 μg/mL BSA, 5 μL 10× NEBuffer 3
MluI & EcoRV	10 units MluI enzyme, 10 units EcoRV enzyme, 1 μg DNA, 100 μg/mL BSA, 5 μL 10× NEBuffer 3
MluI and BglII	10 units MluI enzyme, 10 units BglII enzyme, 1 μg DNA, 5 μL 10× NEBuffer 3

Table 2.15: Restriction Enzyme Reaction Conditions

Where possible, DNA fragments were inserted into vectors cut with two restriction enzymes to generate incompatible ends to minimise recircularisation of vector fragments. Calf intestinal phosphatase treatment of digested vectors was performed if compatible ends were generated to remove the 5' terminal phosphate and prevent recircularisation. This was achieved by the addition of 10 units of calf intestinal phosphatase (New England Biolabs) to heat inactivated digests followed by incubation at 37°C for 60 minutes.

The Wizard® SV Gel and PCR Clean-Up System (Promega) was used to purify vectors digested where calf intestinal phosphatase treatment was required to prevent recircularisation. An equal volume of Membrane Binding Solution (4.5M guanidine isothiocyanate; 0.5M potassium acetate pH 5.0) was added to samples, transferred to a silica membrane column and incubated for 1 minute at room temperature to allow DNA adsorption onto the silica surface. Columns were then centrifuged at 16,000 g for 1 minute and washed twice with Membrane Wash Solution (10mM potassium acetate pH 5.0; 80% [v/v] ethanol; 16.7μM EDTA pH 8.0). The second centrifugation was

performed at 16,000 g for 5 minutes to ensure columns were dry prior to elution of DNA with 50 μL of ultra pure H_2O. Samples were incubated for 1 minute prior to centrifugation at 16,000 g for 1 minute and collection of eluted DNA into micro-centrifuge tubes.

DNA fragments were resolved using horizontal agarose gels. 1-2% [w/v] agarose gels were made by dissolving agarose in 100 mL TBE and adding 10 μL of SYBR® Safe DNA Gel Stain (ThermoFisher Scientific). The gel was poured into a mould, allowed to set and then mounted in an electrophoresis tank and covered with TBE. DNA samples were loaded onto the gel following the addition of 1× blue/orange loading dye (Promega) and electrophoresed at 100V. 100 bp or 1 kb DNA ladders (Promega) were run alongside samples as a marker.

To maximise the successful generation of recombinant plasmids, both vector and insert fragments were gel-purified to exclude the presence of undigested plasmids in the ligation reaction. This was achieved through the use of the QIAquick gel extraction kit (QIAGEN) according to manufacturer's instructions. DNA fragments were excised from agarose gels with a clean scalpel blade to ensure the smallest gel fragments possible. 3 volumes of buffer QG (5.5 M guanidine thiocyanate, 20 mM Tris HCl pH 6.6) per gel volume were added prior to sample incubation at 55°C until gel slices were dissolved (approximately 10 minutes). 1 gel volume of isopropanol was added prior to transferring samples onto a silica membrane column. Columns were then centrifuged at 17,900 g for 1 minute prior to being washed once with buffer PE (10 mM Tris-HCl pH 7.5, 80% [v/v] ethanol). Columns were additionally centrifuged at 17,900 g for 1 minute to remove residual wash buffer. 30 μL of ultra pure H_2O was added to the middle of the columns and allowed to stand for 1 minute prior to centrifugation at 17,900 g for 1 minute to elute purified DNA fragments into micro-centrifuge tubes.

Ligation of 1 μg of digested vectors and inserts in a 1:3 molar ratio was performed in 20 μL reaction volumes using 400 units of T4 DNA ligase (New England Biolabs) and 2 μL of 10× T4 DNA Ligase Reaction Buffer. Ligation reaction mixtures were incubated overnight at 16°C.

2.2.4 Bacterial transformation

Bacterial transformation for production of plasmid DNA was achieved through heat shock of chemically competent TOP10F bacteria. 50 μL of chemically competent cells were thawed on ice prior to the addition of 5 μL of a ligation reaction or 0.1 μg of plasmid DNA. Cells and DNA were mixed gently prior to incubation on ice on 5 minutes. Samples were heat shocked at 42°C for exactly 60 seconds and placed immediately back on ice for a further 2 minutes. 1 mL of pre-warmed SOC media was then added to the mixture and incubated at 37°C in a rotary shaker-incubator for 1 hour at 225 rpm. Immediately following this, 300 μL of the transformation mixture was plated on a LB plate and incubated overnight.

2.2.5 Bacterial culture

Plated cultures were grown at 37°C overnight on LB plates. Bacterial suspension cultures were grown in LB at 37°C overnight. To allow the selection of bacteria transformed with plasmid DNA expressing the gene of interest, media was supplemented with ampicillin (100 μg/mL).

2.2.6 Large scale plasmid DNA preparation from *E. coli*

Large scale plasmid DNA preparation from *E. coli* was performed using the QIAGEN Plasmid Maxi kit according to manufacturer's instructions. A single bacterial colony was used to inoculate a 5 mL LB starter culture containing the appropriate selection antibiotic and incubated at 37°C for 6 - 8 hours. This starter culture was then used to inoculate a subsequent 100 mL culture which was grown overnight at 37°C. Bacteria were harvested by centrifugation at 6000 g for 15 minutes at 4°C. The bacterial pellet was resuspended in 10 mL P1 solution (50 mM Tris-HCl pH 8.0, 10 mM EDTA, 100 μg/ml RNase A) and then lysed by the addition of 10 mL P2 solution (200 mM NaOH, 1% [w/v] SDS) before incubation at room temperature for 5 minutes. Following this, 10 mL chilled P3 (3.0 M potassium acetate pH 5.5) was added, the lysate mixed by inversion and incubated on ice for 20 minutes. The lysate was cleared by centrifugation at 20,000 g for 30 minutes at 4°C. The supernatant was then further centrifuged at 20,000 g for 15 minutes at 4°C and applied to a QIAGEN-tip 500 column, previously

equilibrated with 10 mL QBT buffer (750 mM NaCl, 50 mM MOPS pH 7.0, 15% [v/v] isopropanol, 0.15% [v/v] Triton® X-100). The column was washed twice with 30 mL QC buffer (1.0 M NaCl, 50 mM MOPS pH 7.0, 15% [v/v] isopropanol). DNA was then eluted with 15 mL QF buffer (1.25 M NaCl, 50 mM TrisHCl pH 8.5, 15% [v/v] isopropanol) and precipitated by the addition of 10.5 mL room temperature isopropanol. DNA was pelleted by centrifugation at 15,000 g for 30 minutes at 4°C prior to being washed with 70% [v/v] ethanol and pelleted again by centrifugation at 15,000 g for 10 minutes. The pellet was dried completely prior to being dissolved in ultra-pure H_2O. DNA concentration was determined by measuring absorbance at 260 nm using a spectrophotometer (NanoDrop™ 2000, ThermoFisher Scientific).

2.2.7 Retroviral transduction

HEK 293T cells were used for the production of viral particles. 2.5×10^6 HEK 293T cells in 10 mL were seeded in 10 cm dishes the day prior to transfection with GeneJuice® transfection reagent (Merck Millipore) according to manufacturer's instructions. 18 μL of the transfection reagent was added drop-wise to 500 μL of Opti-MEM®, mixed thoroughly with a vortex mixer and incubated at room temperature for 5 minutes. 3 μg of insert plasmid vector and 3 μg of packaging plasmid vector were then added to the mixture and incubated for a further 15 minutes at room temperature. This mixture was then added drop-wise to the plates containing HEK 293T cells ensuring that there was even distribution across the dish. Following transduction, HEK 293T cells were incubated at 32°C to optimise conditions for virus production. Media was changed to appropriate media required for target cells 24 hours following transfection and virus containing supernatant harvested at 48 and 72 hours.

Viral transduction of target cells was achieved through spin infection. Harvested viral supernatants were filtered through a 0.45 μm filter prior to the addition of 8 μg/mL polybrene (Merck Millipore) to enhance receptor independent virus adsorption on target cell membranes. Target cells were then centrifuged at 400 g for 5 minutes, supernatant aspirated and subsequently resuspended in virus containing media at $5 - 10 \times 10^5$ cells/mL in 6-well tissue culture plates. These plates were then spun at 1250 g for 90 minutes and incubated at 37°C for 4.5 hours in a humidified incubator. Following a total

exposure time to viral supernatant of 6 hours, media was changed to minimise polybrene toxicity.

2.2.8 Generation of immortalised primary murine haematopoietic stem and progenitor cell lines and derivation of clonal cell lines

Initial generation of immortalised parental cell lines was achieved through magnetic bead selection of HSPCs, obtained from whole bone marrow of male and female C57BL/6 mice, and subsequent retroviral transduction with either an MSCV-MLL-AF9-IRES-YFP or MSCV-MLL-ENL construct.

Mice were humanely euthanized prior to harvest of pelvic bones, femurs and tibias. Bones were flushed with PBS, the resultant cell suspension passed through a 40μm filter and cells pelleted by centrifugation at 400 g for 5 minutes. Cells were resuspended in 10 mL RBC lysis buffer per 1×10^7 cells, incubated on ice for 10 minutes and washed once with an equivalent volume of cold MACS buffer. Magnetic microbead labelling of $CD117^+$ cells was achieved through incubation with 100 μL per 1×10^7 cells of a microbead conjugated CD117 antibody solution, on ice, for 15 minutes. Following a wash with MACS buffer, positive selection of labelled cells then proceeded according to manufacturer's instructions utilising MACS™ LS columns (Miltenyi Biotec). The microbead labelled cell suspension was applied to a separator column in the presence of a magnetic field, the column washed three times with MACS buffer and $CD117^+$ HSPCs eluted in MACS buffer following removal of the magnetic field. Isolated HSPCs were then transduced with oncogenic expression vectors according to the retroviral transduction protocol detailed in 2.2.7, located on page 68.

To generate clonal resistant cell lines, the MLL-AF9 bearing parental cell line was serially re-plated in cytokine supplemented methylcellulose (Methocult™ M3434, Stemcell Technologies) containing either vehicle (0.1% [v/v] DMSO) or drug (400 nM I-BET151). Following the establishment of robust colony growth, individual vehicle treated or resistant colonies were picked with the assistance of an inverted microscope and transferred to liquid culture to generate clonal cell lines. Colonies were initially seeded in 48-well tissue culture plates containing 300 μL of pre-warmed media. Media

was then refreshed daily with pre-warmed media until robust growth was seen whereupon cells were transferred to 6-well tissue culture plates and subsequently to 25 cm^2 tissue culture flasks. Resistant cell lines were maintained continuously in drug whilst being incrementally exposed to increasing concentrations of drug (up to 1 μM I-BET151). Vehicle treated clones were also continuously maintained in 0.1% [v/v] DMSO and passaged in identical fashion. The parental cell line was continuously maintained in liquid culture alone with no exposure to vehicle or drug.

Similarly, to generate resistant cell lines bearing the MLL-ENL translocation, the parental cell line was serially re-plated in cytokine supplemented methylcellulose containing either vehicle (0.1% [v/v] DMSO) or drug (400 nM I-BET151). Following the establishment of robust colony growth, cells in each plate were washed in PBS and transferred to liquid culture to generate cell lines. Resistant cell lines were maintained continuously in drug whilst being incrementally exposed to increasing concentrations of drug (up to 1 μM I-BET151). Vehicle treated clones were also continuously maintained in 0.1% [v/v] DMSO and passaged in identical fashion. The parental cell line was continuously maintained with no exposure to vehicle or drug.

2.2.9 Cell proliferation assays

Cells were seeded at 1×10^4 cells/mL in 6-well tissue culture plates in the presence of I-BET151, JQ1 or vehicle (0.1% [v/v] DMSO) and followed over 96 hours to assess the proliferative capacity of sensitive and resistant clones in the presence of investigational compounds. Cell counts were performed every 24 hours using a haemocytometer.

For long-term proliferation assays, cells were seeded at 1×10^4 cells/mL in 6-well tissue culture plates in the presence of either I-BET151, IMG98, vehicle or combinations thereof to obtain a 0.2% [v/v] DMSO concentration. Cultures were split 1:50 on days 3, 6 and 9. Daily cell counts (total and live cells) were obtained using a flow cytometer (FACSVerse™, BD Biosciences). 50 μL aliquots of cell cultures were mixed with 150 μL FACS buffer containing 1 μg/mL DAPI.

For dose-response assays, serial dilutions of I-BET151, JQ1, pyrvinium or IMG98 were further diluted in complete growth media prior to addition to 96-well plates, seeded with between 5×10^3 and 1×10^4 cells per well in 100 μL, to obtain a 0.1% [v/v] DMSO final concentration. Following 48 to 72 hour incubation, 20 μL resazurin was added to

each well and plates were further incubated for 3 hours prior to assessment of fluorescence.

Similarly, determination of *in vitro* synergy in proliferation assays was undertaken by diluting and combining 5-point serial dilutions of I-BET151 and pyrvinium in a 5 × 5 matrix in 96-well plates containing complete growth media. Drug containing media was then added to 96-well cell plates seeded with 5×10^3 cells per well in 100 μL, to obtain a 0.2% DMSO final concentration. Following 48 to 72 hour incubation, 20 μL resazurin solution was added to each well and plates were further incubated for 3 hours prior to assessment of fluorescence.

Seeding of cells, media and resazurin in 96-well plates was performed with the assistance of a liquid handing instrument (EL406, BioTek) and liquid handling robot (ALH3000, Caliper SciClone). Fluorescence was read at 560 nm/590 nm on a Cytation 3 Imaging Reader (BioTek) and was normalised to control wells containing media only and media containing untreated cells. Statistical analysis and curve fitting was performed using Prism 6 (GraphPad). The determination of synergy was performed according to the method of Zhao et al[229].

2.2.10 Clonogenic assays in methylcellulose

Clonogenic potential was assessed through colony growth of derived cell lines plated in cytokine supplemented methylcellulose (Methocult™ M3434, Stemcell Technologies). 3 mL aliquots of frozen methylcellulose were thawed prior to the addition of cells in 300 μL of complete growth media. Differential response to investigational compounds was determined through the addition of drug or vehicle to obtain a 0.1% [v/v] DMSO final concentration. Single cell suspensions were generated through thorough mixing with a vortex mixer. Mixtures were then divided equally between two 35 mm gridded tissue culture plates (Sarstedt). Cells were incubated at 37°C and 5% CO_2 for 7 to 10 days at which time colonies were counted. The details of specific cell and treatment conditions are outlined below.

Derived vehicle treated and resistant cell lines were plated in duplicate at a cell dose of 2×10^2 per plate in the presence of vehicle (0.1% [v/v] DMSO) or drug (1 μM I-BET151). $Gr1^-/CD11b^-$ and $Gr1^+/CD11b^+$ fractions of resistant cell lines were plated in duplicate following FACS at a cell dose of between 2×10^2 and 2×10^3 cells per plate.

FACS isolated L-GMP populations obtained from whole mouse bone marrow following primary syngeneic transplant of vehicle treated clones were plated in duplicate at a cell dose of between 2×10^2 and 2×10^3 cells per plate in the presence of vehicle (0.1% [v/v] DMSO) or drug (1 μM I-BET151). For assessment of colony forming capacity following LSD1 inhibitor therapy, cells were plated in duplicate at a cell dose of 2×10^4 per plate in the presence of vehicle (0.1% [v/v] DMSO) or drug (1 μM I-BET151, 1 μM IMG98 or a combination of both).

2.2.11 Flow cytometric analyses

Flow cytometry analyses were performed on a LSRFortessa X-20 flow cytometer (BD Biosciences) and all data analysed with FlowJo software (vX.0.7, Tree Star). Cell sorting was performed on a FACSAria Fusion flow sorter (BD Biosciences).

Apoptosis in response to investigational compounds was assessed using APC conjugated Annexin V and PI staining according to manufacturer's instructions. Cells were seeded at 1×10^4 cells/mL in 6-well tissue culture plates in the presence of I-BET151 or vehicle (0.1% [v/v] DMSO) for 72 hours. Following this, cells were washed twice with cold PBS, resuspended in Annexin V binding buffer containing a 1:150 dilution of Annexin V antibody and 0.2 mg/mL PI and incubated at room temperature for 15 minutes prior to flow cytometric analysis.

For cell cycle analysis, cells were seeded at 1×10^4 cells/mL in 12-well tissue culture plates in the presence of I-BET151 or vehicle (0.1% [v/v] DMSO) for 72 hours. Cells were then harvested, washed once in cold PBS and fixed overnight at -20°C in 70% EtOH (v/v) in PBS. The following day, cells were centrifuged and EtOH decanted thoroughly and washed once with and equivalent volume of PBS. Prior to flow cytometric analysis, cells were incubated at 37°C for 30 minutes in PI staining solution (0.02 mg/mL PI, 0.05% v/v Triton-X in PBS, supplemented with 0.2 mg/mL DNase-free RNase A (Qiagen)) or incubated at room temperature for 10 minutes with DAPI staining solution (1 μg/mL DAPI, 0.05% v/v Triton-X in PBS).

Immunophenotype assessments were undertaken using the antibody panels detailed below in Table 2.16, Table 2.17, Table 2.18 and Table 2.19. Stably growing cell lines were harvested and washed twice with cold FACS buffer prior to antibody staining. Cells harvested from murine tissues were resuspended in 10 mL RBC lysis buffer per 1

$\times 10^7$ cells, incubated on ice for 10 minutes and washed twice with an equivalent volume of cold FACS buffer prior to antibody staining. Antibody staining was undertaken by resuspending up to 3×10^6 cells in 30 μL of antibody cocktail in individual wells of a 96-well tissue culture plate. Cells were then incubated in the dark on ice for 45 minutes. If secondary antibody staining was required, cells were washed once with cold FACS buffer and resuspended in 30 μL of secondary antibody cocktail and incubated further in the dark on ice for 20 minutes. Cells were washed twice with cold FACS buffer and resuspended in FACS buffer containing a viability dye prior to flow cytometric analysis. PI or DAPI was used as a viability dye to ensure that immunophenotyping analyses were performed on viable cells. Appropriate unstained, single stained and fluorescence minus one controls were used to determine background staining and compensation in each channel.

Target	Fluorochrome	Dilution
Gr-1	Alexa Fluor 700	1:80
CD11b	Brilliant Violet 605	1:80
DAPI		1 μg/mL

Table 2.16: Antibody panel for assessment of murine markers of committed myeloid differentiation

Target	Fluorochrome	Dilution
CD117/c-kit	APC/Cy7	1:80
CD16/32	PerCP/Cy5.5	1:80
CD34	eFluor 660	1:25
Lineage	Biotin	1:25
Ly-6A (sca-1)	Pacific Blue	1:100
Biotin	V500 streptavidin	1:50
PI		1 μg/mL

Table 2.17: Antibody panel for assessment of murine stem and progenitor populations

Target	Fluorochrome	Dilution
CD117/c-kit	APC/Cy7	1:180
CD16/32	PerCP/Cy5.5	1:300
CD34	eFluor 660	1:125
CD86	PE	1:500
Gr-1	Alexa Fluor 700	1:90
CD11b	Brilliant Violet 605	1:90
PI		1 µg/mL

Table 2.18 Antibody panel for assessment of murine stem and progenitor populations following LSD1 inhibitor treatment

Target	Species	Fluorochrome	Dilution
CD45.1	Mouse	APC/Cy7	1:125
Ter119	Mouse	ef450	1:66.7
CD123	Human	PE/Cy5	1:50
CD19	Human	Biotin	1:80
CD3	Human	Biotin	1:80
CD33	Human	PE/Cy7	1:80
CD34	Human	APC	1:50
CD38	Human	Brilliant Violet 711	1:25
CD45	Human	FITC	1:100
CD45RA	Human	PerCP/Cy5.5	1:50
CD90	Human	PE	1:50
Biotin		V500 streptavidin	1:50
PI			1 µg/mL

Table 2.19: Antibody panel for assessment of human stem and progenitor populations in patient derived xenografts

2.2.12 RNAi studies

shRNA inserts utilised in inducible RNAi studies were sub-cloned from plasmid vectors with a pGIPZ backbone that constitutively express shRNAs (GIPZ Human Protein

Kinase Gene Family Library #RHS6039, Dharmacon) into the tetracycline responsive TtRMPVIR (27995, addgene) vector using the DNA cloning techniques detailed in section 2.2.3, located on page 64. The shRNA sequences used are listed in Table 2.20 below.

As shRNA inserts in the pGIPZ backbone are cloned between MluI and XhoI restriction sites, TtRMPVIR was modified to introduce a new MluI restriction site to enable sub-cloning of shRNA inserts. This was achieved by ligating the annealed oligonucleotide sequence GATCGAATTCACGCGTGAATTC, following EcoRI restriction enzyme digest of both the oligonucleotide and TtRMPVIR, into the sole EcoRI restriction site found on TtRMPVIR. The EcoRI digested TtRMPVIR vector was treated with calf intestinal phosphatase to prevent recircularisation of digested vector during ligation and purified using the Wizard® SV Gel and PCR Clean-Up System (Promega) according to manufacturer's instructions. Insertion of the MluI restriction site was confirmed by double restriction enzyme digest with MluI and EcoRV, where successful insertion of MluI resulted in the generation of novel 6285 bp and 2768 bp products identified through visualisation on an 1% [w/v] agarose gel.

shRNA inserts were then excised from plasmid vectors with a pGIPZ backbone through double restriction digest with MluI and XhoI. The approximately 300 - 400 bp inserts were isolated on a 2% [w/v] agarose gel and purified using a QIAquick gel extraction kit (QIAGEN) as per manufacturer's instructions. Similarly, the successfully modified TtRMPVIR vector was double digested with MluI and XhoI restriction enzymes and gel purified to create a donor template for subsequent ligation of shRNA inserts. Ligation of shRNA inserts and the modified TtRMPVIR vector was performed as described in section 2.2.3, page 64. Successful ligation of shRNA inserts was confirmed by double restriction enzyme digest with MluI and BglII, where successful ligation resulted in the identification of a larger, approximately 1700 bp product on an 1% [w/v] agarose gel compared to digestion of empty vector which produces a 1300 bp product. Successful ligation of shRNA inserts was confirmed by Sanger sequencing using the standard miR30 5' sequencing primer: TGTTTGAATGAGGCTTCAGTAC.

For competitive proliferation assays, retrovirus transduced cells were sorted for shRNA-containing ($Venus^+/YFP^+$) and non shRNA-containing (YFP^+ only) populations and recombined at a 1:1 ratio. Retroviral transduction was performed as described in section 2.2.7, page 68. Following this, cells were cultured with 1 mg/mL doxycycline to induce

shRNA expression. The proportion of shRNA-expressing (dsRED$^+$/Venus$^+$/YFP$^+$) cells were determined by flow cytometric analysis and followed over time. To achieve this, cells were passaged 1:20 every 48 hours in doxycycline containing media and an aliquot washed twice with FACS buffer prior to flow cytometric analysis. mRNA knockdown efficiency of shRNA-expressing (dsRED$^+$/Venus$^+$/YFP$^+$) and non shRNA-containing cells (YFP$^+$) was assessed by qRT-PCR (section 2.2.13, page 77) and immunoblotting (section 2.2.14, page 78), 48 to 72 hours after doxycycline exposure, following FACS isolation.

shRNA directed against APC were cloned into pLMPC (pMSCV-miRE-PGK-PuroR-IRES-mCherry) and were a kind gift from Dr Johannes Zuber. Constitutive expression of shRNAs was linked to mCherry expression. After retroviral transduction (detailed in section 2.2.7, page 68), the proportion of mCherry positive cells was determined by flow cytometric analysis following treatment with vehicle (0.1% [v/v] DMSO) or I-BET151 and observed over time. Cells were passaged 1:20 every 48 hours at which time an aliquot was obtained and washed twice with FACS buffer prior to flow cytometric analysis. Selective advantage consequent to shRNA expression results in enrichment of mCherry positive cells. Knockdown efficiency of APC mRNA in shRNA-expressing cells was assessed following FACS isolation of mCherry positive cells by qRT-PCR (section 2.2.13, page 77). The detailed validation of shRNAs directed against APC can be found in Rathert et al.[230].

shRNA	Target	Sequence
#2253	APC	ACACGAAGAAGAGAGATTCGAA
#498	BRD4	ACTATGTTTACAAATTGTT
#499	BRD3/4	AGGACTTCAACACTATGTT
#500	BRD4	AGCAGAACAAACCAAAGAA
#5011	APC	TGACGATGATATTGAAATATTA
#793	Renilla	TAGATAAGCATTATAATTCCTA
#851	BRD2	CGGATTATCACAAAATTAT

Table 2.20: shRNA sequences

2.2.13 Quantitative real-time RT-PCR

mRNA was prepared using the Qiagen RNeasy kit and cDNA synthesis was performed using the SuperScript™ VILO™ kit (Life Technologies) as per manufacturer's instructions. Quantitative PCR analysis was undertaken on an Applied Biosystems StepOnePlus System with Fast SYBR® Green reagents (Life Technologies).

To extract RNA, cells were pelleted by centrifugation and lysed through the addition of 350 μL of the guanidine thiocyanate containing buffer RLT supplemented with 0.01% [v/v] β-mercaptoethanol. Samples were mixed thoroughly with a vortex mixer. An equivalent volume of isopropanol was then added to enhance binding of RNA to silica based membrane columns prior to transfer of the sample RNeasy spin columns and centrifugation at 8,000 g for 15 seconds. Columns were washed once with 350 μL of buffer RW1 prior to on-column DNase digestion. 10 μL (30 units) of DNase I was diluted in 70 μL of buffer RDD prior to application to and incubation of columns at room temperature for 15 minutes. Following DNase digestion, DNase solution, excess salt and protein contaminants were removed from columns by washing once with 350 μL of buffer RW1 followed by two washes with 500 μL of buffer RPE. During the second wash, columns were spun at 8,000 g for 2 minutes to remove any residual ethanol prior to elution of RNA. 30 μL of ultra pure H_2O was added to the centre of the spin column prior to centrifugation at 8,000 g for 1 minute and collection of eluted RNA into micro-centrifuge tubes.

First strand cDNA synthesis was performed in 20 μL reaction volumes by adding 4 μL SuperScript™ VILO™ master mix to 500 ng RNA made up to 16 μL with ultra pure H_2O. The proprietary SuperScript™ VILO™ master mix contains SuperScript™ III reverse transcriptase, RNaseOUT™ Recombinant Ribonuclease Inhibitor, random primers, $MgCl_2$ and dNTPs. Samples were initially incubated at 25°C for 10 minutes prior to cDNA synthesis through incubation at 42°C for 60 minutes. Reactions were inactivated for 5 minutes at 85°C.

Primers utilised for qRT-PCR are detailed in section 2.1.8, located on page 60. 10 μL reaction volumes were used on 96-well plates containing 5 μL Fast SYBR Green master mix, 0.05 μL forward primer (200 μM), 0.05 μL reverse primer (200 μM), 0.5 μL cDNA and 4.4 μL ultra pure H_2O. Each biological replicate sample was run in triplicate

technical replicate. PCR amplification was performed with an initial step of 20 seconds at 95°C, followed by 40 cycles of 95°C at 3 seconds and 30 seconds at 60°C.

For analysis of murine cell line samples, expression levels were determined using the ΔCT method and normalised to beta-2-microglobulin (*B2m*) and/or *Gapdh*. Differences in expression were assessed using a *t*-test for statistical significance.

For determination of baseline WNT/β-catenin pathway and target gene expression in primary human AML samples, expression relative to the mean of all samples was determined using the ΔCT method and normalised to GAPDH and actin.

2.2.14 Immunoblotting

Preparation of mammalian cell samples for immunoblotting was achieved by lysis of approximately 1×10^6 cells through the addition of 200 μL Western sol buffer (0.5 mM EDTA, 20 mM HEPES, 2% [w/v] SDS). Lysed cells were then sonicated using the high setting (Bioruptor, Diagenode) for 5 minutes (30 seconds on, 30 seconds off).

To ensure equal well loading, protein concentrations were determined using the colorimetric Bio-Rad DC protein assay according to manufacturer's instructions. In 96-well microplates, 5 μL of whole cell lysate samples were combined with 25 μL of reagent A, an alkaline copper tartrate solution containing a 1:50 dilution of reagent S, a surfactant. 200 μL of reagent B, a dilute Folin reagent, was then added and mixed thoroughly. Reduction of the Folin reagent by detergent solubilised, copper treated proteins in an alkaline medium results in colour change which is directly proportional to protein concentration. As such, following a 15 minute incubation period, absorbance was read at 750 nm using a POLARstar Optima microplate fluorescence reader (BMG Labtech) and compared a standard curve generated from measurement of absorbance of solutions containing known concentrations of BSA to determine protein concentration.

Subsequently, proteins were resolved in 8-20% [v/v] acrylamide gels according to size using the standard Laemmli procedure of one-dimensional gel electrophoresis under denaturing and reducing conditions. The mini-protean tetra cell gel apparatus (Bio-Rad) was assembled and utilised according to manufacturer's instructions. 0.75 mm spacers and combs were used. 10% resolving gels were prepared by mixing 1.25 mL 40% [v/v] acrylamide (37.5:1 acrylamide:bisacrylamide), 1.25 mL 1 M Tris-HCl pH 8.8, 50 μL

10% [w/v] SDS and 2.4 mL ddH_2O. Gels with lower or higher acrylamide concentrations were prepared by adjusting the volumes of acrylamide and ddH_2O. 50 μL of 10% [w/v] ammonium persulfate (APS) and 5 μL tetramethylethylenediamine (TEMED) were added to initiate polymerisation of the acrylamide. The gel solution was then applied between sandwiched glass plates until the height of the solution was 2 cm from the top of the small plate. Isopropanol was overlaid on the top of the gel to ensure the top of the resolving gel was set evenly during polymerisation. The overlaid isopropanol was removed following polymerisation. A stacking gel was prepared by mixing 1.25 mL 40% [v/v] acrylamide (37.5:1 acrylamide:bisacrylamide), 1.25 mL 1 M Tris-HCl pH 6.8, 100 μL 10% [w/v] SDS and 6.3 mL ddH_2O, 100 μL of 10% [w/v] APS and 10 μL TEMED. The solution was applied to the glass sandwich overlaying the resolving gel, a comb inserted into the stacking solution and the gel left to polymerise.

Prior to loading onto gels, protein samples were denatured by boiling in 1x SDS loading buffer (200 mM Tris-HCl pH 6.8, 20% [v/v] β-mercaptoethanol, 2% [w/v] SDS, 0.1% [w/v] bromophenol blue, 40% [v/v] glycerol) for 10 minutes. 10 μg of protein was equally loaded into each well. Gels were electrophoresed in Tris-glycine running buffer (25mM Tris-HCl, 250 mM glycine, 0.1% [w/v] SDS) at 150-200 V. Pre-stained high molecular weight protein markers were run alongside the samples (Bio-Rad).

Proteins were transferred from polyacrylamide gels to polyvinylidene fluoride (PVDF) membranes (Millipore) using the mini-protean tetra blotting apparatus (Bio-Rad). Following electrophoresis, gels were transferred into transfer buffer (50mM Tris-HCl, 580 nM glycine, 0.1% [w/v] SDS, 20% [v/v] methanol) and sandwiched next to a PVDF membrane between two pieces of Whatman 3MM filter paper and two sponge pads. The completed sandwich was inserted into the blotting apparatus such that the PVDF membrane was facing the positive anode. The blotting apparatus was filled with ice cold transfer buffer maintained at 4°C and gels transferred overnight at 20V.

Following protein transfer, membranes were blocked in membrane blocking solution (TBS with 0.05% [v/v] Tween-20, 5% [w/v] non-fat milk powder) for 1 hour prior to being washed twice with TBS-T (TBS with 0.05% [v/v] Tween 20) for 10 minutes. The membrane was then probed with primary antibody diluted in blocking buffer (detailed in Table 2.4, page 57) with gentle agitation overnight at 4°C. Membranes were washed twice with TBS-T for 10 minutes prior to incubation with secondary antibodies

conjugated with horseradish peroxidase (Invitrogen) for 1 hour. Proteins were detected by exposure to x-ray film after further washing membranes twice with TBS-T for 10 minutes and incubation with Amersham ECL chemiluminescent detection reagents (GE Healthcare Lifesciences) according to manufacturers instructions.

2.2.15 Examination of drug efflux and metabolism by quantitative mass spectrometry

Between 2×10^5 and 3×10^5 cells per well were seeded in 24-well plates and treated with vehicle (0.1% [v/v] DMSO) or 600 nM I-BET151. Following 48 hours, cells were harvested by centrifugation, washed twice in ice cold PBS and lysed in 500 μL M-PER buffer (Thermo Scientific). Base media, supernatant, wash and cell lysates were quenched with 5% acetonitrile (aq) containing labetalol at 62.5 ng/mL as the internal standard. These samples, in addition to serial dilutions of I-BET151 used to generate standard curves, were then analysed by mass spectrometry. Mass spectrometry was performed by Dr Richard Gregory of the GSK Medicines Research Centre (Gunnels Wood Road, Stevenage, Hertfordshire, SG1 2NY, United Kingdom).

HPLC-mass spectrometry apparatus and conditions: The HPLC system was an integrated CTC PAL auto sampler (LEAP technologies), Jasco XTC pumps (Jasco). The HPLC analytical column was an ACE 2 C18 30mm × 2.1mm (Advanced Chromatography Technologies) maintained at 40°C. The mobile phase solvents were water containing 0.1% formic acid and acetonitrile containing 0.1% formic acid. A gradient ran from 5% to 95% acetonitrile + 0.1 % formic acid up to 1.3 minutes, was held for 0.1 minutes and returned to the starting conditions over 0.05 minutes then held to 1.5 minutes at a flow rate of 1 mL/min. A divert valve was utilised so the first 0.4 min and final 0.2 minutes of flow were diverted to waste.

Mass spectromic detection was performed using an API 4000 triple quadrupole instrument (AB Sciex) with multiple reaction monitoring (MRM). Ions were generated in positive ionization mode using an electrospray interface. The ionspray voltage was set at 4000 V and the source temperature was set at 600°C. For collision dissociation, nitrogen was used as the collision gas. The MRM of the mass transitions for I-BET151 (m/z 416.17 to 311.10), and Labetalol (m/z 329.19 to 162.00), were used for data acquisition.

Data interpretation: Data was collected and analysed using Analyst 1.4.2 (AB Sciex), for quantification, area ratios (between analyte/internal standard) were used to construct a standard line, using weighted ($1/x^2$) linear least squared regression, and results extrapolated the area ratio of samples from this standard line.

2.2.16 Murine models of leukaemia

Primary syngeneic transplantation studies of stably growing derived vehicle treated or resistant cell lines in limit dilution analyses were performed with intravenous tail vein injection of between 10 to 2×10^6 cells per mouse.

Serial syngeneic transplantation studies of drug efficacy, generation of *in vivo* resistance and limit dilution analyses were performed with intravenous injection of between 10 to 2.5×10^6 cells per mouse obtained from bone marrow or spleen. Treatment with vehicle or I-BET151 at 20-30 mg/kg began between days 9-13. Pyrvinium, alone or in combination with I-BET151, was delivered between days 9 & 26.

Following stable retroviral transduction of resistant cell lines with a DKK1 containing construct, 5×10^6 cells per mouse were injected intravenously in primary syngeneic transplants. Treatment with vehicle or I-BET151 at 20 mg/kg began at day 16.

Syngeneic transplantation studies were performed in C57BL/6 mice (wild type or expressing $Ptprc^a$). All mice were 6-10 weeks old at the time of sub-lethal irradiation (300 cGy) and intravenous cell injection. Treatment with vehicle, I-BET151 or pyrvinium was commenced following engraftment of leukaemia as determined by >1% YFP expression in peripheral blood in the majority of mice. Mice were randomly assigned treatment groups; treatment administration was not blinded. Sample sizes were determined according to the resource equation method. Differences in Kaplan-Meier survival curves were analysed using the log-rank statistic.

Patient derived xenograft studies were performed in NOD/SCID/$Il2rg^{-/-}$ (NSG) mice. All mice were 6-10 weeks old at the time of sub-lethal irradiation (200 cGy) and intravenous cell injection of 1×10^5 to 5×10^5 cells per mouse. Treatment with vehicle or I-BET151 at 10 mg/kg for a 2 week period began upon detection of >1% circulating human $CD45^+$ cells in mouse peripheral blood at week 14. Treatment cohorts were matched for transplant generation. Mice were randomly assigned treatment groups; treatment administration was not blinded.

I-BET151 was dissolved in DMSO prior to suspension in normal saline containing 10% [w/v] Kleptose HPB to give a 5% [v/v] DMSO final concentration. I-BET151 was delivered daily (5 days on, 2 days off) by IP injection (10 mL/kg) with dose reduction of I-BET151 undertaken if evidence of drug intolerance was observed.

Pyrvinium was dissolved in DMSO prior to suspension in normal saline to give a 15% [v/v] DMSO final concentration. Pyrvinium was delivered daily by IP injection (10 mL/kg). Dosing of pyrvinium was commenced at 0.1 mg/kg and escalated in 0.1 mg/kg increments every second dose to a maximal dose of 0.5 mg/kg.

All mice were kept in a pathogen free animal facility, inspected daily and sacrificed upon signs of distress/disease. All experiments were conducted under either UK home office regulations or institutional animal ethics review board in Australia. Statistical analyses of limit dilutions to identify the frequency of leukaemia initiating cells in transplanted cell populations were undertaken according to the method of Hu and Smyth utilising the web-tool accessed at http://bioinf.wehi.edu.au/software/elda/ [231].

2.2.17 Mouse tissue sample preparation

Peripheral blood samples were collected via tail vein bleeds in EDTA treated tubes (Sarstedt) and counted using a XP-100 analyser (Sysmex). Cell cytospins and blood smears were stained with the Rapid Romanowsky Staining Kit (Thermo Fisher Scientific).

Mice were humanely euthanized prior to harvest of bone marrow from pelvic bones, femurs and tibias. Bones were flushed with cold PBS and the resultant cell suspension passed through a 40μm filter. Prior to use in downstream applications (such as immunophenotype assessment by flow cytometry, viral transduction, DNA/RNA extraction, syngeneic transplant), bone marrow samples were subjected to red blood cell lysis. Following centrifugation at 400 g for 10 minutes, samples were resuspended in10 mL cold RBC lysis buffer per 1×10^7 cells, incubated on ice for 10 minutes and washed twice with an equivalent volume of cold PBS.

2.2.18 Sanger sequencing

DNA was extracted from cell lines using the DNeasy blood and tissue kit (Qiagen) according to manufacturers instructions. Harvested cells were pelleted by centrifugation at 300 g for 5 minutes prior to resuspension in 200 μL PBS. Cells were lysed through the addition of 200 μL buffer AL with 20 μL proteinase K (600 mAU/ml) added to digest protein contaminants. Samples were subsequently mixed thoroughly and incubated at 56°C for 10 minutes. 200 μL ethanol was added and thoroughly mixed to enhance binding of DNA to silica membrane columns prior application of the entire sample to DNeasy mini spin columns and centrifugation at 6,000 g for 1 minute. Columns were then washed once with 500 μL buffer AW1 and centrifuged at 6,000 g for 1 minute prior to a second wash with 500 μL buffer AW2 and centrifugation at 6,000 g for 1 minute. Columns were spun at 20,000 g for 3 minutes to ensure membranes were dry prior to elution of DNA. 200 μL of ultra pure H_2O was added to the centre of column membranes prior to centrifugation at 6,000 g for 1 minute and collection of eluted DNA into micro-centrifuge tubes.

Eluted DNA was quantified using a NanoDrop spectrophotometer (Thermo Scientific) and sent for sequencing at a commercial laboratory (Centre for Translational Pathology, Department of Pathology, University of Melbourne) using the primers described in Table 2.10.

2.2.19 Exome capture sequencing

DNA was extracted from cell lines using the DNeasy blood and tissue kit (Qiagen) according to manufacturers instructions as described above in section 2.2.18, page 83. Eluted DNA was quantified using the Qubit dsDNA HS Assay (Life Technologies) prior to fragmentation to a peak size of approximately 200 bp using the focal acoustic device, SonoLab S2 (Covaris). Library preparations were performed using the SureSelect^{XT} Target Enrichment System for Illumina Paired-End Sequencing Library protocol (Agilent Technologies) with the SureSelect^{XT} Mouse All Exon Kit for the capture process (Agilent Technologies). The quality of libraries submitted for sequencing were assessed using the High Sensitivity DNA assay on the 2100 bioanalyzer (Agilent technologies, Santa Clara, CA). Libraries were quantified with qPCR, normalised and pooled to 2 nM before sequencing with paired end 100 bp reads

using standard protocols on the HiSeq2500 (Illumina). Library preparation, quality control and sequencing were performed by the Molecular Genomics Core Facility (Peter MacCallum Cancer Centre).

The Fastq files generated by sequencing were aligned to the mm10 mouse reference genome using bwa[232]. Copy number variation was analysed using ADTEx[233] to compare the depth of coverage in resistant and vehicle treated clones with the parental cell line. Variant calling was performed with VarScan2[234], MuTect[235] and GATK HaplotypeCaller[236]. The Ensembl Variant Effect Predictor (VEP)[237] was used to predict the functional effect of the identified variants. Mutations detected by at least two variant callers were further analysed for shared mutations between cell lines and mutation spectrum. Genomic regions with coverage of at least 8 reads in all libraries were analysed for the frequency of mutations. Coding exonic, UTRs and intronic regions were obtained from the UCSC Table Browser[238]. Upstream regions were defined as 1000 bp upstream of genes, downstream regions were defined as 1000 bp downstream of genes, and intergenic regions were over 1000 bp from genes. Bioinformatic analysis of exome capture data was performed with the assistance of Dr Enid Lam (Dawson Laboratory, Peter MacCallum Cancer Centre).

2.2.20 Chromatin Immunoprecipitation assay, real-time PCR and sequencing analysis

Chromatin immunoprecipitation (ChIP) was performed on stably growing cell lines with approximately 20×10^6 cells harvested per condition. Cells were cross-linked with 1% formaldehyde for 15 minutes at room temperature with gentle agitation on an orbital shaker. Cross-linking was stopped by the addition of 0.125 M glycine and gentle agitation for 5 minutes on an orbital shaker. Cells were then pelleted by centrifugation at 400 g for 5 minutes, washed twice with cold PBS and subsequently lysed in 300 µL ChIP lysis buffer (1% [w/v] SDS, 10 mM EDTA, 50 mM Tris-HCl pH 8.0 and protease inhibitors). Lysates were sonicated in a Covaris ultrasonicator to achieve a mean DNA fragment size of 500 bp. Chromatin was pelleted prior to resuspension in modified RIPA buffer (1% [v/v] Triton X, 0.1% [w/v] deoxycholate, 90 mM NaCl, 10 mM Tris-HCl pH 8.0 and protease inhibitors). An aliquot (4% of sample) was stored as input material. Immunoprecipitation was performed for a minimum of 12 hours at 4°C in

modified RIPA buffer using antibodies as detailed in section 2.1.4, page 57. Following this, 50 μL of an equal volume of protein A and G magnetic beads (Life Technologies) were added and used to bind antibodies and associated chromatin for 2 hours at 4°C. Protein A/G magnetic beads were washed twice and equilibrated with modified RIPA buffer prior to addition to samples. Chromatin bound beads were washed twice with 1 mL ChIP wash buffer (0.1% [w/v] SDS, 1% [v/v] Triton X-100, 2 mM EDTA, 150 mM NaCl, 20 mM Tris-HCl pH 8.0) and once with 1 mL of high salt containing ChIP final wash buffer (0.1% [w/v] SDS, 1% Triton X-100, 2 mM EDTA, 500 mM NaCl, 20 mM Tris-HCl pH 8.0). Chromatin was eluted off magnetic beads in 200 μL of elution buffer (1% [w/v] SDS, 100 mM $NaHCO_3$) for 30 minutes at 30°C on a thermal shaker set at 1,000 rpm. The input and immunoprecipitated samples were then mixed with 2 μL of RNase (Roche) and incubated at 65°C overnight to reverse crosslinking of DNA. Reverse crosslinking of DNA was followed by DNA purification using the QIAquick PCR purification kit (Qiagen) as per manufacturer's instructions and detailed in section 2.2.3, page 64.

For qRT-PCR analysis of immunoprecipitated DNA (ChIP PCR), analysis was performed on an Applied Biosystems StepOnePlus System with SYBR green reagents as described in section 2.2.13, page 77. The primer pairs used are detailed in Table 2.11, page 62. Enrichment of immunoprecipitated DNA at *Myc* TSS and enhancer regions was compared to a negative control region 20 kb upstream of *Myc*.

For sequencing analysis of immunoprecipitated DNA (ChIP-seq), DNA was quantified using the Qubit dsDNA HS Assay (Life Technologies). Library preparations were performed using the standard ThruPLEX®-FD Prep Kit protocol (Rubicon Genomics) and size selected for 200-400 bp using the Pippen Prep (Sage Science Inc.). Fragment sizes were established using either the High Sensitivity DNA assay or the DNA 1000 kit and 2100 bioanalyzer (Agilent Technologies). Libraries were quantified with qPCR, normalised and pooled to 2 nM before sequencing with single end 50 bp reads using standard protocols on the HiSeq2500 (Illumina). Library preparation, quality control and sequencing were performed by the Molecular Genomics Core Facility (Pete-MacCallum Cancer Centre).

The Fastq files generated by sequencing were aligned to the mm10 mouse reference genome using bwa[232]. Peak-calling was performed using MACS2[239] with default

parameters and the input library as control. Profiles and heat maps of reads and MACS peaks in the 5 kb around TSS were generated with Genomic Tools. Bioinformatic analysis of ChIP-seq data was performed with the assistance of Dr Enid Lam (Dawson Laboratory, Peter MacCallum Cancer Centre).

2.2.21 Expression analysis by microarray and RNA-sequencing

RNA was prepared using the Qiagen RNeasy kit as described in section 2.2.13, page 77. RNA was extracted from cell lines stably maintained in either vehicle (0.1% [v/v] DMSO) or varying concentrations of I-BET151 and harvested mouse tissues (as described in section 2.2.17, page 82).

For microarray analysis, RNA was hybridised to Illumina MouseWG-6 v2 Expression BeadChips. Gene expression data were processed using the lumi package in R. Probe sets were filtered to remove those where the detection p-value (representing the probability that the expression is above the background of the negative control probe) was greater than 0.05 in at least one sample. Expression data was background corrected and quantile normalised. Normalisation and inference of differential expression were performed using limma[240]. Correction for multiple testing was performed using the method of Benjamini and Hochberg[241]. Genes with a false discovery rate below 0.05 and a fold-change greater than 2 were considered significantly differentially expressed. For genes with multiple probe sets, only the probe set with the highest average expression across samples was used. Microarray analysis was performed by Cambridge Genomic Services (Department of Pathology, University of Cambridge). Bioinformatic analysis of microarray data was performed with the assistance of Dr Enid Lam (Dawson Laboratory, Peter MacCallum Cancer Centre).

For RNA sequencing analysis, RNA concentrations were first quantified with the NanoDrop spectrophotometer (Thermo Scientific). The integrity was established using the RNA 6000 kit and 2100 bioanalyzer (Agilent Technologies). Library preparations were performed using the standard TruSeq RNA Sample Preparation protocol (Illumina) with fragment sizes established using the DNA 1000 kit and 2100 bioanalyzer (Agilent Technologies). Libraries were quantified with qPCR, normalised and pooled to 2 nM before sequencing with paired-end 50 bp reads using standard protocols on an Illumina HiSeq2500. Library preparation, quality control and

sequencing were performed by the Molecular Genomics Core Facility (Peter MacCallum Cancer Centre).

Reads were aligned to the mouse genome (Ensembl Release 75, Feb 2014) using Subread[242] and assigned to genes using featureCounts[243]. Differential expression was inferred using limma/voom[240]. Correction for multiple testing using the Benjamini-Hochberg method was performed[241]. Genes with a false discovery rate below 0.05 and a fold-change greater than 2 were considered significantly differentially expressed.

Gene set enrichments were determined using ROAST[244]. ROAST tests for up- or down-regulation of genes in a given pathway were performed on cell lines either stably maintained in vehicle (0.1% [v/v] DMSO) or I-BET. p-values were corrected for multiple testing using the method of Benjamini and Hochberg[241]. Gene sets were obtained from MSigDB[245] and curated. The GSEA terms used are detailed in Table 2.21. Human Entrez accessions from the downloaded gene sets were converted into mouse accessions using orthologue information from the Mouse Genome Database at the Mouse Genome Informatics website (http://www.informatics.jax.org; accessed June 2014). ROAST tests were performed to assess for an enrichment of a L-GMP gene expression signature (GSE4416)[177] and a L-GMP derived from HSC signature (GSE18483)[179] in the I-BET resistant compared with vehicle treated cell lines. The gene expression program associated with human leukaemia stem cells was obtained from GSE30375[227] and analysed with LIMMA[240]. Gene expression of LSC was compared with leukaemia progenitor cells (LPC) and genes upregulated in LSC were analysed for an enrichment of the Wnt/β-catenin pathway using ROAST[244]. Bioinformatic analysis of RNA sequencing data was performed with the assistance of Dr Enid Lam (Dawson Laboratory, Peter MacCallum Cancer Centre) and Dr Alan Rubin (Bioinformatics Division, Walter & Eliza Hall Institute of Medical Research, Melbourne, Australia).

Pathway	GSEA Terms
WNT/beta-catenin	ST_WNT_BETA_CATENIN_PATHWAY
JAK/STAT	KEGG_JAK_STAT_SIGNALING_PATHWAY
PI3K/AKT/mTOR	REACTOME_PI3K_AKT_ACTIVATION
nF-kB	REACTOME_ACTIVATION_OF_NF_KAPPAB_IN_B_CELLS
RAS/ERK/MAPK	KEGG_MAPK_SIGNALING_PATHWAY
NOTCH	KEGG_NOTCH_SIGNALING_PATHWAY
hippo	REACTOME_SIGNALING_BY_HIPPO
hedgehog	KEGG_HEDGEHOG_SIGNALING_PATHWAY
TGP-beta	KEGG_TGF_BETA_SIGNALING_PATHWAY

Table 2.21: GSEA terms

2.2.22 Correlation of expression of WNT/β-catenin pathway expression and response to I-BET151

A principal component analysis was performed on the qRT-PCR data of β-catenin pathway and target gene expression from primary human AML samples obtained as described in section 2.2.13, page 77. Pearson's correlation was calculated between the expression of the pathway genes in the first principal component, and the responsiveness to I-BET151.

Correlation of log gene expression of selected WNT/β-catenin pathway genes was assessed using a corrgram and correlation between log expression and apoptosis was examined using scatterplots. As expression between genes was typically highly correlated, or inversely correlated, the log-expression data was summarised using the first principle component and compared to the level of apoptosis. A multiple linear regression model was also fitted to the data. As the full model was close to saturated (8 samples, 6 genes), a stepwise model selection procedure based on the Akaike Information Criteria (AIC), which was implemented in the R function STEP, was used. The model that minimized the AIC excluded one gene (*AXIN2*). Statistical analysis of expression data was performed with the assistance of Professor Anthony Papenfuss (Bioinformatics Division, Walter & Eliza Hall Institute of Medical Research, Melbourne, Australia).

Chapter 3 - Establishing ex vivo models of BET Inhibitor Resistance

3.1 Generation of a clonal murine model of resistance to BET inhibition using MLL-AF9 transformed HSPCs

To generate a model of resistance to the novel epigenetic targeted therapies know as the BET inhibitors, a clonal approach was undertaken in a clean genetic background using magnetic bead selection of c-kit positive HSPCs obtained from whole bone marrow of C57BL/6 mice (Figure 4). This approach was utilised as previous attempts by our laboratory, and the experience of others (unpublished data), to generate models of resistance through stepped escalation of BET inhibitor exposure in human MLLfp bearing cell lines (MV4;11, MOLM13 and NOMO1) have been unsuccessful.

Murine HSPCs were transformed using a retroviral human MLL-AF9 construct to generate an immortal primary cell line. Previous work has demonstrated the exquisite sensitivity of this model system to both genetic and pharmacologic inhibition of BET proteins.[75,181] Furthermore, this system has served as an effective model of LSC hierarchy and is able to faithfully recapitulate human leukaemia in an *in vivo* setting.[177,178]

Following stable generation of a parental cell line in liquid culture, cells were plated in cytokine supplemented methylcellulose and exposed to either 0.1% DMSO (vehicle) or I-BET151 at the IC_{50} value of the parental cell line (400 nM) (Figure 6b). Cytokine supplemented and nutrient enriched methylcellulose is designed to support optimal growth of progenitor cells and is a more permissive *in vitro* environment, allowing for cellular adaptation, as compared with standard liquid culture.[246] Cells were serially passaged at weekly intervals with the robust generation of resistant colonies observed after eight weeks. In order to follow the fate of individual clones, blast colonies (each derived from a single cell) were isolated and transferred to liquid culture. Although multiple colonies were independently isolated at each passage, only a minority of either vehicle treated or resistant colonies were successfully able to generate clonal cell lines

due to the paucity of isolated cells or culture contamination. In all, four independent vehicle-treated and five independent BET inhibitor resistant cell lines were established. Thereafter, the selective pressure imposed upon BET inhibitor resistant cell lines was sequentially escalated over a six month period to establish clones stabling growing at various concentrations, including those greater than the IC_{90} value of the parental and vehicle treated cells (1 μM I-BET151).

To control for bystander effects and dissect the true genetic, epigenetic and signalling alterations accounting for acquired resistance, vehicle-treated clones were subjected to an identical passage procedure in methylcellulose and liquid culture. The vehicle-treated and BET inhibitor resistant cell lines were maintained under constant exposure to vehicle or drug, whilst the parental cell line was continuously maintained in liquid culture with no exposure to vehicle or drug.

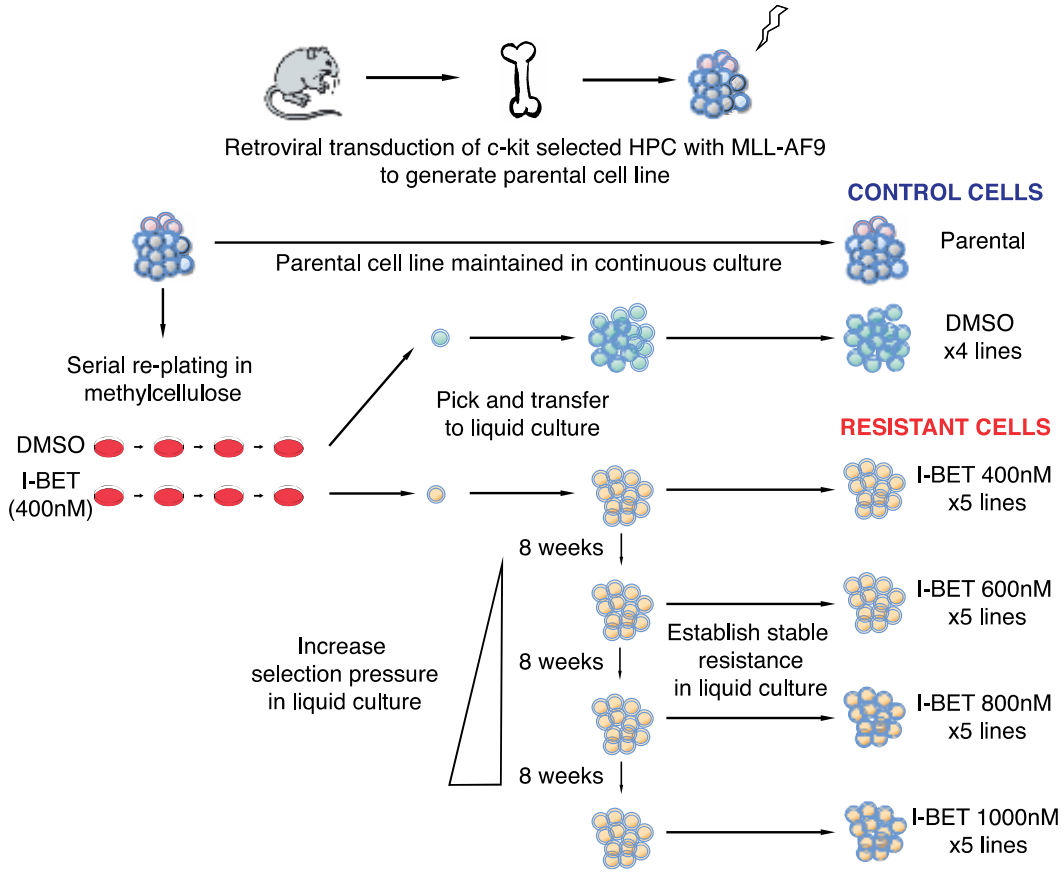

Figure 4 – Generation of murine MLL-AF9 model of resistance

Strategy for the generation of clones resistant to BET inhibition utilising a primary murine MLL-AF9 model of HSPCs.

3.2 Generation of a murine model of resistance to BET inhibition using MLL-ENL transformed HSPCs

An independent MLL-ENL bearing murine model of BET inhibitor resistance was similarly generated through retroviral transformation of c-kit positive HSPCs obtained from C57BL/6 mice (Figure 5).

Following transformation, cells were again plated in cytokine supplemented methylcellulose and exposed to either 0.1% DMSO (vehicle) or I-BET151 at the IC_{50} value of the parental cell line (Figure 13b). In the generated MLL-ENL model, bulk populations of cells as opposed to individual colonies were transferred to liquid culture following the robust generation of resistant colonies. This process increased the reliability of stable cell line generation. Robust colony formation was observed after six weeks.

In all, five vehicle-treated and five BET inhibitor resistant cell lines were established. Selective pressure was subsequently escalated to establish cell lines which were stably growing at greater than the IC_{90} value of the vehicle-treated cells (1 μM I-BET151).

Vehicle-treated and BET inhibitor resistant cell lines were maintained under constant exposure to vehicle or drug and identically passaged in methylcellulose and liquid culture. The parental cell line was continuously maintained in liquid culture with no exposure to vehicle or drug.

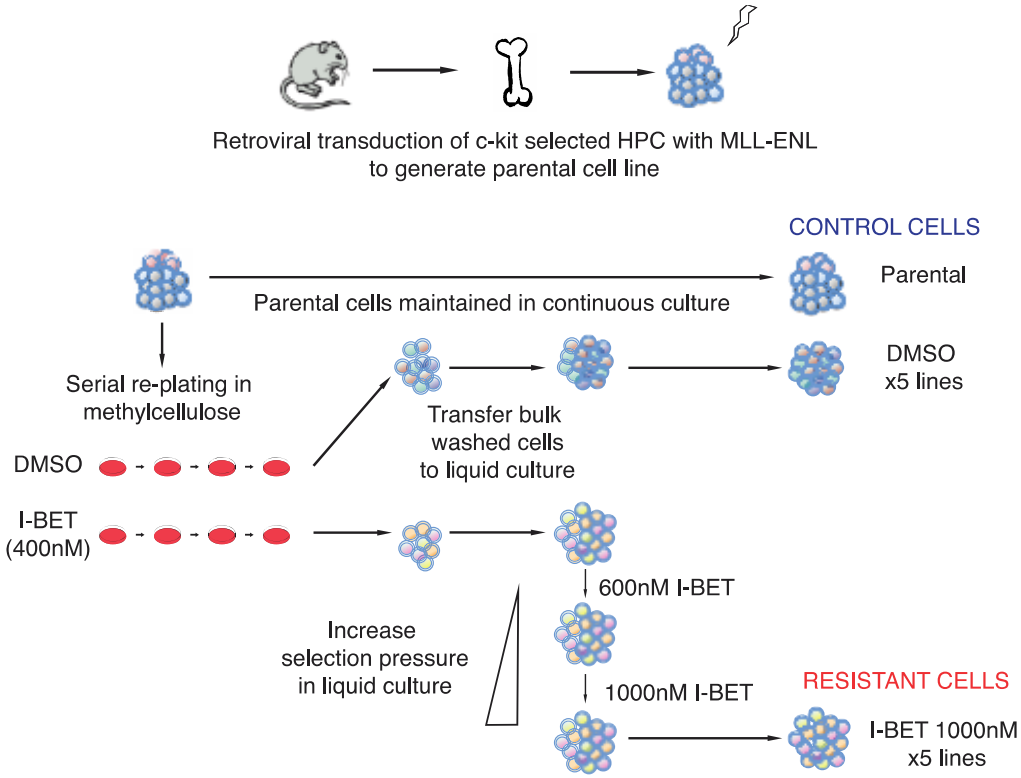

Figure 5 – Generation of murine MLL-ENL model of resistance

Strategy for the generation of clones resistant to BET inhibition utilising a primary murine MLL-ENL model of HSPCs

3.3 Resistant cells are impervious to pharmacological BET inhibition

3.3.1 Proliferation, apoptosis, cell cycle and clonogenic assays in MLL-AF9 cells

Direct comparison of derived cell lines demonstrate that although vehicle-treated clones remained exquisitely sensitive to I-BET151 mediated suppression of proliferation, induction of apoptosis, cell cycle arrest and loss of clonogenic capacity, resistant clones were impervious to these established phenotypic responses.

Examination of the proliferative capacity of resistant clones demonstrates no inhibition despite exposure to 1 μM I-BET151, a concentration greater than the IC_{90} of the vehicle-treated clones or the parental cell line (Figure 6a). Indeed, in assays of cell proliferation to determine the concentration of inhibitor resulting in half-maximal response (IC_{50}), the IC_{50} of resistant clones were more than four times that of corresponding vehicle-treated clones (Figure 6b). Of note, clones stably resistant at higher concentrations of I-BET151 demonstrate increased levels of therapeutic resistance (Figure 6c, Figure 9b).

Intracellular fluorescent labelling using carboxyfluorescein diacetate succinimidyl ester (CFSE) was used to track the proliferation of control and vehicle clones in response to I-BET151 treatment. Discrimination of successive rounds of cell division is achieved through flow cytometric analysis of covalently bound CFSE which is divided equally between daughter cells. Resistant clones demonstrate minimal inhibition of proliferative activity in the presence of I-BET151, whereas cell division is impaired in vehicle treated control clones (Figure 7).

Rapid induction of apoptosis and profound G0/G1 cell-cycle arrest is demonstrated in sensitive AML cells following treatment with all classes of BET inhibitors.[75,181] Whilst these effects were observed in vehicle-treated control clones, induction of apoptosis was not prominent in resistant clones (Figure 8). Furthermore, no effect on cell-cycle progression was observed in resistant clones despite increasing concentrations of I-BET151 (Figure 9a).

Confirming the phenotype of resistant clones, clonogenic assays demonstrate no inhibition of colony formation following treatment of resistant-clones with 1 μM I-BET151 (Figure 10).

Finally, morphological analysis of cells by light microscopy demonstrated no significant difference between sensitive and resistant clones (Figure 11).

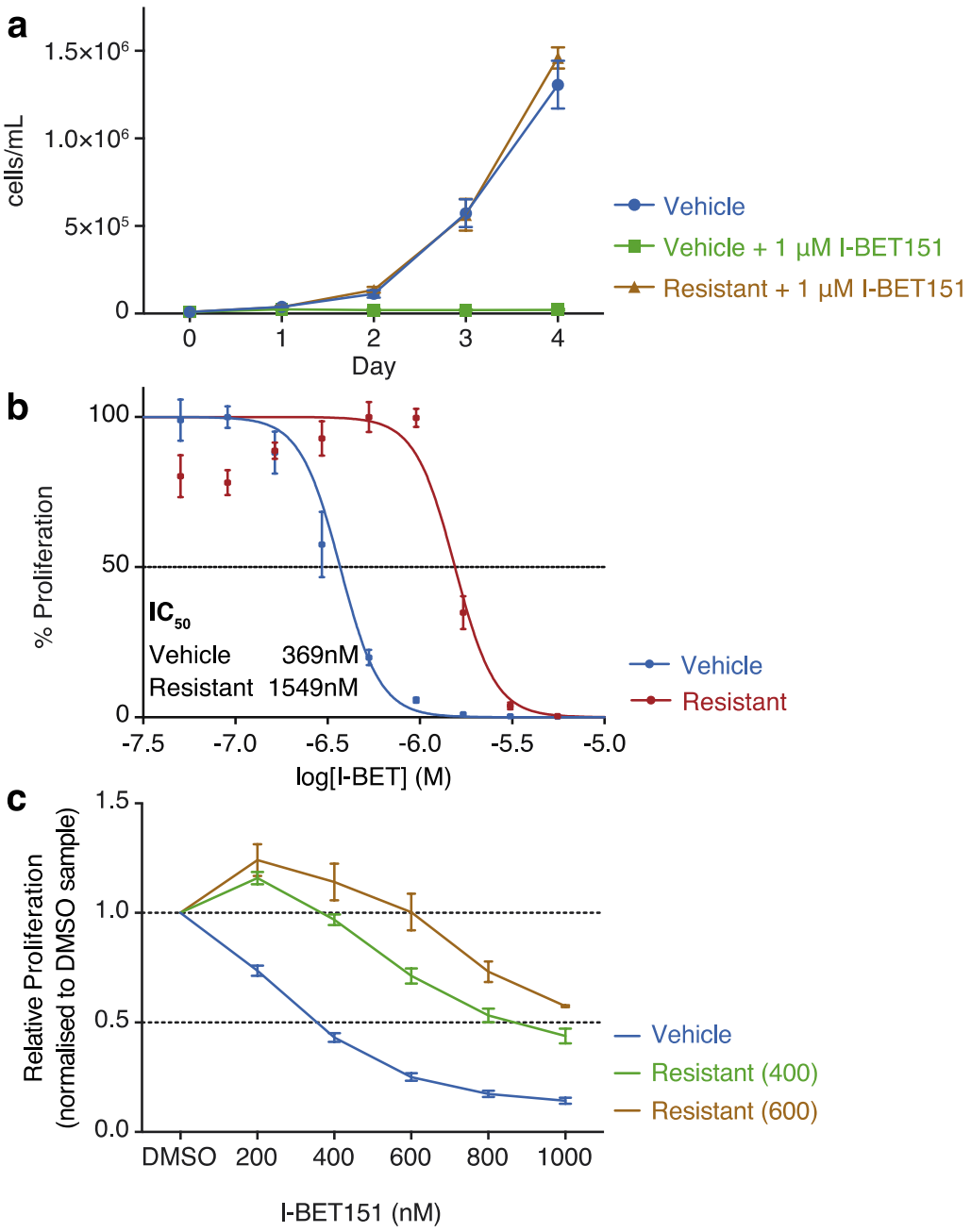

Figure 6 – MLL-AF9 proliferation assays

Resistance to I-BET151 of derived MLL-AF9 cell lines is demonstrated in cell proliferation assays. ***a****, Daily cell counts of vehicle-treated and resistant clones seeded at 1 × 10⁴ cells/mL, performed in biological triplicate (mean ± s.d.).* ***b****, Representative dose-response curve of a vehicle-treated clone and a resistant clone stably maintained in 1 μM I-BET151 after 72hrs of drug exposure (mean ± s.d., n = 4 per group).* ***c****, Resistant cell lines stably maintained at increasing concentrations of I-BET151 (400 nM and 600 nM respectively) demonstrate increased levels of therapeutic resistance in dose-response curves after 72hrs of drug exposure (mean ± s.e.m., n = 6 per group).*

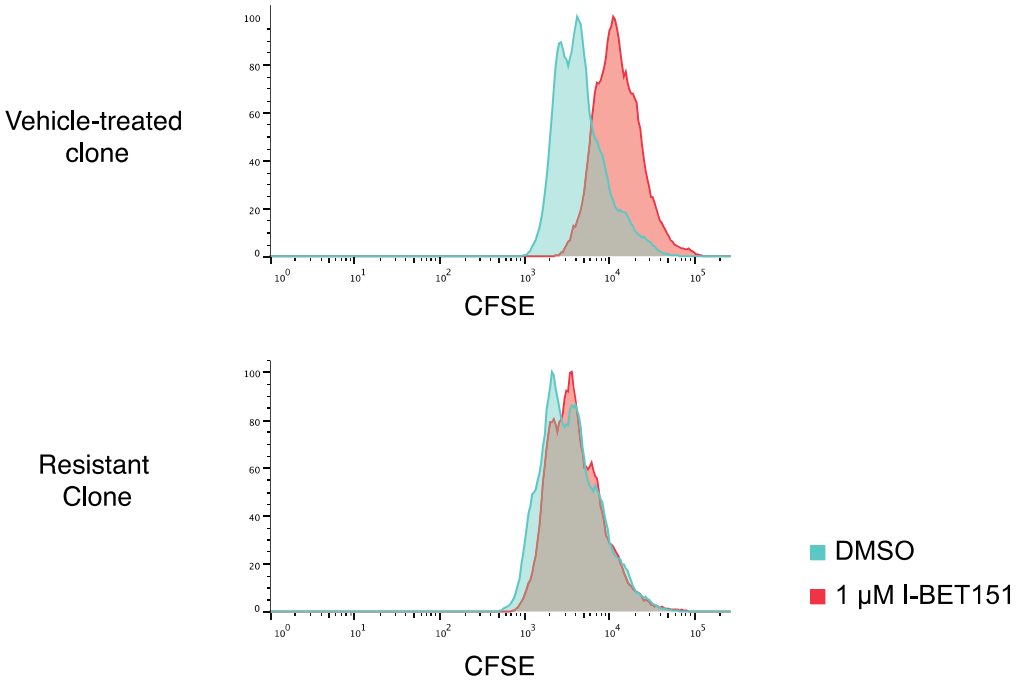

Figure 7 – MLL-AF9 CFSE assays

Examination of proliferative capacity following CFSE labelling of vehicle-treated and resistant clones. Resistant clones demonstrate no impairment in proliferative capacity despite exposure to 1 µM I-BET151. Representative flow cytometric analysis following 72hrs of drug exposure is presented.

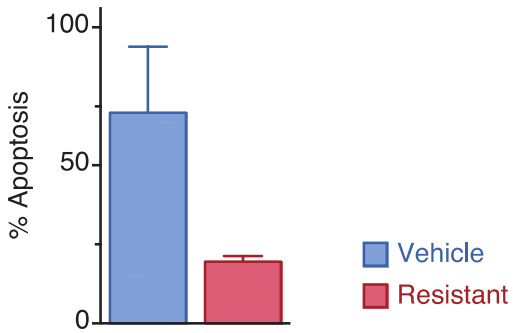

Figure 8 – MLL-AF9 apoptosis assays

Resistance to I-BET151-mediated induction of apoptosis in derived MLL-AF9 cell lines is observed in flow cytometric assays of apoptosis. Proportions of apoptotic cells (annexin V and/or PI positive) following 72 hours of exposure to 1 µM I-BET151 observed in biological triplicate experiments (mean ± s.e.m.) are presented.

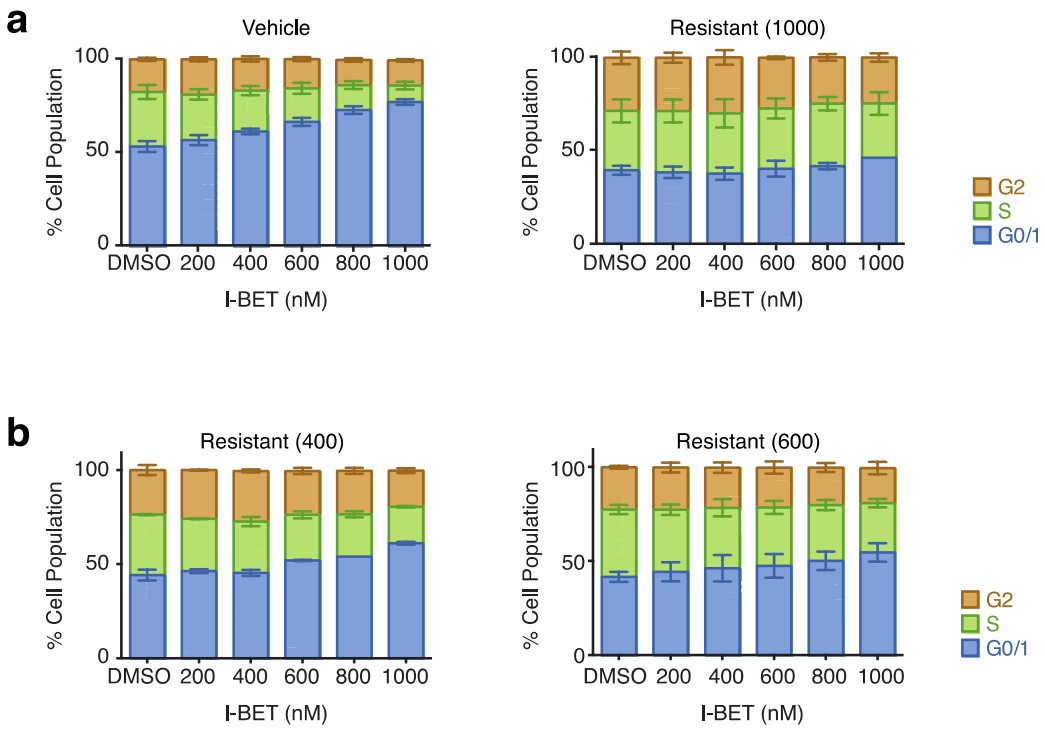

Figure 9 – MLL-AF9 cell cycle assays

Abrogation of response to I-BET151-mediated cell cycle arrest demonstrated in cell cycle assays. ***a****, Resistant clones do not demonstrate cell cycle arrest in biological triplicate experiments following 72hrs of drug exposure (mean ± s.e.m.).* ***b****, This is more evident in resistant clones stably maintained in higher concentrations of I-BET151. Data from biological duplicate experiments (mean ± s.e.m.) is presented.*

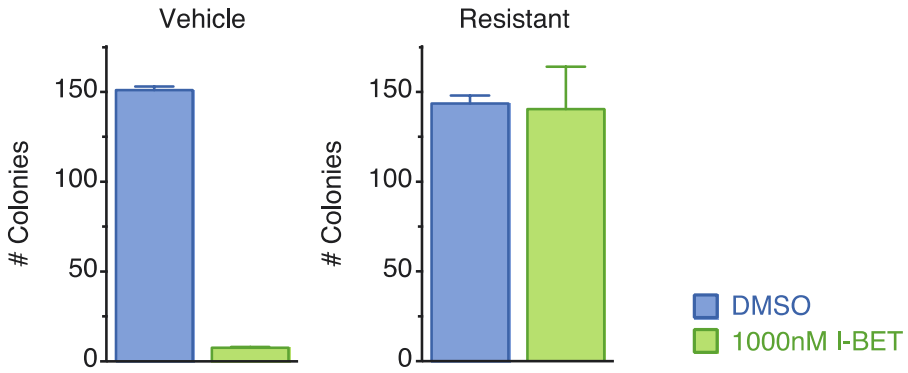

Figure 10 – MLL AF9 clonogenic assays

Resistance to I-BET151 of derived MLL-AF9 clonal cell lines is demonstrated in clonogenic assays. Colony counts were measured following 7 days of drug exposure and performed in biological duplicate (mean ± s.e.m.).

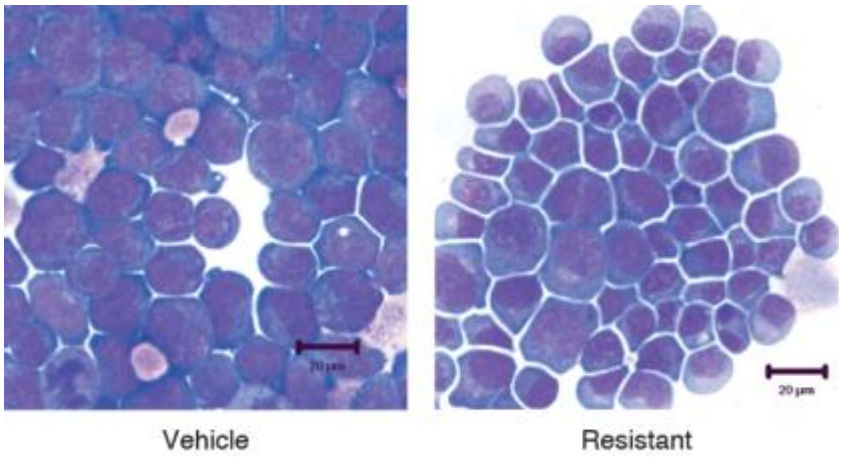

Figure 11 – Morphology of sensitive and resistant clones

Cell morphology of vehicle-treated and resistant clones as examined by light microscopy following cytospin and Romanowsky staining.

3.3.2 Cross resistance to JQ1 in proliferation assays

While chemically distinct inhibitors directed against the same target have sometimes overcome resistance[208], resistance to I-BET151 also confers cross-resistance to the chemically distinct BET inhibitor JQ1[102] (Figure 12).

Similar to the observation following treatment with I-BET151, resistant clones treated with JQ1 demonstrated no proliferative disadvantage despite exposure to JQ1 concentrations greater than the IC_{90} of corresponding vehicle-treated clones (Figure 12a). Furthermore, the IC_{50} of resistant clones was three times that of corresponding vehicle-treated clones (Figure 12b).

Drug class resistance to structurally distinct inhibitors highlights robust resistance to pharmacological inhibition of BET proteins in the derived model of resistance in AML.

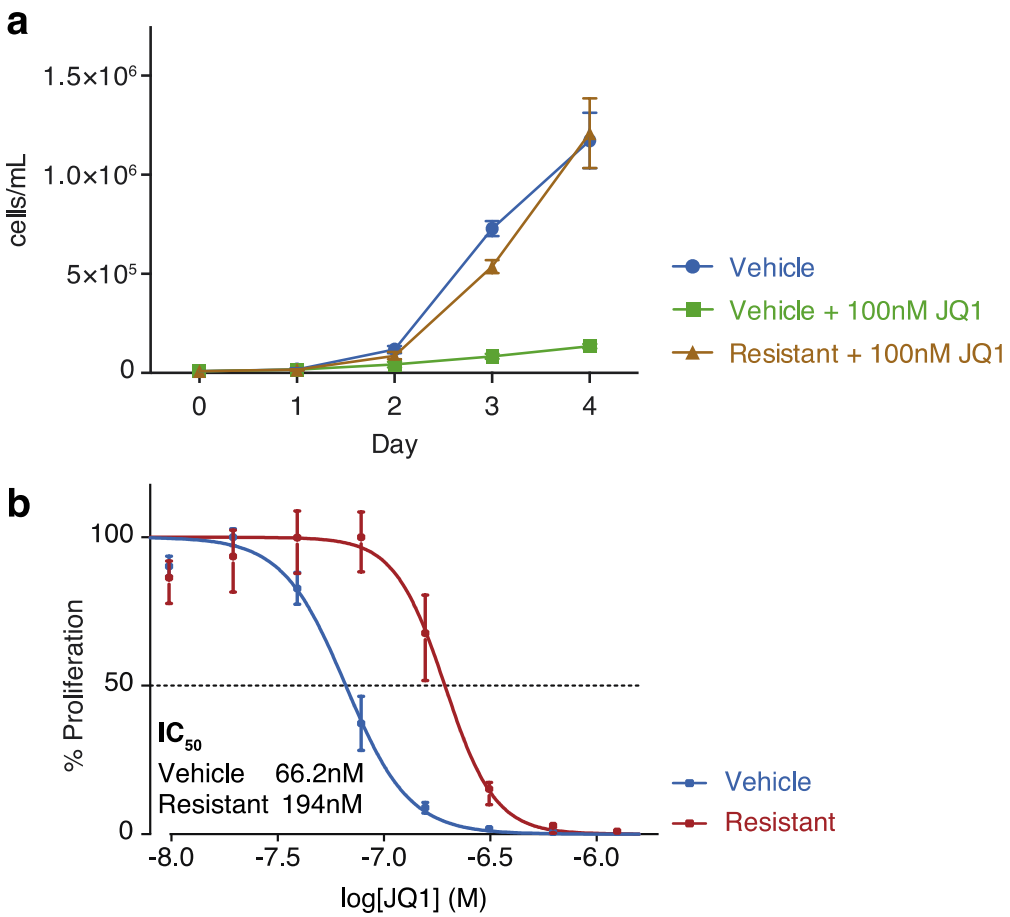

Figure 12 – JQ1 cross resistance

Cross resistance to the chemically distinct BET inhibitor, JQ1, is demonstrated in proliferation assays of derived MLL-AF9 clonal cell lines. ***a****, Daily cell counts of vehicle-treated and resistant clones seeded at 1 × 10⁴ cells/mL, performed in biological triplicate (mean ± s.d.).* ***b****, Representative dose–response curve of a vehicle-treated clone and a resistant clone after 72 h of growth (mean ± s.d., n = 4 per group).*

3.3.3 Proliferation assays in MLL-ENL cells

Similar to the observation in the clonal MLL-AF9 model, BET inhibitor resistant cells bearing the MLL-ENL fusion demonstrated preserved proliferative capacity in the presence of 1 μM I-BET151 (Figure 13a). Although the proliferative capacity of BET inhibitor resistant MLL-ENL cells was moderately decreased in comparison to that observed in BET inhibitor resistant MLL-AF9 cells (Figure 6a), MLL-ENL bearing resistant cells were comfortably maintained in drug concentrations representing > IC_{90} of corresponding vehicle-treated cell lines. Furthermore, the IC_{50} of resistant cells was three times greater than that observed in corresponding sensitive vehicle-treated cell lines (Figure 13b).

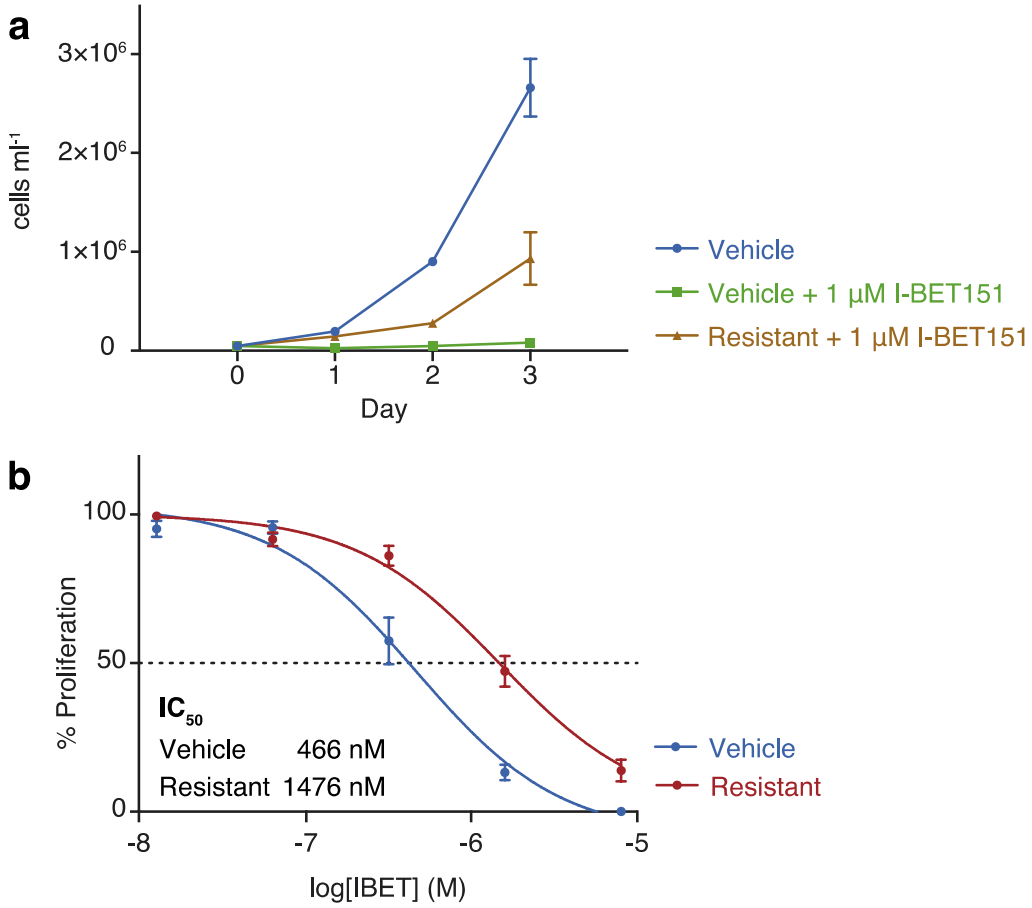

Figure 13 – MLL-ENL proliferation assays

Resistance to I-BET151 of MLL-ENL cell lines demonstrated in cell proliferation assays. ***a****, Daily cell counts of vehicle-treated and resistant cell lines seeded at 1 × 10⁴ cells/mL, performed in biological duplicate (mean ± s.e.m.).* ***b****, Representative dose-response curve of a vehicle-treated cell line and a resistant cell line stably maintained in 1 µM I-BET151 after 72hrs of growth (mean ± s.e.m., n = 4 per group).*

3.4 Resistant cells are impervious to genetic knockdown of BET proteins

3.4.1 The use of an inducible shRNA system for selective knockdown of BET proteins

High-content short hairpin RNA (shRNA) screens in a MLL-AF9 model has previously identified Brd4 as the major therapeutic target of BET inhibitors[181]. In order to evaluate the impact of genetic knockdown of BET proteins in our model of BET inhibitor resistance we adapted an all-in-one inducible shRNA system (TtRMPVIR), [see section 2.2.12, page 74].[228] This Tet-On retroviral vector system contains both a reverse tetracycline transactivator (rtTA) and an optimised tetracycline-response element (TREtight) promoter in one vector. Furthermore, this system enables precise tracking of retroviral transduction and shRNA expression by flow cytometry through the expression of two fluorescent reporters. Retroviral insertion of this construct into target cells results in constitutive expression of the Venus fluorophore driven by a phosphoglycerate kinase (PGK) promoter. The TREtight promoter drives the expression of shRNAs in the presence of doxycycline and is linked to a dsRED fluorescent reporter (Figure 14). This system may be utilised in competitive proliferation assays where shRNA expressing cells are followed over time and proliferative capacity/survival compared to non-shRNA expressing cell populations.

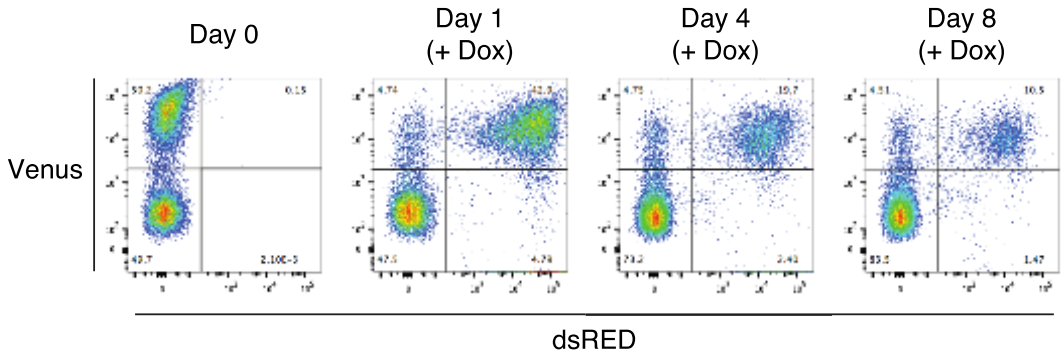

Figure 14 – Competitive proliferation assays utilising an inducible shRNA system

Representative flow cytometry plots of cell lines stably transduced with the adapted TtRMPVIR inducible shRNA vector. Three populations are identified and may be tracked over time: i) a YFP$^+$/Venus$^-$/dsRED$^-$ population which does not contain the inducible shRNA vector, ii) a YFP$^+$/Venus$^+$/dsRED$^-$ population which has been successfully transduced with the inducible shRNA vector but is not actively expressing the shRNA and, iii) a YFP$^+$/Venus$^+$/dsRED$^+$ population which contains the inducible shRNA vector and is actively expressing the shRNA following exposure to doxycycline. Selective disadvantage consequent to shRNA expression results in drop out of dsRED-positive cells from culture over time.

3.4.2 Competitive shRNA assays using hairpins against BRD2, BRD3 and BRD4

Using this inducible system, we were able to replicate the identification of Brd4 as a critical requirement for the survival and proliferation of vehicle-treated clones (Figure 15a). Vehicle treated clones maintain exquisite sensitivity to Brd4 loss. However, BET-inhibitor resistant clones were significantly less susceptible to genetic depletion of Brd4 (Figure 15a). mRNA and protein knockdown consequent to doxycycline exposure (Figure 15b, c), results in relative proliferative disadvantage and loss of sensitive populations over time in competitive proliferation assays.

This effect was observed utilising two independent shRNAs directed against Brd4 (shRNA #498 & #500) and a dual targeting Brd3/4 shRNA (shRNA #499) (Figure 16). No effect was observed with targeting Brd2 (shRNA #851) or a non-targeting scramble shRNA in resistant cells.

Mild toxicity of the scramble shRNA was observed in vehicle-treated cells which may reflect a proliferative disadvantage, relative to untransduced isogenic cells, consequent to shRNA production. This toxicity was not observed in resistant cells and may represent a dose-dependent toxicity. Nonetheless, no decrease in BRD2/3/4 mRNA or protein levels was observed in comparison to targeted shRNAs.

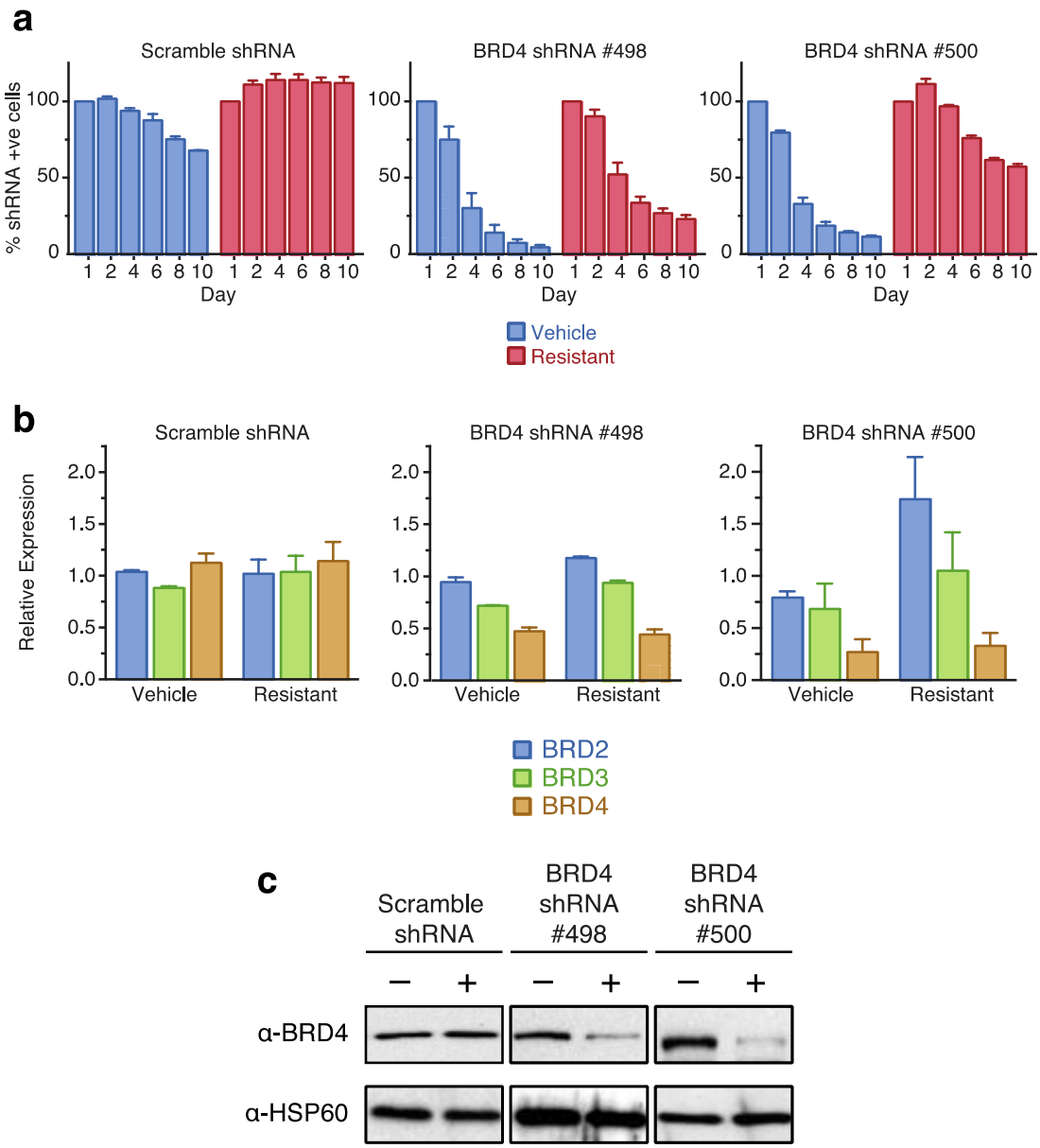

Figure 15 – BRD4 shRNA studies

Resistance to shRNA-mediated selective knockdown of Brd4 is observed in resistant clones but not vehicle-treated clones. ***a****, Competitive proliferation assays of vehicle-treated and resistant clones transduced with inducible shRNA vectors following doxycycline exposure. The proportion of shRNA expressing dsRED-positive cells in culture is normalized to day 1 after doxycycline exposure in biological duplicate experiments (mean ± s.e.m.)* ***b****, Independent inducible shRNAs specifically reduce the expression of Brd4, but not Brd2 or Brd3, after 48–72 h of doxycycline. mRNA levels in shRNA-positive cells is normalized to mRNA expression in shRNA-negative cells in biological duplicate experiments (mean ± s.e.m.).* ***c****, Brd4 protein levels are reduced in shRNA-positive cells following 72 hours of doxycycline induction (+).*

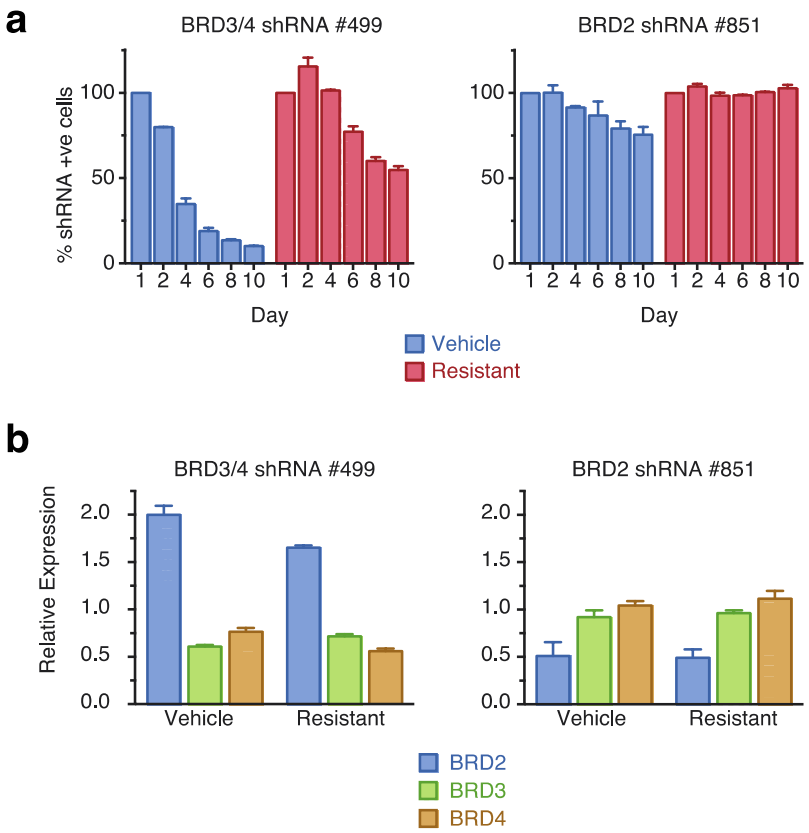

Figure 16 – BRD2 and BRD3/4 shRNA studies

In addition to resistance to selective knockdown of Brd4, BET-inhibitor-resistant cells are also refractory to RNAi-mediated dual knockdown of Brd3 and Brd4. shRNA-mediated knockdown of Brd2 has minimal effect on both vehicle-treated and resistant clones. ***a****, Competitive proliferation assays of vehicle-treated and resistant clones transduced with inducible shRNA vectors following doxycycline exposure. The proportion of shRNA expressing dsRED-positive cells in culture is normalized to day 1 after doxycycline exposure in biological duplicate experiments (mean ± s.e.m.)* ***b****, Reduction of Brd3/4 mRNA expression and Brd2 mRNA expression with two independent shRNAs after 48–72 h of doxycycline. mRNA levels in shRNA-positive cells normalized to mRNA expression in shRNA-negative cells in biological duplicate experiments (mean ± s.e.m.).*

3.5 Resistant clones maintain intermediate resistance phenotype following withdrawal of selective pressure

Compensatory mechanisms that confer resistance to targeted therapies may be reversible upon drug withdrawal.[204] This is purported to occur as a result of selection of a less 'fit' clone which has inherent insufficiencies in the absence of selective pressure. Upon withdrawal of selective pressure, more fit clones may prevail with a reduction in the size or disappearance of the resistant clone. Therapeutically, this concept allows for a trial of drug holiday and subsequent re-challenge to re-establish sensitivity to a previously efficacious targeted therapy.

To understand whether BET inhibitor resistance in the derived model was reversible, selective pressure was withdrawn from resistant clones for a period of 4-8 weeks. During this period, resistant clones continued to be exposed to drug vehicle (0.1% DMSO). Phenotypic responses to BET inhibitor exposure were then re-examined.

Partial restoration of BET inhibitor sensitivity was observed in dose-response proliferation and cell cycle assays (Figure 17). Resistant clones also demonstrated partial reacquisition of the immunophenotype of sensitive, BET inhibitor naïve cells (Figure 21, page 116) and also adopt an intermediate transcriptional state in microarray analysis (Figure 43, page 151).

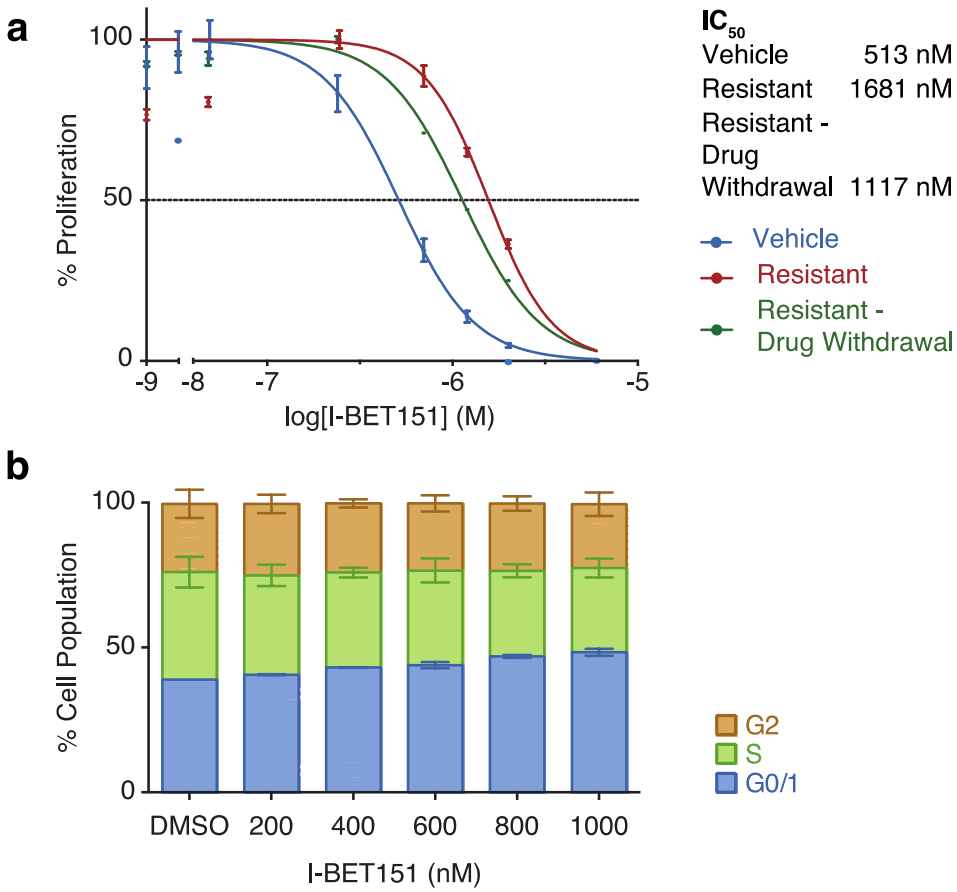

Figure 17 – Phenotypic responses to BET inhibitor exposure following withdrawal of selective pressure in resistant clones

Resistant clones demonstrate partial restoration of BET inhibitor sensitivity following drug withdrawal. ***a****, Representative dose-response curves of sensitive clones, resistant clones maintained in 1 μM I-BET151 and resistant clones following 8 weeks of drug withdrawal. Data obtained following 72 hours of drug exposure (mean ± s.d., n= 12 per group) is presented.* ***b****, Resistance to I-BET151 mediated cell cycle arrest is maintained in resistant clones following 8 weeks of drug withdrawal. Data obtained from biological triplicate experiments following 72hrs of drug exposure (mean ± s.e.m.) is presented.*

3.6 Resistance to BET inhibition is not related to increased drug metabolism or efflux

Alterations in drug efflux and metabolism are major potential mechanisms of acquired drug resistance. Quantitative mass spectrometry was employed to assess if increased drug efflux and/or alterations in metabolism were a feature of acquired resistance to BET inhibition. Unpublished data, derived from liver microsomes from rat, dog and human performed by GlaxoSmithKline, has identified that I-BET151 undergoes an oxidation reaction (+16 Da mass shift) via the cytochrome P450 pathway.

No significant difference was observed in the intracellular and extracellular concentrations of I-BET151 when resistant clones were compared with control counterparts (Figure 18). Furthermore, detailed examination of mass spectrometry data did not detect metabolic products of I-BET151.

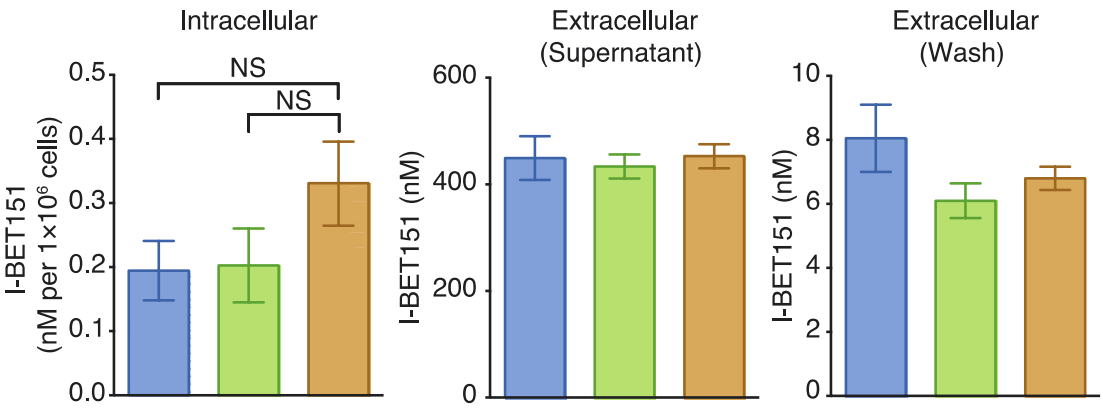

Figure 18 – Quantitative mass spectrometry

Comparison of parental cell line, vehicle treated clones and resistant clones demonstrates no significant difference in the intracellular or extracellular concentrations of I-BET151 following 48 hours of exposure to 600 nM I-BET151. Data from biological duplicate experiments (mean ± s.e.m., statistical significance calculated using a two-tailed Student's t-test) is presented. NS, not significant.

3.7 Resistant cells demonstrate *in vivo* resistance to BET inhibition

Syngeneic transplantation of murine HSPCs transduced with MLLfp results in robust initiation of leukaemia with a short disease latency. Consistent with previous observations, I-BET leads to a significant survival advantage in this AML model (Figure 19a).[75] In contrast, this survival advantage is abrogated following an identical treatment strategy in recipients of resistant cells (Figure 19b). No difference was observed in the pattern of disease between mice transplanted with sensitive or resistant clones. Hind limb paralysis and marked splenomegaly were prominent features of terminal disease following transplantation.

Together, the findings in this chapter establish a robust model of BET inhibitor resistance *in vitro* and *in vivo*, and show that resistant clones are refractory to either chemical or genetic perturbation of Brd4.

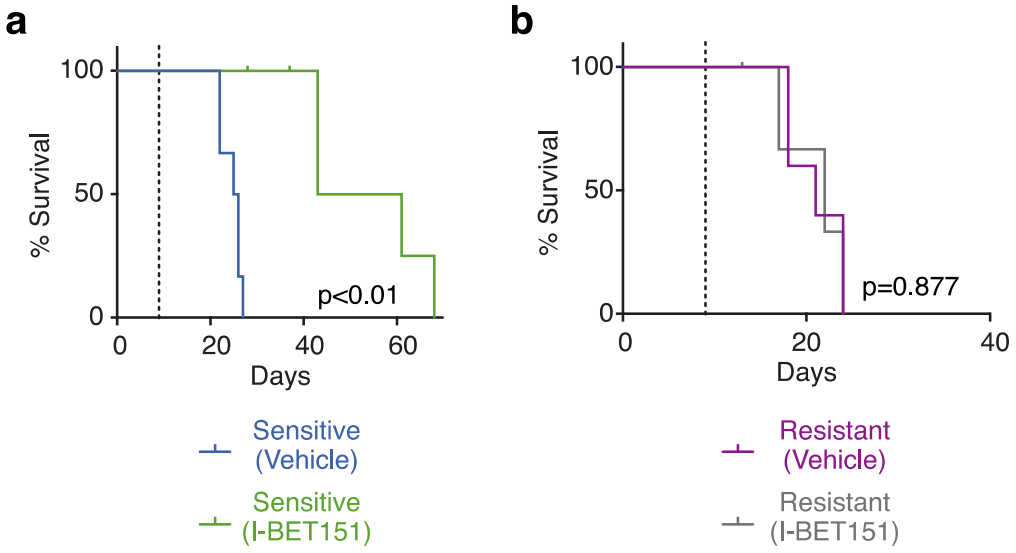

Figure 19 – in vivo resistance to BET inhibition

*Kaplan–Meier curves of secondary syngeneic transplant of sensitive (**a**) and resistant (**b**) clones (n=6 per group, statistical significance calculated using a log-rank test) is presented. 1 × 10^6 cells per mouse were transplanted following sub-lethal irradiation at day 0. Dotted line denotes treatment starting on day 9. Mice in both groups were treated with 30 mg/kg I-BET151.*

Chapter 4 - Resistance to BET Inhibitors Arises from the LSC Compartment

4.1 Resistant cells demonstrate immunophenotypic immaturity

4.1.1 Flow cytometry demonstrating loss of terminal markers of differentiation in MLL-AF9 and MLL-ENL cell lines

Haematopoietic progenitors propagated in liquid culture following retroviral transduction with MLL-AF9 display a mature myeloid immunophenotype (Gr1+, CD11b+).[177,178] Immunophenotypic analysis of *in vitro* generated vehicle-treated control clones emulates these findings (Figure 20a). However, MLL-AF9 bearing resistant clones which have been stably maintained in I-BET151 demonstrate an immature, progenitor like phenotype with loss of terminal markers of myeloid differentiation, Gr1 and CD11b (Figure 20b). Interestingly, stably resistant clones evaluated following an 8 week period of drug withdrawal display an intermediate phenotype (Figure 21).

Similarly, MLL-ENL bearing murine HSPCs demonstrate a mature myeloid immunophenotype.[176] Vehicle-treated cells maintain this immunophenotype, whereas resistant cell lines stably maintained in I-BET151 demonstrate loss of expression of Gr1 and CD11b (Figure 22).

These findings are consistent with acquired resistance to BET inhibition resulting in the enrichment of immunophenotypically immature sub-populations and raise the possibility that BET inhibitor resistant cells are LSCs.

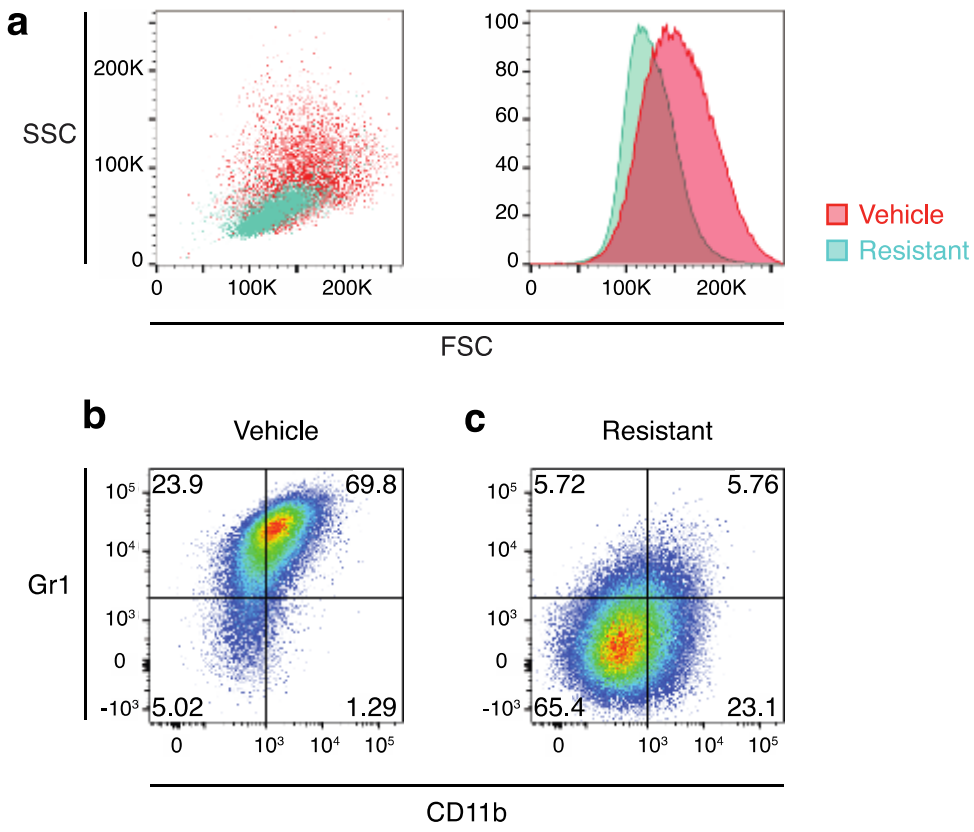

Figure 20 – Gr1/CD11b expression in MLL-AF9 clonal model of resistance

Representative flow cytometry plots demonstrating: ***a****, resistant clones are smaller and demonstrate homogeneity in size and complexity (FSC* ^{mid}*/SSC* ^{low}*),* ***b****, the expected expression of murine markers of terminal myeloid differentiation Gr1 and CD11b in vehicle-treated clones and* ***c****, loss of Gr1 and CD11b expression in resistant clones stably maintained in 1 μM I-BET151.*

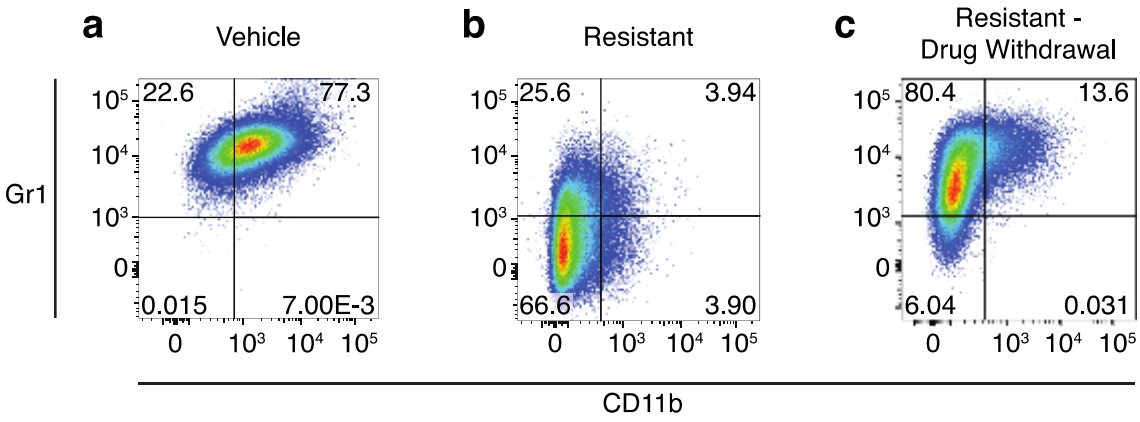

Figure 21 – Gr1/CD11b expression following withdrawal of selective pressure

Representative flow cytometry plots of Gr1 and CD11b expression demonstrating ***a****, expected expression of terminal markers of differentiation in vehicle-treated clones,* ***b****, loss of terminal makers of differentiation in resistant clones stably maintained in 1 μM I-BET151 and* ***c****, reacquisition of an intermediate immunophenotype in resistant clones following withdrawal of drug for 8 weeks.*

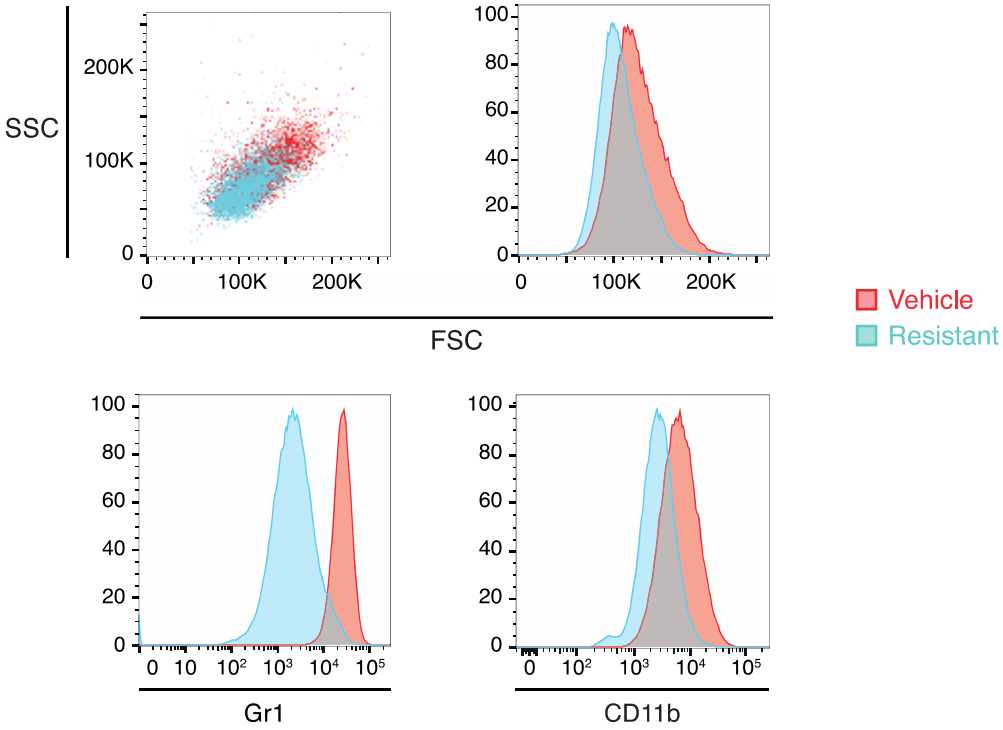

Figure 22 – MLL-ENL resistance immunophenotype

Representative flow cytometry plots demonstrating the smaller, more homogenous nature of resistant cell lines in a MLL-ENL model of BET inhibitor resistance. Resistant cell lines also demonstrate reduced expression of Gr1 and CD11b compared with vehicle-treated cell lines.

4.1.2 Flow sorting of lineage negative population demonstrates enrichment for colony forming cells in clonogenic assays

In vitro colony forming cell (CFC) assays have been extensively used to characterise normal and malignant stem cells. CFC capacity is a surrogate marker of *in vivo* stem cell frequency and is reflective of stem cell functional capacity. [247] Therefore, to examine the functional LSC capacity of resistant clones, FACS sort of lineage negative (Gr1−/CD11b−) and lineage positive (Gr1+/CD11b+) populations was undertaken prior to seeding in cytokine supplemented methylcellulose. Consistent with the notion that resistant clones were enriched for LSCs, we noted a significant increase in the blast colony forming potential of the lineage negative (Gr1−/CD11b−) population (Figure 23).

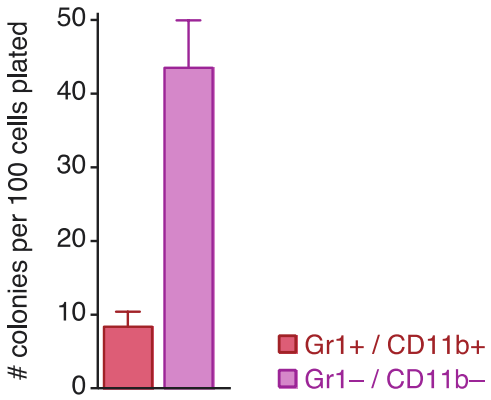

Figure 23 – Colony assays of FACS isolated subpopulations in resistant clones

Lineage negative (Gr1−/CD11b−) cells from resistant clones demonstrate increased colony forming capacity in cytokine supplemented methylcellulose when compared with lineage positive populations. FACS of resistant clones performed in biological duplicate, colony count displayed as mean ± s.e.m..

4.1.3 Flow cytometry demonstrating enrichment of L-GMP population in MLL-AF9 cell lines

Although the precise immunophenotype of LSCs in murine MLLfp leukaemia models has been debated, it has been demonstrated that LSC potential primarily resides in the lineage negative, leukaemic granulocyte macrophage progenitor (L-GMP) population.[177-179,248] This population bears the immunophenotype: Lin^{-}, $Sca\text{-}1^{-}$, $c\text{-}kit^{+}$, $CD34^{+}$, $Fc\gamma RII/III^{+}$.[176,177]

A marked increase in L-GMP cells was observed in resistant clones stably maintained in I-BET151 (Figure 24). This was observed in cells prior to primary transplantation and further highlights the stem cell like nature of cells demonstrating acquired resistance to BET inhibition.

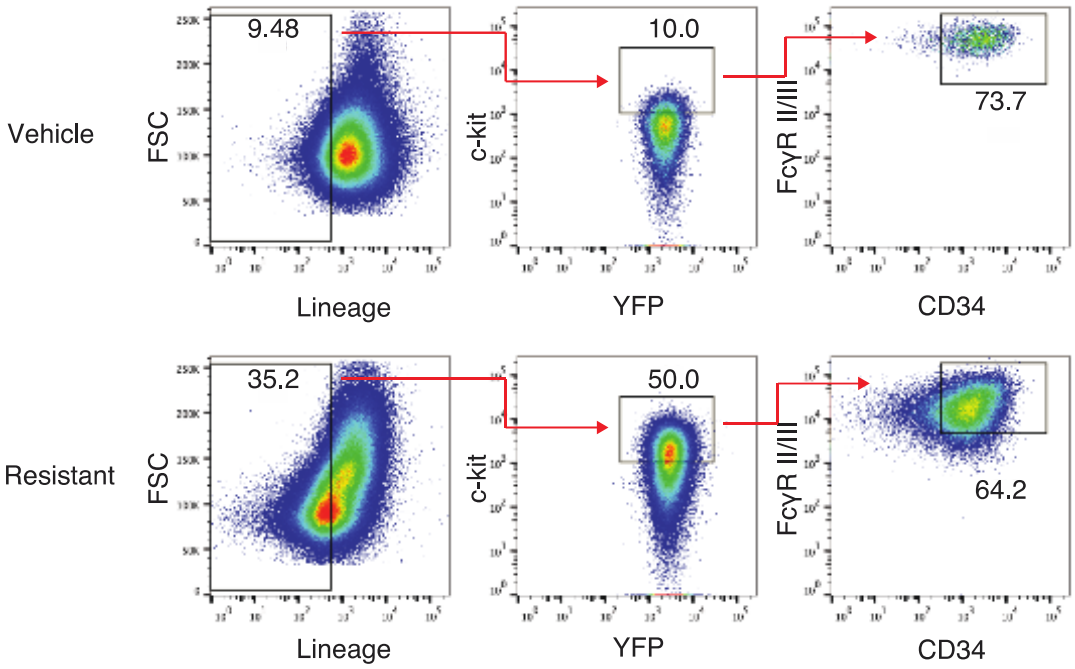

Figure 24 – L-GMP immunophenotype of resistant clones

Representative flow cytometry plots demonstrating enrichment of L-GMPs in resistant clones. Reported percentages represent proportions of parent gate. Non-viable events (PI positive) were excluded.

4.2 BET inhibitor resistant cells are enriched for functional LSCs

4.2.1 Limiting dilution analyses of stably growing resistant cell lines

To address the functional LSC capacity of L-GMP enriched resistant clones in liquid culture, limiting dilution assays of cultured cells in primary syngeneic transplantation were performed. LDA enables mathematical modelling of stem cell frequency within a larger population. The extreme limited dilution analysis method of Hu and Smyth designed for stem cell analysis was utilised in statistical analysis.[231]

While primary transplantation of vehicle-treated clones paralleled the natural history of this AML model, remarkably, primary transplantation of I-BET resistant clones resulted in considerably shorter leukaemia latency (Figure 25a, b). Moreover, limiting dilution analyses confirm that I-BET resistant cells were markedly enriched for LSC potential (Figure 25c). In comparison to vehicle-treated clones, there was a >85 fold enrichment of functional LSCs to 1:5,932 cultured cells. Indeed, transplant of 10^3 cells from cultures of resistant cells was able to successfully engraft 33.3% of mice reflecting the stem cell nature of resistant clones (Table 4.1).

This is a notable finding. Whilst L-GMP cells are easily propagated in liquid culture, these cells rapidly differentiate and the majority adopt a lineage$^+$ immunophenotype resulting in loss of functional LSC capacity.[177] The novel ability to indefinitely maintain a L-GMP population with functional LSC capacity in indefinite culture enables high-throughput examination of LSC function and the development of approaches to eradicate them.

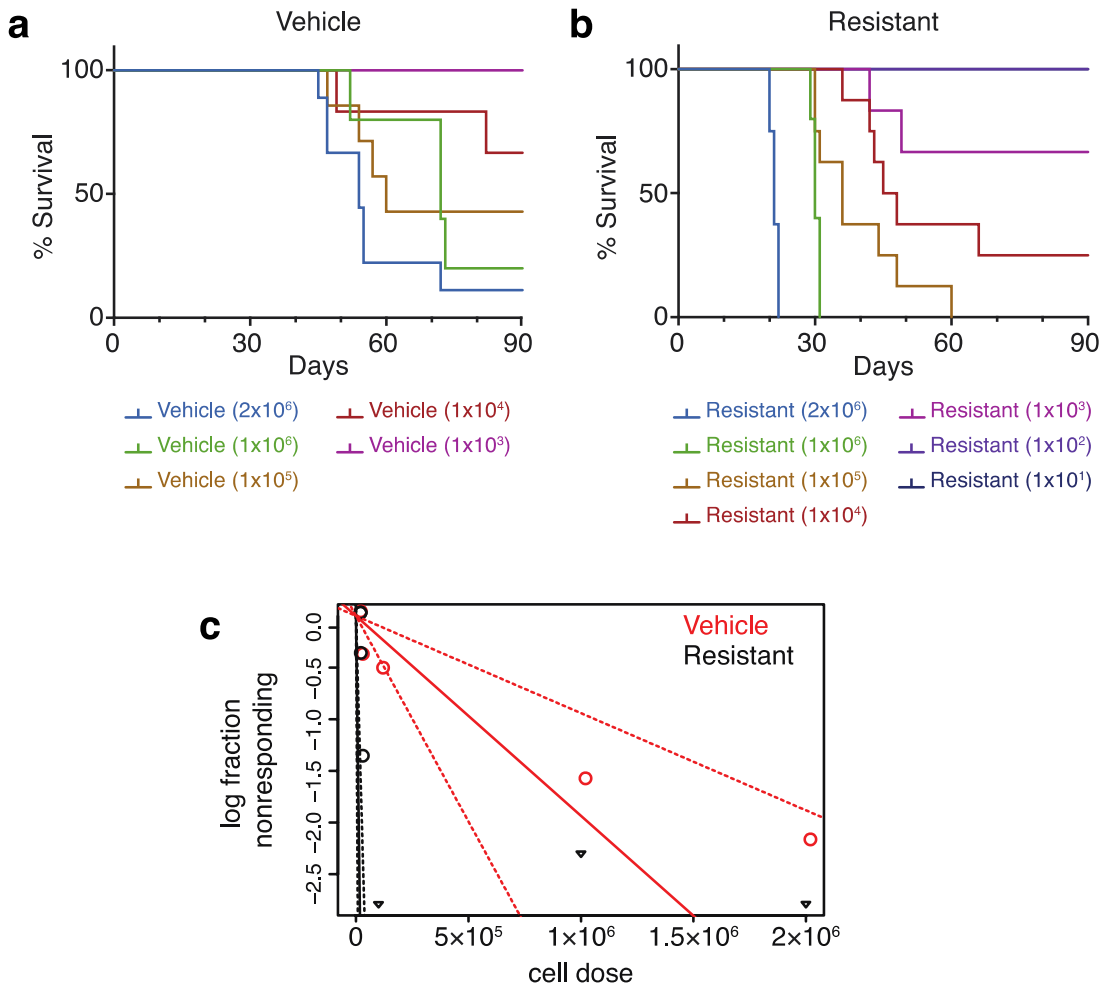

Group	Stem Cell Frequency	CI	p-value
Resistant	1:5,932	[2698-13042]	
Vehicle	1:516,900	[251317-1063141]	5.94E-16

Figure 25 – Enrichment of LSCs in LDA of stably growing BET inhibitor resistant clones following primary transplantation

Limiting dilution primary transplantation analysis of vehicle-treated and resistant clones stably maintained in liquid culture demonstrating enrichment of functional LSCs in resistant clones. ***a*** *&* ***b****, Kaplan–Meier curves of C57BL/6 mice injected with indicated number of cells; detailed cohort and survival data can be found in Table 4.1.* ***c****, LSC frequency determined by LDA. Dotted lines indicate 95% confidence intervals (CI).*

Group	Cell Dose	Transplanted mice	AML		Median Survival (Days)
Sensitive	1000	6	0	(0%)	-
Sensitive	10000	6	2	(33.3%)	-
Sensitive	100000	7	4	(57.1%)	55.5
Sensitive	1000000	5	4	(80%)	72
Sensitive	2000000	9	8	(88.9%)	54
Resistant	10	4	0	(0%)	-
Resistant	100	5	0	(0%)	-
Resistant	1000	6	2	(33.3%)	-
Resistant	10000	8	6	(75%)	36.5
Resistant	100000	8	8	(100%)	36
Resistant	1000000	5	5	(100%)	30
Resistant	2000000	8	8	(100%)	21

Table 4.1: Primary LDA summary

Transplant cohorts and survival of mice injected with vehicle-treated and resistant clones in LDA of primary syngeneic transplants displayed in Figure 25.

4.3 Resistance to BET inhibition derived *in vivo* arises from a LSC compartment

4.3.1 Derivation of *in vivo* resistance through a serial transplant approach

To assess the relevance of these findings to resistance that emerges *in vivo* after sustained exposure to pharmacological BET inhibition, in parallel to the clinical development of acquired resistance, we derived an independent *in vivo* model of BET inhibitor resistance in a murine MLL-AF9 system (Figure 26).

This was achieved by transplanting initially sensitive leukaemias derived from primary transplant of vehicle-treated clones. Subsequently, transplanted mice were exposed to I-BET151 and leukaemias derived from diseased mice treated with I-BET151 were serially transplanted. Mice in subsequent transplant generations were again treated with I-BET151 until loss of I-BET151 mediated survival advantage was observed (Figure 27a). Loss of I-BET151 mediated survival advantage was observed to occur following quaternary transplant. In parallel, leukaemias from mice who were I-BET151 naïve were serially transplanted to control for non-pharmacological effects on stem cell frequency and leukaemia aggressiveness.

Data obtained from this model validated findings from the *ex vivo* model of resistance, and demonstrate that *in vivo* BET inhibitor resistance also emerges from an L-GMP population (Figure 27b & Figure 28). With subsequent transplant generations, chronic I-BET151 exposure resulted in the increased frequency of L-GMPs and shorter leukaemia latency.

The LSC frequency of BET inhibitor resistant leukaemias derived in vivo was examined in LDA following quaternary transplant (Figure 29 & Table 4.2). Importantly, these BET inhibitor resistant AML cells have a functional LSC frequency of approximately 1:6; this is virtually identical to what has previously been reported for a purified L-GMP population (Figure 29b).[177]

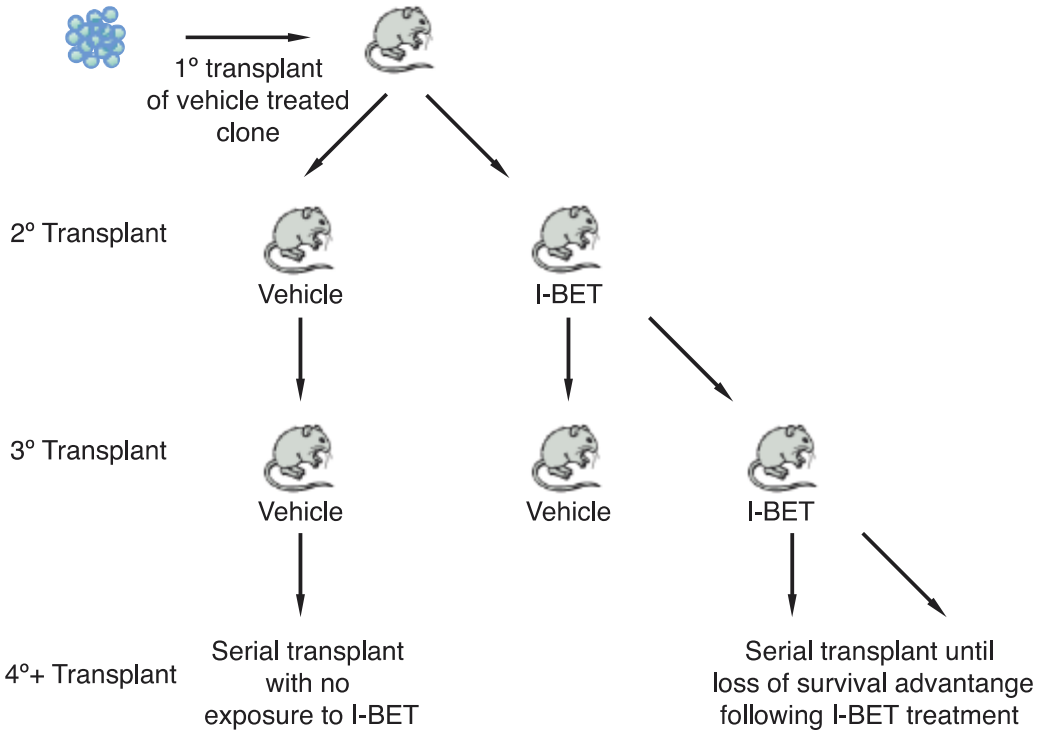

Figure 26 – Generation of murine MLL-AF9 model of in vivo resistance

Experimental strategy for derivation of in vivo resistance to BET inhibitors in a murine MLL–AF9 leukaemia model. Following primary transplant of a vehicle-treated clone, serial transplant of I-BET151-exposed leukaemias, derived from whole bone marrow of diseased mice, was undertaken until loss of I-BET-mediated survival advantage was observed. Treatment was commenced on days 11–13. A cohort of I-BET151-naïve leukaemias was serially transplanted in parallel as a control arm.

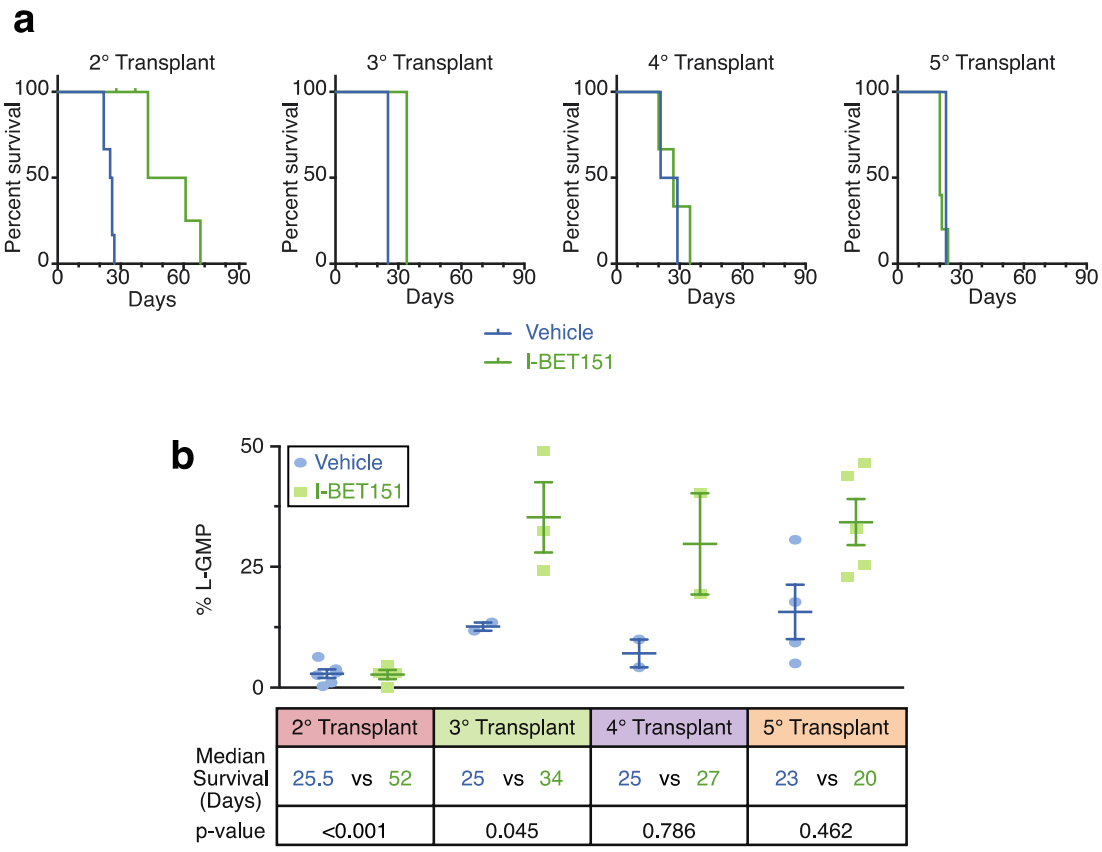

Figure 27 – Enrichment of L-GMPs in an in vivo model of BET inhibitor resistance

Progressive loss of I-BET151 mediated survival advantage observed in serial transplant generations correlating with enrichment of a L-GMP population. ***a****, Kaplan–Meier curves of serial transplant generations from I-BET151 exposed mice. Secondary transplant: vehicle treated n = 6, I-BET151 treated n = 6. Tertiary transplant: vehicle treated n = 2, I-BET151 treated n = 3. Quaternary transplant: vehicle treated n = 2, I-BET151 treated n = 3. Quinary transplant: vehicle treated n = 4, I-BET151 treated n = 5.* ***b****, L-GMP frequency in whole mouse bone marrow (mean ± s.e.m.) after serial transplantation of I-BET-exposed leukaemias from in vivo resistance model. Gating strategy outlined in Figure 28. Statistical significance of survival outcomes determined using log-rank test of Kaplan–Meier survival estimates.*

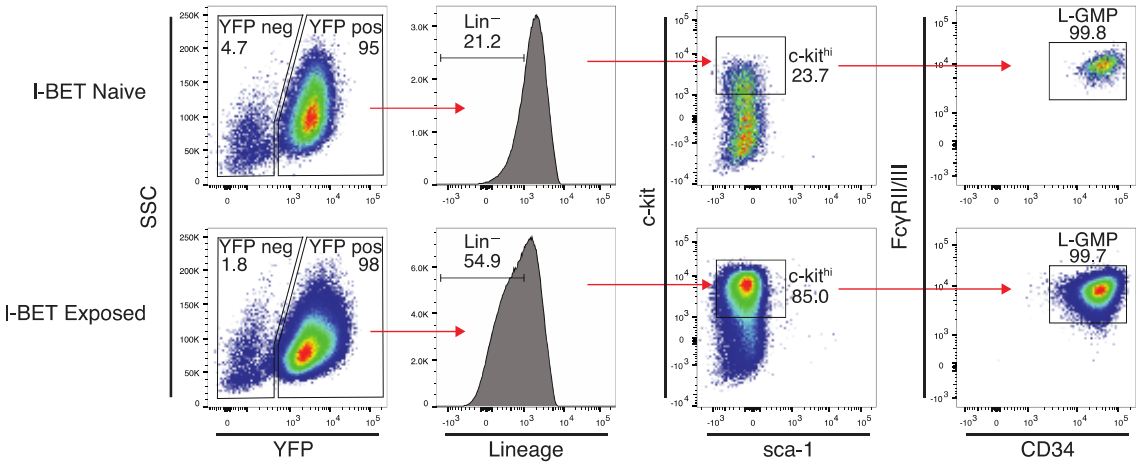

Figure 28 – in vivo L-GMP gating strategy

Gating strategy for identification of L-GMPs in whole mouse bone marrow. Representative flow cytometry plots demonstrating enrichment of L-GMP population observed in I-BET151 exposed mice following quaternary transplantation. Reported percentages represent proportions of parent gate. Non-viable events (PI positive) were excluded.

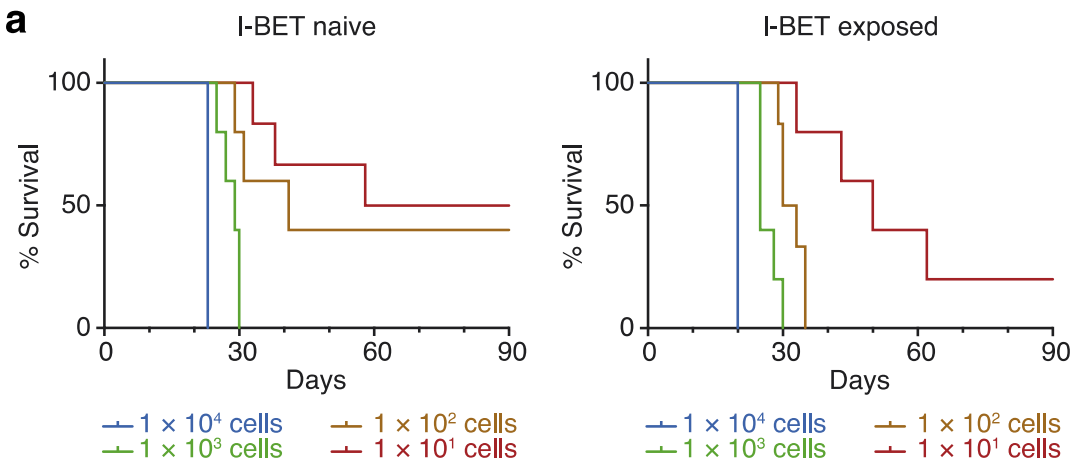

b

Group	Stem Cell Frequency	CI	p-value
Resistant	1:6	[2.09-18.5]	
Sensitive	1:59	[22.59-154.2]	0.003

Figure 29 – Enrichment of LSCs in LDA of BET inhibitor resistant leukaemias generated in vivo

LDA of leukaemias derived from bone marrow of diseased mice following chronic I-BET151 exposure demonstrates that less than 10 cells are reliably able to transfer leukaemia. LDA was performed using leukaemias derived following quaternary transplant. ***a****, Kaplan–Meier curves of C57BL/6 mice injected with indicated number of leukaemic cells from either I-BET naïve (sensitive) or I-BET exposed (resistant) mice.* ***b****, Chronic I-BET exposure significantly enriches for leukaemia stem cells in vivo in LDA.*

Group	Cell Dose	Transplanted mice	AML	Median Survival (Days)
Sensitive	10	6	3 (50%)	74.5
Sensitive	100	5	3 (60%)	41
Sensitive	1000	5	5 (100%)	29
Sensitive	10000	2	2 (100%)	23
Resistant	10	5	4 (80%)	50
Resistant	100	6	6 (100%)	31.5
Resistant	1000	5	5 (100%)	25
Resistant	10000	2	2 (100%)	20

Table 4.2: in vivo resistance LDA summary

Transplant cohorts and survival of mice injected with I-BET naïve (sensitive) or I-BET exposed (resistant) leukaemias derived from mice following quaternary transplant in the LDA presented in Figure 29.

4.4 Intrinsic resistance to BET inhibition is not a characteristic of immunophenotypic LSCs

As enrichment of L-GMP LSCs is evident in both *ex vivo* and *in vivo* models of resistance to BET inhibition, the possibility of intrinsic resistance in L-GMP sub-populations was investigated.

To achieve this, L-GMPs from mice that were I-BET-naïve were isolated through FACS (Figure 30a). These L-GMP populations were then challenged with 1 μM I-BET151 in clonogenic assays. This dose virtually eradicates the clonogenic potential of I-BET151 naïve bulk leukaemia cells as previously demonstrated in Figure 10 (page 99) and in prior published data.[75] However, between 30 and 40% of L-GMPs are able to survive (Figure 30b).

Furthermore, L-GMP frequency does not immediately rise as a consequence of *in vivo* I-BET151 exposure and was instead observed as a population which progressively emerges with continuous and sustained exposure (Figure 27b).

These findings suggest that immunophenotypically homogenous L-GMPs/LSCs show marked heterogeneity in their response to BET inhibition, and that not all L-GMPs are intrinsically resistant to BET inhibitors.

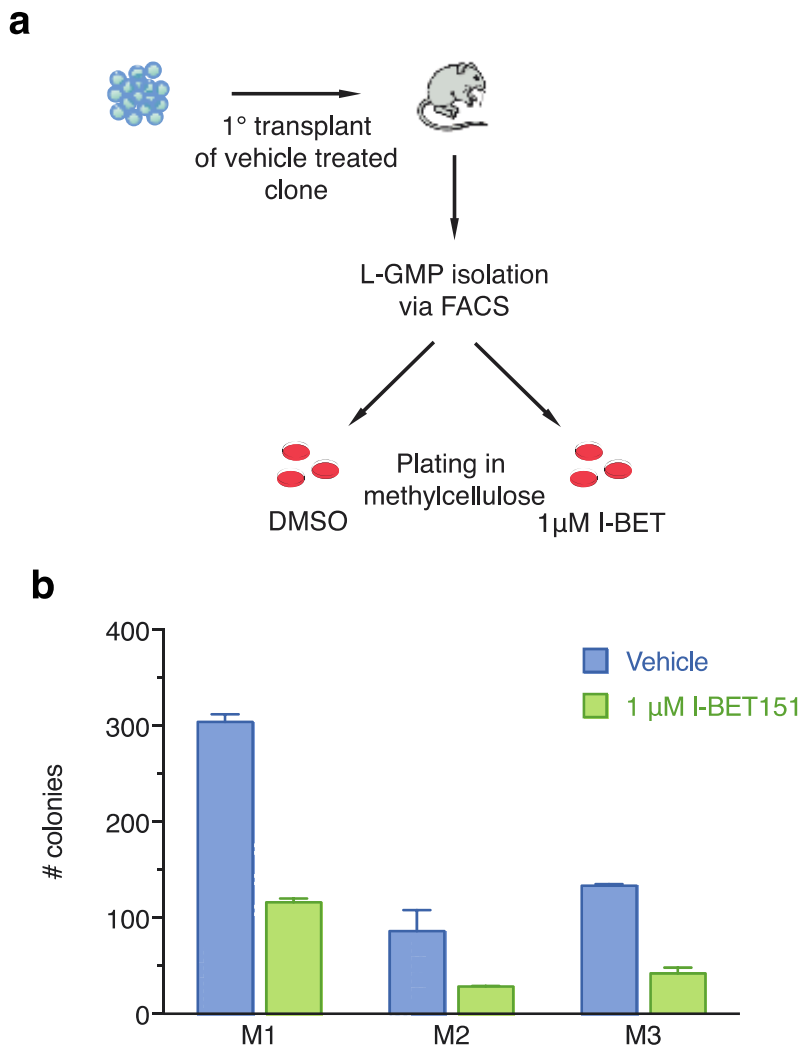

Figure 30 – Clonogenic assays of FACS isolated L-GMPs

Flow sorting of L-GMP cells from I-BET naïve leukaemias and clonogenic assays demonstrating sensitivity to BET inhibition. Only a sub-population of L-GMPs demonstrate resistance to BET inhibitor therapy. ***a****, Experimental strategy for testing intrinsic resistance of L-GMPs to BET inhibition. After syngeneic transplant of a vehicle-treated clone, L-GMPs were FACS-isolated from whole mouse bone marrow of diseased mice and cultured in cytokine supplemented semi-solid media containing either vehicle (0.1% DMSO) or 1 mM I-BET.* ***b****, Colony counts after 7 days of growth biological duplicate experiments (mean ± s.e.m.) of FACS- isolated L-GMPs after primary transplant of vehicle-treated clones. M1, mouse 1; M2, mouse 2; M3, mouse 3.*

4.5 BET inhibitor treatment enriches for a LSC compartment in patient derived xenografts

To further expand the clinical relevance of findings derived from a murine model of MLL leukaemia, we examined the behaviour of a patient derived xenograft (PDX) model of AML in response to BET inhibitor therapy. Xenotransplanted primary AML samples in immunodeficient NSG mice faithfully recapitulate the clonal genetic architecture of human leukaemia.[249] Furthermore, PDX models are a potentially inexhaustible resource for *in vivo* assessment of novel therapeutic approaches in human leukaemias.

4.5.1 Development of a flow cytometric approach for characterisation of LSC compartments in NSG mice bearing PDX

While the immunophenotype of human AML LSCs can be variable, several models have shown that LSCs are enriched within CD34+ cells,[223,227] which immunophenotypically parallel GMPs or lymphoid-primed multipotent progenitors (LMPPs).[250] GMP-like LSCs bear the immunophenotype: $CD45^{+}/CD33^{+}/CD3^{-}/CD19^{-}/CD34^{+}/CD38^{+}/CD45RA^{+}/CD123^{+}$. LMPP-like LSCs bear the immunophenotype: $CD45^{+}/CD33^{+}/CD3^{-}/CD19^{-}/CD34^{+}/CD38^{-}/CD45RA^{+}/CD90^{-}$. To identify these human LSC bearing populations in PDX a multicolour flow cytometry panel was developed (Figure 31). This panel enabled the exclusion of mouse derived cells from analysis.

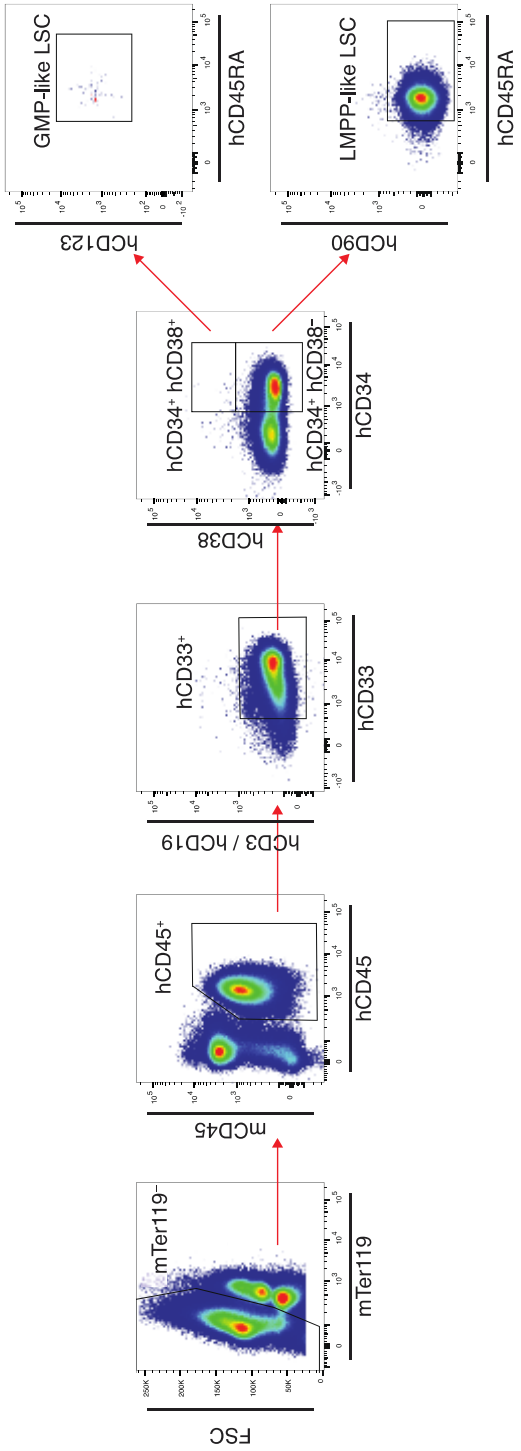

Figure 31 – Gating strategy for the identification of human LSCs in a PDX model

Gating strategy for identification of LMPP-like LSCs and GMP-like LSCs from mouse bone marrow. mTer119 / mCD45 denotes mouse Ter119 / CD45; hCD45 / hCD3 / hCD19 / hCD33 / hCD34 / hCD38 / hCD123 / hCD45RA / hCD90 denotes human CD45 / CD3 / CD19 / CD33 / CD34 / CD38 / CD123 / CD45RA / CD90, respectively. Non-viable events (PI positive) were excluded.

4.5.2 Short term I-BET151 treatment results in enrichment of LMPP-like LSCs in a non-MLL bearing PDX

Utilising a non-MLLfp bearing AML PDX model we undertook short term I-BET151 treatment to examine the impact of pharmacological BET inhibition in a humanised *in vivo* setting. The AML PDX model utilised was a kind gift from Dr Omar Abdel-Wahab at Memorial Sloane Kettering Cancer Center, NY, USA. This PDX model had demonstrated robust engraftment and serial transplantability and has had cytogenetic and molecular characterisation performed (Figure 32b).

Treatment with vehicle or I-BET151 (10 mg/kg) was commenced after engraftment of human cells was detected through assessment of human CD45 expression in peripheral blood (Figure 32a). >1% circulating human cells was detected at week 14.

Consistent with data from murine AML models, I-BET151 treatment resulted in immunophenotypic enrichment for a leukaemic LMPP LSC-like population (Figure 33). Although a non-functional assay of LSC capacity, these data are consistent with BET inhibitor resistance emerging from leukaemia stem cells.

a

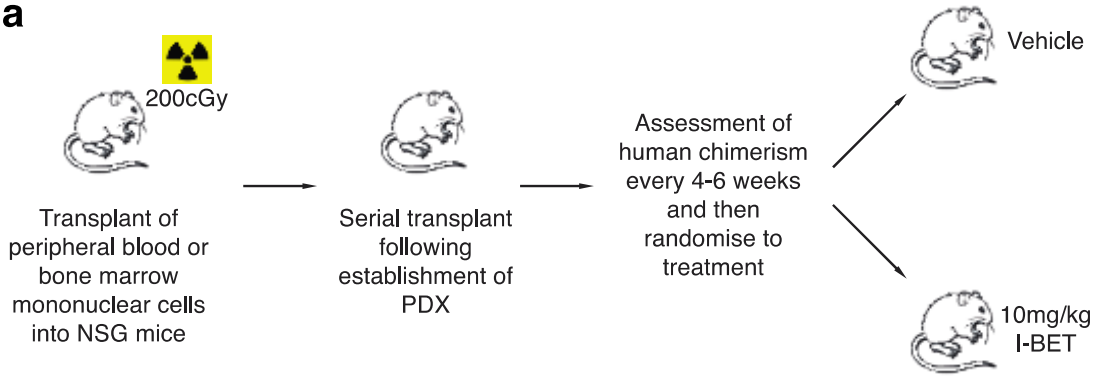

b

PDX ID	Cytogenetics	Genetic Mutations
001	Trisomy 13	ASXL1, KRAS, TET2, SRSF2

Figure 32 – PDX experimental strategy

***a**, Experimental strategy for treatment of NOD/SCID/Il2rg$^{-/-}$ (NSG) mice bearing AML PDXs. Treated mice (with either vehicle or 10 mg/kg I-BET151) belonged to identical transplant generations. **b**, Cytogenetic and genetic information of PDX model used.*

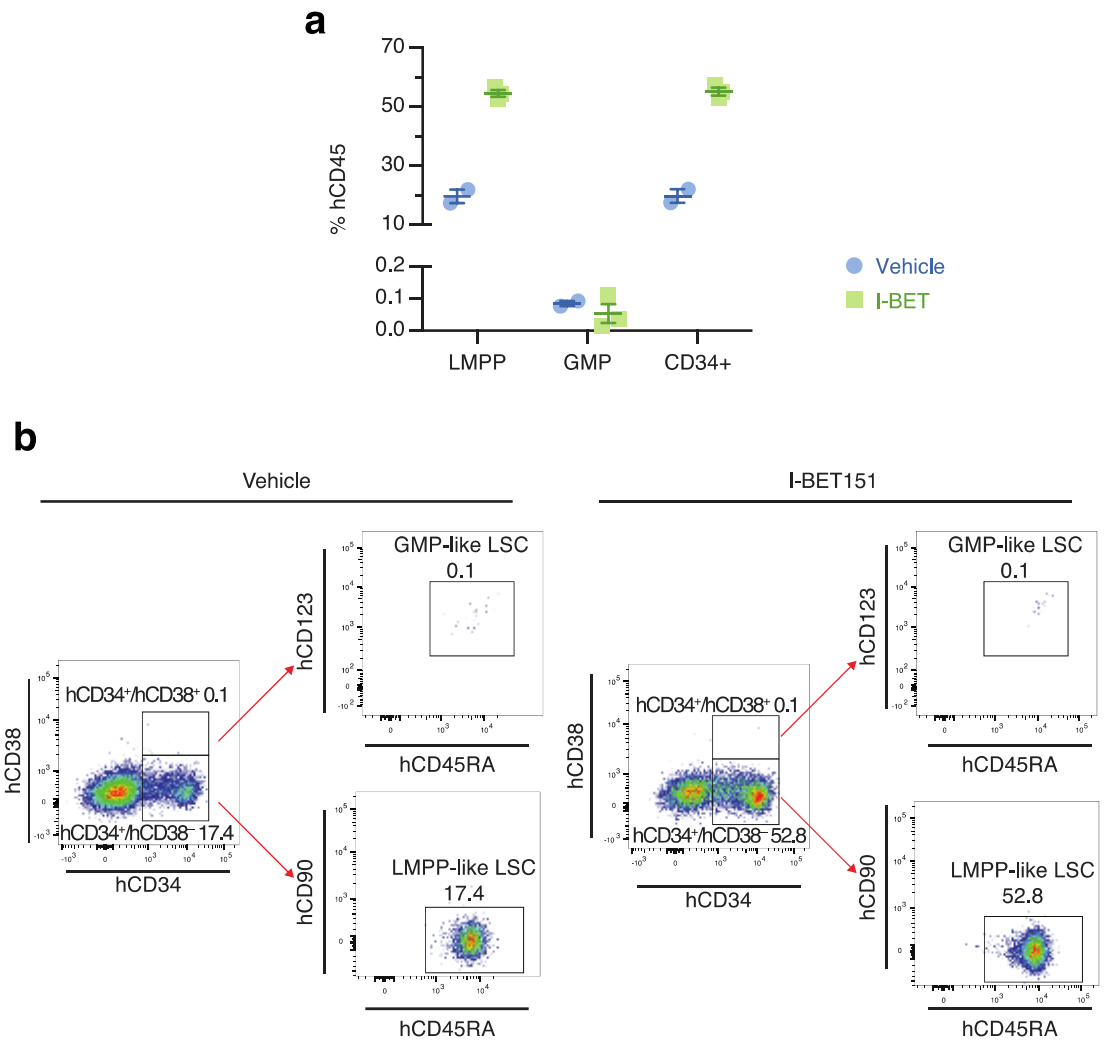

Figure 33 – LSC enrichment following I-BET151 therapy in a PDX model

***a**, Proportion of human leukaemic CD34+ cells, GMPs and LMPPs in whole mouse bone marrow (mean ± s.e.m.) after I-BET exposure in an AML PDX model (n = 5) Proportions expressed as percentage of total human CD45$^+$ cells. **b**, Representative FACS analysis of bone marrow obtained from vehicle- and I-BET151-treated mice demonstrating enrichment of LMPP-like LSCs in I-BET-treated mice. Events displayed are gated on mouse Ter119$^-$ / human CD45$^+$ / human CD33$^+$ cells and are expressed as a percentage of total hCD45$^+$ cells.*

Chapter 5 - Identifying the molecular mechanism of resistance to BET inhibitors

5.1 Genetic abnormalities do not mediate resistance to BET inhibition

To examine the underlying molecular aetiology of resistance, mutation analysis was undertaken at locus specific and genomic levels.

As mutations in bromodomain 1 of *Brd4* have been demonstrated to alter BET inhibitor affinity for *Brd4* without affecting *Brd4* function we undertook an initial examination of potential mutation hotspots by Sanger sequencing.[251] No mutations were identified in resistant clones as compared with vehicle-treated clones or parental cell line controls.

Subsequently, whole exome sequencing (WES) in the parental cell line, two independent vehicle-treated clones and two independent resistant clones was undertaken (Figure 34 & Figure 35). Validating our targeted Sanger sequencing, no gatekeeper mutations in the bromodomains of *Brd2/3/4* were identified.

WES was performed at two time points, early and late, to assess genetic stability in the presence of selective pressure (Figure 34). Similar to human leukaemias driven by MLLfp, genetic instability was not a prominent feature of the derived murine MLL-AF9 model of resistance to BET inhibition. Mutational frequency across both vehicle-treated and resistant clones was low (median 1.36 mutations per million bp) and representative of AML mutational burden in The Cancer Genome Atlas (TCGA) analyses (Figure 35b).[252] No consistent gene mutation signature was identified (Figure 35c).

Furthermore, although independently established resistant clones behaved identically in all functional analyses described previously, no common copy number aberrations were identified and only 24 mutations were shared across resistant clones that were not present in vehicle-treated clones (Figure 34 and Figure 35a). These mutations have no apparent functional relevance to AML and/or BET activity. To ensure validity of identified mutations, RNA-seq data from identical clones were examined (Figure 36).

Finally, WES data was utilised to confirm the clonal nature of resistant cell lines through identification of both male and female clones (Figure 37).

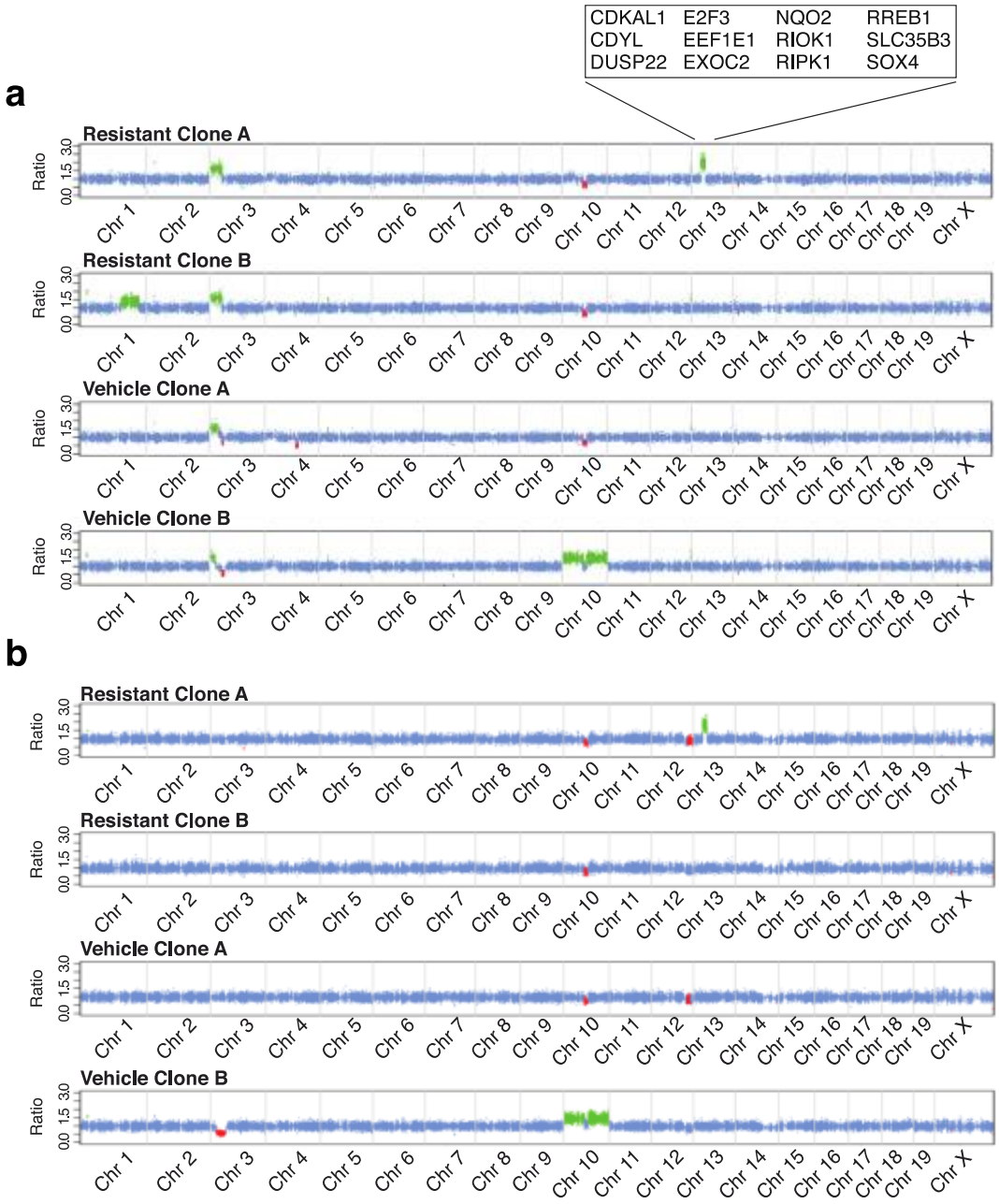

Figure 34 – Copy number analysis by WES

*Comparison of WES data from early (**a**) and late (**b**) time points identifies non-advantageous passenger mutations. WES data from vehicle-treated and resistant clones is normalized to the parental cell line; red regions denote copy number loss and green regions denote copy number gain. Call out box identifies genes within a small region on chromosome 13 in one resistant clone which demonstrates persistent copy number gain and are associated with increased mRNA expression relative to non-resistant cells (Table 5.1).*

Gene	Resistant Clone A	Resistant Clone B
Cdkal1	1.82	1.17
Cdyl	1.98	1.28
Dusp22	1.97	1.19
E2f3	1.64	-1
Eef1e1	1.64	1.15
Exoc2	2.57	1.41
Nqo2	1.68	-1.19
Tiok1	1.74	1.07
Ripk1	2.12	1.17
Rreb1	1.84	1.23
Slc35b3	1.86	1.01
Sox4	3.36	-1.79

Table 5.1: WES gene expression correlation data

Correlation of genes identified in copy number gain region on chromosome 13 in one resistant clone with gene expression data from the two resistant clones examined by WES. Fold change in gene expression compared to vehicle-treated clones obtained from microarray analysis is shown.

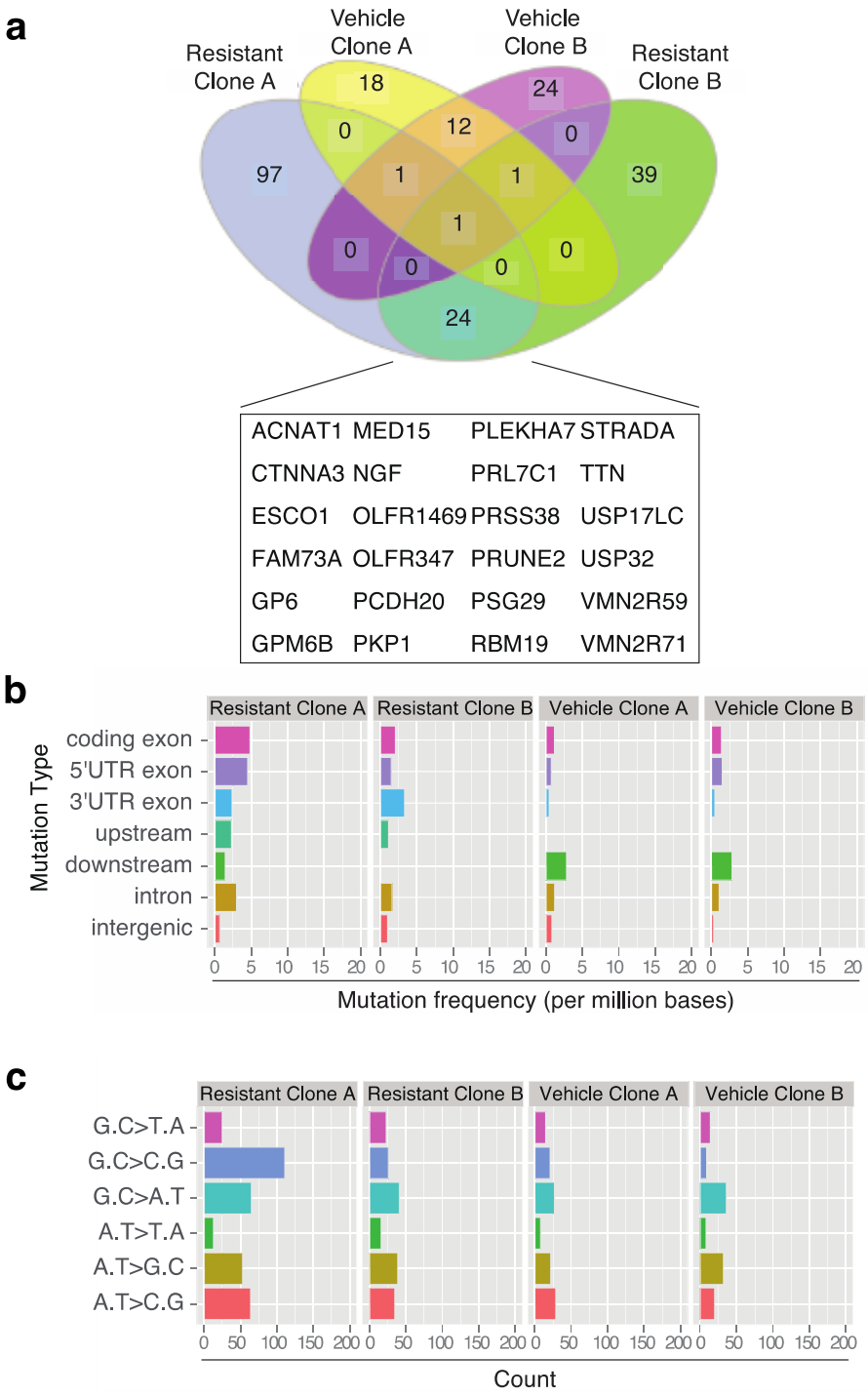

Figure 35 – Mutation analysis by WES

***a**, Venn diagram demonstrating gene mutations shared between vehicle-treated and resistant clones. Highlighted in the call out box are 24 gene mutations shared between resistant clones but not found in vehicle-treated clones. **b**, Resistant clones do not exhibit marked genetic instability with low mutation frequency observed. **c**, No specific mutation signature is identified in resistant clones.*

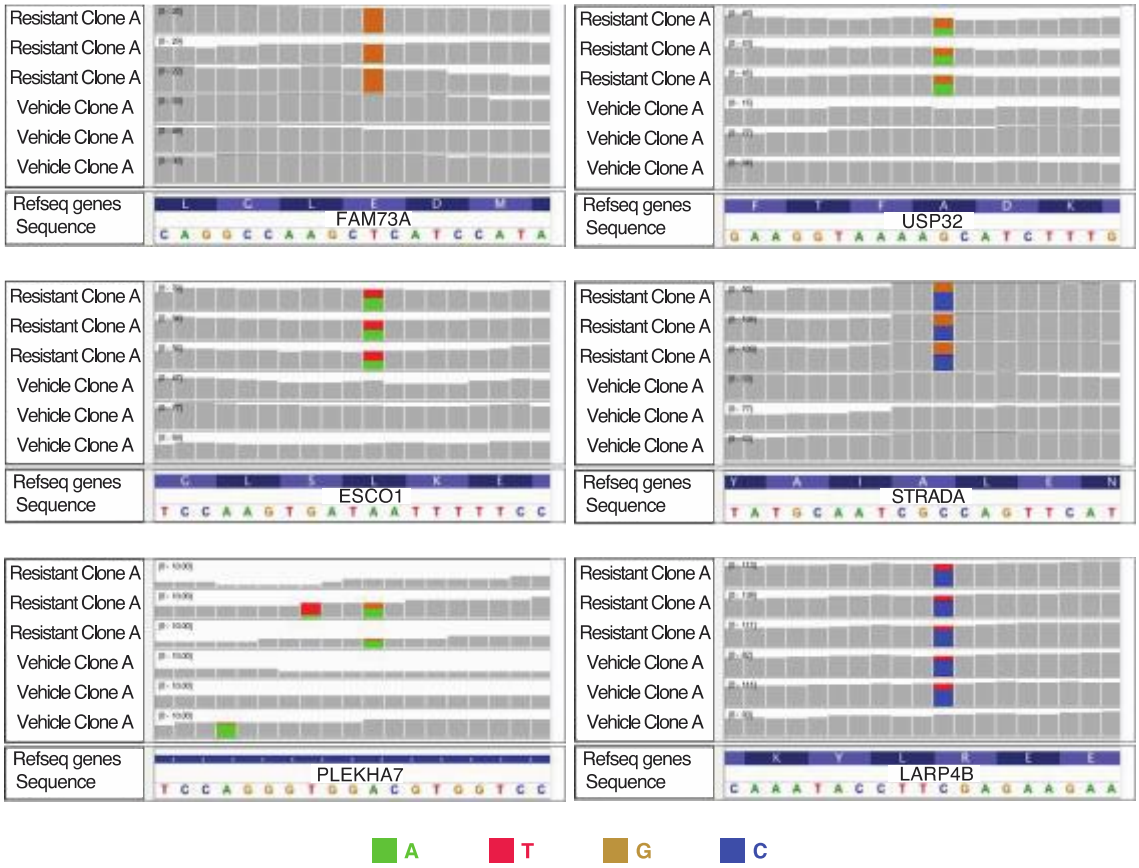

Figure 36 – Validation of WES mutation data by RNA-seq

Mutations detected by WES can be validated with data obtained from RNA-seq of the same clones. Selected examples of mutations unique to resistant clones and shared between vehicle-treated and resistant clones is shown in integrative genomics viewer (IGV) tracks.

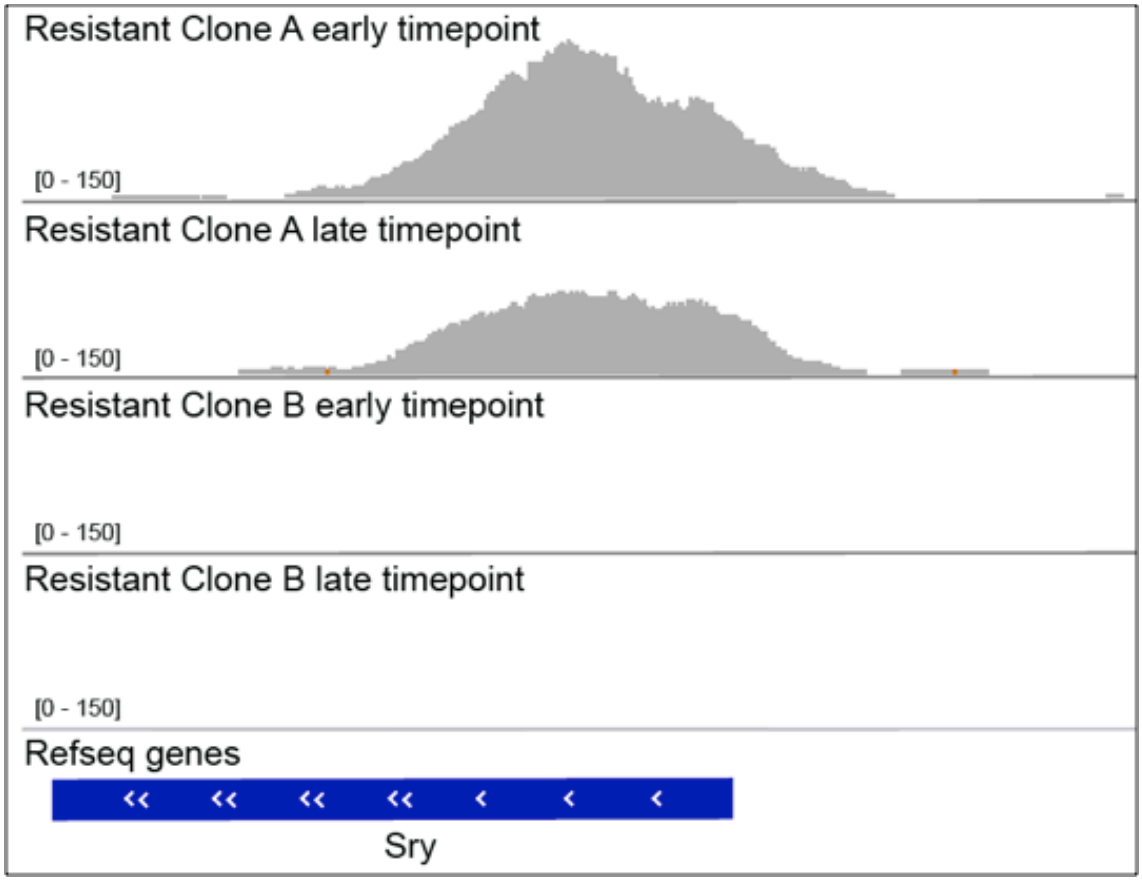

Figure 37 – Confirming clonality of resistant clones by WES

Clonality of resistant cell lines demonstrated in WES. As detailed in methods (section 2.2.8, page 69), the parental MLL-AF9 cell line was derived from both male and female mice. Reads detected at Sry, present on the Y chromosome are displayed.

5.2 Examination of the chromatin interface demonstrates maintenance of expression of key oncogenes despite loss of key transcription factors at TSSs

Pharmacological inhibition of the BET proteins results in incomplete displacement of Brd2, Brd3 and Brd4 from chromatin.[75,101,182,183] In particular, preferential displacement of Brd4 is observed from genomic regions described as 'superenhancers' although the underlying mechanism behind this observation remains controversial.[183,253]

Consistent with the pharmacological activity of I-BET151 in resistant cell lines stably maintained in inhibitor, decreased levels of chromatin bound Brd2, Brd3 and Brd4 were observed in comparison to vehicle-treated controls at TSSs genome wide (Figure 38). Furthermore, this affect was observed to be more prominent in superenhancers (Figure 39).

Of note, examination of key Brd4 targets such as *Myc* demonstrated equal expression in resistant cells despite loss of Brd4 from functional *Myc* enhancer elements in qRT-PCR, microarray and RNA-seq experiments (Figure 40). Loss of Brd4 binding did not occur genome wide with some enhancer elements demonstrating no significant loss (Figure 41). These findings are suggestive of active alternative compensatory transcriptional programs in BET inhibitor resistant cells driving the persistent expression of key oncogenes.

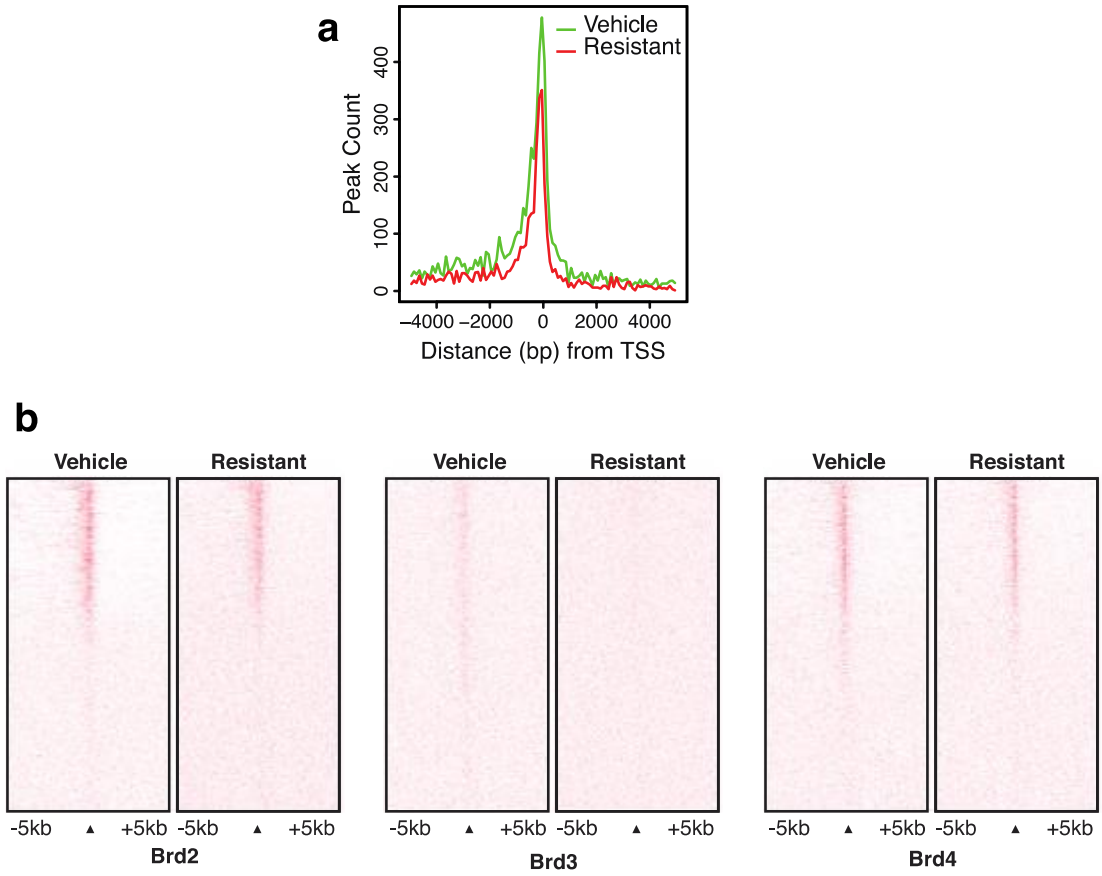

Figure 38 – BET protein binding at TSSs genome wide in ChIP-seq data

Decreased binding of BET proteins is observed genome wide in resistant clones. ***a****, Brd4 binding profiled across annotated TSSs genome wide.* ***b****, Genome wide profiling of Brd2, Brd3 and Brd4 binding at TSSs genome wide in vehicle-treated and resistant clones. A heat map representation of protein binding is presented where red indicates higher density of reads in ChIP-seq data. These data are centred upon the TSS of annotated genes with 5 kb flanking sequences either side and ranked by amount of binding.*

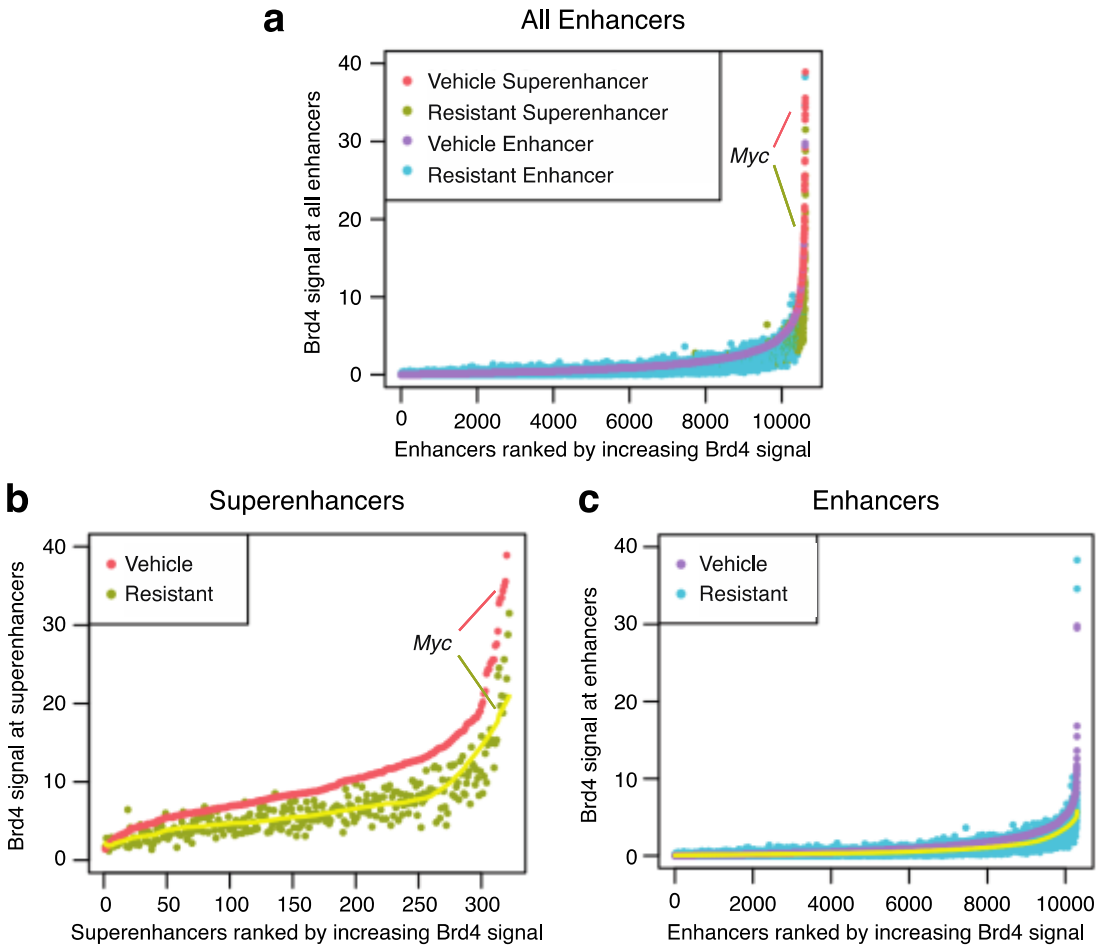

Figure 39 – Brd4 binding at superenhancers in ChIP-seq data

*BET inhibitor resistant clones demonstrate preferential loss of Brd4 at superenhancers. Binding of Brd4 across (**a**) all enhancer elements (**b**) 'superenhancers' and (**c**) 'typical' enhancers in resistant clones in comparison to vehicle-treated clones is presented. Brd4 binding at H3K27ac peaks is ranked by increasing Brd4 signal in vehicle-treated clones. Individual enhancer elements are denoted by dots. Myc is highlighted as an example of a superenhancer associated gene. The yellow trend line in panels b and c reflects the average Brd4 signal in resistant clones across ranked genes.*

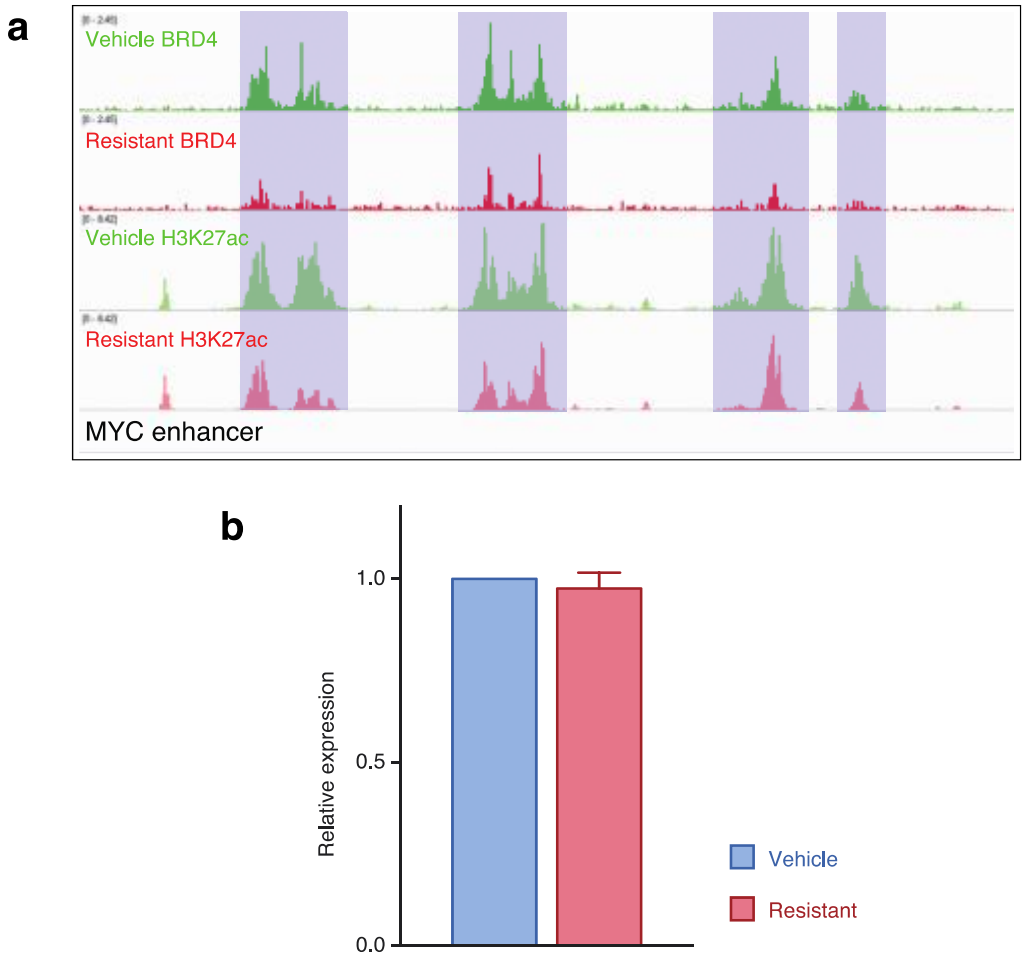

Figure 40 – Myc ChIP-seq and qRT-PCR data

Despite loss of Brd4 binding at Myc enhancer elements, no corresponding decrease in mRNA expression is observed between vehicle-treated and resistant clones. ***a****, Brd4 binding and histone 3 lysine 27 acetylation (H3K27ac) at Myc enhancer elements in IGV plots obtained from ChIP-seq is presented in IGV tracks. Shaded regions are designated enhancer elements.* ***b****, Myc expression from biological triplicate experiments by qRT-PCR (mean ± s.d.).*

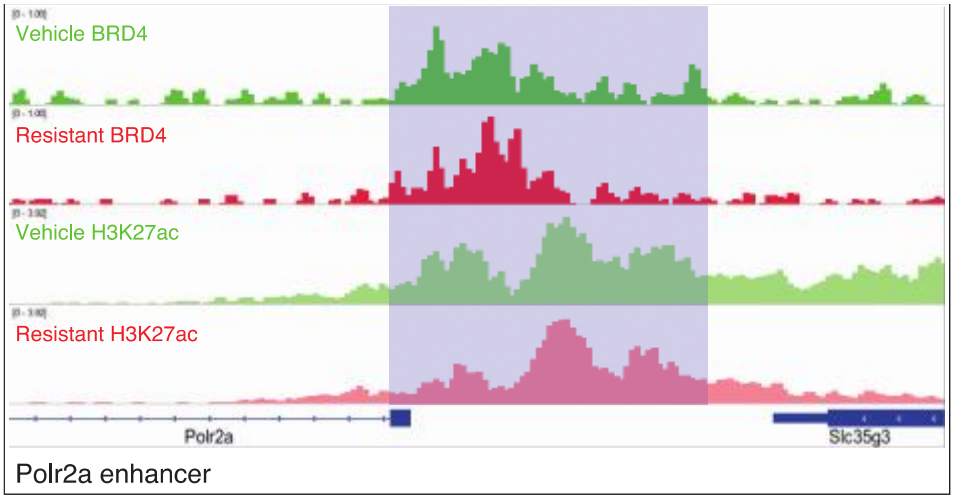

Figure 41 – Polr2a ChIP

Brd4 binding is not consistently lost genome wide. Brd4 binding profile at Polr2a enhancer elements demonstrates no significant loss of Brd4 binding or H3K27ac levels in resistant clones constantly maintained in BET inhibitor. IGV plots of the Polr2a enhancer from ChIP-seq is presented. Shaded regions are designated enhancer elements.

5.3 Gene expression analysis identifies key pathways mediating resistance phenotype

5.3.1 Distinct expression signatures are identified in microarray and RNA-seq data and highlight LSC nature of resistant clones derived *in vitro*

Global transcriptome analyses using two distinct technologies were utilised to further investigate the underlying transcriptional programs driving the molecular mechanism of resistance. These methodologies (microarray and RNA-seq) demonstrated a very high degree of correlation and highlighted several transcriptional changes that clearly distinguished the sensitive parental cell line and vehicle-treated clones from resistant clones (Figure 42, Figure 43 and Figure 44).

Microarray data was obtained from the parental cell line, all derived vehicle-treated clones (x4) and all derived resistant clones (x5) stably maintained at increasing I-BET151 concentrations (400 nM x2, 600 nM x5 and 800 nM x2) (Figure 43). Whilst, as expected, the expression profile of BET inhibitor sensitive vehicle-treated clones clustered closely with the parental cell line on principle component analysis, resistant clones demonstrated clustering of expression profiles according to degree of resistance to BET inhibition. Resistant clones which were stably resistant at the IC_{50} of I-BET151 clustered separately to clones maintained at doses greater than the IC_{80} of I-BET151 suggestive of a threshold of gene expression changes required to tolerate increased drug concentrations. Interestingly, the transcriptome of resistant clones examined four to eight weeks following withdrawal of selective pressure maintained a distinct, intermediate expression profile between BET inhibitor sensitive and resistant clones stably maintained in drug.

Closer examination of a single vehicle-treated clone and a single resistant clone by RNA-seq demonstrated distinct transcriptional changes which were identified by unstructured hierarchical structuring (Figure 44a). Notably, and consistent with our functional data, gene set enrichment analyses (GSEA) of our resistant cells strongly overlapped with previously published transcriptome data of LSCs from this AML model (Figure 44b).[177,179] This LSC signature was derived from comparison of gene

expression in LSC associated L-GMPs with the gene expression of MLL–AF9 cells propagated in liquid culture. Furthermore, examination of microarray data of the bank of derived resistant clones by GSEA demonstrated enrichment of a LSC transcriptome which was proportional to the degree of resistance to BET inhibition (Figure 45).

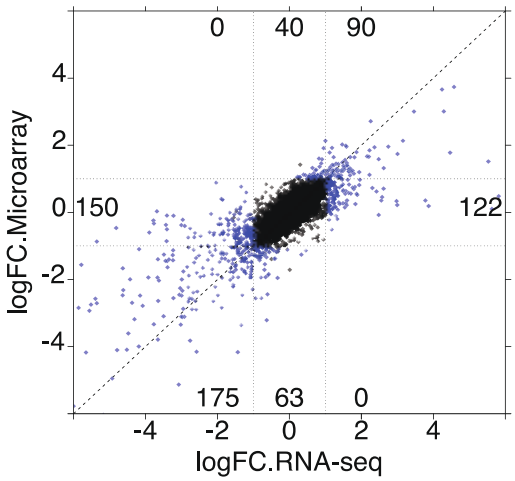

Figure 42 – Global transcriptome analyses

Global transcriptome analyses by microarray and RNA-seq demonstrate a high degree of correlation. Correlation of log2 fold change (logFC) between RNA-seq and microarray data across all genes is presented. No genes show opposing expression changes. Dotted line indicates y = x, blue dots represent genes that are significantly differentially expressed (gene expression log(FC) at least ± 1.0, FDR corrected P < 0.05).

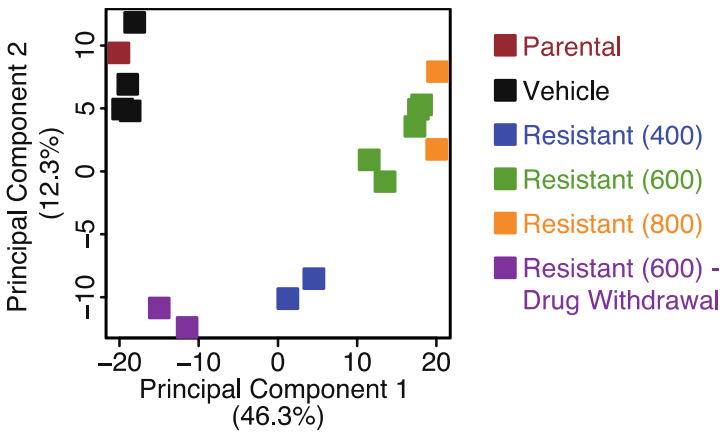

Figure 43 – Transcriptome analysis by microarray

Principle component analysis of parental cell line, vehicle-treated clones (n = 4), resistant clones (n = 9) and resistant clones after drug withdrawal (n = 2). Parentheses denote concentration of I-BET151 (nM) in which resistant clones have been stably maintained.

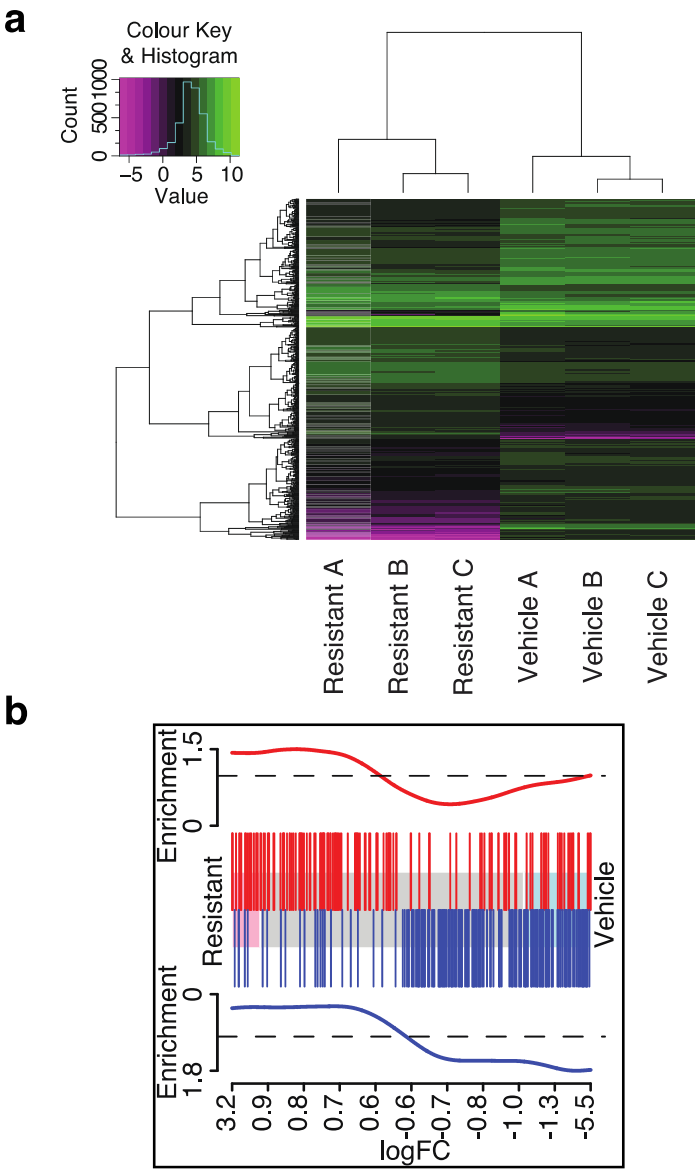

Figure 44 – in vitro RNA-seq data

Distinct transcriptional changes are evident in sensitive and resistant clones. ***a****, Heat map of differential mRNA expression data from a vehicle-treated and resistant clone (maintained in 1 μM I-BET151) performed by RNA-seq obtained in biological triplicate.* ***b****, GSEA identifies enrichment of a published LSC signature associated with a L-GMP self-renewal program in resistant clones. Shaded area in the centre of plot shows genes ranked by fold change in expression in resistant relative to vehicle clones. Pink and blue shading represent significantly up- and down- regulated genes, respectively. Up- and down- regulated genes in the published LSC signature are shown in red and blue, respectively, and correlate with up- and down- regulated (false discovery rate (FDR) p-value <5.0 × 10^{-5} for both) genes in BET inhibitor resistant clones.*

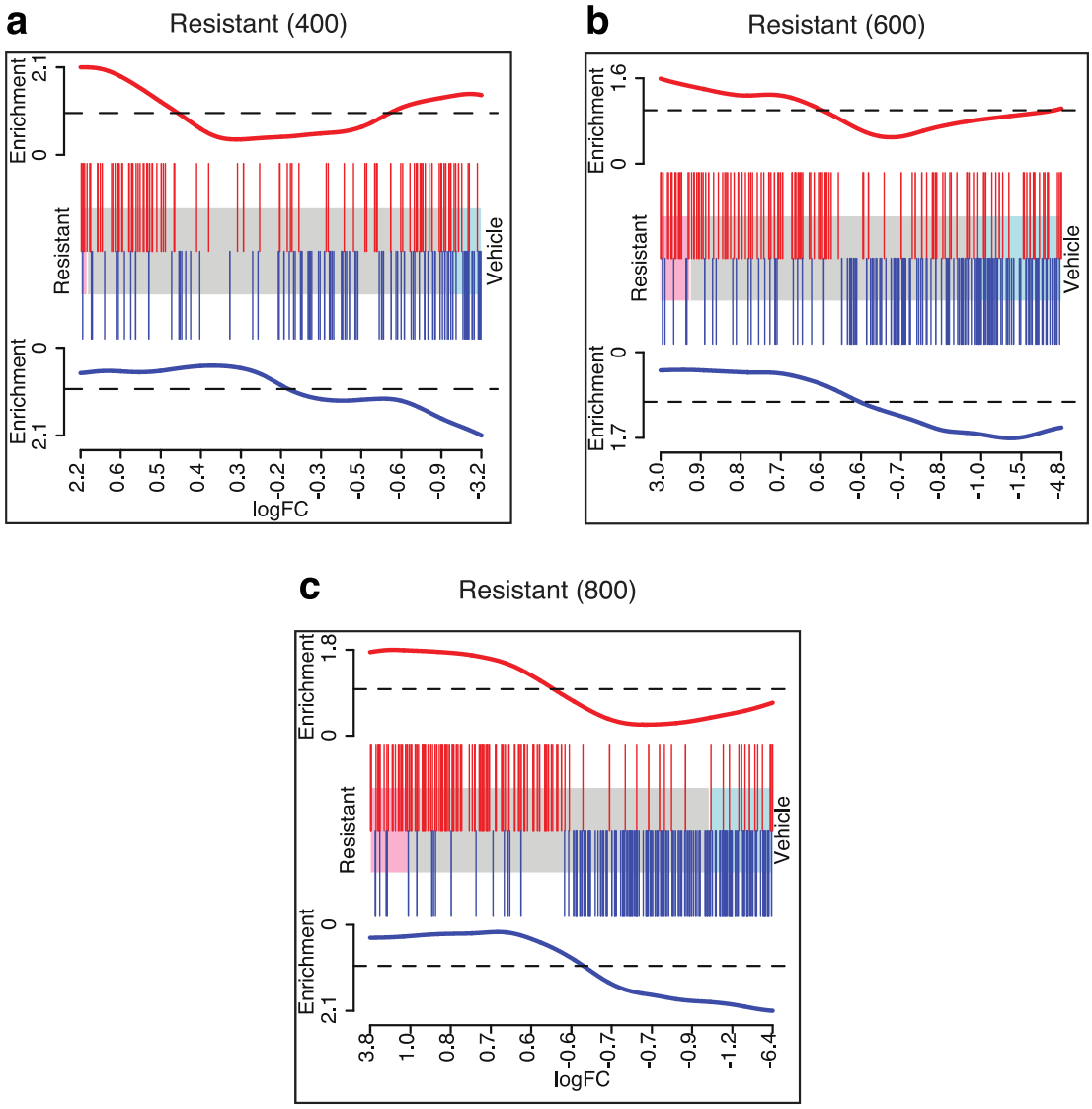

Figure 45 – Microarray GSEA

GSEA shows enrichment of a LSC signature BET inhibitor resistant clones, with resistant clones stably maintained in progressively higher concentrations of I-BET151 demonstrating increasing enrichment of a LSC signature. Resistant (400) upregulated FDR p-value = 1.2 × 10^{-1}, downregulated FDR p-value = 9.3 × 10^{-3}. Resistant (600) upregulated FDR p-value <1.0 × 10^{-4}, downregulated FDR p-value <2.5 × 10^{-4}. Resistant (800) upregulated FDR p-value <5.0 × 10^{-5}, downregulated FDR p-value <5.0 × 10^{-5}.

5.3.2 GSEA demonstrates enrichment for LSC signature following development of *in vivo* resistance

To further extend these findings into the *in vivo* derived model of resistance, the transcriptome of tumours derived from BET inhibitor exposed and BET inhibitor naïve mice were examined by RNA-seq (Figure 46). These tumours were obtained from mice following quaternary transplant which were concurrently used for LDA demonstrating enrichment of LSC frequency (Figure 29, page 128).

Unstructured hierarchical clustering again demonstrated distinct transcriptional changes distinguishing BET inhibitor resistant and BET inhibitor sensitive tumours (Figure 46a). Furthermore, enrichment of the previously described LSC gene expression signature was observed in GSEA (Figure 46b). These findings confirm the LSC nature of BET inhibitor resistant leukaemias in this model.

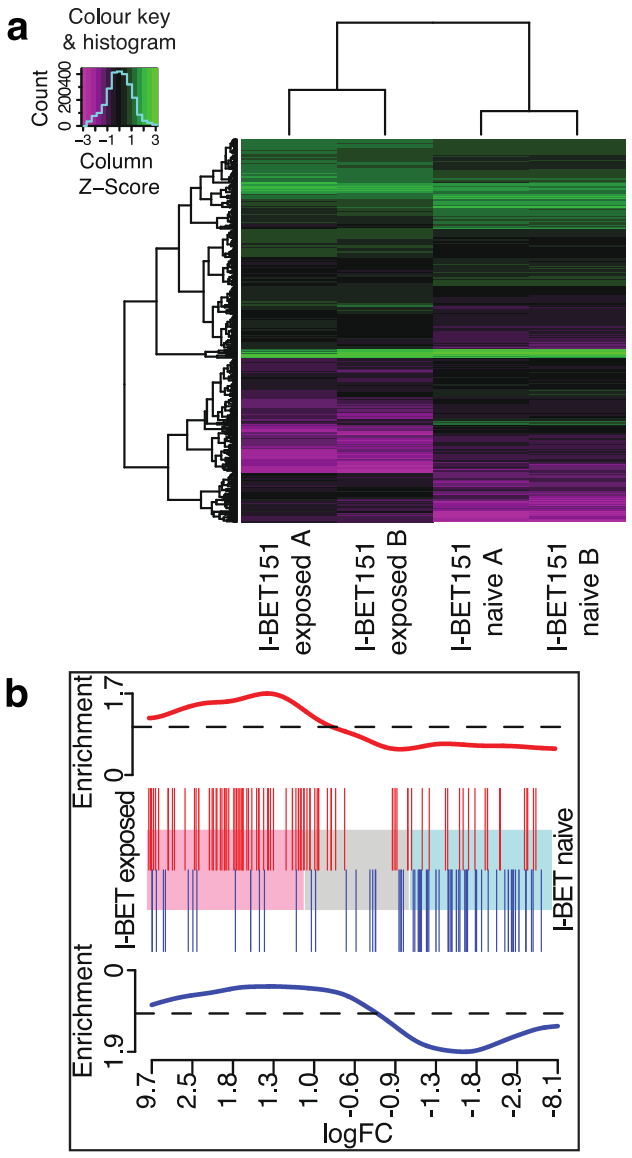

Figure 46 – in vivo RNA-seq data identifies enrichment of LSC gene expression signature following chronic in vivo BET inhibitor exposure

***a**, Heat map of differential mRNA expression data from RNA-seq of leukaemias from the bone marrow of I-BET151-exposed (n = 2) and I-BET151-naive (n = 2) mice after quaternary transplant. **b**, GSEA of RNA-seq data from in vivo leukaemias. Shaded area in the centre of plot shows genes ranked by fold change in expression in BET inhibitor exposed relative to BET inhibitor naïve leukaemias. Pink and blue shading represent significantly up- and down- regulated genes, respectively. Up- and down- regulated genes in the LSC signature are shown in red and blue, respectively, and correlate with up- and down- regulated genes (FDR p-value = 5.0×10^{-2} for both) in BET inhibitor exposed leukaemias.*

5.3.3 Pathway analysis reveals the role of WNT/β-catenin signalling in the regulation of sensitivity to BET inhibition in MLL-AF9 cells

To identify precise transcriptional programmes differentially expressed in BET inhibitor resistant clones, we performed GSEA for major signalling pathways in microarray data obtained from multiple resistant clones. These major signalling pathways have been demonstrated to play a role in the initiation, maintenance or progression of AML or in oncogenesis. [254,255]

These findings demonstrated that the NF-kB pathway was significantly downregulated, whereas both the Wnt/β-catenin and TGF-β pathways were significantly upregulated in resistant clones. In particular, these pathways can potentially be modulated for therapeutic effect in the restoration of BET inhibitor sensitivity or in the prevention of BET inhibitor resistance

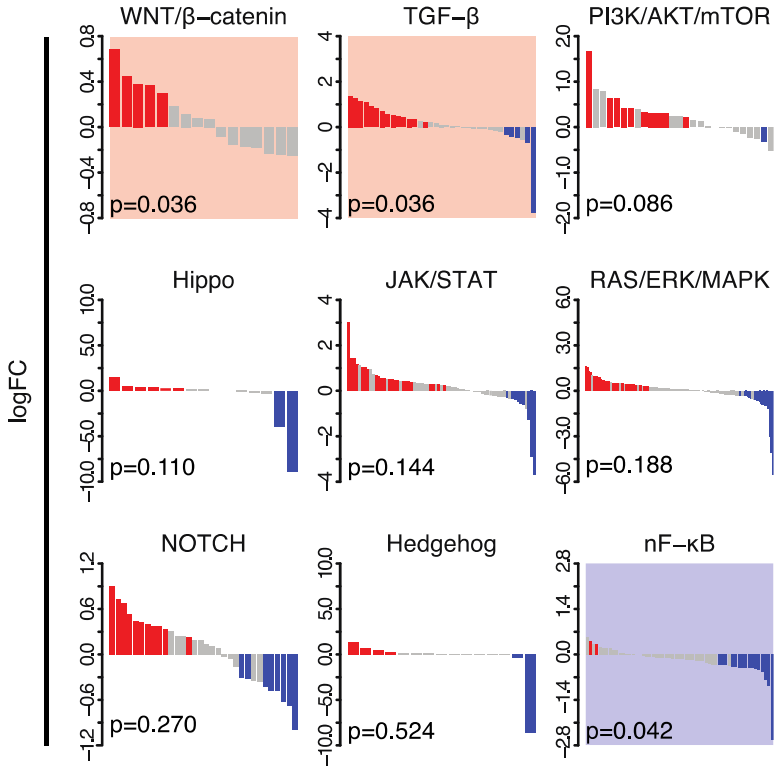

Figure 47 – Pathway GSEA analysis

Statistically significant upregulation (shaded red) of the WNT/β-catenin and TGF-β pathways and downregulation (shaded blue) of the NF-kB pathway is observed in all resistant clones (n = 11). FDR p-values are presented.

Chapter 6 - Examining the role of the WNT/β-catenin pathway in BET inhibitor resistance

Upregulation of the Wnt/β-catenin pathway in resistant clones is an intriguing finding as it has been previously shown to be a major protagonist involved in sustaining LSCs in MLLfp driven murine models of leukaemia.[248,256] Furthermore, the Wnt/β-catenin pathway can be demonstrated to be integral to LSC function in human AML (Figure 48) and has been demonstrated to be integral to LSC function in other cancer stem cell models such as blast crisis CML.[227,257] As such, attention was focussed upon the Wnt/β-catenin pathway and its role in BET inhibitor resistance.

Examination of the Wnt/β-catenin pathway in greater detail demonstrated that several components, from ligand receptors to transcriptional co-activators, were transcriptionally upregulated in MLL-AF9 bearing resistant clones (Figure 49). Furthermore, examination of Wnt/β-catenin pathway genes in resistant cell lines bearing MLL-ENL also demonstrated increased expression of this pathway (Figure 50).

The Wnt/β-catenin pathway is a critical pathway involved in the pathogenesis of many other malignancies, particularly colorectal cancer.[258] In canonical Wnt signalling, β-catenin is maintained in its 'off' state through the action of a negative regulatory complex including adenomatous polyposis coli (APC), Axin, casein kinase 1α (CK1α and GSK3β. In the absence of Wnt ligand binding, this negative regulatory complex phosphorylates β-catenin thereby tagging the protein for proteosomal degradation. Activation of signalling, either through Wnt ligand interaction with frizzled receptors or Lrp5/6, results in inhibition of negative regulatory complex through the recruitment of Dvl proteins. This releases β-catenin, which translocates to the nucleus to bind key transcription factors Tcf4/Lef and modulates transcription of downstream targets such as Myc and Ccnd1 (Figure 49).[259,260] Many approaches are under active development to target aberrant Wnt signalling in oncogenesis.[258] To interrogate the function of the Wnt/β-catenin pathway in mediating resistance to BET inhibition we adopted robust genetic and pharmacological approaches.[261,262]

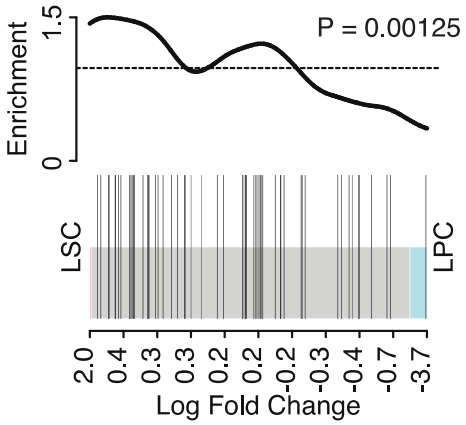

Figure 48 – WNT/β-catenin gene expression signature in LSCs

GSEA of previously published human LSC gene expression data from Eppert et al.[227] demonstrates enrichment of the WNT/β-catenin pathway. Gene expression of LSCs were compared with leukaemia progenitor cells (LPC) and genes upregulated in LSC were analysed for enrichment of the Wnt/β-catenin pathway using ROAST. Shaded area in the centre of plot shows genes ranked by fold change in expression in leukaemia stem cells (LSC) populations relative to leukaemia progenitor cells (LPC). Pink and blue shading represent significantly up- and down- regulated genes, respectively.

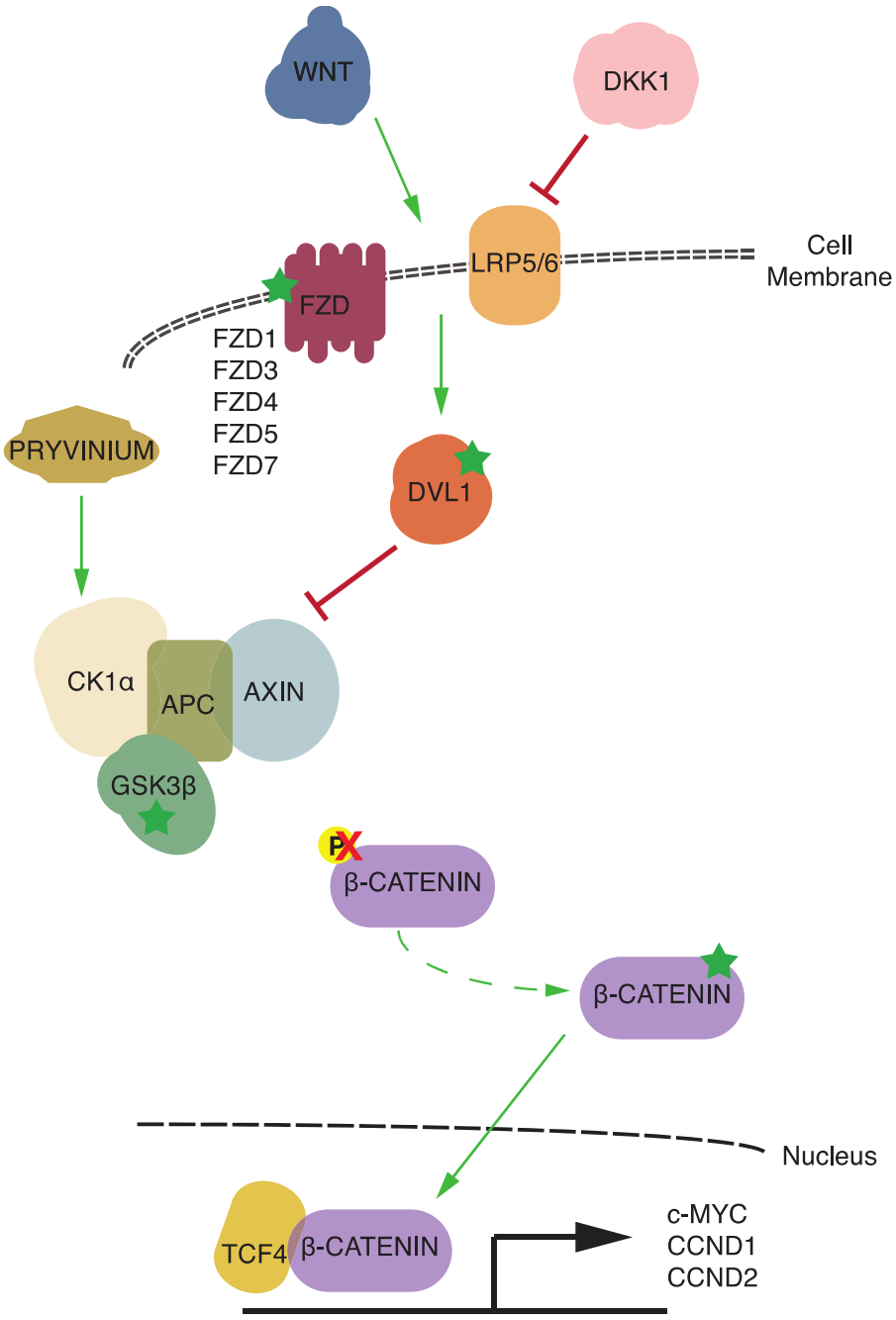
WNT
DKK1
LRP5/6
Cell
Membrane
FZD
FZD1
FZD3
FZD4
FZD5
FZD7
PRYVINIUM
DVL1
CK1α
APC
AXIN
GSK3β
P
β-CATENIN
β-CATENIN
Nucleus
TCF4
β-CATENIN
c-MYC
CCND1
CCND2

Figure 49 – Wnt/β-catenin pathway in resistance to BET inhibitors

Schematic representation of the canonical Wnt/β-catenin pathway. Activation of the canonical Wnt signalling pathway results in inhibition of the negative regulatory complex consisting of scaffold proteins APC and Axin and the kinases GSK3β and CK1α. This allows β-catenin to translocate to the nucleus and exert its role as a transcriptional co-activator. Highlighted by green stars are components of the pathway identified from transcriptome data which are significantly upregulated (>1.5-fold change, FDR <0.05) in resistant clones relative to vehicle-treated clones. Also of note is the action of DKK1 in inhibiting the LRP5/6 interaction with WNT ligands and the action of pyrvinium, a small molecule which enhances the activity of the negative regulatory complex through potentiation of CK1α activity.

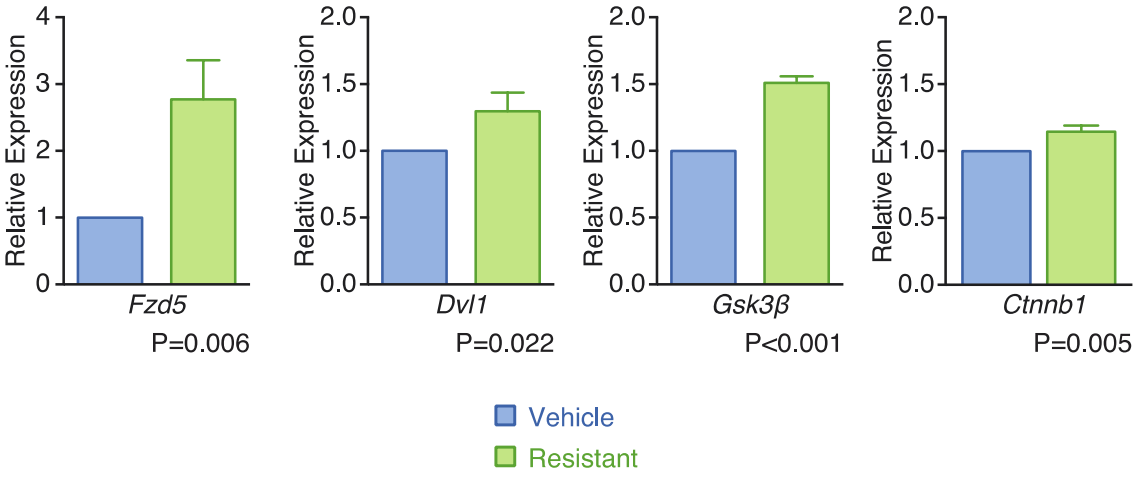

Figure 50 – Wnt/β-catenin pathway expression in MLL-ENL resistant cell lines

Resistant cell lines bearing MLL–ENL demonstrate increased expression of WNT/β-catenin pathway genes. qRT–PCR data performed in biological triplicate (mean ± s.d.). Statistical significance determined by Student's t-test.

6.1 Genetic modulation of the WNT/β-catenin pathway in resistant cell lines restores sensitivity to BET inhibition

6.1.1 Introduction of DKK1 restores immunophenotype, sensitivity to cell cycle arrest and apoptosis

To specifically antagonise Wnt/β-catenin signalling, the Dickkopf Wnt signalling pathway inhibitor 1 (Dkk1) protein was genetically overexpressed (Figure 51). This was achieved through retroviral insertion of a Dkk1 overexpression construct which was a kind gift from A/Prof Steven Lane, QIMR Berghofer Medical Research Institute, Queensland, Australia.

Overexpression of Dkk1 in resistant clones resulted in differentiation to more mature leukaemic blasts with restoration of expression of Gr1 and CD11b (Figure 52a) and reduction in L-GMP frequency (Figure 24 and Figure 52b). These findings are consistent with restoration of a more differentiated immunophenotype which is similar to BET inhibitor sensitive vehicle-treated clones.

Exposure to I-BET151 confirmed restoration of *in vitro* sensitivity to BET inhibition in proliferation (Figure 53) and cell cycle assays (Figure 54). Furthermore, overexpression of Dkk1 in resistant clones resulted in decreased *Myc* mRNA and protein expression (Figure 55). Finally, restoration of *in vivo* sensitivity to BET inhibition was observed in resistant clones overexpressing Dkk1 (Figure 56).

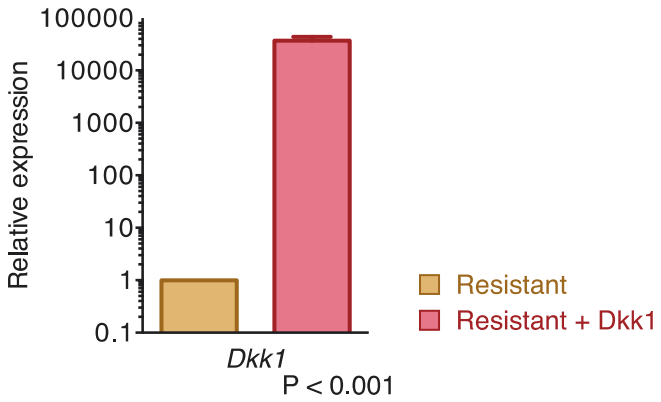

Figure 51 – Dkk1 expression following stable transduction in resistant clones

Dkk1 mRNA expression in resistant cells before and after stable retroviral transduction of murine Dkk1. qRT–PCR data from biological triplicate experiments normalised to untransduced clones is presented (mean ± s.d.).

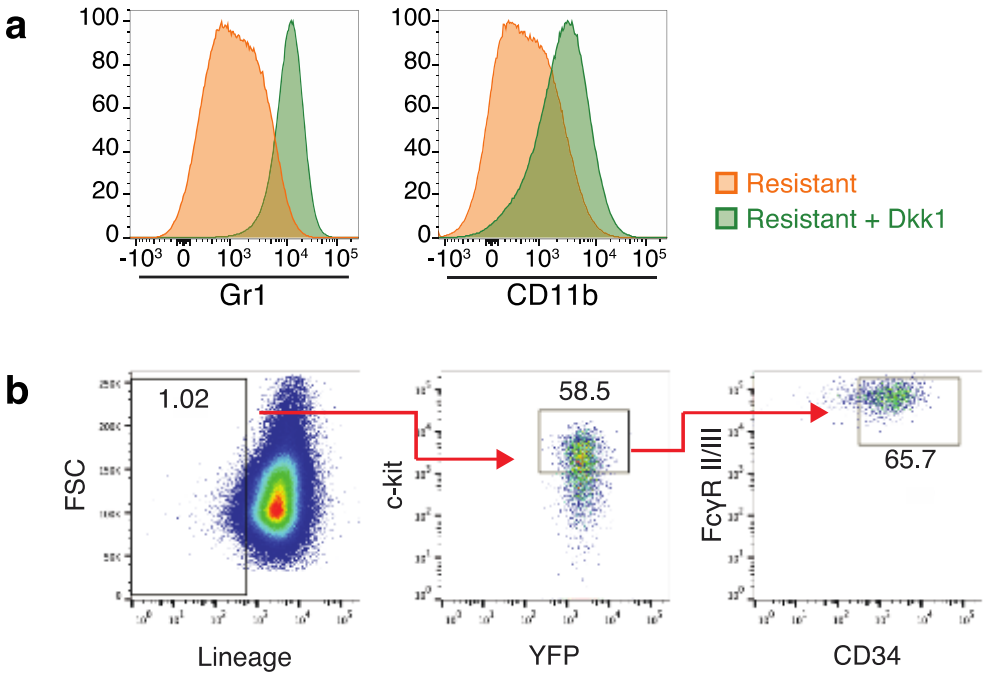

Figure 52 – Immunophenotype of resistant clones following Dkk1 overexpression

Dkk1 overexpression results in restoration of a mature immunophenotype in resistant clones. ***a****, Dkk1 overexpression results in restoration of Gr1 and CD11b expression in resistant clones. Representative FACS analysis of a resistant clone before and after stable retroviral transduction of Dkk1. Non-viable events (PI positive) were excluded.* ***b****, Resistant clones stably expressing Dkk1 do not show immunophenotypic enrichment for L-GMPs (see Figure 24, page 120 for comparison). Representative FACS analysis of resistant clone overexpressing Dkk1 is presented, percentages represent proportion of parent gate. Non-viable events (PI positive) were excluded.*

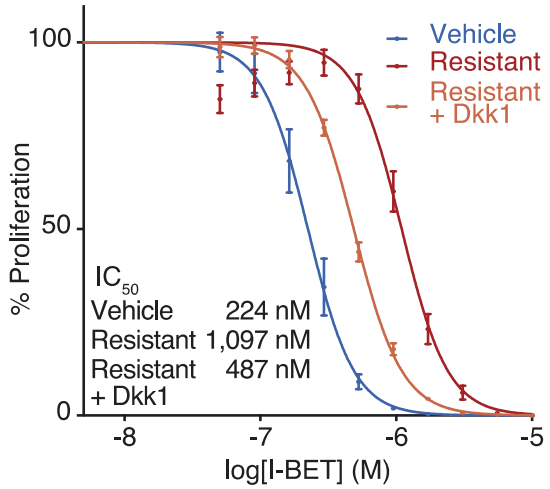

Figure 53 – Proliferation assays following overexpression of Dkk1 in resistant clones

Partial restoration of sensitivity to BET inhibition is observed in resistant clones following stable transduction with Dkk1. Representative dose-response curve of a vehicle-treated clone and resistant clone with and without expression of Dkk1 after 72 hours of growth (mean ± s.e.m., n = 16 per group).

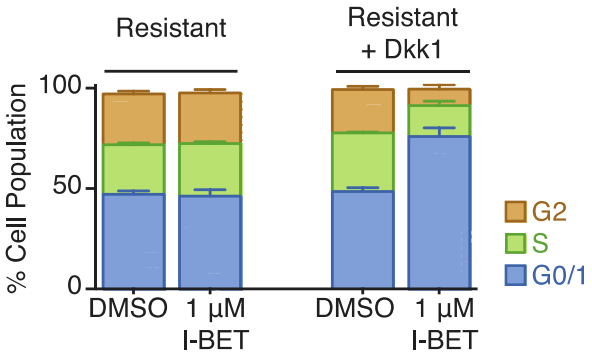

Figure 54 – Cell cycle assays following overexpression of Dkk1 in resistant clones

Restoration of BET inhibitor induced cell-cycle arrest is observed in resistant clones stably transduced with Dkk1. Flow cytometric analysis after 48 hour exposure to either vehicle or 1 μM I-BET151 in biological triplicate experiments (mean ± s.e.m.) is presented.

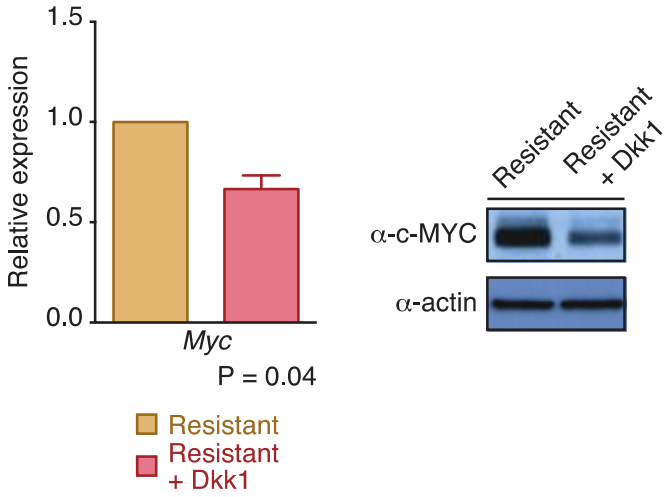

Figure 55 – Myc expression following overexpression of Dkk1 in resistant clones

Negative regulation of Wnt/b-catenin signalling by Dkk1 in resistant clones results in decreased expression of Myc mRNA and protein. qRT–PCR data from biological triplicate experiments (mean ± s.d.) is presented.

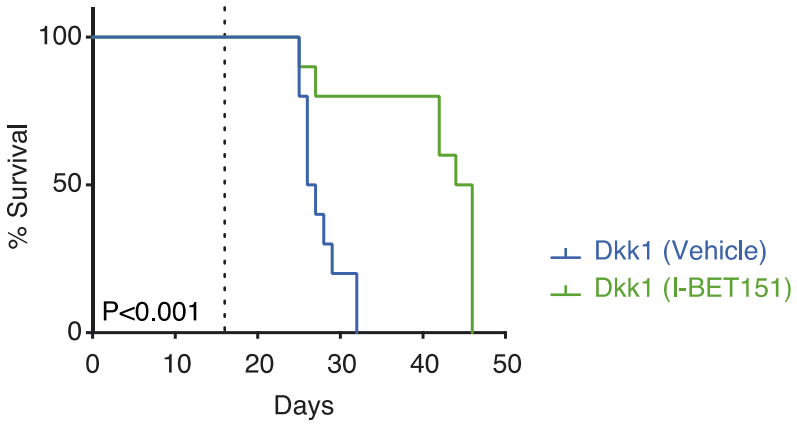

Figure 56 – Restoration of in vivo sensitivity to BET inhibition following overexpression of Dkk1 in resistant clones

Kaplan–Meier curve of vehicle and I-BET151 treated mice after syngeneic transplantation of a resistant clone stably transduced with Dkk1 (n = 10 per group, statistical significance calculated using a log-rank test). Dotted line denotes treatment beginning on day 16 with 30 mg/kg I-BET151.

6.2 Pharmacological inhibition of the WNT/β-catenin pathway restores sensitivity to BET inhibition

Further examination of the role Wnt/β-catenin signalling plays in resistance to BET inhibition was undertaken utilising the tool compound pyrvinium, an established small-molecule inhibitor of Wnt signalling. Pyrvinium functions by selectively potentiating the activity of CK1α through allosteric activation.[262] It is a FDA approved antihelminthic drug with potential translatability as a Wnt pathway inhibitor in humans. However, *in vivo* toxicity is a significant limiting factor in further drug development.[262,263]

In vitro assessment of pyrvinium activity in vehicle-treated clones demonstrates reduction in the expression of Wnt/β-catenin target genes *Myc* and *Ccnd2* (Figure 57). Indeed, both vehicle-treated and resistant clones demonstrated nanomolar sensitivity to pyrvinium (Figure 58a). Interestingly, when the activity of pyrvinium was assessed in combination with BET inhibition, synergy was demonstrated in resistant clones at a range of drug concentrations (Figure 58b). Accordingly, when utilised in combination with I-BET151, the expression of *Myc* and *Ccnd2* in resistant clones was reduced (Figure 59). This was not observed in vehicle-treated clones suggesting that resistant clones were particularly dependent on Wnt/β-catenin signalling.

Similar to the findings observed with genetic inhibition of Wnt/β-catenin signalling, exposure of resistant clones to pyrvinium resulted in the restoration of expression of Gr1 and CD11b (Figure 60). Although, in combination with I-BET151, pyrvinium exposure resulted in a modest restoration of sensitivity to BET inhibitor induced cell cycle arrest in resistant clones, this was associated with an increase in the induction of cell death (Figure 61). These findings are consistent with Wnt/β-catenin signalling playing a key role in mediating resistance to BET inhibitors.

To assess the *in vivo* efficacy of combination therapy, the stepped pyrvinium dosing regimen of Xu et al was utilised to minimise toxicity.[263] Initial maximal tolerated dose (MTD) assessments demonstrated that >0.5 mg/kg pyrvinium in combination with >20 mg/kg I-BET151 resulted in unacceptable toxicity in mice following syngeneic transplant of resistant clones. In particular, distressed mice who were euthanized were observed to have anorexia and marked thrombocytopenia in the absence of significant

disease burden. Therefore, drug dosing was modified to adopt a short 14 day dosing schedule of drugs delivered at lower doses. Despite this, mice cohorts administered combination therapy with pyrvinium and I-BET151 demonstrated a statistically significant survival advantage (Figure 62).

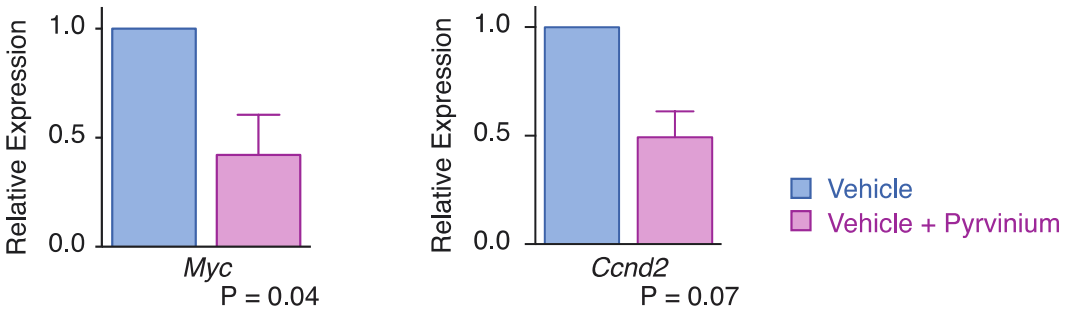

Figure 57 – Wnt/β-catenin target gene expression by qRT-PCR in vehicle-treated clones

Pyrvinium reduces the expression of Wnt/β-catenin target genes Myc and Ccnd2 in vehicle-treated clones following treatment with 30 nM pyrvinium for 48 hours. qRT-PCR data from biological duplicate experiments (mean ± s.e.m.) is presented.

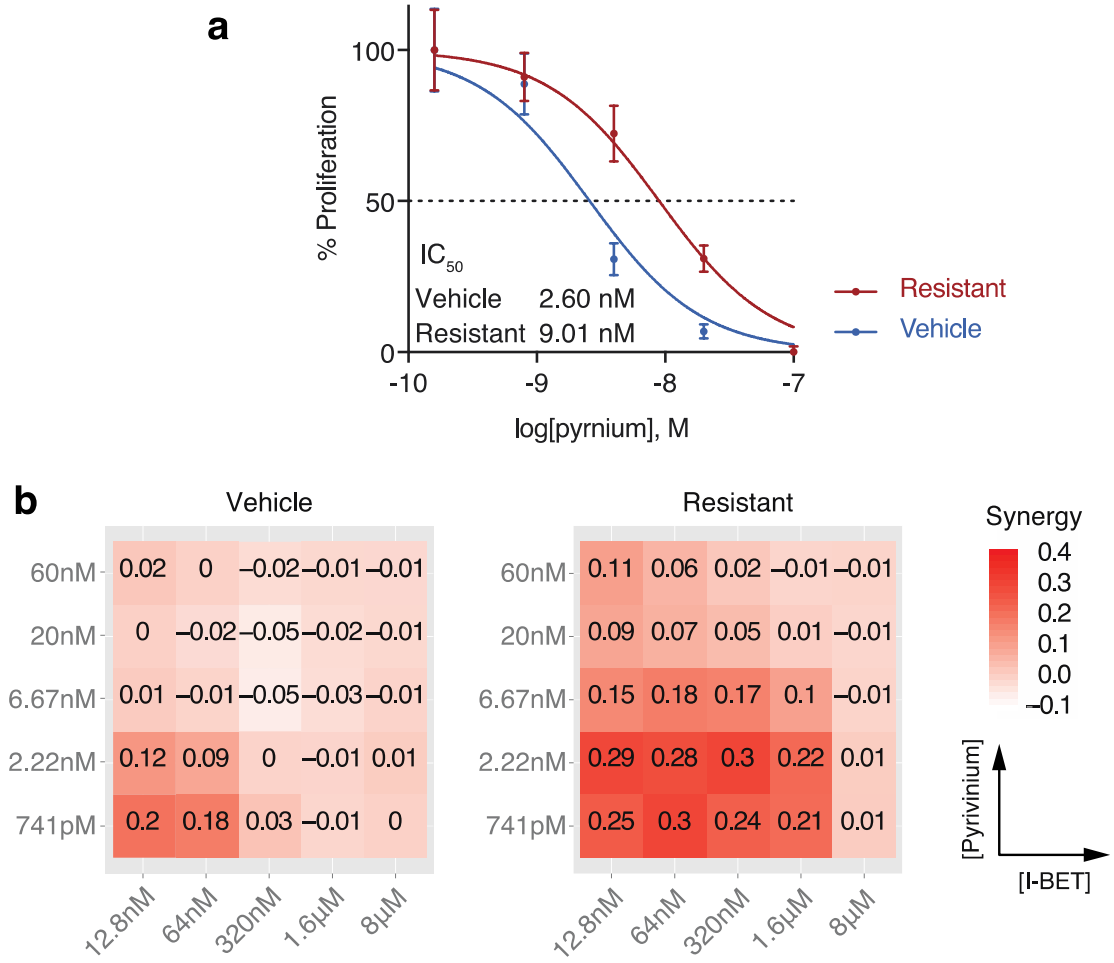

Figure 58 – Pyrvinium proliferation assays

Pyrvinium demonstrates synergistic activity with I-BET151 in resistant clones. ***a****, Representative dose-response curve of a vehicle-treated clone and resistant clone treated with pyrvinium after 48 hours of drug exposure (mean ± s.e.m., n = 4 per group).* ***b****, Heat map representation of Bliss interaction index[229] across five-point dose range of pyrvinium and I-BET151 performed in biological quadruplicate proliferation assays following 48 hours of drug exposure. Synergy is observed following treatment of resistant clones which is not evident in vehicle-treated clones.*

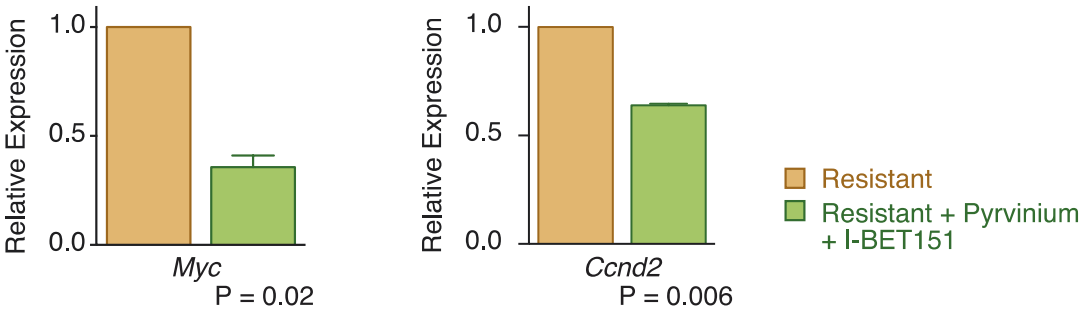

Figure 59 – Wnt/β-catenin target gene expression by qRT-PCR in resistant clones

Pyrvinium, when utilised in combination with I-BET151, results in reduced expression of Myc and Ccnd2 in resistant clones. qRT-PCR data from resistant clones treated with a combination of 1 μM I-BET151 and 30 nM pyrvinium (mean ± s.e.m.) is presented.

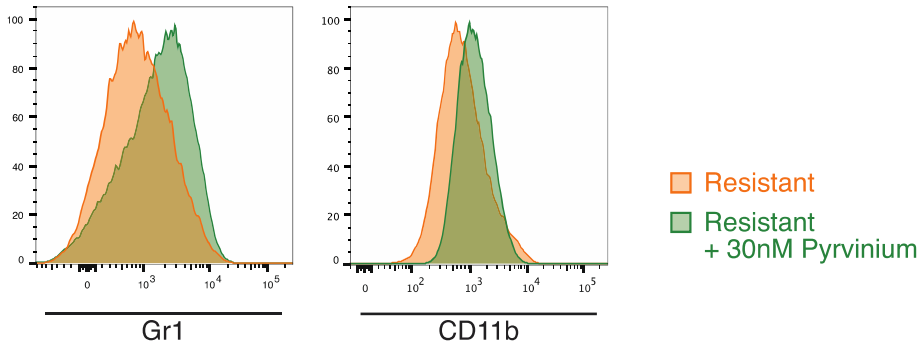

Figure 60 – Immunophenotype of resistant clones following exposure to pyrvinium

Exposure of resistant clones to the Wnt/β-catenin pathway inhibitor pyrvinium results in re-expression of Gr11 and CD11b. Representative FACS analysis of resistant clone in the presence or absence of 30 nM pyrvinium following 48 hours of growth is presented. Non-viable events (PI positive) were excluded.

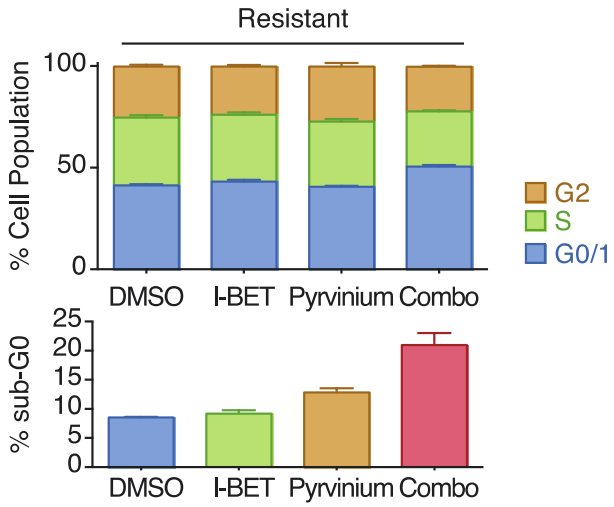

Figure 61 – Response of resistant clones to pyrvinium in cell cycle assays

Pyrvinium synergises with I-BET151 to induce a modest cell cycle arrest and an induction of cell death (sub-G0 cell fraction). Resistant clones were treated for 24 hours with vehicle (0.1% DMSO), 1 μM I-BET151, 30 nM pyrvinium or a combination of both active compounds. Data from biological triplicate experiments (mean ± s.e.m.) is presented.

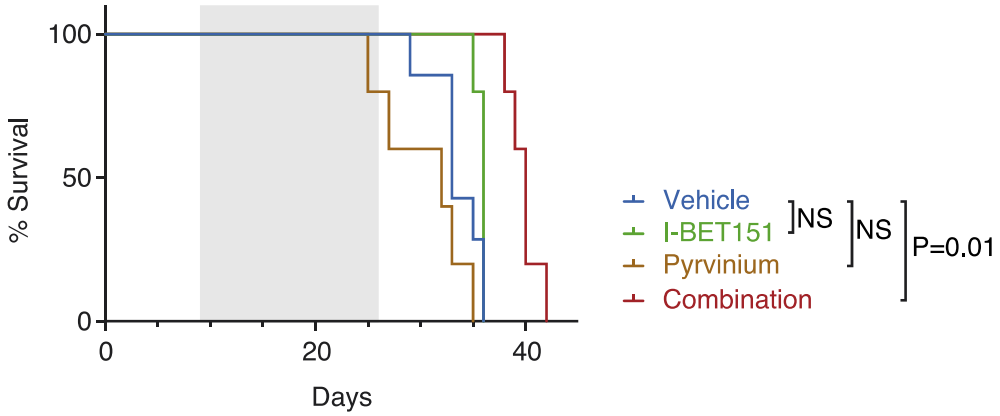

Figure 62 – Combination therapy with Pyrvinium restores sensitivity to BET inhibition in vivo

Treatment of mice following syngeneic transplant of resistant clones with pyrvinium restores sensitivity to BET inhibition. Treatment with pyrvinium alone resulted in toxicity. Kaplan-Meier curve of mice treated with vehicle, I-BET151, pyrvinium or a combination of both active drugs after syngeneic transplantation of resistant clones. Shaded area denotes active treatment between days 9 and 26 (vehicle n = 7, I-BET n = 5, pyrvinium n = 5, combination n = 5, statistical significance calculated using a log-rank test). Mice were administered 20 mg/kg I-BET151 and/or pyrvinium in incremental doses to a maximum of 0.5 mg/kg.

6.3 Genetic activation of Wnt/ β-catenin signalling results in the rapid development of resistance

To confirm the role of Wnt/β-catenin signalling in mediating resistance to BET inhibition, genetic knockdown studies of Apc were undertaken. shRNA mediated downregulation of *Apc*, a negative regulator of Wnt signalling, results in activation of the Wnt/β-catenin signalling pathway.[230] Competitive proliferation assays were performed using constitutively expressed shRNAs directed against *Apc* that were a kind gift from Dr Johannes Zuber, The Research Institute of Molecular Pathology (IMP), Vienna, Austria (Figure 63).

Successful transduction of shRNAs results in the detectable fluorescent expression of mCherry by flow cytometry (Figure 63), the decreased expression of *Apc* (Figure 64a) and increased expression of the Wnt/β-catenin target gene *Myc* (Figure 64b). Cell populations can be tracked over time in competitive proliferation assays where proliferative advantage/disadvantage in the face of selective pressure results in the enrichment/loss of cells as observed by flow cytometry.

This model system was used to assess the activation of Wnt signalling in sensitive clones. Stimulation of the Wnt/β-catenin pathway in sensitive cells, by downregulation of *Apc*, confers BET inhibitor resistance, further highlighting the crucial influence of this pathway on BET inhibitor efficacy (Figure 65). As opposed to the clonal derivation of resistance over many months as previously described, the acquisition of rapid resistance was observed.

Time to the development of resistance varied between shRNAs employed but was robustly observed between 5 to 7 days with Apc shRNA #5011 (Figure 65a) whereas time to robust resistance with Apc shRNA #2253 (Figure 65b) was 9 to 13 days. Sensitivity of vehicle-treated cells to BET inhibition was maintained with the viability of these cells allowing for culture in the presence of BET inhibitor for only 3 days (Figure 65c).

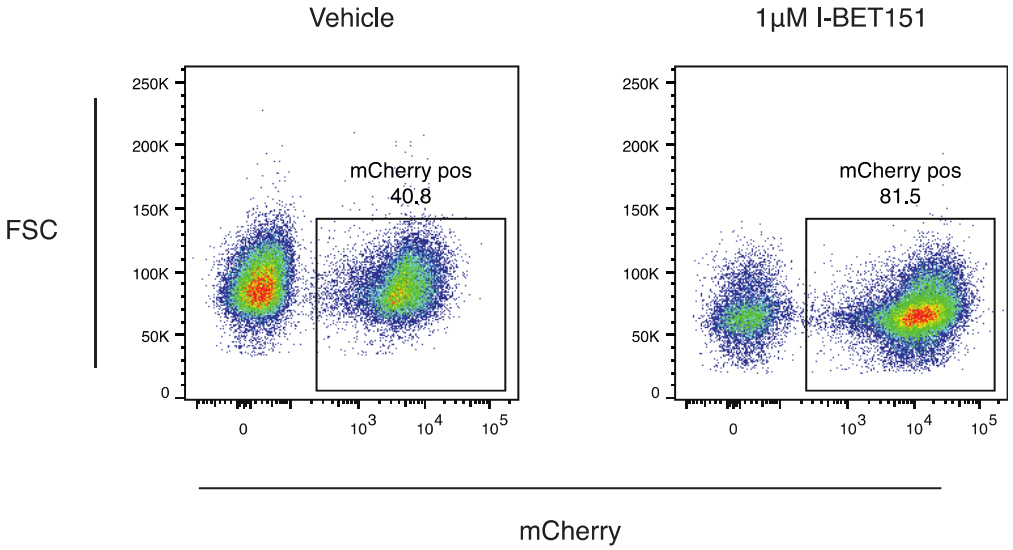

Figure 63 – Competitive shRNA assays by flow cytometry

Successful transduction of a miRE shRNA containing vector pLMPC (pMSCV-miRE-PGK-PuroR-IRES-mCherry) results in the constitutive expression of shRNAs linked to mCherry expression. These cells can be followed over time in competitive proliferation assays to evaluate competitive advantage/disadvantage which shRNA expression confers. Representative FACS plots after 7 days of cumulative drug exposure to either vehicle (0.1% DMSO) or 1 µM I-BET in a vehicle-treated clone transduced with an Apc shRNA is presented.

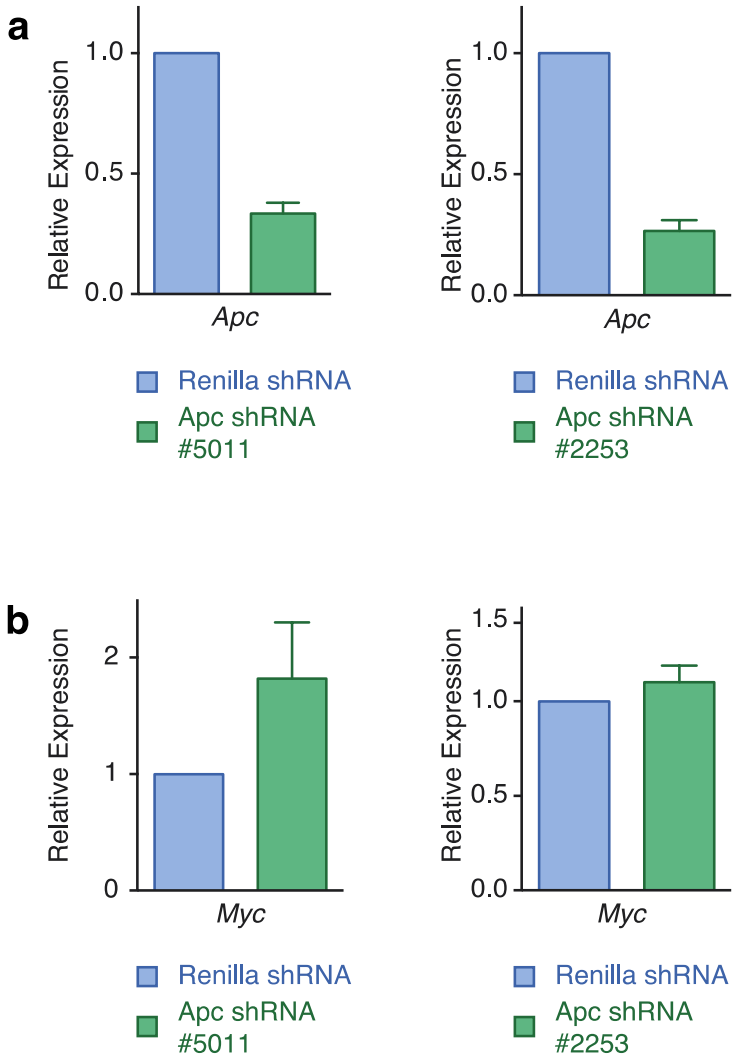

Figure 64 – Validation of Apc shRNAs by qRT-PCR

Two independent shRNAs result in the decreased expression of Apc which result in increased Wnt pathway signalling. ***a****, Apc expression by qRT–PCR from FACS-isolated shRNA-containing cells performed in biological duplicate (mean ± s.e.m.).* ***b****, shRNA-mediated knockdown of Apc results in increased expression of Wnt/β-catenin target gene Myc. qRT–PCR data from FACS isolated shRNA containing cells performed in biological duplicate (mean ± s.e.m.) is presented.*

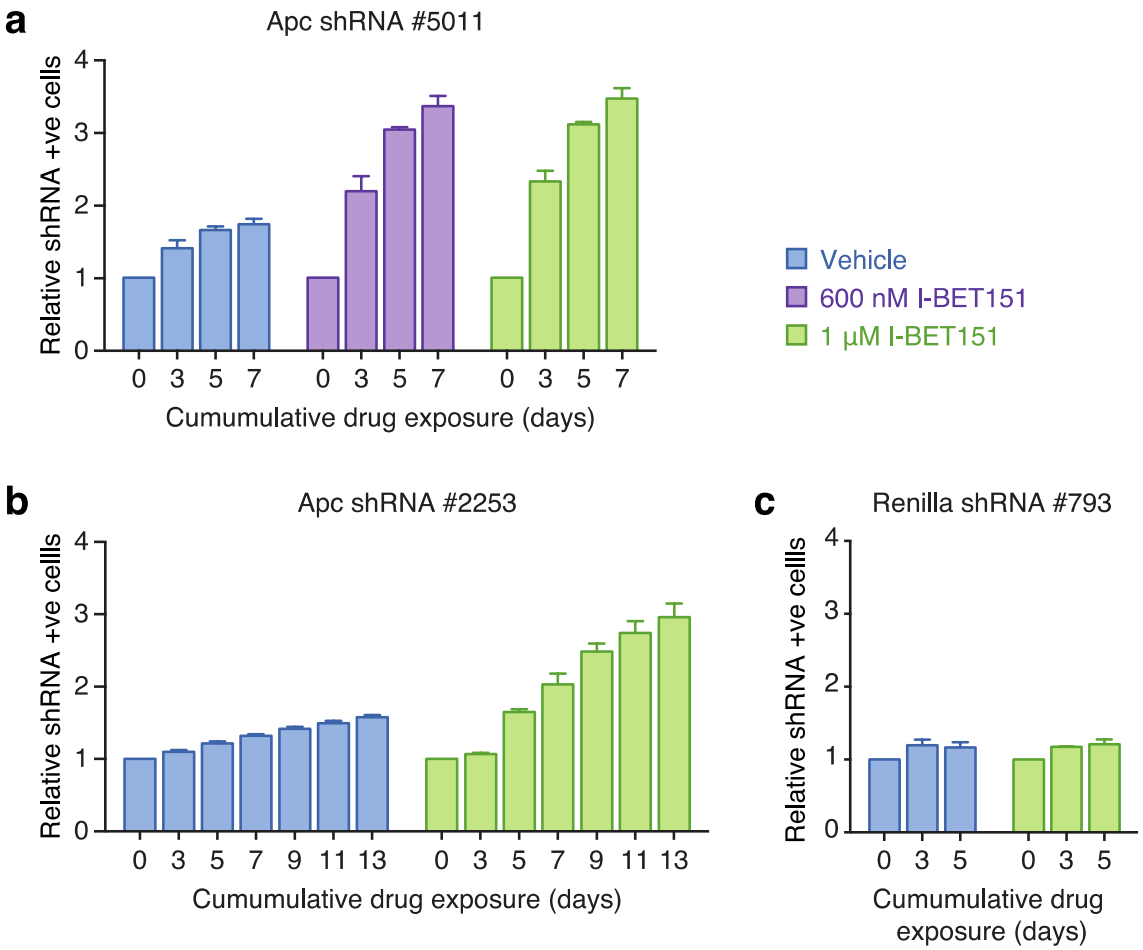

Figure 65 – Apc knockdown confers proliferative advantage and BET inhibitor resistance to vehicle-treated clones

shRNA-mediated knockdown of Apc, a negative regulator of Wnt/β-catenin signalling, confers resistance to vehicle-treated clones. BET inhibitor treatment enriches for shRNA-containing (mCherry-positive) cells over time as demonstrated by flow cytometry in competitive proliferation assays. ***a-b****, Independent shRNAs directed against Apc confer resistance to vehicle-treated clones whilst* ***c****, a shRNA directed against Renilla luciferase conferred no proliferative advantage/disadvantage. Viable, shRNA-positive cells after treatment with either vehicle or I-BET151 at indicated doses normalized to day 0 performed in biological triplicate (mean ± s.d.) is displayed.*

6.4 WNT/β-catenin signalling is a biomarker of response to BET inhibition in human MLLfp driven AML

BET inhibitors have demonstrated a broad range of efficacy against primary human AML samples.[75,182] To explore the translational relevance of these findings, correlation of baseline Wnt/β-catenin pathway and target gene expression was undertaken against the degree of I-BET151 induced apoptosis in these samples (Figure 66 & Figure 67). A high degree of correlation was observed in preliminary (Figure 68) and subsequent (

Figure 69) statistical analysis (see also Methods section 2.2.22, page 88). These data support of the finding of increased activity of the WNT/β-catenin pathway negating the effects of BET inhibition and highlight the potential for examination of the pathways as a biomarker of response in clinical trials.

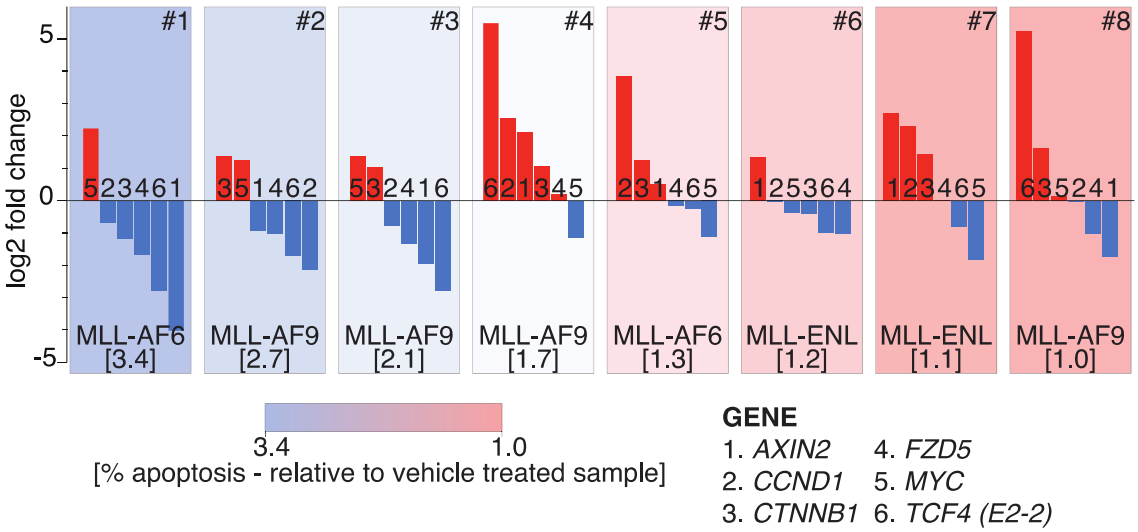

Figure 66 – Examination of WNT/β-catenin pathway and target genes by qRT-PCR in primary human AML samples

Assessment of β-catenin pathway gene expression in eight primary human AML samples with associated response to I-BET151 exposure. Each panel represents an individual primary human AML sample, with genetic abnormality denoted. Waterfall plot of relative qRT–PCR expression data of key β-catenin pathway genes (AXIN2, CCND1, CTNNB1, FZD5, MYC, TCF4 (also known as E2-2)) is displayed. The relative expression of each gene is normalised to the median expression across samples. Each bar is labelled 1–6 according to gene represented. Relative apoptosis observed after 48 hour exposure to 500 nM I-BET151 versus vehicle (0.1% DMSO) is denoted in square parenthesis and is also represented as a heat map background shading in each panel (further details found in Figure 67).

a

Patient	MLL-FUSION	% Viable cells		% Apoptosis (Annexin V+/PI+)	
		DMSO	I-BET	DMSO	I-BET
1	MLL-AF6	51	15	49	85
2	MLL-AF9	43	16	57	84
3	MLL-AF9	46	22	54	78
4	MLL-AF9	34	20	66	80
5	MLL-AF6	55	41	45	59
6	MLL-ENL	65	53	35	47
7	MLL-ENL	68	64	32	36
8	MLL-AF9	73	70	27	30

b

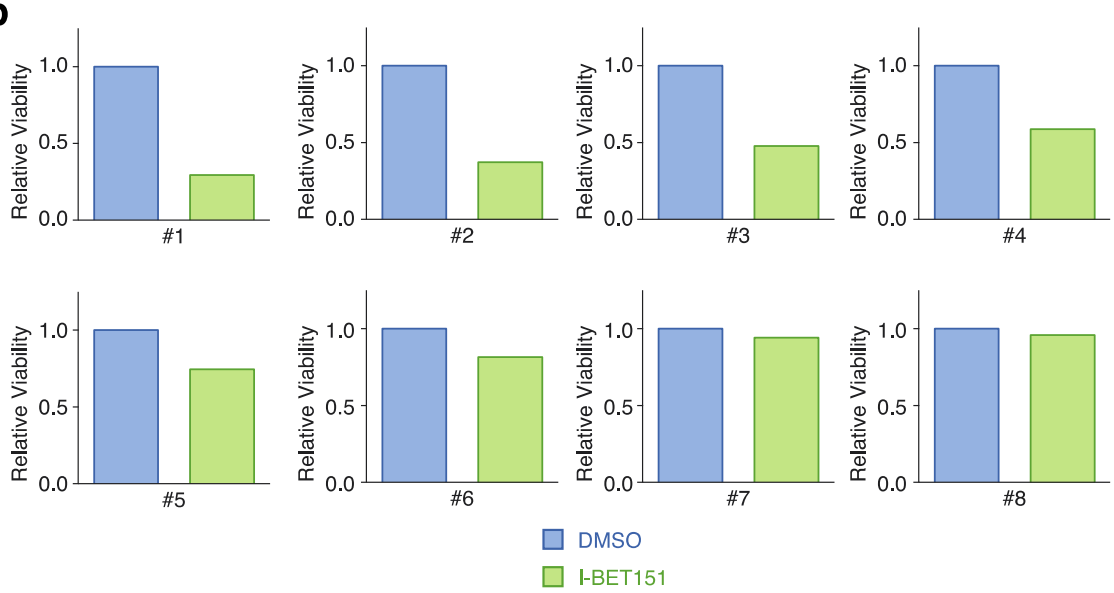

Figure 67 – Response to I-BET151 treatment in primary human AML samples

Examination of response to BET inhibitor treatment across a panel of eight primary human AML samples by flow cytometric analysis of apoptosis. ***a****, Apoptosis observed after 48 h exposure to either vehicle (0.1% DMSO) or 500 nM I-BET151.* ***b****, Relative viability of primary human AML samples after treatment with I-BET151. Comparison is made of the proportion of viable cells identified in the I-BET151 treated sample relative to the vehicle treated sample.*

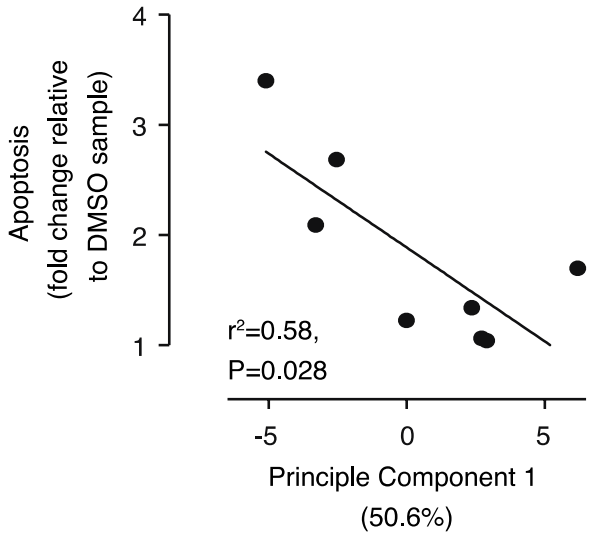

Figure 68 – Correlation of WNT/β-catenin expression with I-BET151 responsiveness in primary human AML

WNT/β-catenin pathway and target gene expression correlates with responsiveness to I-BET151 in primary human AML samples. Correlation between aggregate relative expression of examined β-catenin pathway genes with responsiveness to I-BET151 therapy is presented. Statistical significance determined using Pearson's correlation.

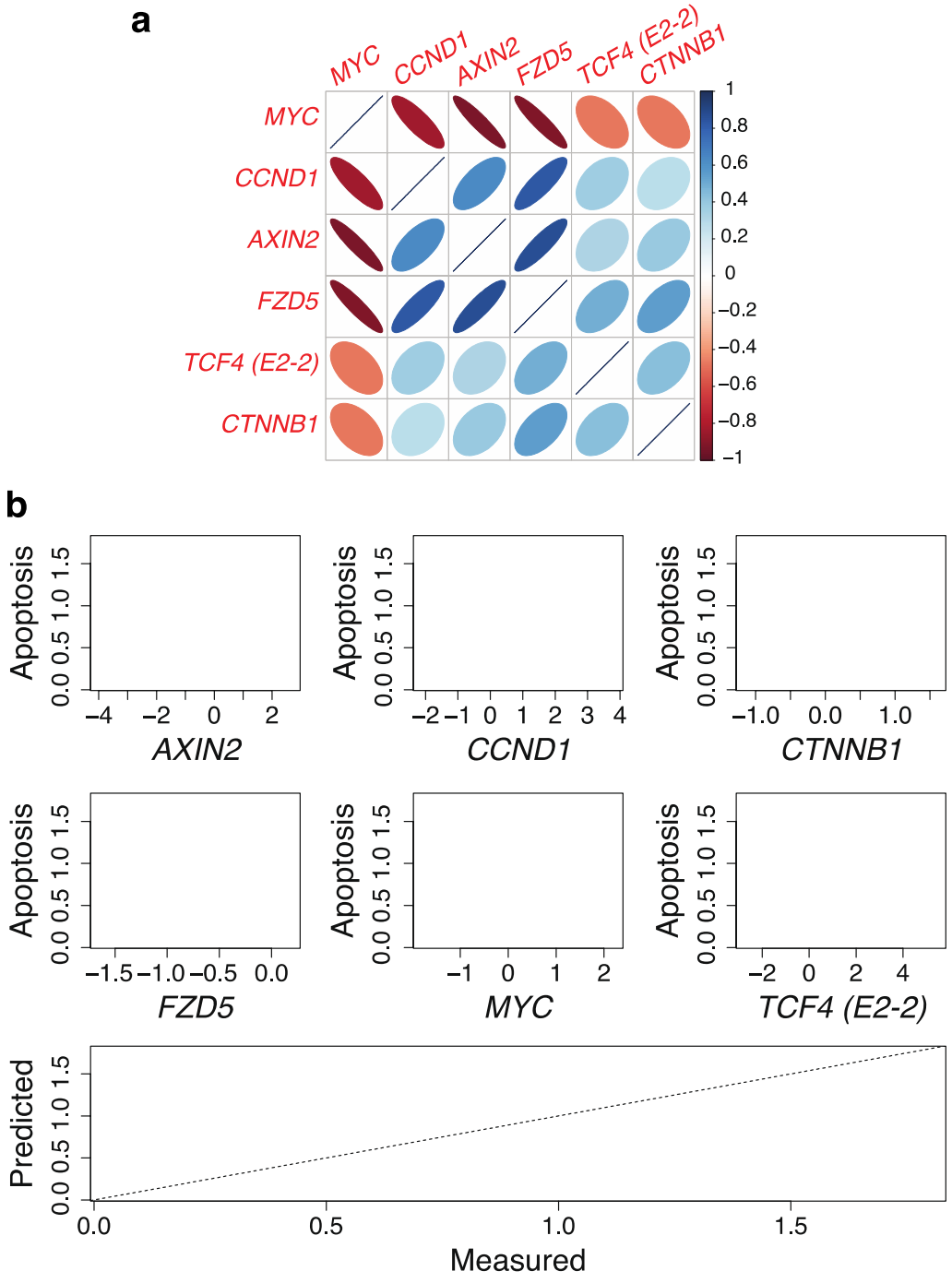
a
MYC
CCND1
AXIN2
FZD5
TCF4 (E2-2)
CTNNB1
1
0.8
0.6
0.4
0.2
0
−0.2
−0.4
−0.6
−0.8
−1
b
Apoptosis
AXIN2
CCND1
CTNNB1
FZD5
MYC
TCF4 (E2-2)
Predicted
Measured

Figure 69 – Correlation of WNT/β-catenin expression with I-BET151 responsiveness in primary human AML using a multiple linear regression model

***a**, Log2-transformed expression levels of selected genes in the WNT/β-catenin pathway were measured using qRT–PCR in a panel of eight primary human AML samples. A corrgram shows high correlation of gene expression of individual genes with each other. The colour and thinness of the ellipse indicate the strength of correlation (a line is perfect correlation; a circle is uncorrelated). The ellipse direction indicates the sign of the correlation (correlated: right/blue, inversely correlated: left/red). **b**, Expression of selected genes is correlated with apoptosis. Scatterplots show apoptosis versus the log2 expression level of each gene. Expression of five genes (CCND1, CTNNB1, FZD5, MYC and TCF4) predicts apoptosis. The relationship is highlighted in a plot of apoptosis predicted using a multiple linear regression model with the five genes versus the actual data.*

6.5 β-catenin binds at sites of BRD4 loss genome wide and mediates resistance through epigenetic plasticity

Examination of the role β-catenin plays at cis-regulatory elements of target genes highlights the mechanistic role of Wnt/β-catenin signalling in resistance to BET inhibition.

In vehicle-treated BET inhibitor sensitive clones, Brd4 is bound to the cis-regulatory elements of target genes such as Myc (Figure 40a, page 147), whereas β-catenin is essentially absent (Figure 70a). However, in resistant clones, Brd4 binding is decreased (Figure 40a) but β-catenin is now bound at these sites and able to sustain the expression of *Myc* (Figure 70 a & b). Negative regulation with Dkk1 reduces chromatin bound β-catenin and subverts its ability to maintain the expression of *Myc* (Figure 70 a, b & Figure 55).

When examined on a genome wide basis, analogous to the events at Myc, in resistant clones chromatin occupancy of β-catenin is increased at sites where Brd4 is displaced from chromatin at TSSs (Figure 71). This increased β-catenin occupancy is abrogated by the expression of Dkk1. β-catenin demonstrates little co-occupancy at Brd4 binding sites.

Taken together, these data are consistent with β-catenin functioning as an alternative transcription factor in the maintenance of malignant gene expression. This epigenetic plasticity allows for the adaptation and survival of resistant clones in the face of sustained selective pressure with BET inhibitors.

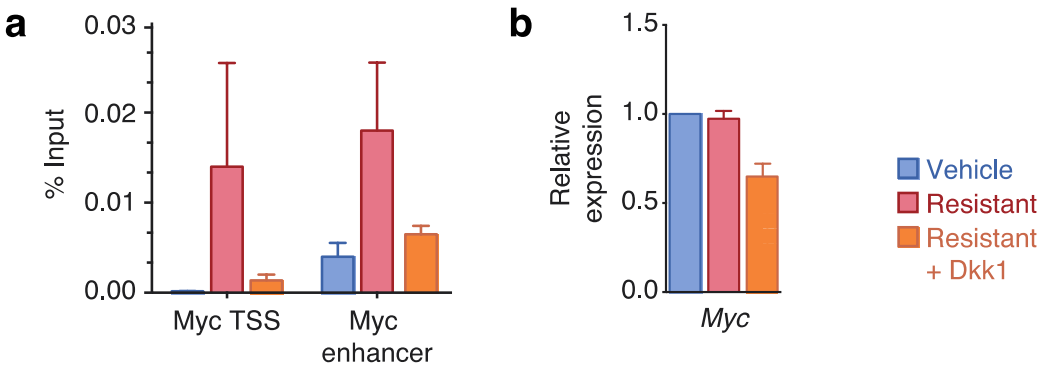

Figure 70 – ChIP-PCR and qRT-PCR data at Myc TSS and enhancer elements for β-catenin

β-catenin functions at Myc TSS and enhancer elements as an alternative transcription factor maintaining the expression of the key oncogene Myc. ***a****, Binding of β-catenin at Myc TSS and enhancer elements in vehicle-treated clones, resistant clones and resistant clones stably overexpressing Dkk1. Mean enrichment relative to input (± s.e.m.) in ChIP analysis from biological triplicate experiments.* ***b****, Myc expression by qRT-PCR from biological triplicate experiments (mean ± s.d.).*

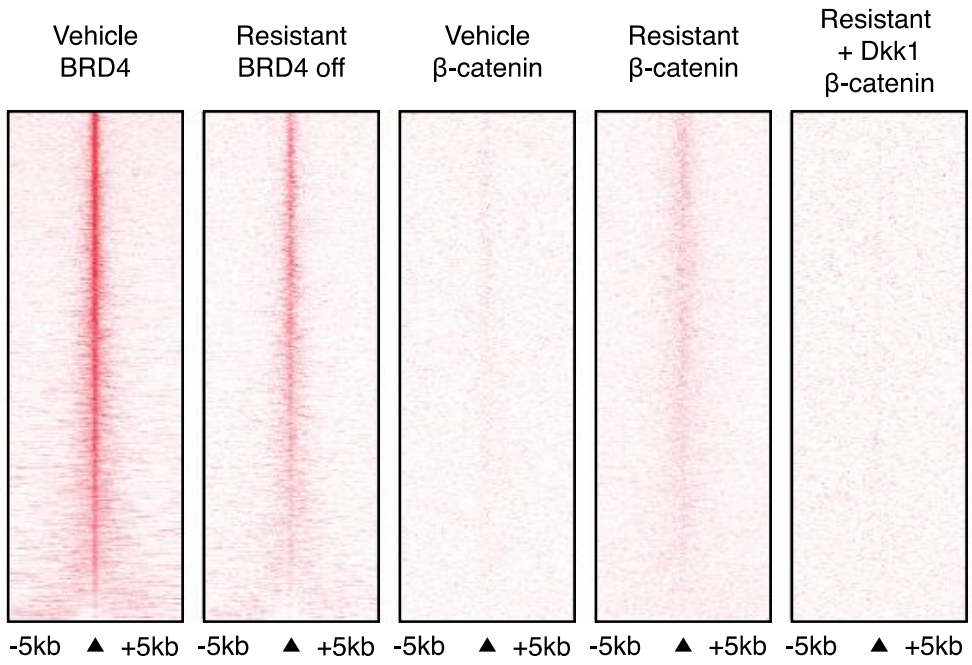

Figure 71 – β-catenin genome wide ChIP

Increased β-catenin binding is observed genome wide in resistant clones at regions where Brd4 binding is lost relative to vehicle-treated clones. Heat map representation of Brd4 peaks genome wide in vehicle-treated clones ranked according to amount of Brd4 binding is shown in the first panel; loss of Brd4 across identically ranked peaks in resistant clones is demonstrated in the second panel; β-catenin binding in vehicle treated clones, resistant clones and resistant clones stably overexpressing Dkk1 across identically ranked Brd4 peaks is demonstrated in subsequent panels. Heat map representation of protein binding is presented where red indicates higher density of reads in ChIP-seq data. These data are centred upon the TSS of annotated genes with 5 kb flanking sequences either side and ranked by amount of binding observed in vehicle-treated clones.

Chapter 7 - Modulating epigenetic targets to overcome resistance to BET inhibition

To further interrogate the role of aberrant epigenetic signalling in the maintenance of LSC function, attention was focused on the epigenetic eraser LSD1. LSD1 has been identified as a key node of epigenetic regulation underpinning malignant phenotypes in acute leukaemia. This has culminated in the ongoing development of small molecule inhibitors targeting LSD1.[139,140] Akin to the BET inhibitors, LSD1 inhibitors have shown pre-clinical promise in the treatment of AML and have entered early phase clinical trials (NCT02842827, NCT02177812). Central to the efficacy of LSD1 inhibitors is the induction of differentiation of leukaemic cells observed both *in vitro* and *in vivo* leading to loss of LSC function.[139,140]

As such, the role of LSD1 in the context of LSC enrichment and BET inhibitor resistance was examined using the reversible LSD1 inhibitor IMG98 (Imago BioSciences, Inc.). This tool compound was used in conjunction with BET inhibitor therapy to assess the feasibility of combination targeted epigenetic therapy with the aim to develop rationally scheduled therapy in the prevention or management of resistance to single agent therapy.

7.1 Combination therapy with LSD1 inhibitors results in restoration of sensitivity to BET inhibitors

Limited *in vitro* single agent efficacy was observed following treatment of vehicle-treated and BET inhibitor resistant clones with IMG98 in proliferation assays (Figure 72, Figure 73 & Figure 74). LSD1 inhibition appeared to have a greater impact on vehicle-treated clones representative of bulk tumour populations in comparison to LSC enriched BET-inhibitor resistant clones. In short-term (48 hour) proliferation assays, vehicle-treated clones demonstrated an estimated IC_{50} >10 μM whilst an IC_{50} was unable to be determined for BET inhibitor resistant clones (Figure 72). Longer-term treatment with IMG98 as a single agent likewise had a modest effect on proliferation in vehicle-treated and BET inhibitor resistant clones and minimal effect on viability (Figure 74), cell cycle progression (Figure 75) and apoptosis (Figure 76).

Contrary to previously published data,[139] LSD1 inhibition with IMG98 had limited effect on colony formation as a single agent in MLLfp mediated murine AML (Figure 77). However, the discrepancy in colony assays may partially be accounted for by a difference in methodology with previous work accounting for differences in colony type. In these studies, overall colony number was not significantly different between vehicle and LSD1 inhibitor treated samples.

The efficacy of pharmacological LSD1 inhibition was more pronounced when utilised in combination with BET inhibitors. As expected, vehicle-treated clones maintained single agent sensitivity to BET inhibitors in proliferation, viability, cell cycle, apoptosis and clonogenic assays (Figure 73, Figure 74, Figure 75, Figure 76 & Figure 77). In combination with LSD1 inhibition, the inhibitory effect was additive in vehicle-treated clones. Similarly, the proliferative capacity of BET inhibitor resistant/LSC enriched clones was abolished in combination therapy (Figure 73) with a reduction in cell viability (Figure 74). This was underpinned by an induction in cell cycle arrest (Figure 75), and induction of apoptosis (Figure 76). Suggestive of an effect on LSC capacity, the colony forming capacity of BET inhibitor resistant clones was reduced (Figure 77).

These data are consistent with co-treatment of BET inhibitor resistant/LSC enriched clones with LSD1 inhibitors and BET inhibitors resulting in restoration of sensitivity to BET inhibitors.

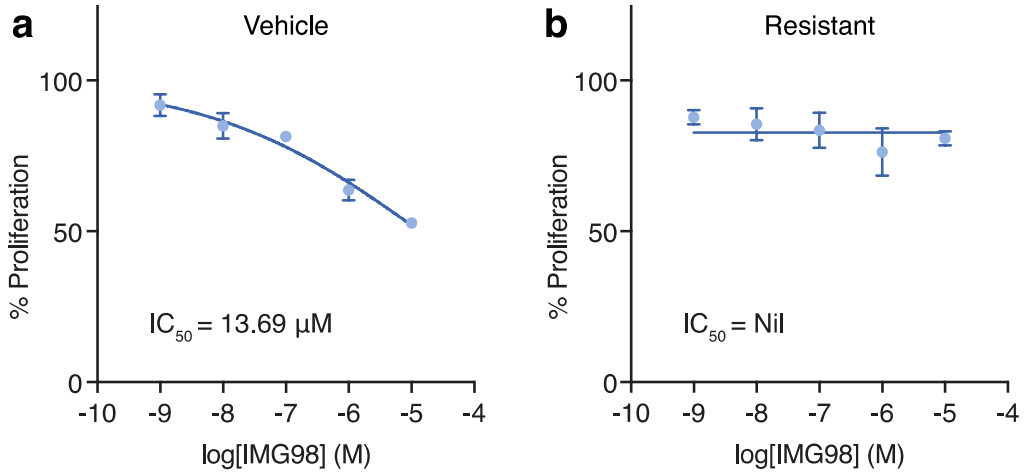

Figure 72 – LSD1 inhibitor dose-response assays

*LSD1 inhibition has limited single agent efficacy in short-term proliferation assays. Representative dose-response curves of (**a**) vehicle-treated and (**b**) BET inhibitor resistant clones obtained following 48 hours of drug exposure (mean ± s.e.m., n=4 per group) is presented.*

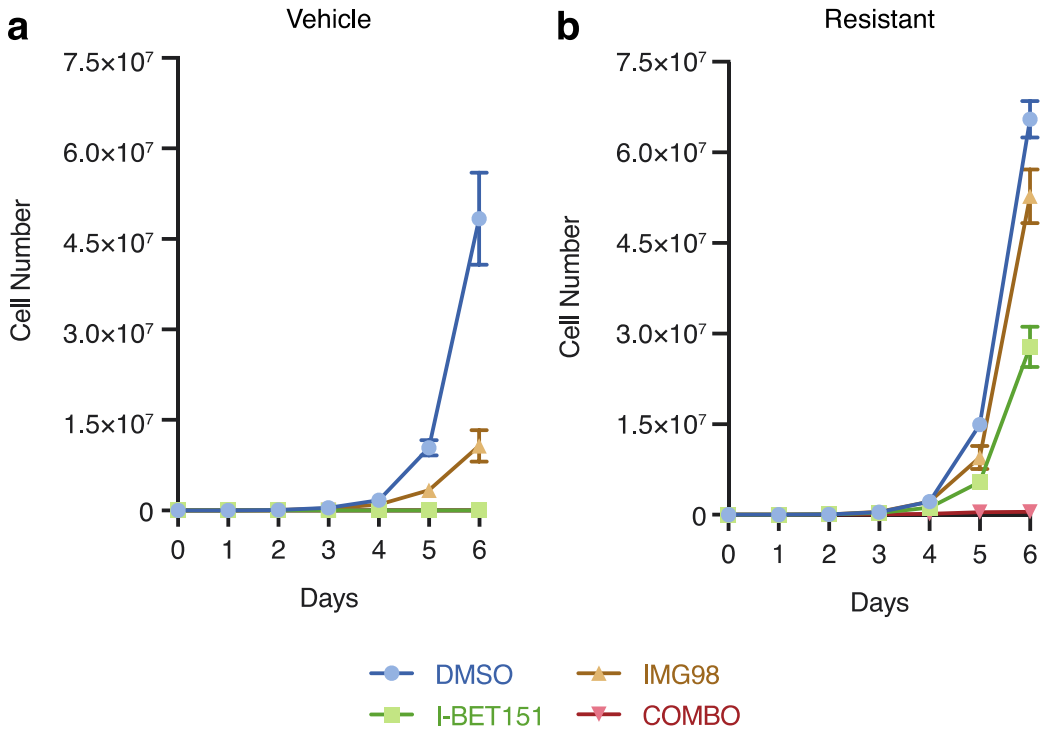

Figure 73 – LSD1 inhibitor long-term proliferation assays

*Combination therapy with LSD1 inhibitors and BET inhibitors results in abrogation of proliferative capacity in BET inhibitor resistant/LSC enriched clones. Daily cell counts of vehicle-treated (**a**) and BET inhibitor resistant (**b**) clones seeded at 1 × 10^4 cells/mL, performed in biological quadruplicate (mean ± s.e.m.) is presented. Cells were treated with vehicle (0.1% DMSO), 1 μM I-BET151, 1 μM IMG98 or a combination of both active drugs.*

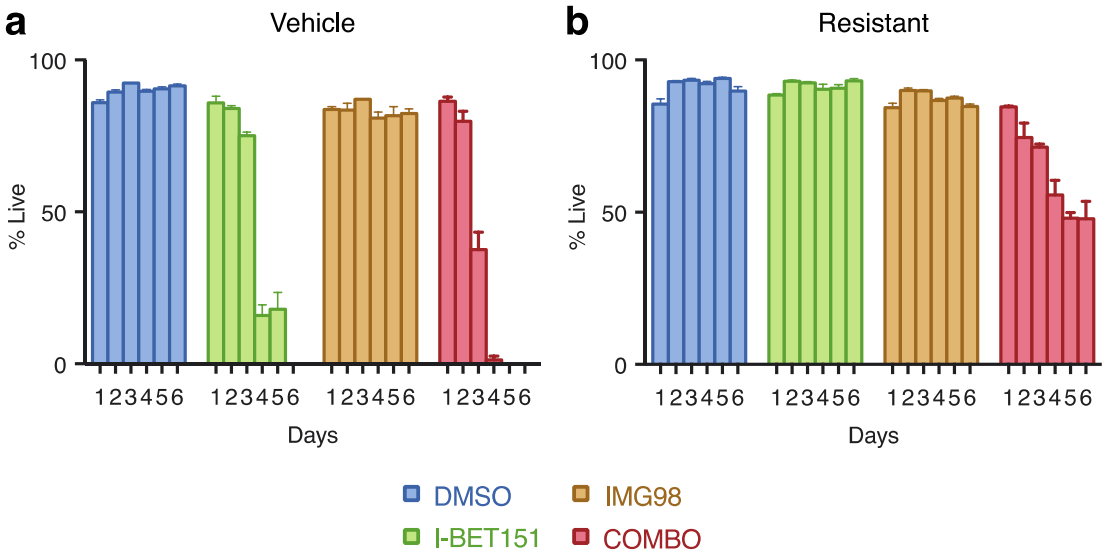

Figure 74 – Cell viability following treatment with LSD1 inhibitors in long-term proliferation assays

*An additive effect on cell viability is observed in vehicle-treated clones following combination therapy with LSD1 inhibitors and BET inhibitors. Cell viability is also reduced in BET-inhibitor resistant/LSC enriched clones following combination therapy. Assessment of cell viability in vehicle-treated (**a**) and BET inhibitor resistant (**b**) clones at identical time points and treatments presented in Figure 73. Proportion of live cells determined as DAPI negative cells in the sample obtained from biological quadruplicate experiments is presented (mean ± s.e.m.).*

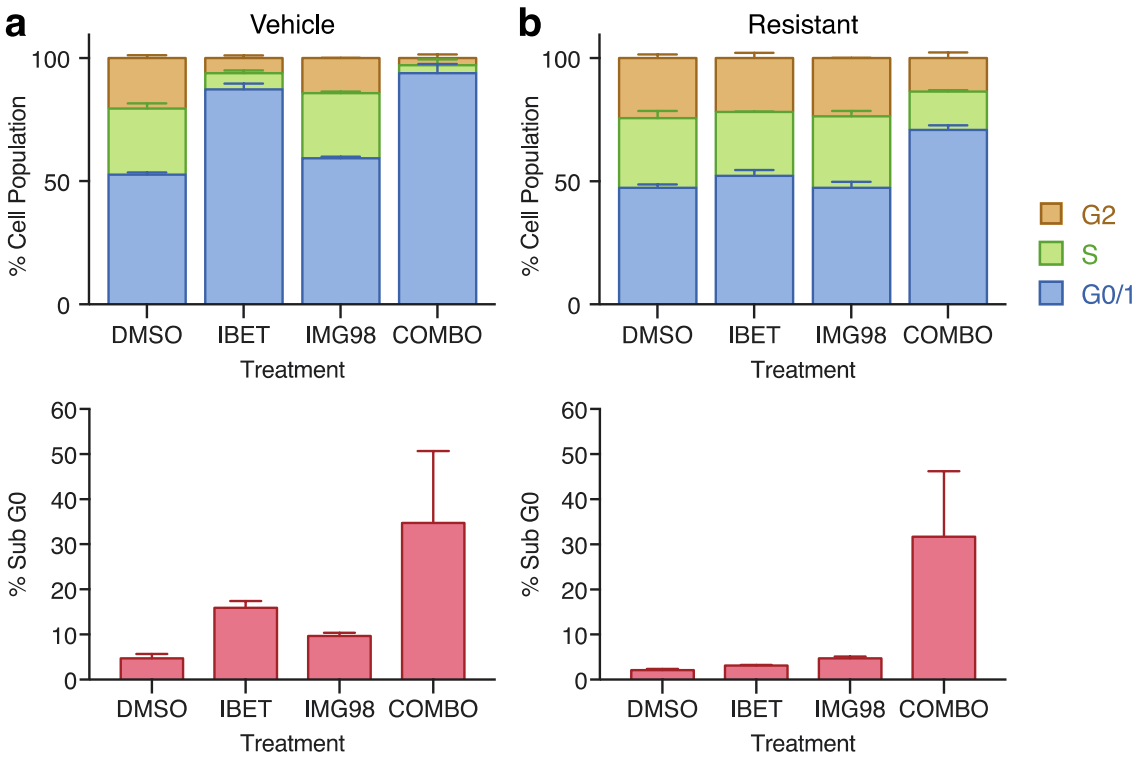

Figure 75 – LSD1 inhibitor cell cycle analysis

*Combination therapy with LSD1 inhibitors and BET inhibitors induces cell cycle arrest in BET inhibitor resistant/LSC enriched clones. Assessment of cell cycle progression performed in vehicle-treated (**a**) and BET inhibitor resistant (**b**) clones seeded at 1 × 10^4 cells/mL, in biological duplicate (mean ± s.e.m.) is presented. Cells were treated with vehicle (0.1% DMSO), 1 μM I-BET151, 1 μM IMG98 or a combination of both active drugs for three days.*

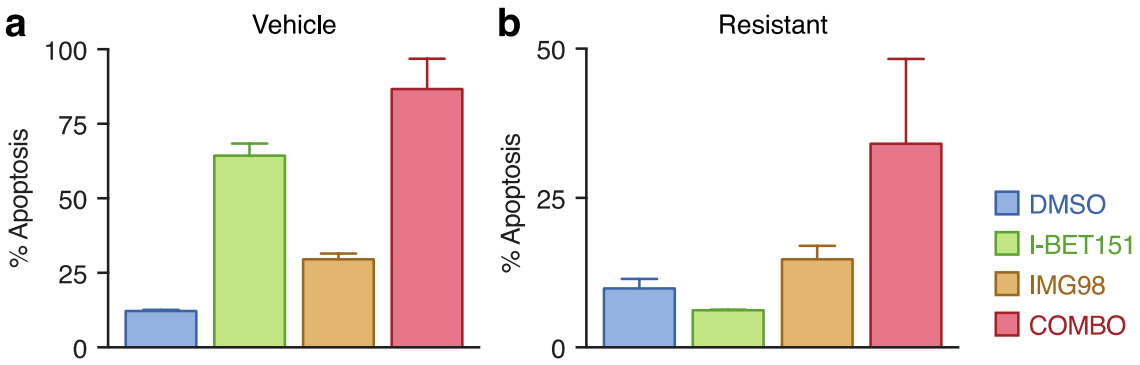

Figure 76 – LSD1 inhibitor apoptosis analysis

*Combination therapy with LSD1 inhibitors and BET inhibitors results in induction of apoptosis in BET inhibitor resistant/LSC enriched clones. Assessment of apoptosis in vehicle-treated (**a**) and BET-inhibitor resistant (**b**) clones seeded at 1 × 10^4 cells/mL. Proportions of apoptotic cells (annexin V and/or PI positive) following treatment with vehicle (0.1% DMSO), 1 μM I-BET151, 1 μM IMG98 or a combination of both active drugs for six days, performed in biological duplicate (mean ± s.e.m.) is presented.*

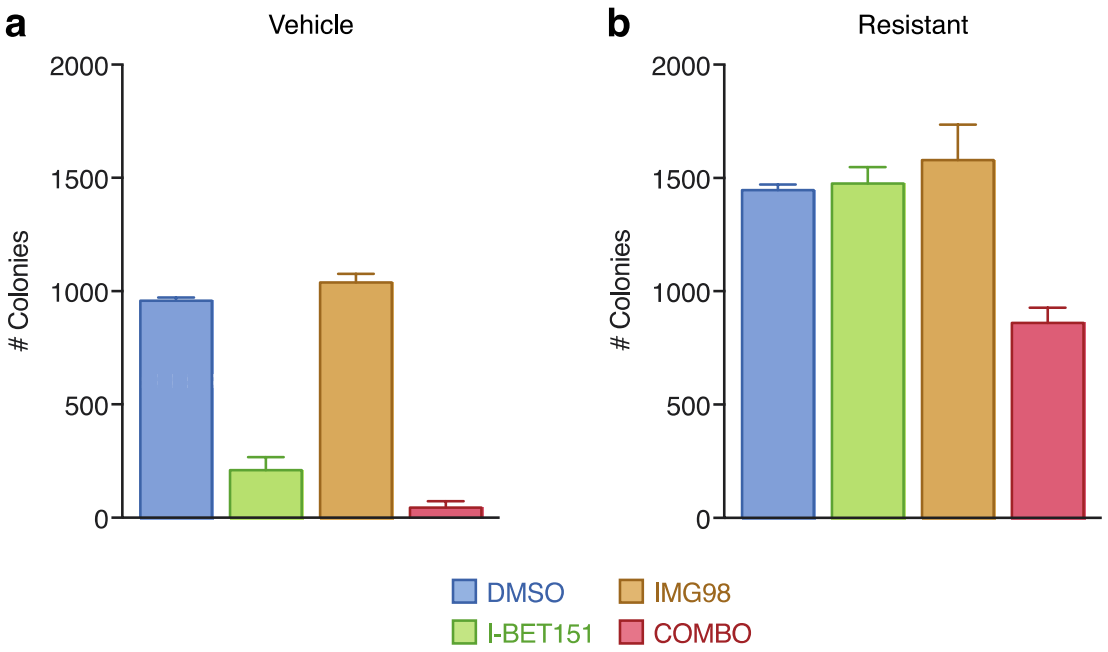

Figure 77 – LSD1 inhibitor colony assays

Colony assays demonstrate effectiveness of dual epigenetic combination therapy in the reduction of colony formation in both vehicle-treated and BET inhibitor resistant/LSC clones. Colony counts after 7 days of growth following treatment with vehicle (0.1% DMSO), 1 μM I-BET151, 1 μM IMG98 or a combination of both active drugs in biological duplicate experiments (mean ± s.e.m.) is presented.

7.2 Pre-treatment with LSD1 inhibitors results in restoration of sensitivity to BET inhibitors

To delineate the changes induced by LSD1 inhibition in BET inhibitor resistant/LSC enriched clones in the restoration of sensitivity to BET inhibitors, pre-treatment of cells was undertaken with IMG98.

Pre-treatment with IMG98 resulted in restoration of nanomolar sensitivity to BET inhibitors in BET inhibitor resistant/LSC enriched clones as demonstrated in dose-response proliferation assays (Figure 78). Although resistant clones were withdrawn from BET inhibitor selective pressure during pre-treatment, the degree of restoration of BET inhibitor sensitivity exceed the partial restoration observed following BET inhibitor withdrawal where the IC_{50} remained > 1 μM (see Figure 17a, page 111). No discernable effect on BET inhibitor sensitivity was observed in vehicle-treated clones following pre-treatment with LSD1 inhibitors (Figure 78).

Detailed examination of this phenomena in BET inhibitor resistant/LSC enriched clones confirmed restoration of sensitivity to BET inhibition in proliferation assays following LSD1 pre-treatment (Figure 79 & Figure 80). Furthermore, sensitivity was restored in the absence of ongoing, concurrent LSD1 inhibition. These findings were further reflected in cell cycle (Figure 81) and apoptosis assays (Figure 82) and are consistent with LSD1 inhibition inducing a phenotypic change in LSC enriched clones resulting in sensitivity to BET inhibitors.

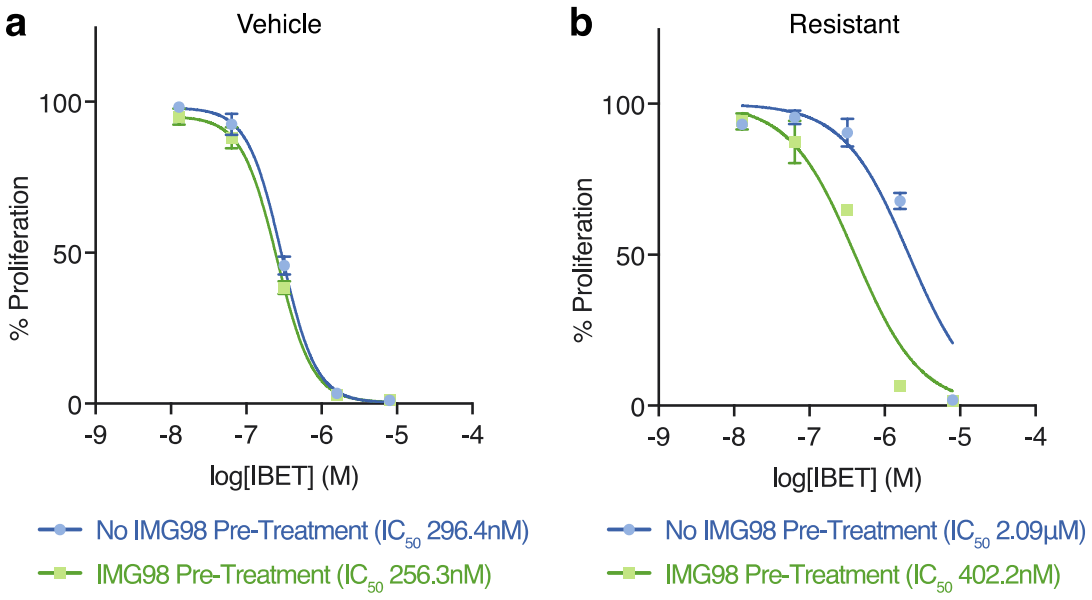

Figure 78 – I-BET151 dose-response assays following LSD1 inhibitor pre-treatment

*Pre-treatment with LSD1 inhibitor for 7 days restores sensitivity to BET inhibition in BET inhibitor resistant/LSC enriched clones in dose-response proliferation assays. No effect was observed on vehicle-treated clones. Representative dose-response curves of (**a**) vehicle-treated clones and (**b**) BET inhibitor resistant clones obtained following 72 hours of exposure to I-BET151 (mean ± s.e.m., n=4 per group) is presented. Cells were pre-treated with 500 nM IMG98 for 7 days and washed prior to seeding at 1 × 10^4 cells/mL.*

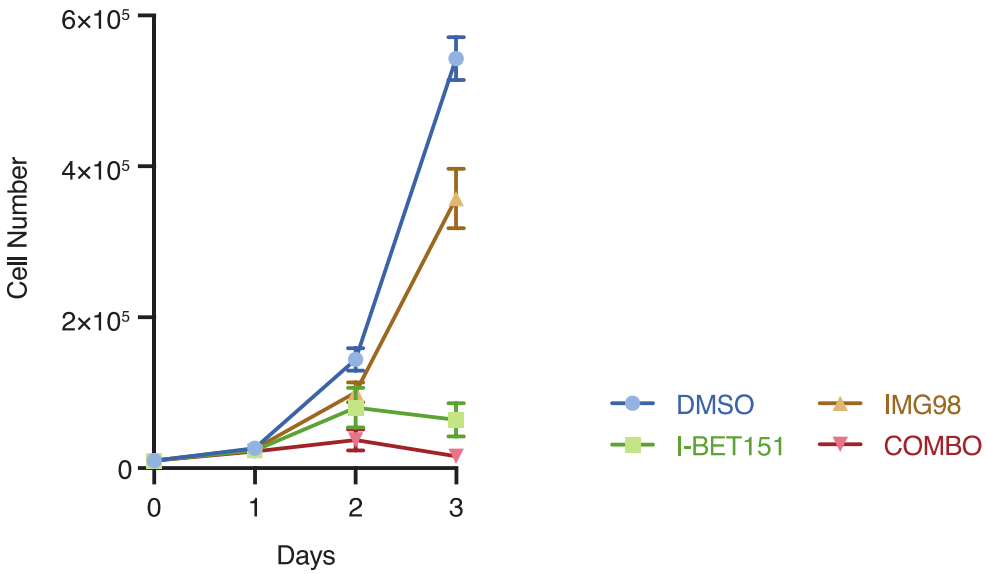

Figure 79 – Proliferation assays following LSD1 inhibitor pre-treatment

Pre-treatment with LSD1 inhibitor for 6 days restores sensitivity to BET inhibitors in BET inhibitor resistant/LSC enriched clones. Sensitivity to I-BET151 is maintained in the absence of IMG98. Following pre-treatment with 1 μM IMG98, cells were washed and treated with vehicle (0.1% DMSO), 1 μM I-BET151, 1 μM IMG98 or a combination of both active drugs. Daily cell counts of resistant clones seeded at 1 × 10^4 cells/mL performed in biological quadruplicate (mean ± s.e.m.) is presented.

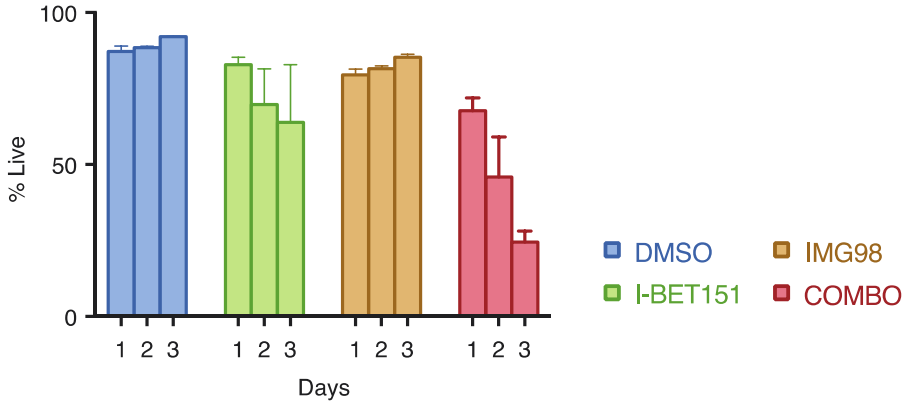

Figure 80 – Cell viability in proliferation assays following LSD1 inhibitor pre-treatment

Assessment of cell viability in BET inhibitor resistant/LSC enriched clones at identical time points and treatments presented in Figure 79. Proportion of live cells, determined as DAPI negative cells in the sample obtained from biological quadruplicate experiments is presented (mean ± s.e.m.).

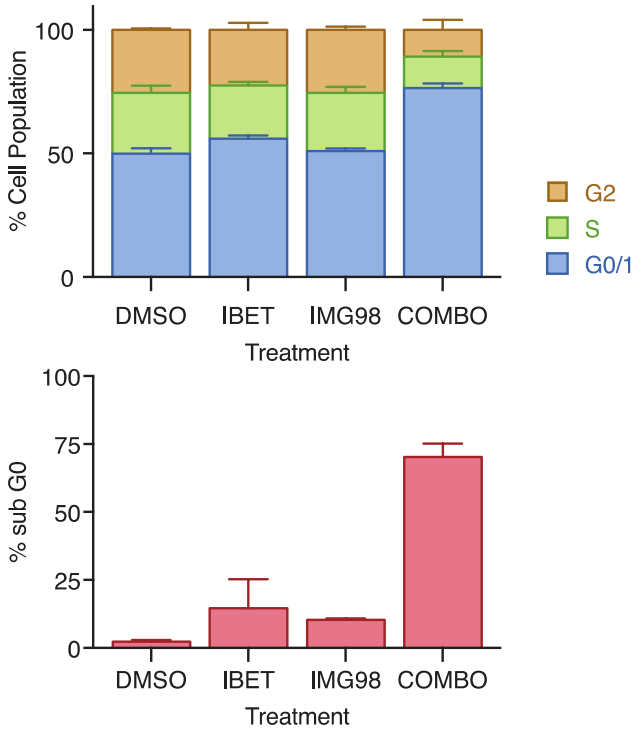

Figure 81 – Cell cycle analysis following LSD1 inhibitor pre-treatment

Pre-treatment of BET inhibitor resistant/LSC enriched clones with LSD1 inhibitor restores sensitivity to BET inhibition in cell cycle analyses. Analysis of cell cycle was performed following pre-treatment with 1 μM IMG98 for six days. Cells were washed, seeded at 1 × 10^4 cells/mL and treated with vehicle (0.1% DMSO), 1 μM I-BET151, 1 μM IMG98 or a combination of both active drugs for a further three days. Data from biological duplicate experiments is presented (mean ± s.e.m.).

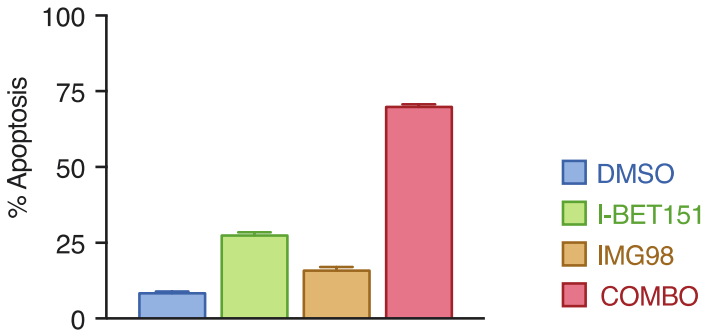

Figure 82 – Apoptosis analysis following LSD1 inhibitor pre-treatment

Pre-treatment of BET inhibitor resistant/LSC enriched clones with LSD1 inhibitor restores sensitivity to BET inhibitor mediated apoptosis. Analysis of apoptosis was performed following pre-treatment with 1 μM IMG98 for six days. Cells were washed, seeded at 1 × 10^4 cells/mL and treated with vehicle (0.1% DMSO), 1 μM I-BET151, 1 μM IMG98 or a combination of both active drugs for a further three days. Proportions of apoptotic cells (annexin V and/or PI positive) from experiments performed in biological duplicate (mean ± s.e.m.) is presented.

7.3 LSD1 inhibition results in differentiation of BET inhibitor resistant clones and loss of LSC immunophenotype

LSD1 inhibitor treatment has been demonstrated to result in morphological and immunophenotypic differentiation with the induction of markers of monocyte/macrophage differentiation.[139] In particular, CD86 expression has been demonstrated to be a surrogate cellular biomarker of pharmacological LSD1 inhibition.[264] Consistent with these findings, treatment with IMG98 alone, or in combination with I-BET151, resulted in the expression of CD86 over time in BET inhibitor resistant/LSC enriched clones (Figure 83). Furthermore, a loss of the LSC containing L-GMP population was observed (Figure 84 & Figure 85).

Examination of the transcriptional changes underlying LSD1 inhibitor induced phenotypic changes in BET inhibitor resistant/LSC enriched clones demonstrates partial reversion of gene expression toward that of vehicle treated clones. This is demonstrated in principle component analysis (Figure 86) and GSEA (Figure 87) of RNA-seq data obtained from vehicle-treated clones, BET-inhibitor resistant clones and BET-inhibitor resistant clones treated with IMG98.

Taken together, these data are consistent with LSD1 inhibitor therapy inducing differentiation of a LSC population resulting in restoration of BET inhibitor sensitivity. As such, differentiation therapy with LSD1 inhibitors could be utilised in combination therapy approaches in rationally scheduled anti-leukaemic therapy to circumvent resistance to BET inhibitors.

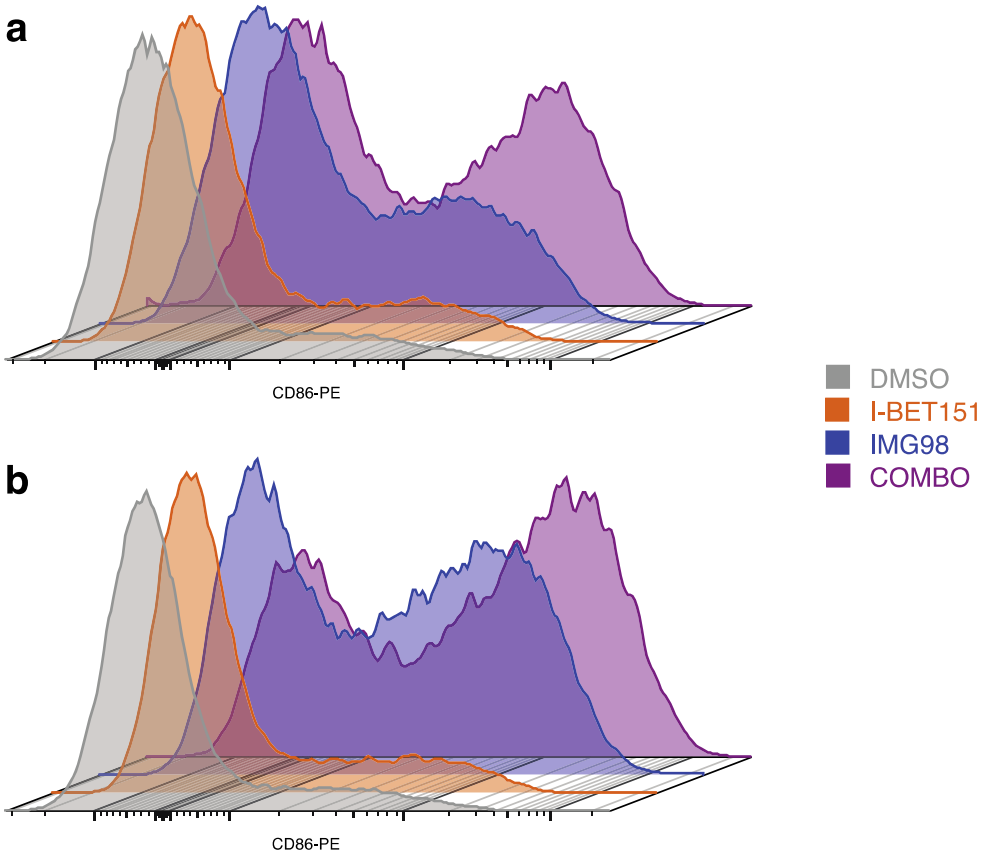

Figure 83 – CD86 expression following LSD1 inhibitor treatment

*Increased CD86 expression is observed in BET inhibitor resistant/LSC enriched clones over time in cells treated with IMG98 consistent with monocyte/macrophage differentiation. Representative FACS plots of CD86 expression in BET inhibitor resistant/LSC enriched clones following (**a**) 3 days and (**b**) 6 days of treatment. Cells were treated with vehicle (0.1% DMSO), 1 μM I-BET151, 1 μM IMG98 or a combination of both active drugs.*

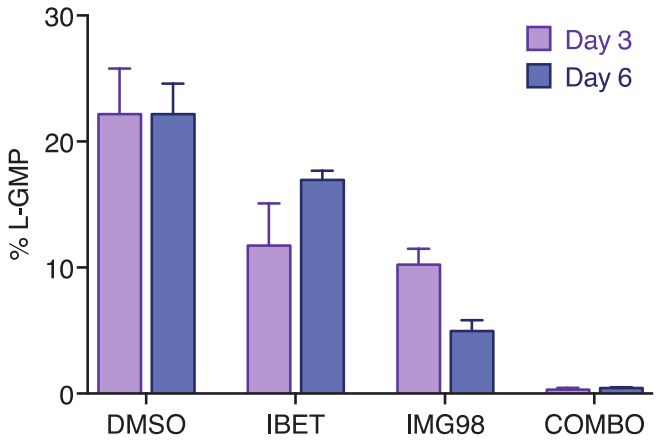

Figure 84 – L-GMP immunophenotype following LSD1 inhibitor treatment

Loss of LSC bearing L-GMP cells is observed following LSD1 inhibitor treatment in BET inhibitor resistant/LSC enriched clones. Cells were treated with vehicle (0.1% DMSO), 1 μM I-BET151, 1 μM IMG98 or a combination of both active drugs. L-GMP proportions (defined in Figure 85) from biological duplicate experiments is presented (mean ± s.e.m.).

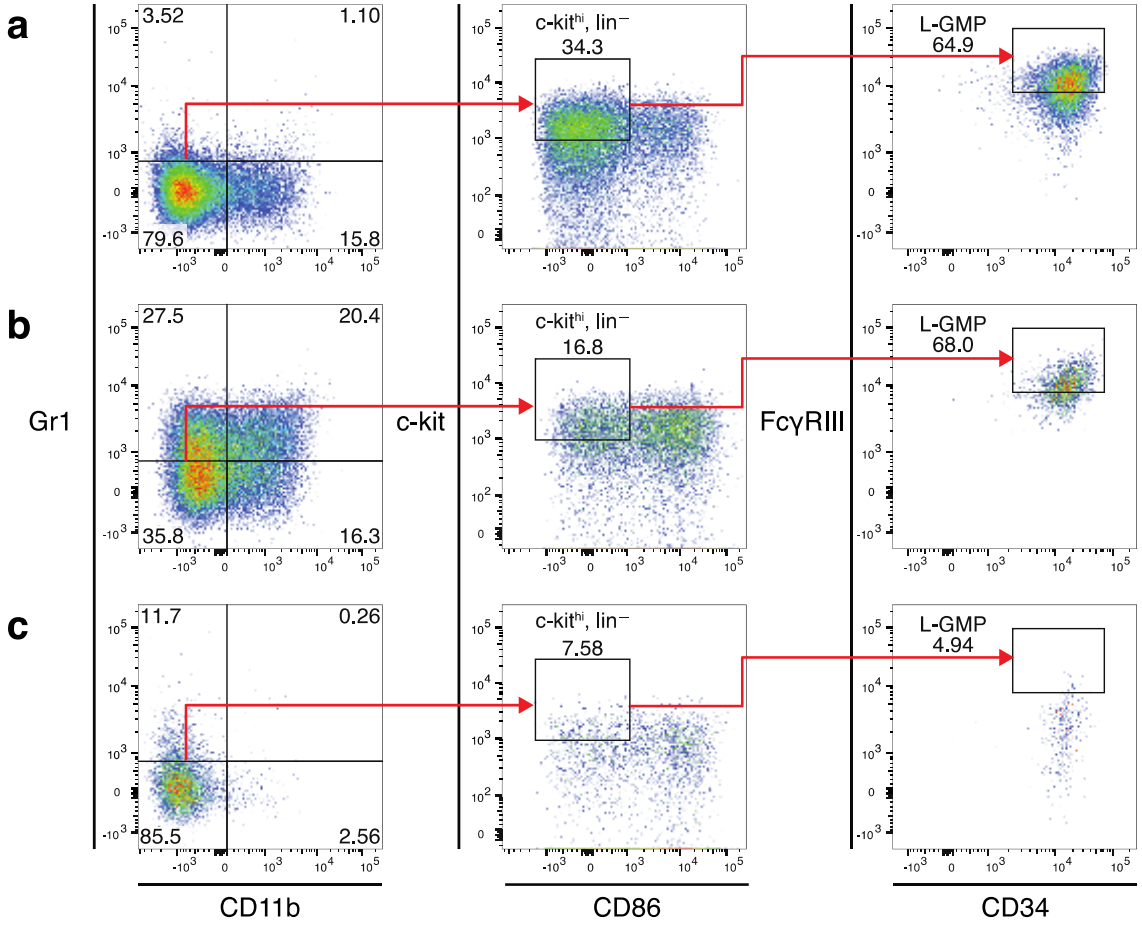

Figure 85 – Gating strategy for the identification of L-GMPs following LSD1 inhibitor therapy

*Representative FACS plots of gating strategy to identify L-GMP in BET inhibitor resistant/LSC enriched clones treated with (**a**) 1 μM I-BET151, (**b**)1 μM IMG98 or (**c**) a combination of both drugs. L-GMPs were identified as cells bearing the immunophenotype: lineage negative (Gr1, CD11b, CD86 negative), c-kit^{hi}, CD34^{+}, FcγRII/III^{hi}. Reported percentages represent proportions of parent gate. Non-viable events (PI positive) were excluded.*

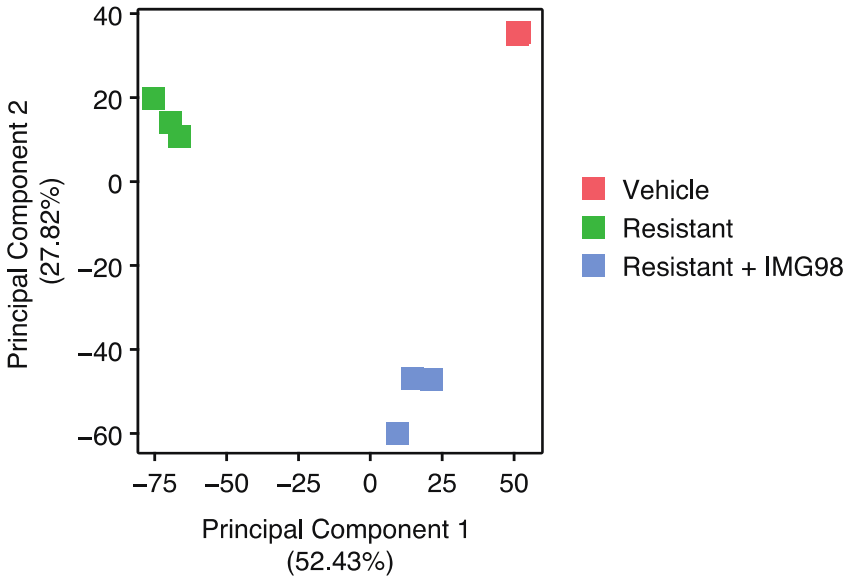

Figure 86 – Transcriptome analysis of LSD1 inhibitor treated cells

Treatment of BET inhibitor resistant/LSC enriched clones with IMG98 results in partial reversion of transcriptome changes in principle component analysis of RNA-seq data. Comparison is made between a vehicle-treated clone, resistant clone maintained in 1 μM I-BET151 and a resistant clone treated with 1 μM IMG98 for six days obtained in biological triplicate.

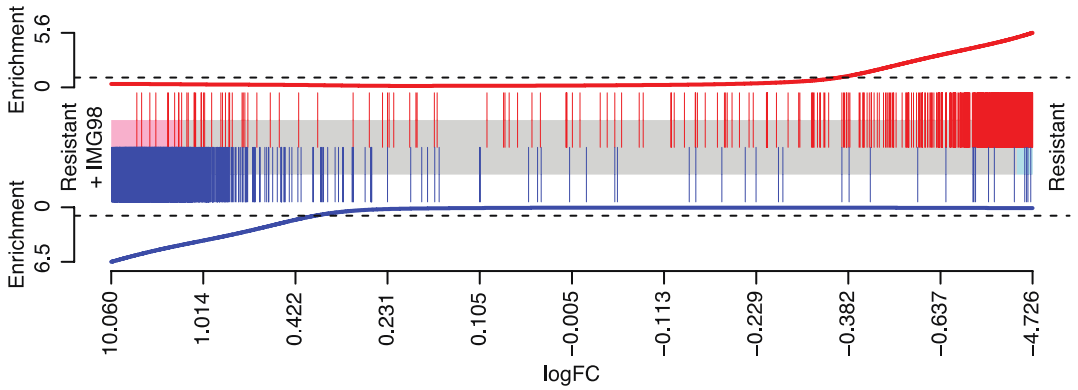

Figure 87 – GSEA of BET-inhibitor resistant clones following LSD1 inhibitor treatment

Following treatment with LSD1 inhibitors, BET inhibitor resistant/LSC enriched clones demonstrate enrichment of a gene expression signature consistent with vehicle-treated clones representative of bulk leukaemic cells. This analysis is achieved through GSEA of gene expression changes determined between resistant cell lines and vehicle-treated cell lines as demonstrated in RNAseq data presented in Figure 44a. Shaded area in the centre of plot shows genes ranked by fold change in expression in resistant clones treated with IMG98 relative to resistant clones maintained in I-BET151. Pink and blue shading represent significantly up- and down- regulated genes, respectively. Up- and down- regulated genes when BET inhibitor resistant clones are compared to vehicle-treated clones are shown in red and blue, respectively. Gene expression changes correlate with reversion of gene expression to vehicle-treated clones in BET inhibitor resistant clones treated with IMG98 (FDR = 1.0×10^{-4} for both upregulated and downregulated genes).

Chapter 8 - Discussion

8.1 The role of epigenetic targeted therapies for AML in the age of genomic technologies

AML is an aggressive haematological malignancy which demonstrates heterogeneity at a clinical, biological and molecular level.[265] However, transcriptional dysregulation resulting in a block in differentiation and increased self-renewal plays a unifying role in leukaemogenesis and is an opportunity for therapeutic intervention.[266]

Induction chemotherapy regimens for AML have remained largely unaltered following their introduction more than 30 years ago.[267-269] Although effective in remission induction in the majority of patients, disease relapse remains a significant cause of mortality. Over 70% of patients continue to succumb to disease despite approaches involving intensive chemotherapy and allogeneic stem cell transplantation.[191,192,270] Therefore, the identification of novel therapeutics driven by greater understanding of leukemogenic drivers and mechanisms of disease persistence is urgently required.

The advent and application of next generation sequencing technologies is central to achieving this goal. These technologies have comprehensively examined the genetic basis of leukaemogenesis.[57,271] This knowledge has allowed us to better understand response to standard therapeutic approaches and subsequently stratify patient exposure to toxic therapies,[3,272,273] in addition to revolutionising approaches to minimal residual disease monitoring.[274] However, the greatest potential impact of these technologies in altering patient outcomes will be the identification of key regulatory pathways and nodes which are amenable to therapeutic targeting. Thus far, the potential success of targeted therapeutics has been demonstrated by the introduction of ATRA in *PML-RARα* positive cases[275] and the use of TKIs in FLT3 positive AML,[276] with a number of additional small molecules in active pre-clinical and clinical development.

The frequency of recurrent somatic mutations in key proteins involved in regulating DNA methylation, post-translational histone modification and chromatin remodelling identified in AML, highlights the possibility of therapeutic invention utilising small

molecules directed against aberrant epigenetic regulators. Indeed, the ability to modulate the function of epigenetic regulators in the control of transcription is likely to play an important role in our therapeutic armamentarium.[7,9,277] However, a key strength and potential weakness of epigenetic therapies is the plasticity of the epigenome. As such, a thorough understanding of the underlying mechanisms of action, determinants of response and resistance to epigenetic targeted therapies is required to identify effective strategies which will optimise the clinical utility of such drugs.

8.2 Resistance to BET inhibitors arises as a consequence of epigenetic plasticity

The pre-clinical utility of targeting epigenetic reader proteins from the BET protein family has been demonstrated utilising murine MLLfp models of leukaemia.[75,181,182] These models have served as effective models of disordered epigenetic regulation, have been extensively characterised *in vitro* and *in vivo* and demonstrate exquisite BET inhibitor sensitivity.[177,178] BET inhibitors directly target protein-protein interactions that are critical to the functional integrity of essential transcriptional machinery and result in established phenotypic responses including decreased proliferation, induction of apoptosis, cell cycle arrest and loss of clonogenic capacity *in vitro*, in addition to prolongation of survival *in vivo*. These promising pre-clinical findings identifying a new class of anti-cancer therapy have been extended into early phase clinical trials.

However, therapeutic resistance is an inevitable consequence of cancer therapies.[190] As the BET inhibitors are non-catalytic inhibitors, no robust pre-existing paradigm was present to guide investigation of resistance mechanisms. The approach undertaken to develop the model of BET inhibitor resistance presented in this work was prompted by multiple failures to develop resistance through stepped escalation of BET inhibitor exposure in human leukaemia cell lines. Notably, the use of primary murine progenitors transformed with MLLfp, successfully generated a flexible model system of clonal BET inhibitor resistance in a clean genetic background which allowed for extensive characterisation of BET inhibitor adaptive changes in comparison to isogenic vehicle-treated BET inhibitor sensitive clones.

Derived resistant clones were resistant to pharmacological BET inhibition with abrogation of established phenotypic responses and cross-resistance to chemically

distinct BET inhibitors observed. The resistance phenotype was stable following withdrawal of BET inhibitor selective pressure and resistance to genetic knockdown of BET proteins was demonstrated in inducible shRNA assays. Although increased drug efflux or metabolism are frequently identified resistance mechanisms, no evidence of these phenomena was identified in resistant clones. Furthermore, *in vivo* resistance was demonstrated following syngeneic transplantation with no difference in disease distribution or morphology observed. Together, these findings establish a robust model of BET inhibitor resistance.

Further examination of the molecular mechanism underlying resistance did not identify any genetic mutations accounting for the observed resistance phenotype. However, transcriptome analyses demonstrated increased Wnt/β-catenin signalling and through genetic and small molecule approaches, resistance in murine leukaemias was confirmed to be, in part, a consequence of increased function of the Wnt pathway. This included the demonstration of increased Wnt/β-catenin signalling resulting in the rapid development of resistance through shRNA mediated knockdown of Apc. These findings were further reinforced by the identification of increased WNT/β-catenin signalling as a biomarker of response in human MLLfp driven leukaemias.

The functional consequence of increased Wnt/β-catenin signalling and its role in resistance was demonstrated in ChIP assays examining the chromatin interface. The expression of key oncogenes normally facilitated by BRD4 remained unchanged in resistant clones despite the loss of BRD4 at enhancers and transcriptional start sites. Indeed, in place of BRD4, binding of β-catenin at transcriptional start sites was observed in the maintenance of malignant gene expression.

Adaptive transcriptional plasticity is an emerging theme by which malignant cells are able to escape therapeutic pressure,[278] and these findings are consistent with the findings of Rathert et al. highlighting the WNT/β-catenin pathway as a mechanism to circumvent BET inhibition.[230] Rathert et al. utilised an orthogonal approach involving a chromatin-regulator targeted RNAi screen in a similar murine MLLfp driven model to identify factors which were vital in determining sensitivity to BET inhibitors. This screen identified suppression of the PRC2 complex as a context dependent mediator of BET inhibitor resistance. PRC2 loss facilitated the remodelling of enhancer landscapes and de-repression of WNT/β-catenin signalling resulting in the rapid restoration of transcription of the key oncogene *MYC* following BET inhibitor therapy. Indeed,

dynamic transcriptional profiles demonstrated universal suppression of *MYC* in both sensitive and resistant leukaemic cell lines in immediate response to BET inhibition. It was only in resistant leukaemia cell lines where rapid rebound of *MYC* transcription was observed, whereas sensitive cell lines demonstrated durable repression and subsequent suppression of MYC protein. This rapid rebound was facilitated by increased WNT signalling with increased chromatin occupancy of WNT-dependent transcription factors observed in response to BET inhibition.

Although these findings are encouraging in the development of a rational combination treatment strategy to circumvent the development of BET inhibitor resistance, enthusiasm is tempered by the early phase of clinical development of WNT/β-catenin pathway inhibitors despite persistent research efforts.[258] Pyrvinium, a FDA approved antihelminthic drug, was utilised as a tool compound in this work but significant *in vivo* toxicity was encountered. No clinical trials of pyrvinium as a WNT pathway inhibitor are currently underway. As such, alternative strategies in rational combination therapies need to be explored.

8.3 The role of LSC in BET inhibitor resistance

The most striking finding in the development of a model of BET inhibitor resistance was the identification of treatment resistance emerging from LSCs. Although postulated as the nidus for treatment resistance, prior work has been unable to definitively demonstrate the stem cell origins of drug resistance in leukaemia.[219,279] As resistant/recurrent disease plays a central role in treatment failure in AML, a substantial change in the natural history of this aggressive and often fatal disease will only be achieved through a greater understanding of the biology of LSC and the identification and validation of effective therapeutics targeting this population. However, attempts to develop strategies to eradicate the LSC population have been hampered not only by limitations in immunophenotypic identification of LSCs but also by the challenge of maintaining an enriched LSC population *in vitro*.

Consistent with BET inhibitor resistance arising from a stem cell population, resistant cells derived *in vitro* demonstrated immunophenotypic immaturity with the loss of markers of terminal myeloid differentiation, Gr1 and CD11b. Furthermore, BET inhibitor resistant $Gr1^{-}/CD11b^{-}$ cells demonstrated enrichment for colony forming cells

in clonogenic assays. The identification of lineage negative cells with increased colony forming capacity parallel findings by Krivstov et al. in the identification of a LSC bearing subpopulation in murine models of MLLfp leukaemia.[177] In particular, Krivstov et al. identified enrichment of LSCs in a lineage negative population bearing the immunophenotypic hallmarks of GMP cells, a population termed L-GMPs. However, this is in contrast to the findings of Somervaille et al. who demonstrate the existence of LSC in downstream differentiated cells.[178] To reconcile these differences, functional validation of stem cell frequency through *in vivo* syngeneic transplantation LDAs was undertaken.

Examination of resistant clones propagated *in vitro* in liquid culture demonstrated not only immunophenotypic enrichment for L-GMP cells but also functional enrichment for LSCs in LDAs *in vivo*. A >85 fold enrichment of functional LSCs was observed in BET inhibitor resistant clones in comparison with vehicle-treated clones. These findings were reinforced by GSEA of transcriptome data which demonstrated enrichment of a previously identified LSC signature[177] and corroborate the finding of LSCs residing in an immunophenotypically defined L-GMP population in murine models of MLL-AF9 leukaemia.

These findings are notable as attempts to maintain a LSC population *in vitro* have thus far been unsuccessful. Indeed, previous observations demonstrate that LSC bearing L-GMPs derived from murine MLLfp models propagated in liquid culture differentiate into lineage positive, c-kit negative cells with a corresponding loss of LSC frequency. Therefore, the development of a model of resistance to BET inhibition has serendipitously enabled the indefinite maintenance of a highly enriched, functional population of LSCs in liquid culture. This method is analogous to the findings in embryonic stem cells (ESC), whereby ESC can be maintained in an undifferentiated state with small molecules in defined culture conditions.[280] This provides a bulk resource to extensively characterize LSCs in order to identify targetable dependencies in their eradication.

The enrichment of LSCs in the development of resistance to BET inhibitors is further reinforced by similar findings in an *in vivo* model of resistance. A serial transplantation approach with chronic exposure to BET inhibitors utilising a murine MLLfp model was undertaken to parallel the clinical development of acquired resistance. Previous studies, in the absence of BET inhibitor exposure, demonstrate primary syngeneic transplant of

bulk tumours resulting in the development of leukaemia within 3 to 5 months.[75,177,178] Following secondary or tertiary transplantation, the time to disease onset is less variable and substantially shortened to weeks.[75,177] Concurrent enrichment of LSCs occurs with 1:150 cells observed to be LSCs in the bone marrow of disease mice through LDAs.[177] Consistent with these findings, serial transplant of BET inhibitor naïve leukaemias resulted in reliable onset of disease between day 23 to 26. Additionally, enrichment of LSCs was observed with 1:59 cells demonstrating LSC capacity. In comparison, BET inhibitor resistant leukaemias demonstrated further enrichment of LSCs. A 10 fold enrichment was observed in resistant leukaemias compared to BET inhibitor naïve leukaemias with LSCs accounting for 1:6 cells transplanted. Furthermore, immunophenotypic enrichment of L-GMPs was seen. Of note, the LSC frequency in BET inhibitor resistant leukaemias bore striking similarity to the LSC frequency of purified L-GMP populations (1:6) in the work of Krivtsov et al..[177]

Extension of these findings into humanised PDX models of AML further identify enrichment of a LSC compartment following BET inhibitor exposure. Although challenges remain in the establishment of PDXs in immunodeficient mice,[281] they faithfully model the clonal architecture of human leukaemia and allow for the immunophenotypic identification of LSC compartments *in vivo*.[282] Ongoing debate surrounds the immunophenotypic identification of LSCs in human AML reflecting the biological heterogeneity of this disease.[250,282-284] However, LSCs have been consistently demonstrated to predominantly reside in $CD34^+$ GMPs or LMPPs.[227,250,285] On this basis, enrichment of a LMPP LSC-like population following *in vivo* exposure to BET inhibitors was observed in a non MLLfp bearing PDX model. Although examination of functional LSC capacity through LDA in these models would be required to confirm the LSC nature of LMPP or GMP cells following BET inhibitor therapy, the resource intensive nature of these models limit the feasibility of this approach. Nevertheless, this finding further supports the contention that BET inhibitor resistance arises in a LSC population.

Intrinsic resistance of LSCs to BET inhibition was examined through clonogenic assays of LSC bearing L-GMPs from BET inhibitor naïve leukaemias. Exposure of these cells to BET inhibitors not only highlight the marked heterogeneity of LSCs in their response to BET inhibition, but are consistent with a subset of cells, which are transcriptionally primed or able to display rapid transcription plasticity, being able to overcome the

initial BET inhibitor challenge. As Wnt/β-catenin signalling is demonstrated to be a major protagonist involved in sustaining LSCs in models of AML and in other cancer stem cells,[227,248,256,257] these findings are compatible with BET inhibitor resistant cells which are able to co-opt this pathway to maintain a survival advantage likewise demonstrating LSC characteristics. These cells are thereby able to subsequently thrive and become the dominant population (Figure 88).

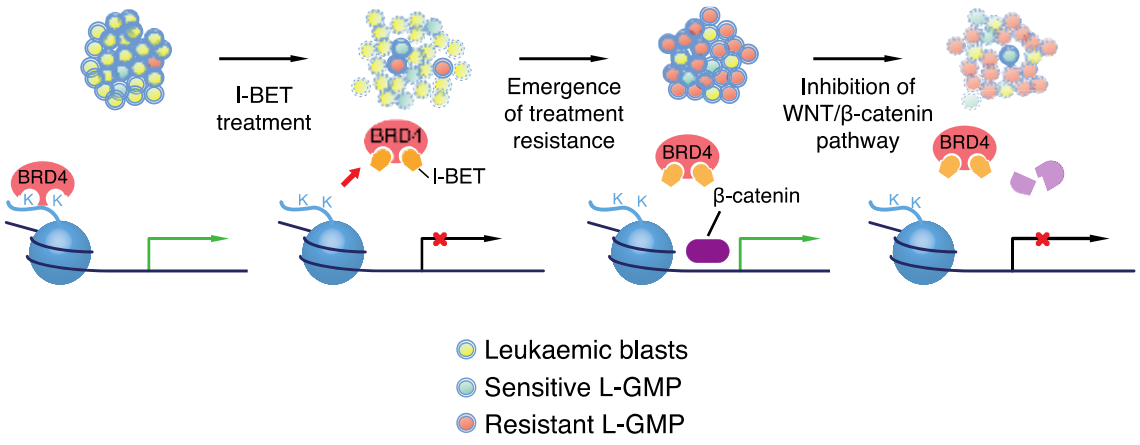

Figure 88 - Model of resistance to BET inhibitors

The functional integrity of BRD4 is essential in the maintenance of malignant gene expression (green arrow) in MLLfp driven acute leukaemia. Following BET inhibitor treatment, malignant gene expression is disrupted in the majority of cells (red cross). However, a subset of cells demonstrate rapid transcriptional plasticity or are transcriptionally primed resulting in the ability to survive the initial BET inhibitor onslaught. These cells are enriched for LSCs and co-opt components of the Wnt/β-catenin pathway to maintain malignant gene expression. Over time, these cells grow out to be the predominant population during the emergence of treatment resistance. Negative regulation of the WNT/β-catenin pathway results in restoration of sensitivity to the BET inhibitors.

8.4 The use of LSD1 inhibitors as differentiation therapy

LSD1 has been identified as a key epigenetic regulatory node underpinning malignant phenotypes in AML and a promising target for pharmacological inhibition.[139,140,286] LSD1 plays a critical role in regulating normal haematopoietic development by restraining progenitor proliferation whilst fostering differentiation.[287,288] Perturbation of LSD1 function in leukaemogenesis results in alteration of this balance with the functional consequence of disordered cellular maturation manifesting as a block in differentiation and enhanced stem cell function.[144] Accordingly, LSD1 expression correlates with LSC function and genetic/pharmacological inhibition of LSD1 results in induction of differentiation and loss of LSC capacity in murine leukaemias and xenograft studies.[139,140]

This capacity to induce differentiation was examined in LSC enriched BET inhibitor resistant clones to assess the feasibility of utilising LSD1 inhibitors as differentiation therapy. Although limited single agent efficacy was observed with LSD1 inhibition in both vehicle-treated and BET inhibitor resistant clones, the pharmacological efficacy of LSD1 inhibition was enhanced when combined with BET inhibition in assays assessing proliferation, cell cycle and apoptosis. Whereas this effect was additive in vehicle treated clones representative of bulk leukaemic populations, restoration of sensitivity to BET inhibitors was observed in BET inhibitor resistant clones. Furthermore, pre-treatment of BET inhibitor resistant clones with LSD1 inhibitors resulted in the restoration of nanomolar sensitivity to BET inhibition. Indeed, sensitivity to BET inhibition was restored in the absence of ongoing LSD1 inhibition in proliferation assays.

Consistent with published findings, induction of differentiation was observed in BET inhibitor resistant clones culminating in a loss of the LSC bearing L-GMP population in immunophenotypic assays. This induction of LSC differentiation is reflected in transcriptome analyses demonstrating reversion to an intermediate state similar to more mature, BET inhibitor sensitive cell populations. Although functional validation of loss of LSC capacity in LSD1 inhibitor treated clones needs to be undertaken in LDA transplant assays, these findings suggest the possibility of utilising LSD1 inhibitors as differentiation therapy. Indeed, the potential for LSD1 inhibitors and BET inhibitors as

a rationally selected combination therapy warrant exploration *in vivo* as a strategy to enhance the clinical utility of both drugs.

However, exploration of this combination in *in vivo* studies will require care in the scheduling of drug therapies to maximise efficacy and minimise potential toxicity. For example, does a period of initial treatment with LSD1 inhibitors result in the loss of BET inhibitor resistant LSCs with inherent transcriptional plasticity and capacity to up-regulate Wnt/β-catenin signalling? Importantly, this approach could limit the exposure of normal HSCs to LSD1 inhibitors.

Of particular concern is the effect of LSD1 inhibition on normal HSC function. LSD1 is highly expressed in normal HSPCs.[289] Mx1-Cre mediated LSD1 knockout produces a defect in HSC self-renewal in competitive transplantation assays in addition to severely impairing the capacity of LSD1 deficient HSC to undergo terminal granulocytic and erythroid differentiation.[287] Furthermore, inducible *in vivo* shRNA mediated knock down of LSD1 in murine models resulted in severe inhibition of terminal granulopoiesis, erythropoiesis and megakaryopoiesis.[288] Although this effect was reversible, careful identification of an adequate therapeutic window with LSD1 inhibitors must be undertaken. This may be assisted by the ongoing development of reversible LSD1 inhibitors.[290]

Data to identify the most appropriate combination approach could be obtained through single cell transcriptome analysis of FACS isolated LSC populations following pre-treatment with LSD1 inhibitors and subsequent exposure to BET inhibitors. In particular, such data would initially inform the effect of LSD1 inhibition on intratumoural transcriptional heterogeneity and subsequently, adaptive responses to BET inhibition. Emerging techniques such as ATAC-seq (Assay for Transposase-Accessible Chromatin with high throughput sequencing)[291] may also be employed to map dynamic changes in the enhancer landscape of LSC enriched cells in response to therapies. Together, these data would provide mechanistic insight into the reversion of transcriptional plasticity modulating BET inhibitor sensitivity in LSCs, identify the timing of essential changes and mitigate any unintended consequences.

8.5 Future Research

The possibility of specifically targeting protein-protein interactions critical to the functional integrity of epigenetic reader proteins has uncovered a new class of anti-cancer therapy. To realise the potential of BET inhibitors in clinical practice, an evaluation of their limitations and mechanisms of resistance is imperative to develop strategies to enhance their efficacy and circumvent therapeutic futility.

The presented work identifies transcriptional plasticity in LSCs as a key mediator of resistance to BET inhibitors. Using models which recapitulate the hierarchical structure of AML, resistance is demonstrated to emerge from a subset of LSCs which are capable of adopting alternate transcription factor networks to maintain malignant gene expression in the face of selective pressure. In particular, increased Wnt/β-catenin signalling is identified to account in part for the observed resistance phenotype, may serve as a potential biomarker of response and can be negatively regulated to restore sensitivity to BET inhibitors. Furthermore, exploration of LSD1 inhibitors in the context of BET inhibitor resistance, as a compound with mechanistic rationale in overcoming resistance through eradication of LSCs, has identified a potential combination therapy approach to enhance the clinical utility of both drugs.

This work highlights an underappreciated attraction of epigenetic therapies. Homogenous responses in a heterogeneous cancer cell population may be utilised to generate unique bottlenecks or synthetic lethal opportunities which can exploited. As such, epigenetic therapies can be used to guide adaptive transcriptional changes in a predictable manner for therapeutic gain. Whilst these adaptive changes may be context dependent and arise only in the absence of gatekeeper mutations and genetic evolution, they provide an enticing backdrop for the development of rational therapeutic combinations.

Epigenetic therapies have been modestly effective thus far as single agents in clinical trials. Indeed, our broader clinical experience with cancer therapeutics highlights the unlikely ability of single agent therapy to deliver sustained benefits in the management of aggressive malignancies. However, combination therapy approaches should be based upon a sound understanding of the molecular pathogenesis of disease. Failure to do so could result in unintended poor patient outcomes. For example, although HDACi have

been demonstrated to have activity in MDS,[292] empirical combination with hypomethylating agents failed to demonstrate any discernible synergy.[40,293,294] Poorer outcomes were observed in combination therapy than with hypomethylating agents alone suggestive of functional antagonism.[293,294] Further evidence of unintended consequences in the modulation of context dependent epigenetic regulators arises from pre-clinical data examining the role of PRC2 complex members in the context of BET inhibitor therapy. Inhibition of PRC2 complex members, including EZH2, facilitates resistance to BET inhibitors in MLLfp leukaemias but conversely, in nerve sheath tumours results in increased BET inhibitor sensitivity.[230,295] Therefore, future combination therapies must be based upon thorough preclinical evaluation and comprehensive molecular rationale.

Importantly, this work establishes a robust model allowing for the indefinite maintenance of an enriched, functional LSC population. This unique resource will enable high-throughput screening to be undertaken to identify targetable dependencies and synthetic lethal interactions. Differential sensitivity of LSCs in comparison to matched tumour populations will be highly informative in the identification of critical cellular pathways for LSC persistence and maintenance. However, the identification of any targetable dependencies must be tempered by the need to validate any findings to ensure selectivity against LSCs whilst sparing normal HSCs to minimise potential toxicity.

Complimentary high-throughput approaches include genetic approaches in the form of RNAi[228] and CRISPR[286] screens as well as pharmacological compound screens[296] and is the focus of future work. A multi-pronged screening approach leverages the strengths of each technique. RNAi screens allow for extensive screening of molecular targets in a non-biased approach to identify and validate genes encoding putative drug targets.[228] However, many epigenetic regulators function as integral components of multi-subunit protein complexes and may exist in several distinct complexes with context dependent roles. Therefore, genetic ablation of epigenetic proteins may disrupt complexes with flow on effects on other complex members resulting in the incorrect identification of the true druggable target. Furthermore, RNAi approaches demonstrate limited selectivity for individual protein domains. This may be critical, particularly when considering epigenetic regulators as therapeutic targets. Domains within each epigenetic protein modulate interactions between complex members and play distinct roles in exerting

regulatory functions. CRISPR screening approaches, with the ability to specifically abrogate the function of individual domains whilst preserving full length proteins, may overcome some of these limitations.[286] Utilising both approaches will allow for cross validation and provide greater finesse in the identification of protein domains underpinning the phenotype of interest to inform rational drug design. Whilst compound screens will not initially provide this level of specificity, utilising therapeutic compounds which are already in widespread use or in advanced clinical development may enable rapid clinical translation of exploitable pathways whilst informing potential mechanisms of LSC persistence.[296] Integration of these approaches will provide the best opportunity to identify appropriate therapeutic approaches.

Together, the studies presented provide novel insights into the biology of AML and the adaptation of LSCs in the face of epigenetic targeted therapies through transcriptional plasticity. The generation and validation of a robust model of LSC function stands as an achievement which has the potential to identify therapeutic approaches that may ultimately deliver the opportunity to eradicate the LSC population.

Chapter 9 - References

1 Mardis, E. R. *et al.* Recurring mutations found by sequencing an acute myeloid leukemia genome. *N Engl J Med* **361**, 1058-1066, doi:10.1056/NEJMoa0903840 (2009).

2 Bejar, R. *et al.* Clinical effect of point mutations in myelodysplastic syndromes. *N Engl J Med* **364**, 2496-2506, doi:10.1056/NEJMoa1013343 (2011).

3 Patel, J. P. *et al.* Prognostic relevance of integrated genetic profiling in acute myeloid leukemia. *N Engl J Med* **366**, 1079-1089, doi:10.1056/NEJMoa1112304 (2012).

4 Haferlach, T. *et al.* Landscape of genetic lesions in 944 patients with myelodysplastic syndromes. *Leukemia* **28**, 241-247, doi:10.1038/leu.2013.336 (2014).

5 Luger, K., Mader, A. W., Richmond, R. K., Sargent, D. F. & Richmond, T. J. Crystal structure of the nucleosome core particle at 2.8 A resolution. *Nature* **389**, 251-260, doi:10.1038/38444 (1997).

6 Kornberg, R. D. Chromatin structure: a repeating unit of histones and DNA. *Science* **184**, 868-871 (1974).

7 Dawson, M. A. & Kouzarides, T. Cancer epigenetics: from mechanism to therapy. *Cell* **150**, 12-27, doi:10.1016/j.cell.2012.06.013 (2012).

8 Hanahan, D. & Weinberg, R. A. Hallmarks of cancer: the next generation. *Cell* **144**, 646-674, doi:10.1016/j.cell.2011.02.013 (2011).

9 Dawson, M. A., Kouzarides, T. & Huntly, B. J. Targeting epigenetic readers in cancer. *N Engl J Med* **367**, 647-657, doi:10.1056/NEJMra1112635 (2012).

10 Smith, Z. D. & Meissner, A. DNA methylation: roles in mammalian development. *Nature reviews. Genetics* **14**, 204-220, doi:10.1038/nrg3354 (2013).

11 Baylin, S. B. & Jones, P. A. A decade of exploring the cancer epigenome - biological and translational implications. *Nature reviews. Cancer* **11**, 726-734, doi:10.1038/nrc3130 (2011).

12 Jones, P. A. & Baylin, S. B. The fundamental role of epigenetic events in cancer. *Nature reviews. Genetics* **3**, 415-428, doi:10.1038/nrg816 (2002).

13 Saied, M. H. *et al.* Genome wide analysis of acute myeloid leukemia reveal leukemia specific methylome and subtype specific hypomethylation of repeats. *PloS one* **7**, e33213, doi:10.1371/journal.pone.0033213 (2012).

14 Akalin, A. *et al.* Base-pair resolution DNA methylation sequencing reveals profoundly divergent epigenetic landscapes in acute myeloid leukemia. *PLoS genetics* **8**, e1002781, doi:10.1371/journal.pgen.1002781 (2012).

15 Stein, R., Gruenbaum, Y., Pollack, Y., Razin, A. & Cedar, H. Clonal inheritance of the pattern of DNA methylation in mouse cells. *Proceedings of the National Academy of Sciences of the United States of America* **79**, 61-65 (1982).

16 Jones, P. A. & Liang, G. Rethinking how DNA methylation patterns are maintained. *Nature reviews. Genetics* **10**, 805-811, doi:10.1038/nrg2651 (2009).

17 Okano, M., Xie, S. & Li, E. Cloning and characterization of a family of novel mammalian DNA (cytosine-5) methyltransferases. *Nature genetics* **19**, 219-220, doi:10.1038/890 (1998).

18 Yan, X. J. *et al.* Exome sequencing identifies somatic mutations of DNA methyltransferase gene DNMT3A in acute monocytic leukemia. *Nature genetics* **43**, 309-315, doi:10.1038/ng.788 (2011).

19 Yamashita, Y. *et al.* Array-based genomic resequencing of human leukemia. *Oncogene* **29**, 3723-3731, doi:10.1038/onc.2010.117 (2010).

20 Ley, T. J. *et al.* DNMT3A mutations in acute myeloid leukemia. *N Engl J Med* **363**, 2424-2433, doi:10.1056/NEJMoa1005143 (2010).

21 Yang, L., Rau, R. & Goodell, M. A. DNMT3A in haematological malignancies. *Nature reviews. Cancer* **15**, 152-165, doi:10.1038/nrc3895 (2015).

22 Walter, M. J. *et al.* Recurrent DNMT3A mutations in patients with myelodysplastic syndromes. *Leukemia* **25**, 1153-1158, doi:10.1038/leu.2011.44 (2011).

23 Stegelmann, F. *et al.* DNMT3A mutations in myeloproliferative neoplasms. *Leukemia* **25**, 1217-1219, doi:10.1038/leu.2011.77 (2011).

24 Genovese, G. *et al.* Clonal hematopoiesis and blood-cancer risk inferred from blood DNA sequence. *N Engl J Med* **371**, 2477-2487, doi:10.1056/NEJMoa1409405 (2014).

25 Fried, I. *et al.* Frequency, onset and clinical impact of somatic DNMT3A mutations in therapy-related and secondary acute myeloid leukemia. *Haematologica* **97**, 246-250, doi:10.3324/haematol.2011.051581 (2012).

26 Kim, S. J. *et al.* A DNMT3A mutation common in AML exhibits dominant-negative effects in murine ES cells. *Blood* **122**, 4086-4089, doi:10.1182/blood-2013-02-483487 (2013).

27 Xu, J. *et al.* DNMT3A Arg882 mutation drives chronic myelomonocytic leukemia through disturbing gene expression/DNA methylation in hematopoietic cells. *Proceedings of the National Academy of Sciences of the United States of America* **111**, 2620-2625, doi:10.1073/pnas.1400150111 (2014).

28 Russler-Germain, D. A. *et al.* The R882H DNMT3A mutation associated with AML dominantly inhibits wild-type DNMT3A by blocking its ability to form active tetramers. *Cancer cell* **25**, 442-454, doi:10.1016/j.ccr.2014.02.010 (2014).

29 Challen, G. A. *et al.* Dnmt3a is essential for hematopoietic stem cell differentiation. *Nature genetics* **44**, 23-31, doi:10.1038/ng.1009 (2012).

30 Shlush, L. I. *et al.* Identification of pre-leukaemic haematopoietic stem cells in acute leukaemia. *Nature* **506**, 328-333, doi:10.1038/nature13038 (2014).

31 Hou, H. A. *et al.* DNMT3A mutations in acute myeloid leukemia: stability during disease evolution and clinical implications. *Blood* **119**, 559-568, doi:10.1182/blood-2011-07-369934 (2012).

32 Thol, F. *et al.* Incidence and prognostic influence of DNMT3A mutations in acute myeloid leukemia. *J Clin Oncol* **29**, 2889-2896, doi:10.1200/JCO.2011.35.4894 (2011).

33 Metzeler, K. H. *et al.* DNMT3A mutations and response to the hypomethylating agent decitabine in acute myeloid leukemia. *Leukemia* **26**, 1106-1107, doi:10.1038/leu.2011.342 (2012).

34 Dinardo, C. D. *et al.* Lack of association of IDH1, IDH2 and DNMT3A mutations with outcome in older patients with acute myeloid leukemia treated with hypomethylating agents. *Leuk Lymphoma*, doi:10.3109/10428194.2013.855309 (2014).

35 Silverman, L. R. *et al.* Randomized controlled trial of azacitidine in patients with the myelodysplastic syndrome: a study of the cancer and leukemia group B. *J Clin Oncol* **20**, 2429-2440 (2002).

36 Kantarjian, H. *et al.* Decitabine improves patient outcomes in myelodysplastic syndromes: results of a phase III randomized study. *Cancer* **106**, 1794-1803, doi:10.1002/cncr.21792 (2006).

37 Fenaux, P. *et al.* Efficacy of azacitidine compared with that of conventional care regimens in the treatment of higher-risk myelodysplastic syndromes: a randomised, open-label, phase III study. *The lancet oncology* **10**, 223-232, doi:10.1016/S1470-2045(09)70003-8 (2009).

38 Fenaux, P. *et al.* Azacitidine prolongs overall survival compared with conventional care regimens in elderly patients with low bone marrow blast count acute myeloid leukemia. *J Clin Oncol* **28**, 562-569, doi:10.1200/JCO.2009.23.8329 (2010).

39 Sauntharajah, Y. Key clinical observations after 5-azacytidine and decitabine treatment of myelodysplastic syndromes suggest practical solutions for better outcomes. *Hematology Am Soc Hematol Educ Program* **2013**, 511-521, doi:10.1182/asheducation-2013.1.511 (2013).

40 Platzbecker, U. & Germing, U. Combination of azacitidine and lenalidomide in myelodysplastic syndromes or acute myeloid leukemia-a wise liaison? *Leukemia* **27**, 1813-1819, doi:10.1038/leu.2013.140 (2013).

41 Grövdal, M. *et al.* Maintenance treatment with azacytidine for patients with high-risk myelodysplastic syndromes (MDS) or acute myeloid leukaemia following MDS in complete remission after induction chemotherapy. *British Journal of Haematology* **150**, 293-302, doi:10.1111/j.1365-2141.2010.08235.x (2010).

42 Liang, P. *et al.* Genome-wide survey reveals dynamic widespread tissue-specific changes in DNA methylation during development. *BMC genomics* **12**, 231, doi:10.1186/1471-2164-12-231 (2011).

43 Tahiliani, M. *et al.* Conversion of 5-methylcytosine to 5-hydroxymethylcytosine in mammalian DNA by MLL partner TET1. *Science* **324**, 930-935, doi:10.1126/science.1170116 (2009).

44 Ito, S. *et al.* Role of Tet proteins in 5mC to 5hmC conversion, ES-cell self-renewal and inner cell mass specification. *Nature* **466**, 1129-1133, doi:10.1038/nature09303 (2010).

45 Ito, S. *et al.* Tet proteins can convert 5-methylcytosine to 5-formylcytosine and 5-carboxylcytosine. *Science* **333**, 1300-1303, doi:10.1126/science.1210597 (2011).

46 He, Y. F. *et al.* Tet-mediated formation of 5-carboxylcytosine and its excision by TDG in mammalian DNA. *Science* **333**, 1303-1307, doi:10.1126/science.1210944 (2011).

47 Branco, M. R., Ficz, G. & Reik, W. Uncovering the role of 5-hydroxymethylcytosine in the epigenome. *Nature reviews. Genetics* **13**, 7-13, doi:10.1038/nrg3080 (2012).

48 Raiber, E. A. *et al.* 5-Formylcytosine alters the structure of the DNA double helix. *Nature structural & molecular biology* **22**, 44-49, doi:10.1038/nsmb.2936 (2015).

49 Wu, H. & Zhang, Y. Tet1 and 5-hydroxymethylation: a genome-wide view in mouse embryonic stem cells. *Cell cycle* **10**, 2428-2436 (2011).

50 Delhommeau, F. *et al.* Mutation in TET2 in myeloid cancers. *N Engl J Med* **360**, 2289-2301, doi:10.1056/NEJMoa0810069 (2009).

51 Langemeijer, S. M. *et al.* Acquired mutations in TET2 are common in myelodysplastic syndromes. *Nature genetics* **41**, 838-842, doi:10.1038/ng.391 (2009).

52 Kosmider, O. *et al.* TET2 gene mutation is a frequent and adverse event in chronic myelomonocytic leukemia. *Haematologica* **94**, 1676-1681, doi:10.3324/haematol.2009.011205 (2009).

53 Abdel-Wahab, O. *et al.* Genetic characterization of TET1, TET2, and TET3 alterations in myeloid malignancies. *Blood* **114**, 144-147, doi:10.1182/blood-2009-03-210039 (2009).

54 Itzykson, R. *et al.* Impact of TET2 mutations on response rate to azacitidine in myelodysplastic syndromes and low blast count acute myeloid leukemias. *Leukemia* **25**, 1147-1152, doi:10.1038/leu.2011.71 (2011).

55 Bejar, R. *et al.* TET2 mutations predict response to hypomethylating agents in myelodysplastic syndrome patients. *Blood* **124**, 2705-2712, doi:10.1182/blood-2014-06-582809 (2014).

56 Tefferi, A. *et al.* TET2 mutations and their clinical correlates in polycythemia vera, essential thrombocythemia and myelofibrosis. *Leukemia* **23**, 905-911, doi:10.1038/leu.2009.47 (2009).

57 Cancer Genome Atlas Research, N. Genomic and epigenomic landscapes of adult de novo acute myeloid leukemia. *N Engl J Med* **368**, 2059-2074, doi:10.1056/NEJMoa1301689 (2013).

58 Figueroa, M. E. *et al.* Leukemic IDH1 and IDH2 mutations result in a hypermethylation phenotype, disrupt TET2 function, and impair hematopoietic differentiation. *Cancer cell* **18**, 553-567, doi:10.1016/j.ccr.2010.11.015 (2010).

59 Ward, P. S. *et al.* The common feature of leukemia-associated IDH1 and IDH2 mutations is a neomorphic enzyme activity converting alpha-ketoglutarate to 2-hydroxyglutarate. *Cancer cell* **17**, 225-234, doi:10.1016/j.ccr.2010.01.020 (2010).

60 Dang, L. *et al.* Cancer-associated IDH1 mutations produce 2-hydroxyglutarate. *Nature* **462**, 739-744, doi:10.1038/nature08617 (2009).

61 Xu, W. *et al.* Oncometabolite 2-hydroxyglutarate is a competitive inhibitor of alpha-ketoglutarate-dependent dioxygenases. *Cancer cell* **19**, 17-30, doi:10.1016/j.ccr.2010.12.014 (2011).

62 Lu, C. *et al.* IDH mutation impairs histone demethylation and results in a block to cell differentiation. *Nature* **483**, 474-478, doi:10.1038/nature10860 (2012).

63 Kats, L. M. *et al.* Proto-oncogenic role of mutant IDH2 in leukemia initiation and maintenance. *Cell stem cell* **14**, 329-341, doi:10.1016/j.stem.2013.12.016 (2014).

64 Chen, C. *et al.* Cancer-associated IDH2 mutants drive an acute myeloid leukemia that is susceptible to Brd4 inhibition. *Genes & development* **27**, 1974-1985, doi:10.1101/gad.226613.113 (2013).

65 Schnittger, S. *et al.* IDH1 mutations are detected in 6.6% of 1414 AML patients and are associated with intermediate risk karyotype and unfavorable prognosis in adults younger than 60 years and unmutated NPM1 status. *Blood* **116**, 5486-5496, doi:10.1182/blood-2010-02-267955 (2010).

66 Abbas, S. *et al.* Acquired mutations in the genes encoding IDH1 and IDH2 both are recurrent aberrations in acute myeloid leukemia: prevalence and prognostic value. *Blood* **116**, 2122-2126, doi:10.1182/blood-2009-11-250878 (2010).

67 Green, C. L. *et al.* The prognostic significance of IDH1 mutations in younger adult patients with acute myeloid leukemia is dependent on FLT3/ITD status. *Blood* **116**, 2779-2782, doi:10.1182/blood-2010-02-270926 (2010).

68 Green, C. L. *et al.* The prognostic significance of IDH2 mutations in AML depends on the location of the mutation. *Blood* **118**, 409-412, doi:10.1182/blood-2010-12-322479 (2011).

69 Paschka, P. *et al.* IDH1 and IDH2 mutations are frequent genetic alterations in acute myeloid leukemia and confer adverse prognosis in cytogenetically normal acute myeloid leukemia with NPM1 mutation without FLT3 internal tandem duplication. *J Clin Oncol* **28**, 3636-3643, doi:10.1200/JCO.2010.28.3762 (2010).

70 Wang, F. *et al.* Targeted inhibition of mutant IDH2 in leukemia cells induces cellular differentiation. *Science* **340**, 622-626, doi:10.1126/science.1234769 (2013).

71 Chaturvedi, A. *et al.* Mutant IDH1 promotes leukemogenesis in vivo and can be specifically targeted in human AML. *Blood* **122**, 2877-2887, doi:10.1182/blood-2013-03-491571 (2013).

72 Stein, E. M. *et al.* Safety and Efficacy of AG-221, a Potent Inhibitor of Mutant IDH2 That Promotes Differentiation of Myeloid Cells in Patients with Advanced Hematologic Malignancies: Results of a Phase 1/2 Trial. *Blood* **126**, 323 (2015).

73 Kouzarides, T. Chromatin modifications and their function. *Cell* **128**, 693-705, doi:10.1016/j.cell.2007.02.005 (2007).

74 Bannister, A. J. & Kouzarides, T. Regulation of chromatin by histone modifications. *Cell research* **21**, 381-395, doi:10.1038/cr.2011.22 (2011).

75 Dawson, M. A. *et al.* Inhibition of BET recruitment to chromatin as an effective treatment for MLL-fusion leukaemia. *Nature* **478**, 529-533, doi:10.1038/nature10509 (2011).

76 Shahbazian, M. D. & Grunstein, M. Functions of site-specific histone acetylation and deacetylation. *Annual review of biochemistry* **76**, 75-100, doi:10.1146/annurev.biochem.76.052705.162114 (2007).

77 Kleff, S., Andrulis, E. D., Anderson, C. W. & Sternglanz, R. Identification of a gene encoding a yeast histone H4 acetyltransferase. *The Journal of biological chemistry* **270**, 24674-24677 (1995).

78 Pasqualucci, L. *et al.* Inactivating mutations of acetyltransferase genes in B-cell lymphoma. *Nature* **471**, 189-195, doi:10.1038/nature09730 (2011).

79 Mullighan, C. G. *et al.* CREBBP mutations in relapsed acute lymphoblastic leukaemia. *Nature* **471**, 235-239, doi:10.1038/nature09727 (2011).

80 Sobulo, O. M. *et al.* MLL is fused to CBP, a histone acetyltransferase, in therapy-related acute myeloid leukemia with a t(11;16)(q23;p13.3). *Proceedings of the National Academy of Sciences of the United States of America* **94**, 8732-8737 (1997).

81 Taki, T., Sako, M., Tsuchida, M. & Hayashi, Y. The t(11;16)(q23;p13) translocation in myelodysplastic syndrome fuses the MLL gene to the CBP gene. *Blood* **89**, 3945-3950 (1997).

82 Carapeti, M., Aguiar, R. C., Goldman, J. M. & Cross, N. C. A novel fusion between MOZ and the nuclear receptor coactivator TIF2 in acute myeloid leukemia. *Blood* **91**, 3127-3133 (1998).

83 Lavau, C., Du, C., Thirman, M. & Zeleznik-Le, N. Chromatin-related properties of CBP fused to MLL generate a myelodysplastic-like syndrome that evolves into myeloid leukemia. *The EMBO journal* **19**, 4655-4664, doi:10.1093/emboj/19.17.4655 (2000).

84 Huntly, B. J. *et al.* MOZ-TIF2, but not BCR-ABL, confers properties of leukemic stem cells to committed murine hematopoietic progenitors. *Cancer cell* **6**, 587-596, doi:10.1016/j.ccr.2004.10.015 (2004).

85 Deguchi, K. *et al.* MOZ-TIF2-induced acute myeloid leukemia requires the MOZ nucleosome binding motif and TIF2-mediated recruitment of CBP. *Cancer cell* **3**, 259-271 (2003).

86 Wang, L. *et al.* The leukemogenicity of AML1-ETO is dependent on site-specific lysine acetylation. *Science* **333**, 765-769, doi:10.1126/science.1201662 (2011).

87 Bowers, E. M. *et al.* Virtual ligand screening of the p300/CBP histone acetyltransferase: identification of a selective small molecule inhibitor. *Chemistry & biology* **17**, 471-482, doi:10.1016/j.chembiol.2010.03.006 (2010).

88 Gao, X. N. *et al.* A histone acetyltransferase p300 inhibitor C646 induces cell cycle arrest and apoptosis selectively in AML1-ETO-positive AML cells. *PloS one* **8**, e55481, doi:10.1371/journal.pone.0055481 (2013).

89 Giotopoulos, G. *et al.* The epigenetic regulators CBP and p300 facilitate leukemogenesis and represent therapeutic targets in acute myeloid leukemia. *Oncogene* **35**, 279-289, doi:10.1038/onc.2015.92 (2016).

90 Bolden, J. E., Peart, M. J. & Johnstone, R. W. Anticancer activities of histone deacetylase inhibitors. *Nature reviews. Drug discovery* **5**, 769-784, doi:10.1038/nrd2133 (2006).

91 Grignani, F. *et al.* Fusion proteins of the retinoic acid receptor-alpha recruit histone deacetylase in promyelocytic leukaemia. *Nature* **391**, 815-818, doi:10.1038/35901 (1998).

92 He, L. Z. *et al.* Distinct interactions of PML-RARalpha and PLZF-RARalpha with co-repressors determine differential responses to RA in APL. *Nature genetics* **18**, 126-135, doi:10.1038/ng0298-126 (1998).

93 Lin, R. J. *et al.* Role of the histone deacetylase complex in acute promyelocytic leukaemia. *Nature* **391**, 811-814, doi:10.1038/35895 (1998).

94 Fazi, F. *et al.* Heterochromatic gene repression of the retinoic acid pathway in acute myeloid leukemia. *Blood* **109**, 4432-4440, doi:10.1182/blood-2006-09-045781 (2007).

95 He, L. Z. *et al.* Histone deacetylase inhibitors induce remission in transgenic models of therapy-resistant acute promyelocytic leukemia. *The Journal of clinical investigation* **108**, 1321-1330, doi:10.1172/JCI11537 (2001).

96 Bojang, P., Jr. & Ramos, K. S. The promise and failures of epigenetic therapies for cancer treatment. *Cancer treatment reviews*, doi:10.1016/j.ctrv.2013.05.009 (2013).

97 Dickinson, M., Johnstone, R. W. & Prince, H. M. Histone deacetylase inhibitors: potential targets responsible for their anti-cancer effect. *Investigational new drugs* **28 Suppl 1**, S3-20, doi:10.1007/s10637-010-9596-y (2010).

98 Bots, M. *et al.* Differentiation therapy for the treatment of t(8;21) acute myeloid leukemia using histone deacetylase inhibitors. *Blood* **123**, 1341-1352, doi:10.1182/blood-2013-03-488114 (2014).

99 Huang, B., Yang, X. D., Zhou, M. M., Ozato, K. & Chen, L. F. Brd4 coactivates transcriptional activation of NF-kappaB via specific binding to acetylated RelA. *Molecular and cellular biology* **29**, 1375-1387, doi:10.1128/MCB.01365-08 (2009).

100 Lamonica, J. M. *et al.* Bromodomain protein Brd3 associates with acetylated GATA1 to promote its chromatin occupancy at erythroid target genes. *Proceedings of the National Academy of Sciences of the United States of America* **108**, E159-168, doi:10.1073/pnas.1102140108 (2011).

101 Nicodeme, E. *et al.* Suppression of inflammation by a synthetic histone mimic. *Nature* **468**, 1119-1123, doi:10.1038/nature09589 (2010).

102 Filippakopoulos, P. *et al.* Selective inhibition of BET bromodomains. *Nature* **468**, 1067-1073, doi:10.1038/nature09504 (2010).

103 Allis, C. D. *et al.* New nomenclature for chromatin-modifying enzymes. *Cell* **131**, 633-636, doi:10.1016/j.cell.2007.10.039 (2007).

104 Collins, R. E. *et al.* In vitro and in vivo analyses of a Phe/Tyr switch controlling product specificity of histone lysine methyltransferases. *The Journal of biological chemistry* **280**, 5563-5570, doi:10.1074/jbc.M410483200 (2005).

105 Wilson, J. R. *et al.* Crystal structure and functional analysis of the histone methyltransferase SET7/9. *Cell* **111**, 105-115 (2002).

106 Barski, A. *et al.* High-resolution profiling of histone methylations in the human genome. *Cell* **129**, 823-837, doi:10.1016/j.cell.2007.05.009 (2007).

107 Rea, S. *et al.* Regulation of chromatin structure by site-specific histone H3 methyltransferases. *Nature* **406**, 593-599, doi:10.1038/35020506 (2000).

108 Heintzman, N. D. *et al.* Distinct and predictive chromatin signatures of transcriptional promoters and enhancers in the human genome. *Nature genetics* **39**, 311-318, doi:10.1038/ng1966 (2007).

109 Cecere, G., Hoersch, S., Jensen, M. B., Dixit, S. & Grishok, A. The ZFP-1(AF10)/DOT-1 complex opposes H2B ubiquitination to reduce Pol II transcription. *Molecular cell* **50**, 894-907, doi:10.1016/j.molcel.2013.06.002 (2013).

110 Klauke, K. *et al.* Polycomb Cbx family members mediate the balance between haematopoietic stem cell self-renewal and differentiation. *Nature cell biology* **15**, 353-362, doi:10.1038/ncb2701 (2013).

111 Cao, R., Tsukada, Y. & Zhang, Y. Role of Bmi-1 and Ring1A in H2A ubiquitylation and Hox gene silencing. *Molecular cell* **20**, 845-854, doi:10.1016/j.molcel.2005.12.002 (2005).

112 Eskeland, R. *et al.* Ring1B compacts chromatin structure and represses gene expression independent of histone ubiquitination. *Molecular cell* **38**, 452-464, doi:10.1016/j.molcel.2010.02.032 (2010).

113 Kondo, Y. *et al.* Gene silencing in cancer by histone H3 lysine 27 trimethylation independent of promoter DNA methylation. *Nature genetics* **40**, 741-750, doi:10.1038/ng.159 (2008).

114 Morin, R. D. *et al.* Somatic mutations altering EZH2 (Tyr641) in follicular and diffuse large B-cell lymphomas of germinal-center origin. *Nature genetics* **42**, 181-185, doi:10.1038/ng.518 (2010).

115 Sneeringer, C. J. *et al.* Coordinated activities of wild-type plus mutant EZH2 drive tumor-associated hypertrimethylation of lysine 27 on histone H3 (H3K27) in human B-cell lymphomas. *Proceedings of the National Academy of Sciences of the United States of America* **107**, 20980-20985, doi:10.1073/pnas.1012525107 (2010).

116 McCabe, M. T. *et al.* EZH2 inhibition as a therapeutic strategy for lymphoma with EZH2-activating mutations. *Nature* **492**, 108-112, doi:10.1038/nature11606 (2012).

117 Kim, K. H. & Roberts, C. W. Targeting EZH2 in cancer. *Nat Med* **22**, 128-134, doi:10.1038/nm.4036 (2016).

118 Ernst, T. *et al.* Inactivating mutations of the histone methyltransferase gene EZH2 in myeloid disorders. *Nature genetics* **42**, 722-726, doi:10.1038/ng.621 (2010).

119 Nikoloski, G. *et al.* Somatic mutations of the histone methyltransferase gene EZH2 in myelodysplastic syndromes. *Nature genetics* **42**, 665-667, doi:10.1038/ng.620 (2010).

120 Abdel-Wahab, O. *et al.* Concomitant analysis of EZH2 and ASXL1 mutations in myelofibrosis, chronic myelomonocytic leukemia and blast-phase myeloproliferative neoplasms. *Leukemia* **25**, 1200-1202, doi:10.1038/leu.2011.58 (2011).

121 Grossmann, V. *et al.* Molecular profiling of chronic myelomonocytic leukemia reveals diverse mutations in >80% of patients with TET2 and EZH2 being of high prognostic relevance. *Leukemia* **25**, 877-879, doi:10.1038/leu.2011.10 (2011).

122 Guglielmelli, P. *et al.* EZH2 mutational status predicts poor survival in myelofibrosis. *Blood* **118**, 5227-5234, doi:10.1182/blood-2011-06-363424 (2011).

123 Score, J. *et al.* Inactivation of polycomb repressive complex 2 components in myeloproliferative and myelodysplastic/myeloproliferative neoplasms. *Blood* **119**, 1208-1213, doi:10.1182/blood-2011-07-367243 (2012).

124 Kroeze, L. I. *et al.* Genetic defects in PRC2 components other than EZH2 are not common in myeloid malignancies. *Blood* **119**, 1318-1319, doi:10.1182/blood-2011-07-365213 (2012).

125 Abdel-Wahab, O. *et al.* ASXL1 mutations promote myeloid transformation through loss of PRC2-mediated gene repression. *Cancer cell* **22**, 180-193, doi:10.1016/j.ccr.2012.06.032 (2012).

126 Gelsi-Boyer, V. *et al.* ASXL1 mutation is associated with poor prognosis and acute transformation in chronic myelomonocytic leukaemia. *Br J Haematol* **151**, 365-375, doi:10.1111/j.1365-2141.2010.08381.x (2010).

127 Scheuermann, J. C. *et al.* Histone H2A deubiquitinase activity of the Polycomb repressive complex PR-DUB. *Nature* **465**, 243-247, doi:10.1038/nature08966 (2010).

128 Lessard, J. & Sauvageau, G. Bmi-1 determines the proliferative capacity of normal and leukaemic stem cells. *Nature* **423**, 255-260, doi:10.1038/nature01572 (2003).

129 Park, I. K. *et al.* Bmi-1 is required for maintenance of adult self-renewing haematopoietic stem cells. *Nature* **423**, 302-305, doi:10.1038/nature01587 (2003).

130 Wang, H. *et al.* Role of histone H2A ubiquitination in Polycomb silencing. *Nature* **431**, 873-878, doi:10.1038/nature02985 (2004).

131 Buchwald, G. *et al.* Structure and E3-ligase activity of the Ring-Ring complex of polycomb proteins Bmi1 and Ring1b. *The EMBO journal* **25**, 2465-2474, doi:10.1038/sj.emboj.7601144 (2006).

132 Mohty, M., Yong, A. S., Szydlo, R. M., Apperley, J. F. & Melo, J. V. The polycomb group BMI1 gene is a molecular marker for predicting prognosis of chronic myeloid leukemia. *Blood* **110**, 380-383, doi:10.1182/blood-2006-12-065599 (2007).

133 Mihara, K. *et al.* Bmi-1 is useful as a novel molecular marker for predicting progression of myelodysplastic syndrome and patient prognosis. *Blood* **107**, 305-308, doi:10.1182/blood-2005-06-2393 (2006).

134 Chowdhury, M. *et al.* Expression of Polycomb-group (PcG) protein BMI-1 predicts prognosis in patients with acute myeloid leukemia. *Leukemia* **21**, 1116-1122, doi:10.1038/sj.leu.2404623 (2007).

135 Shi, Y. *et al.* Histone demethylation mediated by the nuclear amine oxidase homolog LSD1. *Cell* **119**, 941-953, doi:10.1016/j.cell.2004.12.012 (2004).

136 van Haaften, G. *et al.* Somatic mutations of the histone H3K27 demethylase gene UTX in human cancer. *Nature genetics* **41**, 521-523, doi:10.1038/ng.349 (2009).

137 Mar, B. G. *et al.* Sequencing histone-modifying enzymes identifies UTX mutations in acute lymphoblastic leukemia. *Leukemia* **26**, 1881-1883, doi:10.1038/leu.2012.56 (2012).

138 Kruidenier, L. *et al.* A selective jumonji H3K27 demethylase inhibitor modulates the proinflammatory macrophage response. *Nature* **488**, 404-408, doi:10.1038/nature11262 (2012).

139 Harris, W. J. *et al.* The histone demethylase KDM1A sustains the oncogenic potential of MLL-AF9 leukemia stem cells. *Cancer cell* **21**, 473-487, doi:10.1016/j.ccr.2012.03.014 (2012).

140 Schenk, T. *et al.* Inhibition of the LSD1 (KDM1A) demethylase reactivates the all-trans-retinoic acid differentiation pathway in acute myeloid leukemia. *Nat Med* **18**, 605-611, doi:10.1038/nm.2661 (2012).

141 Kooistra, S. M. & Helin, K. Molecular mechanisms and potential functions of histone demethylases. *Nature reviews. Molecular cell biology* **13**, 297-311, doi:10.1038/nrm3327 (2012).

142 Metzger, E. *et al.* LSD1 demethylates repressive histone marks to promote androgen-receptor-dependent transcription. *Nature* **437**, 436-439, doi:10.1038/nature04020 (2005).

143 Berglund, L. *et al.* A genecentric Human Protein Atlas for expression profiles based on antibodies. *Molecular & cellular proteomics : MCP* **7**, 2019-2027, doi:10.1074/mcp.R800013-MCP200 (2008).

144 Lokken, A. A. & Zeleznik-Le, N. J. Breaking the LSD1/KDM1A addiction: therapeutic targeting of the epigenetic modifier in AML. *Cancer cell* **21**, 451-453, doi:10.1016/j.ccr.2012.03.027 (2012).

145 Wang, G. G. *et al.* Haematopoietic malignancies caused by dysregulation of a chromatin-binding PHD finger. *Nature* **459**, 847-851, doi:10.1038/nature08036 (2009).

146 Baek, S. H. When signaling kinases meet histones and histone modifiers in the nucleus. *Molecular cell* **42**, 274-284, doi:10.1016/j.molcel.2011.03.022 (2011).

147 Dawson, M. A. *et al.* JAK2 phosphorylates histone H3Y41 and excludes HP1alpha from chromatin. *Nature* **461**, 819-822, doi:10.1038/nature08448 (2009).

148 Dawson, M. A. *et al.* Three distinct patterns of histone H3Y41 phosphorylation mark active genes. *Cell reports* **2**, 470-477, doi:10.1016/j.celrep.2012.08.016 (2012).

149 Liu, F. *et al.* JAK2V617F-mediated phosphorylation of PRMT5 downregulates its methyltransferase activity and promotes myeloproliferation. *Cancer cell* **19**, 283-294, doi:10.1016/j.ccr.2010.12.020 (2011).

150 Bernt, K. M. & Armstrong, S. A. Targeting epigenetic programs in MLL-rearranged leukemias. *Hematology Am Soc Hematol Educ Program* **2011**, 354-360, doi:10.1182/asheducation-2011.1.354 (2011).

151 Slany, R. K. When epigenetics kills: MLL fusion proteins in leukemia. *Hematological oncology* **23**, 1-9, doi:10.1002/hon.739 (2005).

152 De Braekeleer, M., Morel, F., Le Bris, M. J., Herry, A. & Douet-Guilbert, N. The MLL gene and translocations involving chromosomal band 11q23 in acute leukemia. *Anticancer research* **25**, 1931-1944 (2005).

153 Krivtsov, A. V. & Armstrong, S. A. MLL translocations, histone modifications and leukaemia stem-cell development. *Nature reviews. Cancer* **7**, 823-833, doi:10.1038/nrc2253 (2007).

154 Meyer, C. *et al.* The MLL recombinome of acute leukemias in 2013. *Leukemia*, doi:10.1038/leu.2013.135 (2013).

155 Luo, Z., Lin, C. & Shilatifard, A. The super elongation complex (SEC) family in transcriptional control. *Nature reviews. Molecular cell biology* **13**, 543-547, doi:10.1038/nrm3417 (2012).

156 Nguyen, A. T. & Zhang, Y. The diverse functions of Dot1 and H3K79 methylation. *Genes & development* **25**, 1345-1358, doi:10.1101/gad.2057811 (2011).

157 Daigle, S. R. *et al.* Selective killing of mixed lineage leukemia cells by a potent small-molecule DOT1L inhibitor. *Cancer cell* **20**, 53-65, doi:10.1016/j.ccr.2011.06.009 (2011).

158 Grembecka, J. *et al.* Menin-MLL inhibitors reverse oncogenic activity of MLL fusion proteins in leukemia. *Nature chemical biology* **8**, 277-284, doi:10.1038/nchembio.773 (2012).

159 Bernt, K. M. *et al.* MLL-rearranged leukemia is dependent on aberrant H3K79 methylation by DOT1L. *Cancer cell* **20**, 66-78, doi:10.1016/j.ccr.2011.06.010 (2011).

160 Mueller, D. *et al.* A role for the MLL fusion partner ENL in transcriptional elongation and chromatin modification. *Blood* **110**, 4445-4454, doi:10.1182/blood-2007-05-090514 (2007).

161 Milne, T. A., Martin, M. E., Brock, H. W., Slany, R. K. & Hess, J. L. Leukemogenic MLL fusion proteins bind across a broad region of the Hox a9 locus, promoting transcription and multiple histone modifications. *Cancer research* **65**, 11367-11374, doi:10.1158/0008-5472.CAN-05-1041 (2005).

162 Okada, Y. *et al.* hDOT1L links histone methylation to leukemogenesis. *Cell* **121**, 167-178, doi:10.1016/j.cell.2005.02.020 (2005).

163 Jo, S. Y., Granowicz, E. M., Maillard, I., Thomas, D. & Hess, J. L. Requirement for Dot1l in murine postnatal hematopoiesis and leukemogenesis by MLL translocation. *Blood* **117**, 4759-4768, doi:10.1182/blood-2010-12-327668 (2011).

164 Nguyen, A. T., He, J., Taranova, O. & Zhang, Y. Essential role of DOT1L in maintaining normal adult hematopoiesis. *Cell research* **21**, 1370-1373, doi:10.1038/cr.2011.115 (2011).

165 Feng, Y. *et al.* Early mammalian erythropoiesis requires the Dot1L methyltransferase. *Blood* **116**, 4483-4491, doi:10.1182/blood-2010-03-276501 (2010).

166 Guenther, M. G. *et al.* Aberrant chromatin at genes encoding stem cell regulators in human mixed-lineage leukemia. *Genes & development* **22**, 3403-3408, doi:10.1101/gad.1741408 (2008).

167 Krivtsov, A. V. *et al.* H3K79 methylation profiles define murine and human MLL-AF4 leukemias. *Cancer cell* **14**, 355-368, doi:10.1016/j.ccr.2008.10.001 (2008).

168 Daigle, S. R. *et al.* Potent inhibition of DOT1L as treatment of MLL-fusion leukemia. *Blood* **122**, 1017-1025, doi:10.1182/blood-2013-04-497644 (2013).

169 Stein, E. M. *et al.* The DOT1L Inhibitor EPZ-5676: Safety and Activity in Relapsed/Refractory Patients with MLL-Rearranged Leukemia. *Blood* **124**, 387 (2014).

170 Gilan, O. *et al.* Functional interdependence of BRD4 and DOT1L in MLL leukemia. *Nature structural & molecular biology* **23**, 673-681, doi:10.1038/nsmb.3249 (2016).

171 Yokoyama, A. *et al.* The menin tumor suppressor protein is an essential oncogenic cofactor for MLL-associated leukemogenesis. *Cell* **123**, 207-218, doi:10.1016/j.cell.2005.09.025 (2005).

172 Caslini, C. *et al.* Interaction of MLL amino terminal sequences with menin is required for transformation. *Cancer research* **67**, 7275-7283, doi:10.1158/0008-5472.CAN-06-2369 (2007).

173 Grembecka, J. *et al.* High-affinity small molecule inhibitors of the menin-Mixed Lineage Leukemia (MLL) interaction closely mimic a natural protein-protein interaction. *Journal of medicinal chemistry*, doi:10.1021/jm401868d (2014).

174 Cao, F. *et al.* Targeting MLL1 H3K4 methyltransferase activity in mixed-lineage leukemia. *Molecular cell* **53**, 247-261, doi:10.1016/j.molcel.2013.12.001 (2014).

175 Mishra, B. P. *et al.* The histone methyltransferase activity of MLL1 is dispensable for hematopoiesis and leukemogenesis. *Cell reports* **7**, 1239-1247, doi:10.1016/j.celrep.2014.04.015 (2014).

176 Cozzio, A. *et al.* Similar MLL-associated leukemias arising from self-renewing stem cells and short-lived myeloid progenitors. *Genes & development* **17**, 3029-3035, doi:10.1101/gad.1143403 (2003).

177 Krivtsov, A. V. *et al.* Transformation from committed progenitor to leukaemia stem cell initiated by MLL-AF9. *Nature* **442**, 818-822, doi:10.1038/nature04980 (2006).

178 Somervaille, T. C. & Cleary, M. L. Identification and characterization of leukemia stem cells in murine MLL-AF9 acute myeloid leukemia. *Cancer cell* **10**, 257-268, doi:10.1016/j.ccr.2006.08.020 (2006).

179 Krivtsov, A. V. *et al.* Cell of origin determines clinically relevant subtypes of MLL-rearranged AML. *Leukemia* **27**, 852-860, doi:10.1038/leu.2012.363 (2013).

180 Baud, M. G. *et al.* Chemical biology. A bump-and-hole approach to engineer controlled selectivity of BET bromodomain chemical probes. *Science* **346**, 638-641, doi:10.1126/science.1249830 (2014).

181 Zuber, J. *et al.* RNAi screen identifies Brd4 as a therapeutic target in acute myeloid leukaemia. *Nature* **478**, 524-528, doi:10.1038/nature10334 (2011).

182 Dawson, M. A. *et al.* Recurrent mutations, including NPM1c, activate a BRD4-dependent core transcriptional program in acute myeloid leukemia. *Leukemia*, doi:10.1038/leu.2013.338 (2013).

183 Loven, J. *et al.* Selective inhibition of tumor oncogenes by disruption of super-enhancers. *Cell* **153**, 320-334, doi:10.1016/j.cell.2013.03.036 (2013).

184 Delmore, J. E. *et al.* BET bromodomain inhibition as a therapeutic strategy to target c-Myc. *Cell* **146**, 904-917, doi:10.1016/j.cell.2011.08.017 (2011).

185 Mertz, J. A. *et al.* Targeting MYC dependence in cancer by inhibiting BET bromodomains. *Proceedings of the National Academy of Sciences of the United States of America* **108**, 16669-16674, doi:10.1073/pnas.1108190108 (2011).

186 Ott, C. J. *et al.* BET bromodomain inhibition targets both c-Myc and IL7R in high-risk acute lymphoblastic leukemia. *Blood* **120**, 2843-2852, doi:10.1182/blood-2012-02-413021 (2012).

187 Berthon, C. *et al.* Bromodomain inhibitor OTX015 in patients with acute leukaemia: a dose-escalation, phase 1 study. *Lancet Haematol* **3**, e186-195, doi:10.1016/S2352-3026(15)00247-1 (2016).

188 Amorim, S. *et al.* Bromodomain inhibitor OTX015 in patients with lymphoma or multiple myeloma: a dose-escalation, open-label, pharmacokinetic, phase 1 study. *Lancet Haematol* **3**, e196-204, doi:10.1016/S2352-3026(16)00021-1 (2016).

189 Wander, S. A., Levis, M. J. & Fathi, A. T. The evolving role of FLT3 inhibitors in acute myeloid leukemia: quizartinib and beyond. *Ther Adv Hematol* **5**, 65-77, doi:10.1177/2040620714532123 (2014).

190 Holohan, C., Van Schaeybroeck, S., Longley, D. B. & Johnston, P. G. Cancer drug resistance: an evolving paradigm. *Nature reviews. Cancer* **13**, 714-726, doi:10.1038/nrc3599 (2013).

191 Lim, A. *et al.* in *ASBMT/CIBMTR BMT Tandem Meeting.*

192 Fong, C. Y. *et al.* Fludarabine, cytarabine, granulocyte-colony stimulating factor and amsacrine: an effective salvage therapy option for acute myeloid leukemia at first relapse. *Leuk Lymphoma* **54**, 336-341, doi:10.3109/10428194.2012.713479 (2013).

193 Gottesman, M. M., Fojo, T. & Bates, S. E. Multidrug resistance in cancer: role of ATP-dependent transporters. *Nature reviews. Cancer* **2**, 48-58, doi:10.1038/nrc706 (2002).

194 Begley, D. J. Delivery of therapeutic agents to the central nervous system: the problems and the possibilities. *Pharmacol Ther* **104**, 29-45, doi:10.1016/j.pharmthera.2004.08.001 (2004).

195 Stewart, D. J. Tumor and host factors that may limit efficacy of chemotherapy in non-small cell and small cell lung cancer. *Crit Rev Oncol Hematol* **75**, 173-234, doi:10.1016/j.critrevonc.2009.11.006 (2010).

196 Alfarouk, K. O. *et al.* Resistance to cancer chemotherapy: failure in drug response from ADME to P-gp. *Cancer Cell Int* **15**, 71, doi:10.1186/s12935-015-0221-1 (2015).

197 Bell, D. R., Gerlach, J. H., Kartner, N., Buick, R. N. & Ling, V. Detection of P-glycoprotein in ovarian cancer: a molecular marker associated with multidrug resistance. *J Clin Oncol* **3**, 311-315 (1985).

198 Kartner, N., Riordan, J. R. & Ling, V. Cell surface P-glycoprotein associated with multidrug resistance in mammalian cell lines. *Science* **221**, 1285-1288 (1983).

199 Wu, C. P., Hsieh, C. H. & Wu, Y. S. The emergence of drug transporter-mediated multidrug resistance to cancer chemotherapy. *Mol Pharm* **8**, 1996-2011, doi:10.1021/mp200261n (2011).

200 Dean, M., Fojo, T. & Bates, S. Tumour stem cells and drug resistance. *Nature reviews. Cancer* **5**, 275-284, doi:10.1038/nrc1590 (2005).

201 Shukla, S., Chen, Z. S. & Ambudkar, S. V. Tyrosine kinase inhibitors as modulators of ABC transporter-mediated drug resistance. *Drug Resist Updat* **15**, 70-80, doi:10.1016/j.drup.2012.01.005 (2012).

202 Longley, D. B., Harkin, D. P. & Johnston, P. G. 5-fluorouracil: mechanisms of action and clinical strategies. *Nature reviews. Cancer* **3**, 330-338, doi:10.1038/nrc1074 (2003).

203 Galmarini, C. M., Mackey, J. R. & Dumontet, C. Nucleoside analogues: mechanisms of drug resistance and reversal strategies. *Leukemia* **15**, 875-890 (2001).

204 Koppikar, P. *et al.* Heterodimeric JAK-STAT activation as a mechanism of persistence to JAK2 inhibitor therapy. *Nature* **489**, 155-159, doi:10.1038/nature11303 (2012).

205 Gorre, M. E. *et al.* Clinical resistance to STI-571 cancer therapy caused by BCR-ABL gene mutation or amplification. *Science* **293**, 876-880, doi:10.1126/science.1062538 (2001).

206 Engelman, J. A. *et al.* MET amplification leads to gefitinib resistance in lung cancer by activating ERBB3 signaling. *Science* **316**, 1039-1043, doi:10.1126/science.1141478 (2007).

207 Nazarian, R. *et al.* Melanomas acquire resistance to B-RAF(V600E) inhibition by RTK or N-RAS upregulation. *Nature* **468**, 973-977, doi:10.1038/nature09626 (2010).

208 Weisberg, E., Manley, P. W., Cowan-Jacob, S. W., Hochhaus, A. & Griffin, J. D. Second generation inhibitors of BCR-ABL for the treatment of imatinib-resistant chronic myeloid leukaemia. *Nature reviews. Cancer* **7**, 345-356, doi:10.1038/nrc2126 (2007).

209 O'Hare, T. *et al.* AP24534, a pan-BCR-ABL inhibitor for chronic myeloid leukemia, potently inhibits the T315I mutant and overcomes mutation-based resistance. *Cancer cell* **16**, 401-412, doi:10.1016/j.ccr.2009.09.028 (2009).

210 Cortes, J. E. *et al.* A phase 2 trial of ponatinib in Philadelphia chromosome-positive leukemias. *N Engl J Med* **369**, 1783-1796, doi:10.1056/NEJMoa1306494 (2013).

211 Zhang, J. *et al.* Targeting Bcr-Abl by combining allosteric with ATP-binding-site inhibitors. *Nature* **463**, 501-506, doi:10.1038/nature08675 (2010).

212 Hantschel, O. Allosteric BCR-ABL inhibitors in Philadelphia chromosome-positive acute lymphoblastic leukemia: novel opportunities for drug combinations to overcome resistance. *Haematologica* **97**, 157-159, doi:10.3324/haematol.2012.061812 (2012).

213 Redmond, K. L., Papafili, A., Lawler, M. & Van Schaeybroeck, S. Overcoming Resistance to Targeted Therapies in Cancer. *Semin Oncol* **42**, 896-908, doi:10.1053/j.seminoncol.2015.09.028 (2015).

214 Goldman, A. *et al.* Temporally sequenced anticancer drugs overcome adaptive resistance by targeting a vulnerable chemotherapy-induced phenotypic transition. *Nat Commun* **6**, 6139, doi:10.1038/ncomms7139 (2015).

215 Pratz, K. & Levis, M. Incorporating FLT3 inhibitors into acute myeloid leukemia treatment regimens. *Leuk Lymphoma* **49**, 852-863, doi:10.1080/10428190801895352 (2008).

216 Knapper, S. FLT3 inhibition in acute myeloid leukaemia. *Br J Haematol* **138**, 687-699, doi:10.1111/j.1365-2141.2007.06700.x (2007).

217 Levis, M., Pham, R., Smith, B. D. & Small, D. In vitro studies of a FLT3 inhibitor combined with chemotherapy: sequence of administration is important to achieve synergistic cytotoxic effects. *Blood* **104**, 1145-1150, doi:10.1182/blood-2004-01-0388 (2004).

218 Brown, P., Levis, M., McIntyre, E., Griesemer, M. & Small, D. Combinations of the FLT3 inhibitor CEP-701 and chemotherapy synergistically kill infant and childhood MLL-rearranged ALL cells in a sequence-dependent manner. *Leukemia* **20**, 1368-1376, doi:10.1038/sj.leu.2404277 (2006).

219 Greaves, M. Evolutionary Determinants of Cancer. *Cancer discovery* **5**, 806-820, doi:10.1158/2159-8290.CD-15-0439 (2015).

220 Yates, L. R. & Campbell, P. J. Evolution of the cancer genome. *Nature reviews. Genetics* **13**, 795-806, doi:10.1038/nrg3317 (2012).

221 Navin, N. *et al.* Tumour evolution inferred by single-cell sequencing. *Nature* **472**, 90-94, doi:10.1038/nature09807 (2011).

222 Patel, A. P. *et al.* Single-cell RNA-seq highlights intratumoral heterogeneity in primary glioblastoma. *Science* **344**, 1396-1401, doi:10.1126/science.1254257 (2014).

223 Valent, P. *et al.* Cancer stem cell definitions and terminology: the devil is in the details. *Nature reviews. Cancer* **12**, 767-775, doi:10.1038/nrc3368 (2012).

224 Huntly, B. J. & Gilliland, D. G. Leukaemia stem cells and the evolution of cancer-stem-cell research. *Nature reviews. Cancer* **5**, 311-321, doi:10.1038/nrc1592 (2005).

225 Gottgens, B. Regulatory network control of blood stem cells. *Blood* **125**, 2614-2620, doi:10.1182/blood-2014-08-570226 (2015).

226 Reya, T., Morrison, S. J., Clarke, M. F. & Weissman, I. L. Stem cells, cancer, and cancer stem cells. *Nature* **414**, 105-111, doi:10.1038/35102167 (2001).

227 Eppert, K. *et al.* Stem cell gene expression programs influence clinical outcome in human leukemia. *Nat Med* **17**, 1086-1093, doi:10.1038/nm.2415 (2011).

228 Zuber, J. *et al.* Toolkit for evaluating genes required for proliferation and survival using tetracycline-regulated RNAi. *Nature biotechnology* **29**, 79-83, doi:10.1038/nbt.1720 (2011).

229 Zhao, W. *et al.* A New Bliss Independence Model to Analyze Drug Combination Data. *Journal of biomolecular screening* **19**, 817-821, doi:10.1177/1087057114521867 (2014).

230 Rathert, P. *et al.* Transcriptional plasticity promotes primary and acquired resistance to BET inhibition. *Nature* **525**, 543-547, doi:10.1038/nature14898 (2015).

231 Hu, Y. & Smyth, G. K. ELDA: extreme limiting dilution analysis for comparing depleted and enriched populations in stem cell and other assays. *Journal of immunological methods* **347**, 70-78, doi:10.1016/j.jim.2009.06.008 (2009).

232 Li, H. & Durbin, R. Fast and accurate short read alignment with Burrows-Wheeler transform. *Bioinformatics* **25**, 1754-1760, doi:10.1093/bioinformatics/btp324 (2009).

233 Amarasinghe, K. C., Li, J. & Halgamuge, S. K. CoNVEX: copy number variation estimation in exome sequencing data using HMM. *BMC Bioinformatics* **14 Suppl 2**, S2, doi:10.1186/1471-2105-14-S2-S2 (2013).

234 Koboldt, D. C. *et al.* VarScan 2: somatic mutation and copy number alteration discovery in cancer by exome sequencing. *Genome Res* **22**, 568-576, doi:10.1101/gr.129684.111 (2012).

235 Cibulskis, K. *et al.* Sensitive detection of somatic point mutations in impure and heterogeneous cancer samples. *Nat Biotechnol* **31**, 213-219, doi:10.1038/nbt.2514 (2013).

236 McKenna, A. *et al.* The Genome Analysis Toolkit: a MapReduce framework for analyzing next-generation DNA sequencing data. *Genome Res* **20**, 1297-1303, doi:10.1101/gr.107524.110 (2010).

237 McLaren, W. *et al.* Deriving the consequences of genomic variants with the Ensembl API and SNP Effect Predictor. *Bioinformatics* **26**, 2069-2070, doi:10.1093/bioinformatics/btq330 (2010).

238 Karolchik, D. *et al.* The UCSC Table Browser data retrieval tool. *Nucleic Acids Res* **32**, D493-496, doi:10.1093/nar/gkh103 (2004).

239 Zhang, Y. *et al.* Model-based analysis of ChIP-Seq (MACS). *Genome Biol* **9**, R137, doi:gb-2008-9-9-r137 [pii]
10.1186/gb-2008-9-9-r137 (2008).

240 Smyth, G. in *Bioinformatics and Computational Biology Solutions using R and Bioconductor* (ed V. Carey R. Gentleman, S. Dudoit, R. Irizarry, W. Huber) 397-420 (Springer, 2005).

241 Benjamini, Y. H., Yosef. Controlling the False Discovery Rate: A Practical and Powerful Approach to Multiple Testing. *J. Roy. Statist. Soc. Ser. B* **57**, 289-300 (1995).

242 Liao, Y., Smyth, G. K. & Shi, W. The Subread aligner: fast, accurate and scalable read mapping by seed-and-vote. *Nucleic Acids Res* **41**, e108, doi:10.1093/nar/gkt214 (2013).

243 Liao, Y., Smyth, G. K. & Shi, W. featureCounts: an efficient general purpose program for assigning sequence reads to genomic features. *Bioinformatics* **30**, 923-930, doi:10.1093/bioinformatics/btt656 (2014).

244 Wu, D. *et al.* ROAST: rotation gene set tests for complex microarray experiments. *Bioinformatics* **26**, 2176-2182, doi:10.1093/bioinformatics/btq401 (2010).

245 Subramanian, A. *et al.* Gene set enrichment analysis: a knowledge-based approach for interpreting genome-wide expression profiles. *Proc Natl Acad Sci U S A* **102**, 15545-15550, doi:10.1073/pnas.0506580102 (2005).

246 Miller, C. L. & Lai, B. Human and mouse hematopoietic colony-forming cell assays. *Methods in molecular biology* **290**, 71-89 (2005).

247 Pereira, C., Clarke, E. & Damen, J. Hematopoietic colony-forming cell assays. *Methods in molecular biology* **407**, 177-208, doi:10.1007/978-1-59745-536-7_14 (2007).

248 Wang, Y. *et al.* The Wnt/beta-catenin pathway is required for the development of leukemia stem cells in AML. *Science* **327**, 1650-1653, doi:10.1126/science.1186624 (2010).

249 Wang, K. *et al.* Patient-derived xenotransplants can recapitulate the genetic driver landscape of acute leukemias. *Leukemia*, doi:10.1038/leu.2016.166 (2016).

250 Goardon, N. *et al.* Coexistence of LMPP-like and GMP-like leukemia stem cells in acute myeloid leukemia. *Cancer cell* **19**, 138-152, doi:10.1016/j.ccr.2010.12.012 (2011).

251 Jung, M. *et al.* Affinity map of bromodomain protein 4 (BRD4) interactions with the histone H4 tail and the small molecule inhibitor JQ1. *The Journal of biological chemistry* **289**, 9304-9319, doi:10.1074/jbc.M113.523019 (2014).

252 Kandoth, C. *et al.* Mutational landscape and significance across 12 major cancer types. *Nature* **502**, 333-339, doi:10.1038/nature12634 (2013).

253 Pott, S. & Lieb, J. D. What are super-enhancers? *Nature genetics* **47**, 8-12, doi:10.1038/ng.3167 (2015).

254 Khwaja, A. *et al.* Acute myeloid leukaemia. *Nat Rev Dis Primers* **2**, 16010, doi:10.1038/nrdp.2016.10 (2016).

255 Misaghian, N. *et al.* Targeting the leukemic stem cell: the Holy Grail of leukemia therapy. *Leukemia* **23**, 25-42, doi:10.1038/leu.2008.246 (2009).

256 Yeung, J. *et al.* beta-Catenin mediates the establishment and drug resistance of MLL leukemic stem cells. *Cancer cell* **18**, 606-618, doi:10.1016/j.ccr.2010.10.032 (2010).

257 Jamieson, C. H. *et al.* Granulocyte-macrophage progenitors as candidate leukemic stem cells in blast-crisis CML. *N Engl J Med* **351**, 657-667, doi:10.1056/NEJMoa040258 (2004).

258 Zhan, T., Rindtorff, N. & Boutros, M. Wnt signaling in cancer. *Oncogene*, doi:10.1038/onc.2016.304 (2016).

259 He, T. C. *et al.* Identification of c-MYC as a target of the APC pathway. *Science* **281**, 1509-1512 (1998).

260 Tetsu, O. & McCormick, F. Beta-catenin regulates expression of cyclin D1 in colon carcinoma cells. *Nature* **398**, 422-426, doi:10.1038/18884 (1999).

261 Niehrs, C. Function and biological roles of the Dickkopf family of Wnt modulators. *Oncogene* **25**, 7469-7481, doi:10.1038/sj.onc.1210054 (2006).

262 Thorne, C. A. *et al.* Small-molecule inhibition of Wnt signaling through activation of casein kinase 1alpha. *Nature chemical biology* **6**, 829-836, doi:10.1038/nchembio.453 (2010).

263 Xu, W. *et al.* The antihelmintic drug pyrvinium pamoate targets aggressive breast cancer. *PloS one* **8**, e71508, doi:10.1371/journal.pone.0071508 (2013).

264 Lynch, J. T., Cockerill, M. J., Hitchin, J. R., Wiseman, D. H. & Somervaille, T. C. CD86 expression as a surrogate cellular biomarker for pharmacological inhibition of the histone demethylase lysine-specific demethylase 1. *Anal Biochem* **442**, 104-106, doi:10.1016/j.ab.2013.07.032 (2013).

265 Estey, E. & Dohner, H. Acute myeloid leukaemia. *Lancet* **368**, 1894-1907, doi:10.1016/S0140-6736(06)69780-8 (2006).

266 Tenen, D. G. Disruption of differentiation in human cancer: AML shows the way. *Nature reviews. Cancer* **3**, 89-101, doi:10.1038/nrc989 (2003).

267 Herzig, R. H., Lazarus, H. M., Wolff, S. N., Phillips, G. L. & Herzig, G. P. High-dose cytosine arabinoside therapy with and without anthracycline antibiotics for remission reinduction of acute nonlymphoblastic leukemia. *J Clin Oncol* **3**, 992-997, doi:10.1200/jco.1985.3.7.992 (1985).

268 Wolff, S. N. *et al.* High-dose cytosine arabinoside and daunorubicin as consolidation therapy for acute nonlymphocytic leukemia in first remission: a pilot study. *Blood* **65**, 1407-1411 (1985).

269 Löwenberg, B. *et al.* Cytarabine dose for acute myeloid leukemia. *The New England journal of medicine* **364**, 1027-1036, doi:10.1056/NEJMoa1010222 (2011).

270 Howlader, N. *et al. SEER Cancer Statistics Review, 1975-2012, National Cancer Institute.*, <http://seer.cancer.gov/csr/1975_2012/> (2015).

271 Papaemmanuil, E. *et al.* Genomic Classification and Prognosis in Acute Myeloid Leukemia. *N Engl J Med* **374**, 2209-2221, doi:10.1056/NEJMoa1516192 (2016).

272 Mrozek, K. *et al.* Prognostic significance of the European LeukemiaNet standardized system for reporting cytogenetic and molecular alterations in adults with acute myeloid leukemia. *J Clin Oncol* **30**, 4515-4523, doi:10.1200/JCO.2012.43.4738 (2012).

273 Dohner, H., Weisdorf, D. J. & Bloomfield, C. D. Acute Myeloid Leukemia. *N Engl J Med* **373**, 1136-1152, doi:10.1056/NEJMra1406184 (2015).

274 Ivey, A. *et al.* Assessment of Minimal Residual Disease in Standard-Risk AML. *N Engl J Med* **374**, 422-433, doi:10.1056/NEJMoa1507471 (2016).

275 Wang, Z. Y. & Chen, Z. Acute promyelocytic leukemia: from highly fatal to highly curable. *Blood* **111**, 2505-2515, doi:10.1182/blood-2007-07-102798 (2008).

276 Stone, R. M. *et al.* The Multi-Kinase Inhibitor Midostaurin (M) Prolongs Survival Compared with Placebo (P) in Combination with Daunorubicin (D)/Cytarabine (C) Induction (ind), High-Dose C Consolidation (consol), and As Maintenance (maint) Therapy in Newly Diagnosed Acute Myeloid Leukemia (AML) Patients (pts) Age 18-60 with FLT3 Mutations (muts): An International Prospective Randomized (rand) P-Controlled Double-Blind Trial (CALGB 10603/RATIFY [Alliance]). *Blood* **126** (2015).

277 Kelly, T. K., De Carvalho, D. D. & Jones, P. A. Epigenetic modifications as therapeutic targets. *Nature biotechnology* **28**, 1069-1078, doi:10.1038/nbt.1678 (2010).

278 Knoechel, B. *et al.* An epigenetic mechanism of resistance to targeted therapy in T cell acute lymphoblastic leukemia. *Nature genetics* **46**, 364-370, doi:10.1038/ng.2913 (2014).

279 Greaves, M. Leukaemia 'firsts' in cancer research and treatment. *Nature reviews. Cancer* **16**, 163-172, doi:10.1038/nrc.2016.3 (2016).

280 Ying, Q. L. *et al.* The ground state of embryonic stem cell self-renewal. *Nature* **453**, 519-523, doi:10.1038/nature06968 (2008).

281 Wunderlich, M. *et al.* AML xenograft efficiency is significantly improved in NOD/SCID-IL2RG mice constitutively expressing human SCF, GM-CSF and IL-3. *Leukemia* **24**, 1785-1788, doi:10.1038/leu.2010.158 (2010).

282 Sarry, J. E. *et al.* Human acute myelogenous leukemia stem cells are rare and heterogeneous when assayed in NOD/SCID/IL2Rgammac-deficient mice. *The Journal of clinical investigation* **121**, 384-395, doi:10.1172/JCI41495 (2011).

283 Grimwade, D. & Freeman, S. D. Defining minimal residual disease in acute myeloid leukemia: which platforms are ready for "prime time"? *Blood* **124**, 3345-3355, doi:10.1182/blood-2014-05-577593 (2014).

284 Taussig, D. C. *et al.* Leukemia-initiating cells from some acute myeloid leukemia patients with mutated nucleophosmin reside in the CD34(-) fraction. *Blood* **115**, 1976-1984, doi:10.1182/blood-2009-02-206565 (2010).

285 Kersten, B. *et al.* CD45RA, a specific marker for leukaemia stem cell sub-populations in acute myeloid leukaemia. *Br J Haematol* **173**, 219-235, doi:10.1111/bjh.13941 (2016).

286 Shi, J. *et al.* Discovery of cancer drug targets by CRISPR-Cas9 screening of protein domains. *Nature biotechnology* **33**, 661-667, doi:10.1038/nbt.3235 (2015).

287 Kerenyi, M. A. *et al.* Histone demethylase Lsd1 represses hematopoietic stem and progenitor cell signatures during blood cell maturation. *Elife* **2**, e00633, doi:10.7554/eLife.00633 (2013).

288 Sprussel, A. *et al.* Lysine-specific demethylase 1 restricts hematopoietic progenitor proliferation and is essential for terminal differentiation. *Leukemia* **26**, 2039-2051, doi:10.1038/leu.2012.157 (2012).

289 Lynch, J. T., Harris, W. J. & Somervaille, T. C. LSD1 inhibition: a therapeutic strategy in cancer? *Expert opinion on therapeutic targets* **16**, 1239-1249, doi:10.1517/14728222.2012.722206 (2012).

290 Mould, D. P., McGonagle, A. E., Wiseman, D. H., Williams, E. L. & Jordan, A. M. Reversible inhibitors of LSD1 as therapeutic agents in acute myeloid leukemia: clinical significance and progress to date. *Med Res Rev* **35**, 586-618, doi:10.1002/med.21334 (2015).

291 Buenrostro, J. D., Giresi, P. G., Zaba, L. C., Chang, H. Y. & Greenleaf, W. J. Transposition of native chromatin for fast and sensitive epigenomic profiling of open chromatin, DNA-binding proteins and nucleosome position. *Nat Methods* **10**, 1213-1218, doi:10.1038/nmeth.2688 (2013).

292 Quintas-Cardama, A., Santos, F. P. & Garcia-Manero, G. Histone deacetylase inhibitors for the treatment of myelodysplastic syndrome and acute myeloid leukemia. *Leukemia* **25**, 226-235, doi:10.1038/leu.2010.276 (2011).

293 Prebet, T. *et al.* Prolonged administration of azacitidine with or without entinostat for myelodysplastic syndrome and acute myeloid leukemia with myelodysplasia-related changes: results of the US Leukemia Intergroup trial E1905. *J Clin Oncol* **32**, 1242-1248, doi:10.1200/JCO.2013.50.3102 (2014).

294 Issa, J. P. *et al.* Results of phase 2 randomized study of low-dose decitabine with or without valproic acid in patients with myelodysplastic syndrome and acute myelogenous leukemia. *Cancer* **121**, 556-561, doi:10.1002/cncr.29085 (2015).

295 De Raedt, T. *et al.* PRC2 loss amplifies Ras-driven transcription and confers sensitivity to BRD4-based therapies. *Nature* **514**, 247-251, doi:10.1038/nature13561 (2014).

296 Garnett, M. J. *et al.* Systematic identification of genomic markers of drug sensitivity in cancer cells. *Nature* **483**, 570-575, doi:10.1038/nature11005 (2012).